HYDROISOMERIZATION OF ALKANES OVER METAL-LOADED ZEOLITE CATALYSTS

A thesis submitted to the University of Manchester for the degree of
Doctor of Philosophy
in the Faculty of Engineering and Physical Sciences

2010

RAED H. ABUDAWOOD

School of Chemical Engineering and Analytical Science

TABLE OF CONTENTS

Final word count: 47,500

LIST OF TABLES

LIST OF FIGURES

University of Manchester
Student: Raed H Abudawood
Degree: PhD
Thesis Title: Hydroisomerization of Alkanes over Metal-loaded Zeolite Catalysts
Date: 18 December 2010

ABSTRACT

Zeolite catalysis plays an important role in many industrial applications due to their unique properties and has become widely used in the area of oil refining. Of particular interest is Zeolite Y, which can be hydrothermally treated into its ultrastable form, USY. USY offers a superior practicality, especially when dealuminated and metal-loaded.

The importance of alkanes hydroisomerization arises from the continuingly stricter regulations imposed on the utilization of gasoline as an automotive fuel. The requirements to reduce the aromatics content in gasoline present a need to find an alternative way to maintain its research octane number (RON). An alternative to gasoline's high-octane aromatic content is to increase the RON for the paraffinic content of gasoline, which can be accomplished through hydroisomerization. Commercially, bifunctional metal-loaded zeolites are used to hydroisomerize the light naphtha stream produced at overheads of atmospheric distillation towers. However, no such process exists for the low-value heavy naphtha cut. This targeted process would, if successful, greatly improve refiner's profitability.

In this work, bifunctional USY zeolite catalysts are studied in the hydroisomerization of a normal alkane (nC_7, RON = 0). This nC_7, found in heavy naphtha, has been used as the "model" compound. The impact of different reaction conditions and catalyst properties on catalyst activity and stability, in addition to the catalyst selectivity to high octane isomers is one step towards determining optimum conditions and preferential catalyst formulations that favour octane maximization. Six platinum-loaded USY zeolite catalysts, four in-house and two commercial, were tested in an atmospheric glass fixed-bed reactor and a stainless steel reactor purpose-built during the course of this thesis. Reaction temperatures ranged from 170 to 250^{o}C at pressures between 1 and 15 bar. The hydrogen to hydrocarbon molar ratio was fixed at 9, with feed space time ranging from 35.14 to 140.6 kg.s/mol. In-house catalysts were hydrothermally treated at different severities, while commercial ones were originally dealuminated through acid-leaching treatments.

Results have shown commercial catalyst CBV-712 gave the best performance and highest octane values for product isomers (>30). In addition, there was no coke generation. The next best catalyst was the most severely steamed in-house catalyst (USY-D) that has shown a remarkable performance at high pressures, almost eclipsing the performance of CBV-712, yet produced higher levels of coke. Other USY catalysts tested were less robust during reactions, probably due to imbalance in their acidic to metallic functions, or diffusion limitations arising from their pore structures. The best catalysts were, nonetheless, highly sensitive to sulfur presence in the feed, which severely impacted their activity, especially their metallic functions, and thus require sulfur-free feeds in order to demonstrate their full capacities.

Simple kinetic modelling of experimental data was performed using the initial rates method and estimation of kinetic parameters, whose values were in good agreement with previous literature.

DECLARATION

No portion of the work referred to in this thesis has been submitted in support of an application for another degree or qualification of this or any other university or other institute of learning.

COPYRIGHT STATEMENTS

i. The author of this thesis (including any appendices and/or schedules to this thesis) owns certain copyright or related rights in it (the "Copyright") and s/he has given The University of Manchester certain rights to use such Copyright, including for administrative purposes.

ii. Copies of this thesis, either in full or in extracts and whether in hard or electronic copy, may be made **only** in accordance with the Copyright, Designs and Patents Act 1988 (as amended) and regulations issued under it or, where appropriate, in accordance with licensing agreements which the University has from time to time. This page must form part of any such copies made.

iii. The ownership of certain Copyright, patents, designs, trade marks and other intellectual property (the "Intellectual Property") and any reproductions of copyright works in the thesis, for example graphs and tables ("Reproductions"), which may be described in this thesis, may not be owned by the author and may be owned by third parties. Such Intellectual Property and Reproductions cannot and must not be made available for use without the prior written permission of the owner(s) of the relevant Intellectual Propert and/or Reproductions.

iv. Further information on the conditions under which disclosure, publication and commercialisation of this thesis, the Copyright and any Intellectual Property and/or Reproductions described in it may take place is available in the University IP Policy (see http://www.campus.manchester.ac.uk/medialibrary/policies/intellectual-property.pdf), in any relevant Thesis restriction declarations deposited in the University Library, The University Library's regulations (see http://www.manchester.ac.uk/library/aboutus/regulations) and in The University's policy on presentation of Theses

ACKNOWLEDGEMENTS

I would like to acknowledge my supervisor, Dr. Arthur Garforth, who has been continuously supporting this research and providing ideas and guidance in solving problems, resources allocation and experimental set up, and my mentor in Saudi Aramco, Dr. Omer Refa Koseoglu, for his ideas and helpful input. I would like also to thank my colleague Faisal Al-Humaidan, who gave me advice and helped me in planning lab experiments with their associated procedures in addition to planning the building of my pressure unit. In addition, my sincere appreciation goes to my colleagues Faisal Alotaibi, who provided tremendous help in many aspects of my work and Rashid Usman, who gave a lot of valuable input and support. I am indebted to Saudi Aramco's management, who approved my sponsorship to study in the University of Manchester. Finally, I would like to thank my wife and parents for being always there for me and their continuous support throughout my PhD program.

LIST OF ABBREVIATIONS

MTBE	Methyltertiarybutylether
USY	Ultrastable Y
SBU	Secondary building unit
EFAL	Extraframework aluminium
SEM	Scanning electron microscopy
3D	3 dimentional
SA	Sodium aluminate
RON	Research octane number
PW	Tungstophosphoric acid
UDY	Ultradealuminated Y
TOF	Turnover frequency
HDS	Hydrodesulfurization
DMDS	Dimethyldisulfide
ppm	Part per million
GS	Glycol solution
EDAX	Energy dispersive X-ray
XRD	X-ray diffraction
CRT	Cathode ray tube
MCH	Methylcyclohexane
WHSV	Weighted hourly space velocity
HC	Hydrocarbon
P&ID	Piping & instrumentation diagram
HPLC	High performance liquid chromatography
GC	Gas chromatography
FID	Flame ionization detector

FTIR	Fourier transform infrared spectroscopy
NMR	Nuclear magnetic resonance
BET	Brunauer Emmett Teller
TPD	Temperature programmed desorption
TGA	Thermogravimetric analysis
GC-MS	Gas chromatography – mass spectrometer
BRON	Blending research octane number
NPT	National pipe thread
OD	Outside diameter
I/O	Input/output
Vdc	Volts of continuous current
B/L	Brönsted/Lewis

LIST OF SYMBOLS

β	Beta
I/C	Isomerization to cracking ratio
n_{Pt}	number of accessible platinum sites
n_A	number of acid sites
K_i	Weighting factor
k	Rate constant
X	Conversion
W	Weight of catalyst
F_o	Feed molar flow rate
A	Preexponential factor
E_A	Activation energy
r_o	Initial rate
k_o	Rate constant at initial rate conditions
n	Reaction order in nC_7
m	Reaction order in H_2
P_{C7}	Normal heptane partial pressure
P_{H2}	Hydrogen partial pressure
R	Gas constant
k_{iso}	rate constant of isomerisation
K_{dehydr}	Dehydrogenation equilibrium constant
K_{prot}	Protonation equilibrium constant
p_{nC6}	Normal hexane partial pressure
α	Order of reaction
PAR	Parameter
$p_{n\text{-}alkane}$	normal alkane partial pressure

$E_{act,\ iso}$	n-alkoxy isomerization activation energy
$E_{act,\ app}$	Apparent activation energy
$\theta_{n\text{-}alkoxy}$	Langmuir coverage of n-alkoxy groups
$\Delta H_{prot,\ ads}$	enthalpy of protonation (alkoxy formation) from the alkene adsorbed state
$\Delta H_{ads,\ n=6}$	enthalpy of adsorption of normal hexene
ΔH_{dehydr}	dehydrogenation enthalpy
k_3	Isomerization rate constant
r	Rate of reaction
C_m	Brönsted acid site concentration of the catalyst
K_1	Equilibrium constant of normal hexane dehydrogenation
K_2	Equilibrium constant of carbenium ion formation
nC_7	Normal heptane
$_f$	Final
$_o$	Initial

CHAPTER ONE

INTRODUCTION

1.1 Introduction

The requirement for cleaner energy resources has resulted in stricter environmental regulations with regards to the quality of automotive fuels. In particular, the content of harmful aromatics present in transportation gasoline has to be reduced [1-24], if not completely removed, without affecting the combustion quality of the fuel [2,14,18,19]. Finding a harmless substituent to the high-octane aromatics is not a straightforward task, since main octane enhancers have either been completely phased out due to their toxicity in many countries worldwide, such as in the case of lead-containing additives, or seen their use decline due to their environmental problems, like oxygenates such as MTBE [5,9,13,17-21,25,26]. In addition, using octane-rich reformates fails to do the trick since aromatics are a major constituent of them [1,18,23]. However, the utilization of an upgraded low-value refinery stream to the gasoline pool might present a solution to the problem, as it can considerably lower the cost of gasoline production, while losing only some of its original quality, but still remain environmentally friendly. The application of specifically-made bifunctional zeolite catalysts in upgrading the octane number of the refinery light naphtha stream through hydroisomerization has already been commercialized [1,2,4,6-9,11,15,19,20,23,24,27-30]. This application, however, has not yet been expanded commercially to include the processing of heavy naphtha, which typically contains normal alkanes from the range of heptane to decane [15,18-20,23,27,29].

The use of optimal metal-loaded zeolites in the hydroisomerization of alkanes in the range of heptane to decane is the topic of investigation of this research. The research aim includes acquiring the necessary skills to perform the synthesis, modification, metal-loading, catalysis, and characterization of zeolites. A series of four in-house ultra-stable zeolite Y catalytic supports that possess different catalytic properties as well as two commercially available zeolite Y catalysts were employed in studying the reaction of normal alkanes under various reaction conditions. The aim was to determine the optimum conditions from which a catalyst system with an enhanced activity, selectivity, and stability can be chosen. In addition, the aim was to study the effect of diverse conditions on the

reaction kinetics. Initially, experiments were performed on three catalysts utilizing a glass atmospheric reaction rig while a stainless-steel pressure rig was being built and commissioned. Subsequently, experiments were conducted on the remaining catalysts using the pressure rig at 100 – 1500 kPa pressures.

1.2 Objective

The objective of this thesis is to:

- Provide an introduction about zeolites, their uses, structures, and catalysis, synthesis and modification techniques.
- Review the literature of the hydroisomerization of normal alkanes over zeolitic supports, in order to determine the influence of different reaction conditions and catalytic properties over the reaction and product quality as reported by other researchers, thus providing a starting point for the current work and its experimental design.
- Examine the behaviour and applicability of novel in-house USY zeolite catalytic supports in the hydroisomerization of normal heptane, in comparison to commercial ones, with both being subjected to various reaction conditions for the purpose of identifying supports with the best activity, selectivity and stability, and optimal conditions of the reaction that lead to an improved product research octane number.
- Provide future direction on proposed work and catalyst formulations that can achieve better peformance when applied in this reaction.

1.3 Thesis Outline

This thesis starts with a brief overview of zeolites and their chemistry in chapter two. An insight is given about their synthesis, post-synthesis modification and catalytic properties. Three mainly-covered types of zeolites in the literature of alkane hydroisomerization are also discussed. In chapter three, a detailed discussion about the hydroisomerization of normal alkanes on zeolites is provided. Different factors affecting zeolite activity, selectivity, and stability are commented on as reviewed in recent literature, as well as the reaction mechanisms and kinetics. Chapter four discusses the experimental set up of atmospheric and pressure runs, including the design and commissioning of the

pressure stainless-steel rig. It also covers the experimental part of a zeolite Y synthesis that was performed in year 1 of the program. Chapter five provides an overview of the techniques used in catalyst characterization along with the results. In chapter six, the results of atmospheric and pressure experiments are reported and discussed thoroughly, with comparisons given between obtained results versus those found in the literature. Results of an attempted kinetic modelling are also presented. Finally, chapter seven concludes and lists future work and recommendations on ways to improve the performance of catalysts during the hydroisomerization of heptane.

1.4 Conclusion

The absence of a commercial process to isomerize heavy naphtha into a higher value fraction while minimizing aromatic content makes it appealing to explore ways that make it possible for such a process to exist. One starting way is to hydroisomerize normal heptane as a model compound of heavy naphtha to its octane-rich isomers. Employing different USY zeolite catalysts and a purpose-built reactor unit provides the ability to study the impact of various reaction conditions and catalyst properties on the reaction.

1.5 References

[1] Pope, T. D; Kriz, J. F; Stanciulescu, M. and Monnier, J. (2002). A Study of Catalyst Formulations for Isomerisation of C_7 Hydrocarbons. *Applied Catalysis A: General*, 233, 45-62.

[2] Arribas, M. A; Márquez, F. and Martínez, A. (2000). Activity, Selectivity, and Sulfur Resistance of Pt/WOx–ZrO_2 and Pt/Beta Catalysts for the Simultaneous Hydroisomerization of *n*-Heptane and Hydrogenation of Benzene. *Journal of Catalysis*, 190, 309-319.

[3] Fúnez, A; Thybaut, J. W; Marin, G. B; Sánchez, P; De Lucas, A. and Valverde, J. L. (2008). Assessment of Dominant Factors Affecting Liquid Phase Hydroisomerization on Bifunctional Zeolites. *Applied Catalysis A: General*, 349, 29-39.

[4] Maloncy, M. L; Maschmeyer, T. and Jansen, J. C. (2005). Technical and Economical Evaluation of a Zeolite Membrane Based Heptane Hydroisomerization Process. *Chemical Engineering Journal*, 106, 187-195.

[5] Barsi, F. V. and Cardoso, D. (2009). Bimetallic Pt-Ni Catalysts Supported on USY Zeolite for *n*-Hexane Isomerization. *Brazilian Journal of Chemical Engineering*, 26-2, 353-360.

[6] Matsuda, T; Watanabe, K; Sakagami, H. and Takahashi, N. (2003). Catalytic properties of H_2-reduced MoO_3 and Pt/zeolites for the isomerization of pentane, hexane, and heptane. *Applied Catalysis A: General*, 242, 267-274.

[7] Matsuda, T; Kodama, H; Sakagami, H. and Takahashi, N. (2003). Comparison of the catalytic properties of H_2-reduced Pt/MoO_3 and of Pt/zeolites for the conversions of pentane and heptane. *Applied Catalysis A: General*, 248, 269-278.

[8] Roldán, R; Beale, A. M; Sánchez-Sánchez, M; Romero-Salguero, F. J; Jiménez-Sanchidrián, C; Gómez, J. P. and Sankar, G. (2008). Effect of the Impregnation Order on the Nature of Metal Particles of Bi-functional Pt/Pd-supported Zeolite Beta Materials and on their Catalytic Activity for the Hydroisomerization of Alkanes. *Journal of Catalysis*, 254, 12-26.

[9] Ali, L. I; Ali, Abdel-Ghaffar A; Aboul-Fotouh, S. M. and Aboul-Gheit, A. K. (2001). Hydroconversion of *n*-paraffins in Light Naphtha Using Pt/Al_2O_3 Catalysts Promoted with Noble Metals and/or Chlorine. *Applied Catalysis A: General*, 205, 129-146.

[10] Sánchez, P; Dorado, F; Ramos, M. J; Romero, R; Jiménez, V. and Valverde, J. L. (2006). Hydroisomerization of C_6–C_8 *n*-alkanes, Cyclohexane and Benzene over Palladium and Platinum Beta Catalysts Agglomerated with Bentonite. *Applied Catalysis A: General*, 314, 248-255.

[11] Wei, R; Wang, J. and Xiao, G. (2009). Hydroisomerization of *n*-Heptane Over Cr Promoted Pt-bearing $H_3PW_{12}O_{40}$ Catalysts Supported on Dealuminated USY Zeolite. *Catalysis Letters*, 127, 360-367.

[12] Martins, A; Silva, J. M; Ribeiro, F. R. and Ribeiro, M. F. (2006). Hydroisomerization of *n*-hexane over Pt–Ni/HBEA Using Catalysts Prepared by Different Methods. *Catalysis Letters*, 109, 1-2, 83-87.

[13] Karthikeyan, D; Lingappan, N. and Sivasankar, B. (2008). Hydroisomerization of *n*-Octane over Bifunctional Ni-Pd/HY Zeolite Catalysts. *Industrial* & *Engineering Chemistry Research*, 47, 6538-6546.

[14] Khurshid, M. and Al-Khattaf, S. S. (2009). *n*-Heptane Isomerization over Pt/WO_3-ZrO_2: A Kinetic Study. *Applied Catalysis A: General*, 368, 56-64.

[15] Pham-Huu, C; Del Gallo, P; Peschiera, E. and Ledoux, M. J. (1995). *n*-Hexane and *n*-heptane Isomerization at Atmospheric and Medium Pressure on MoO_3–carbon-modified Supported on SiC and γ-Al_2O_3. *Applied Catalysis A: General*, 132, 77-96.

[16] Eswaramoorthi, I. and Lingappan, N. (2003). Ni–Pt/H-Y Zeolite Catalysts for Hydroisomerization of *n*-hexane and *n*-heptane. *Catalysis Letters*, 87, 3-4, 133-142.

[17] Grau, J. M; Vera, C. R. and Parera, J. M. (2002). Preventing Self-poisoning in [Pt/Al_2O_3 + SO_4^{2-}-ZrO_2] Mixed Catalysts for Isomerization-cracking of Heavy Alkanes by Prereduction of the Acid Function. *Applied Catalysis A: General*, 227, 217-230.

[18] Ramos, M. J; Gómez, J. P; Dorado, F; Sánchez, P. and Valverde, J. L. (2007). Hydroisomerization of a Refinery Naphtha Stream over Platinum Zeolite-based Catalysts. *Chemical Engineering Journal*, 126, 13-21.

[19] Akhmedov, V. M. and Al-Khowaiter, S. H. (2007). Recent Advances and Future Aspects in the Selective Isomerization of High *n*-Alkanes. *Catalysis Reviews*, 49, 33-139.

[20] Li, X; Yang, J; Liu, Z; Asami, K. and Fujimoto, K. (2006). Selective Hydroconversion of *n*-Heptane over Pd-supported Zeolites and Pd-containing Hybrid Catalyst. *Journal of the Japan Petroleum Institute*, 49, 2, 86-90.

[21] Viswanadham, N; Kamble, R; Saxena, S. K. and Garg, M. O. (2008). Studies on Octane Boosting of Industrial Feedstocks on Pt/H-BEA zeolite. *Fuel*, 87, 2394-2400.

[22] Sakagami, H; Ohno, T; Takahashi, N. and Matsuda, T. (2006). The Effects of Na Loading on Catalytic Properties of H_2-reduced Pt/MoO_3 for Heptane Isomerization. *Journal of Catalysis*, 241, 296-303.

[23] Raybaud, P; Patrigeon, A. and Toulhoat, H. (2001). The Origin of the C_7-Hydroconversion Selectivities on Y, β, ZSM-22, ZSM-23, and EU-1 Zeolites. *Journal of Catalysis*, 197, 98-112.

[24] Liu, Y; Guo, W; Zhao, X. S; Lian, J; Dou, J. and Kooli, F. (2006). Zeolite Beta Catalysts for *n*-C_7 hydroisomerization. *Journal of Porous Materials*, 13, 359-364.

[25] Wang, Z. B; Kamo, A; Yoneda, T; Komatsu, T. and Yashima, T. (1997). Isomerization of *n*-heptane over Pt-loaded Zeolite Beta Catalysts. *Applied Catalysis A: General*, 159, 119-132.

[26] Wang, X; Li, C; Wang, Y. and Cai, T. (2004). *n*-Heptane Isomerization over Mesoporous MoO_x and Ni–MoO_x Catalysts. *Catalysis Today*, 93-95, 135-140.

[27] Liu, P; Zhang, X; Yao, Y. and Wang, J. (2010). Alkaline Earth Metal ion-exchanged Beta Zeolite Supported Pt Catalysts for Hydroisomerization of *n*-heptane. *Reaction Kinetics, Mechanisms and Catalysis*, 100, 217-226.

[28] Gu, Y; Wei, R; Ren, X. and Wang, J. (2007). Cs Salts of 12-tungstophosphoric Acid Supported on Dealuminated USY as Catalysts for Hydroisomerization of *n*-heptane. *Catalysis Letters*, 113, 1-2, 41-45.

[29] Gopal, S. and Smirniotis, P. G. (2004). Factors Affecting Isomer Yield for *n*-heptane Hydroisomerization over As-synthesized and Dealuminated Zeolite Catalysts Loaded with Platinum. *Journal of Catalysis*, 225, 278-287.

[30] Matsuda, T; Sakagami, H. and Takahashi, N. (2003). H_2-reduced Pt/MoO_3 as a Selective Catalyst for Heptane Isomerization. *Catalysis Today*, 81, 31-42.

CHAPTER TWO

LITERATURE REVIEW: PART 1:

ZEOLITE SYNTHESIS & CATALYSIS

2.1 Introduction

Zeolites are naturally occurring aluminosilicate crystals. They are found in cavities of basaltic rocks that originate from volcanoes. Flows of the volcanic magma form bubbles that cause zeolite crystals to grow and form cavities. This occurs due to chemical reactions within the volcanic magma. Zeolites that are silica-based originate from silica-rich rocks, whereas ones with high alumina content originate from alumina-based rocks. However, the dispersion of these volcanically occurring zeolites limits their industrial application [1,2].

The name “zeolite” originates from the Greek words *zein*, which means (to boil), and *lithos*, which means (stone) [3]. This name (boiling stone) was used because of the bubbles that zeolites release when heated in blowpipes. The first natural zeolite was discovered in 1756 by Axel F. Cronstedt, a Swedish mineralogist [2,3].

The importance of zeolites arises from the fact that they have uniformly-sized pores in their three-dimensional framework, which allows them to act as sieves on a molecular level, that is, allow the passage of a certain size of molecules, while preventing larger ones [2,4]. This aspect enables zeolites to be used in specific applications on an industrial scale [2].

2.1.1 Zeolites Major Uses

Synthetic zeolites are used in a diverse range of industries. These include laundry detergents, oil refining, petrochemicals industries, gas processing, adsorbents, and agriculture [3,5], as well as waste water treatment and air purification [5,6]. However, the optimum chemical structure of the zeolite varies with different applications. For example, when used for catalytic applications, having high silica content versus alumina is favoured, as it causes the structure to withstand higher temperatures during both the reaction and the

regeneration cycles. In addition, the acidic sites (protons) have to be highly dispersed throughout the structure in order to maximise their strength. On the other hand, any slight modification to the molecular structure can result in a modified shape selectivity that hinders certain molecules from passing and only allows the formation of molecules that can squeeze through the zeolite pores [3].

2.1.2 Zeolite Structures

The main building units in zeolites are silica (SiO_4) and alumina (AlO_4), both tetrahedral. Each of these tetrahedral units is linked in such a way as to form the three-dimensional structure of zeolites. Inside the formed network, each of the four oxygen atoms in a given tetrahedron is shared by an adjacent tetrahedron in addition to its tetrahedron. This way, no oxygen atom is left unshared throughout the network. However, since the aluminium atom has three positive charges and that of silicon has four, the AlO_4 tetrahedron carries a net negative charge, whereas the SiO_4 tetrahedron does not. As a result, the presence of an alumina tetrahedron requires the presence of a positive ion (usually Na, K, Mg, or Ca) to stabilize the negative charge [1,6]. In addition to the cations, zeolites usually contain water molecules that move freely inside the frameworks along with the cations. This property makes it easy for zeolites to undergo ion-exchange [1].

In order to come up with a systematic method of describing zeolite types, secondary building units (SBUs) were identified to classify the diverse range of zeolites (almost 60 topologies [8]). These SBUs are based on groups of tetrahedra that are linked together. These SBUs have been defined as the minimum number of units that a known zeolite topology can be built from [9]. The size of these SBUs determines the pore opening and hence the resulting zeolite topology, since each topology has a characteristic pore opening that is dependent on the size of the SBU. When SBUs are linked together, they form chains, sheets, channels or cages, such as α or β-cages [2,3]. Figure 1 shows examples of SBUs and cages commonly indentified in zeolite frameworks. In the figure, D stands for double, R stands for ring, and 4^6 means that there are 6 of 4-membered planes in the SBU. An example of how SBUs link to form a zeolite structure can be demonstrated in zeolite Y. In this zeolite type, hexagonal prisms (of the structure $[4^6 6^2]$) connect sodalite units (of the structure $[4^6 6^8]$) such that a cubic zeolite unit cell has 8 sodalite units, 9 hexagonal prisms, and 1 supercage or α-cavity (of the structure $[4^{12} 6^8 8^6]$).

Figure 2-1. Some Secondary Building Units and cages that are commonly found in zeolite frameworks [3].

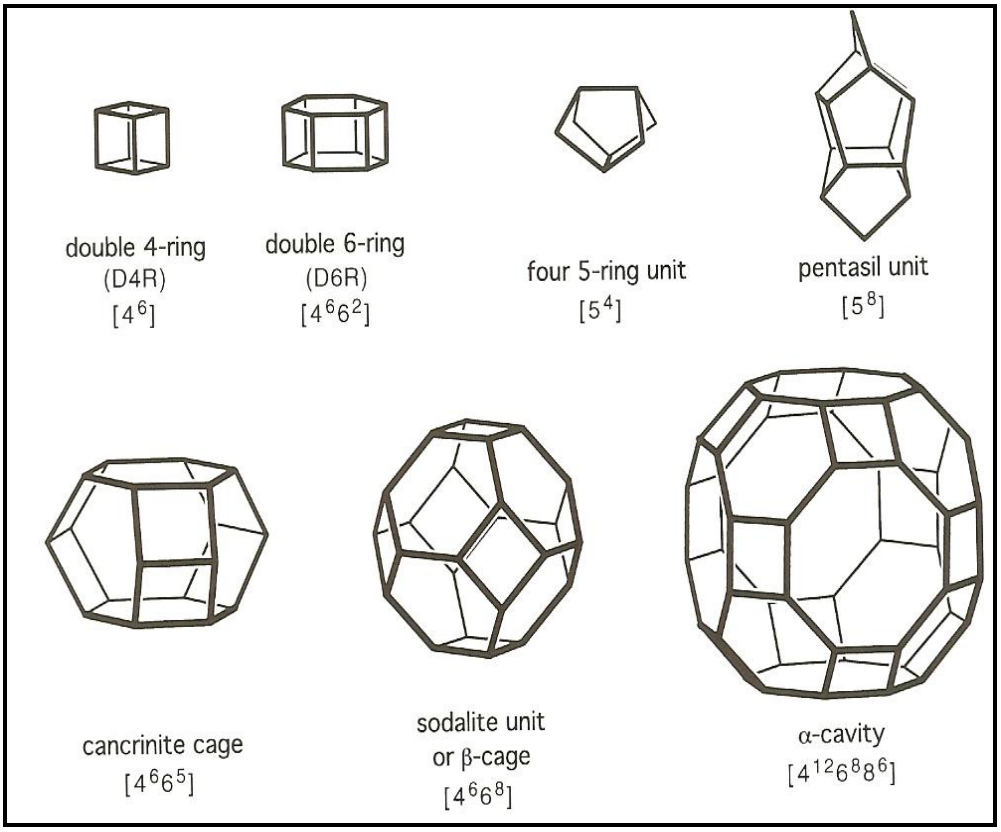

2.2 Hydrothermal Synthesis

The first attempts to synthesize zeolites under high pressures and temperatures were carried out by Richard Barrer in the 1930s. Barrer's work was the starting point for further research at Union Carbide, which resulted in the discovery of synthetic methods at milder conditions in the 1940s, followed by the first commercial application of zeolite Faujasite (Zeolite Y) in oil refining. Moreover, the incorporation of organic cations into the zeolite structures by Mobil in the 1960s and the following applications of MFI type ZSM-5 in the 1970s have growingly fostered research and development in the field of synthetic zeolites for catalytic applications ever since [3].

Zeolites are chemically denoted by an empirical formula as follows:

$$M_{2/n}O \bullet Al_2O_3 \bullet ySiO_2 \bullet wH_2O$$

Here, y ranges between 2 and 10, n represents the cation valence, and w is the number of water molecules present in the framework [3]. There are many sources from which zeolites

can be synthesized. Table 1 lists some commonly-used sources for cations, aluminium, and silicon.

Table 2-1. Reactant components used in hydrothermal synthesis of zeolites [8].

Sources of charge-compensating cations	**Sources of Al**	**Sources of Si**
Alkali metal hydroxides Alkali earth oxides and hydroxides Other oxides and hydroxides Salts (fluorides, other halides, borates, carbonates, phosphates, and sulphates) Organic bases and NH_4OH, especially quaternary bases Soluble silicates and aluminates Mixtures of two or more of the above	Metal aluminates $Al(OH)_3$, Al_2Os, AlO(OH) Al salts Glasses Sediments Minerals, especially clay minerals, felspathoids, felspars, and other zeolites	Silicates Water glass Silica sols Silica gels Silica glass and other glasses Silicon esters Volcanic tufts and sediments Minerals (clay minerals, felspathoids, felspars, other zeolites) Basalts and mineral mixtures Sediments Mixtures of two or more of the above

2.2.1 Reaction Variables

Many factors play a role in shaping the final product during the hydrothermal synthesis of zeolites. The most important ones are temperature (usually shortens crystallization times), pressure, and chemical composition. In addition to these, there are secondary factors that can influence the synthesis, such as [8]:

1. OH^- concentration (pH): The presence of this ion helps aluminium and silicon oxides to come into solution by forming their complex hydroxide forms. Hence, the higher the pH of the system, the faster the reaction takes place and the shorter the zeolite crystallization time.

2. Structure-directing agents: Different cations used in the synthesis result in different zeolite types. The presence of salts also has an effect on the zeolite formed. In addition, organic templates are often used alone or in conjunction with cations in order to control either the zeolite type or a specific property of the zeolite, such as having a high Si/Al ratio. A seeding agent that contains crystals of the targeted zeolite can also be utilized to enhance the crystallization rate, as it is easier for new crystals to form and deposit on the seed crystals [2,10].

2.3 Post-synthesis Modification

Many catalytic applications require the addition or improvement of zeolite properties. These modifications are difficult to achieve through the direct zeolite synthesis. Hence, several post-synthetic methods have been adopted to improve properties such as the zeolite acidity, thermal stability, and porosity. The main methods are ion-exchange, de-alumination by acid leaching, and stabilizing through hydrothermal treatment (steaming) [3,6].

2.3.1 Ion-exchange

The ion-exchange capacity of a certain type of zeolite depends mainly on its Si/Al ratio. The more Al in the zeolite framework structure, the more ion exchange it can undergo. In general, ion-exchange occurs in an aqueous system and involves a cation from the Alkali group or NH_4^+. The rate of ion-exchange depends on the size of the cation, the size of pores in the zeolite structure and temperature. The procedure of ion-exchange is simply carried out by mixing zeolite with a solution of the salt of the targeted cation at room temperature or higher temperatures if the exchange rate is to be enhanced [11].

2.3.2 Acid Leaching

The acid leaching treatment of zeolites causes de-alumination that generally improves their efficiency in processes that result in fast catalyst deactivation through coking, such as cracking [12-14]. This is accomplished by enhancing the thermal stability of zeolite. Acid leaching results in an increase in the Si/Al ratio [12] through the removal of tetrahedral aluminium atoms from the framework [15,16] and the subsequent introduction of mesopores (20-500 Å diameter [17]) into the structure [18]. It has the advantage of not forming extra-framework aluminium inside the zeolite structure, which is found when Al removal is done through steaming [15]. Acid leaching is commonly done with a solution of hydrochloric acid (HCl), ammonium hexafluorosilicate [19], silicon tetrachloride [14,20], fluorine gas or hydrofluoric acid [14]. De-alumination by the acid treatment usually occurs at pH values close to 4 and results in the formation of a hydroxyl nest in place of an aluminium atom from the framework through hydrolysis [3,11].

2.3.3 Steaming

Steaming or hydrothermal treatment involves calcining zeolites, either in the hydrogen or ammonium forms, while steaming at high temperatures. This results in the removal of aluminium from the zeolite framework and the replacement by silicon, which increases the Si/Al ratio of the framework. However, the removed aluminium atoms stay in the zeolite as extra framework aluminium species (EFAL), which can lead to an enhanced acidity through the formation of Lewis acid sites [15]. The formation of EFAL species occurs through the migration of aluminium from the framework into the outer surface of crystals and is rate-controlled, which means it can be accelerated or slowed down by changing the steaming temperature [12]. It has been hypothesized that these EFAL species increase the activity of the zeolite through stabilizing the negative charge that is present in the zeolite structure after protons are removed, possessing a synergy with close Brönsted acid sites, and being themselves active [16].

2.3.4 Metal Loading

Metals from group VIII such as platinum and palladium are commonly loaded into the zeolites used in commercial refining processes, resulting in what is known as bifunctional zeolite catalysts. Bifunctional zeolite catalysts possess both a hydrogenation/dehydrogenation function, provided by the metal, and an acidic function, provided by the zeolite acid sites [21,22]. The metal loading is generally accomplished by ion-exchanging the zeolite in its ammonium form with a salt of the targeted metal in an aqueous solution [22].

2.4 Catalytic Properties

The role of zeolites as primary catalysts in many important commercial applications such as oil refining arises from their unique catalytic activities, selectivities, and stabilities. These catalytic properties are easily modified in zeolites and allow for the flexibility to tailor a zeolitic catalyst for a specific application [2,3,10,11,23,24]. Two of the most important properties that affect the performance of a given zeolite are its acidity and shape-selectivity [5,12], providing zeolites with many advantages over amorphous silica-alumina catalysts [25].

2.4.1 Brönsted & Lewis Acidity

The Brönsted acidity of a zeolite results from the hydroxyl bridge that forms between the aluminium and silicon atoms in the framework, as shown in Figure 2-2 [3,26]. Hence, an increase in the number of framework aluminium atoms (a smaller Si/Al ratio) in a given zeolite causes an increase in the Brönsted acidity of that zeolite, whereas a decrease of aluminium atoms in the framework, resulting from an acid or hydrothermal treatment, decreases it [27]. The Brönsted acid site is formed after the modification of the initial zeolite in its sodium form for example by first exchanging the sodium ion with ammonium and then calcining the zeolite in the ammonium form at high temperatures to transform it into the hydrogen form. This can also be accomplished by ion-exchanging directly with an acid such as HCl or HNO_3 [3,10]. It has been noticed that stronger Brönsted acidic sites are found in areas of the zeolite structure that are highly crystalline whereas weaker ones are found in areas that are less crystalline [27].

Figure 2-2. Formation of the hydroxyl bridge responsible for Brönsted acidity [3].

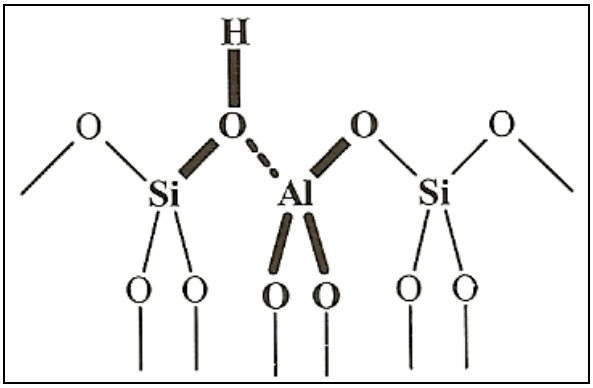

On the other hand, Lewis acidity results when the zeolite is de-aluminated by steaming or calcination, which causes the hydroxyl bridge between aluminium and silicon atoms to break, placing defects in the framework structure and causing some aluminium atoms to migrate to the outer surface of the zeolite and form the EFAL species. The Lewis acidity is caused by the EFAL species in addition to aluminium atoms partly linked (coordinated) but defects in the framework [20,27]. It was found that some type of equilibrium exists between Brönsted and Lewis acid sites, and that this equilibrium is favoured towards Brönsted sites when the density of tetrahedral aluminium is low in the framework or when the zeolite is used at high temperature reactions [28]. It has also been noticed that Lewis acid sites can couple with Brönsted sites and form sites of increased acidity and activity, called superacid sites [29]. However, the EFAL species can reduce the

cracking activity and selectivity of the zeolite by blocking the transfer of bulky molecules and thus enhance the deactivation of the catalyst. This can be resolved by subjecting the zeolite to acid leaching treatments that enable the removal of these EFAL species [16].

2.4.2 Shape-selectivity

The shape-selectivity of zeolites is unique in that crystals with certain pore characteristics are repeated many times in the framework, which results in the high specificity of zeolites to many reactions [3]. When the pore opening of a zeolite is similar to the reactant, the transition state, intermediate, or the product for a certain reaction, shape-selectivity applies and can have different results than when proceeding with the reaction in a homogeneous phase [3,11]. The presence of shape-selectivity in zeolites enhances their activity, selectivity and stability when they are used for specific refining processes [30]. Shape-selectivity can be categorized in three ways [3,30]:

1. Reactant selectivity: This involves the exclusion of reactants of certain size or shape from entering the zeolite structure and reaching the active sites. This is caused by the reactant molecules having a low Gibbs free energy of adsorption onto the zeolite in conjunction with the Gibbs free energy barrier to diffusion through the zeolite structure being low.

2. Product selectivity: Here, the crystal and pore size of the zeolite plays a role in limiting the diffusivity of some molecules and hence its transport out of the zeolite structure. At a molecular level, the Gibbs free energy of adsorption of the product molecules onto the zeolite is high, causing the molecules to desorb, with the Gibbs free energy barrier to diffusion being low, allowing the product molecules to diffuse out of the zeolite structure.

3. Transition-state shape-selectivity: Here, the pore geometry and crystal size of the zeolite forces the transition-state molecules to only form products that can fit inside them and then subsequently leave the crystalline structure.

However, reactions can occur on the outer surface of the zeolite if either the Gibbs free energy of adsorption of reactant molecules onto the zeolite or their Gibbs free energy barrier to diffusion is high, preventing them from entering the zeolite structure.

2.4.3 Zeolite Deactivation

When used in many refining processes, zeolites have been found to deactivate in a number of ways [5,31]:

1. Active site poisoning. This can be caused by impurities in the feed, some component of the feed, or via coke deposition.

2. Pore-mouth blockage, restricting the reactant from entering the zeolite structure. This is also caused by coke deposition, but can also arise from EFAL species.

3. Alterations of the zeolite structure during reaction or regeneration, causing loss of activity.

4. Metal sintering, in the case of bifunctional zeolite catalysts.

2.5 Common Zeolite Types

Three types of zeolite are discussed in this section. These are zeolite Y, Mordenite, and Beta. They are of particular interest due to their catalytic properties during the hydroisomerization of normal alkanes. Given their large pore size structure, they are extensively reported in the litereature for the reaction of high alkanes, since diffusion limitations are low when such large pores are employed in the reaction.

2.5.1 Zeolite Y

This type of zeolite possesses the structure of faujasite. It has a 12 membered-ring structure and a cubic unit cell that is 24.7 Å long. Its three-dimensional structure, large pore diameter (7.4 Å) and low topology density of almost 0.48 solid volume/unit cell volume (0.52 balance is void) makes it attractive in wide catalytic applications [3,30]. The aluminium content in this type of zeolite is high (Si/Al = 2.43) and it is hence highly acidic, which makes it an ideal cracking catalyst [32]. Figure 2-3 shows the typical 3D structure and pore opening of zeolite Y.

Figure 2-3. Pore diameter in Angstroms and a three-dimensional view of zeolite Y framework [33].

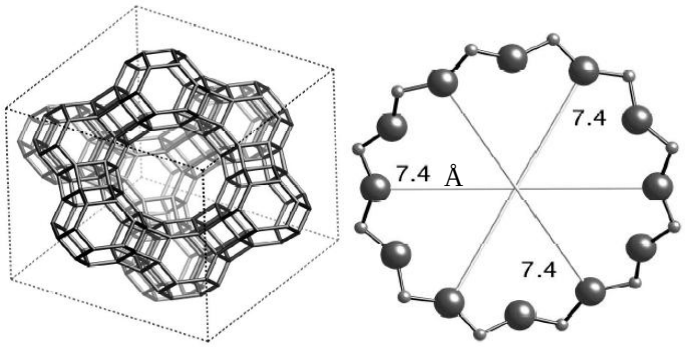

2.5.2 Zeolite Mordenite

The Mordenite structure comprises of units of five rings that are linked together in the form of chains. These chains are inter-connected through oxygen atoms such that they form corrugated sheets. The sheets, in turn, link with one another to make rings having 8 and 12 edges [3]. These 8 and 12-member rings are organized in such a way as to make the access between adjacent channels very limited, leading to the structure being in effect one dimensional [3,34]. Mordenite has rich silica content [34] and a topology density of 0.80 volume/unit cell volume [33]. Commercially, it has a number of applications in the refining industry, such as C_8 aromatics isomerization and C_5-C_6 normal alkane isomerisation [35]. It has been used in such processes because of its strong acid sites. However, since it is effectively a one-dimensional framework, it is prone to fast catalyst deactivation due to pore plugging by coke, although this property makes it have a unique selectivity. In order to reduce the effect of coking, dealumination is often used to increase the number of mesopores in the framework [34]. Figure 2-4 shows the typical structure and pore openings in Mordenite.

Figure 2-4. Pore diameters in Angstroms and a three-dimensional view of zeolite Mordenite framework [33].

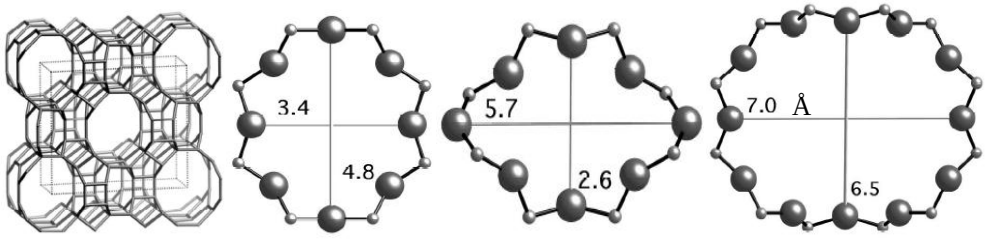

2.5.3 Zeolite Beta

This type of zeolite possesses a 3-dimensional structure with 12-ring inter-connected channels, large pore openings [3,20,36-38] and a topology density of 0.70 volume/unit cell volume [33]. Inside the structure of zeolite Beta, there is always a huge disorder in the way different layers are connected [3], causing a difficulty in providing its

framework description. This is probably why it took a long time for it to have industrial applications [38] although it was initially synthesized in 1967 [37,38]. However, it was found later that it had three different crystalline phases: one tetragonal and two monoclinic [37]. It has a high Si/Al ratio ranging between 10 and more than 100 [20,34] and a small crystal size (20-50 nm), which makes it ideal in many reactions involving the synthesis of bulky or polar molecules, since no diffusion limitations are encountered and hence the reactions are fast [20,27]. Examples of commercial application for zeolite Beta are hydrotreating [38], petrochemical cracking and fine organic catalysis [10], such as the alkylation of isobutane and isobutene, benzene alkylation with propane to produce cumene, and selectively synthesizing many other organic compounds [20,27,38]. Figure 2-5 shows the typical 3D structure and pore openings for zeolite Beta.

Figure 2-5. Pore diameters in Angstroms and a three-dimensional view of zeolite Beta framework [33].

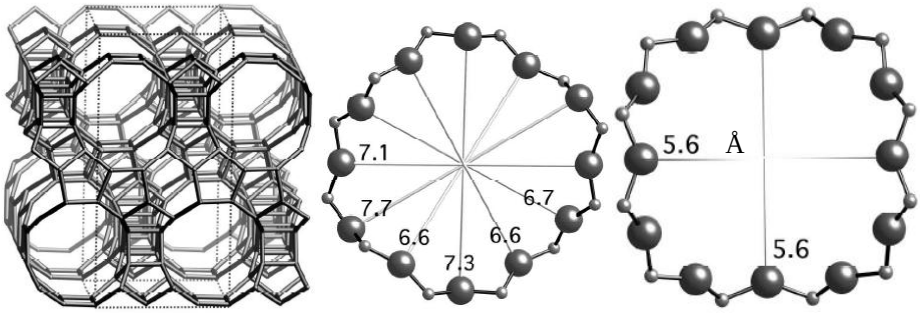

2.6 Conclusion

Zeolites have seen their industrial use expand considerably ever since it was possible to synthesize them due to their unique shape-selective properties. They can be synthesized into various structures with distinct topologies. Their hydrothermal synthesis is positively influenced by temperature, OH^- concentration, and the presence of a structure-directing agent. There are common methods to modify zeolite structures for the purpose of better catalytic use, including steaming, acid-leaching, and metal-loading. These modifications have an effect on catalytic properties and can alter the type and concentration of acid sites as well as the shape-selectivity in zeolites. Of special interest among zeolites are zeolite Y, Beta, and Mordenite. Their large pore systems and strong acidities caused them to be the most commonly used zeolites in alkane hydroisomerization research, which is discussed in depth in the next chapter.

2.7 References

[1] Barrer, R. M. (1978). *Zeolites and Clay Minerals as Sorbents and Molecular Sieves.* London; New York: Academic Press, Inc. p. 1, 4-5.

[2] Barrer, R. M. (1982). *Hydrothermal Chemistry of Zeolites*. London; New York: Academic Press, Inc.

[3] Bekkum, H. V; Flanigen, E. M; Jacobs, P. A. and Jansen, J. C. (2001). *Introduction to Zeolite Science and Practice*. 2nd Edition. Amsterdam: Elsevier. p. 1-2, 5, 7, 11-20, 39-42, 48-51, 56, 263-264.

[4] Frillette, V. J; Haag, W. O. and Lago, R. M. (1981). Catalysis by Crystalline Aluminosilicates: Characterization of Intermediate Pore-Size Zeolites by the "Constraint Index". *Journal of Catalysis*, 67, 218-222.

[5] Guisnet, M; Costa, L. and Ribeiro, F. R. (2009). Prevention of Zeolite Deactivation by Coking. *Journal of Molecular Catalysis A: Chemical*, 305, 69-83.

[6] Batonneau-gener, I; Yonli, A; Hazael-pascal, S; Marques, J. P; Lopes, J. M; Guisnet, M; Ribeiro, F. R. and Mignard, S. (2008). Influence of Steaming and Acid-leaching Treatments on the Hydrophobicity of HBEA Zeolite Determined under Static Conditions. *Microporous and Mesoporous Materials*, 110, 480-487.

[7] Gauw, Franciscus J. M. M. de. (2002). *Kinetic Studies of Alkane Hydroisomerization over Solid Acid Catalysts*. PhD Thesis, Eindhoven University of Technology, Eindhoven.

[8] Barrer, R. M. (1981). Zeolites and their Synthesis. *Zeolites*, 1, 130-140.

[9] Meier, W. M. (1968). *Molecular Sieves*. London: Society for Chemical Industry. P. 20-22.

[10] Jansen, J. C; Stöcker, M; Karge, H. G. and Weitkamp, J. (1994) *Advanced Zeolite Science and Applications*. Amsterdam: Elsevier.

[11] Weitkamp, J. and Puppe, L. (1999). *Catalysis and Zeolites*. Berlin: Springer.

[12] Roldán R; Romero, F. J; Jiménez-Sanchidrián, C; Marinas, J. M. and Gómez, J. P. (2005). Influence of Acidity and Pore Geometry on the Product Distribution in the Hydroisomerization of Light Paraffins on Zeolites. *Applied Catalysis*, 288, 104-115.

[13] Wang, Q. L; Torrealba, M; Giannetto, G; Guisnet, M; Perot, G; Cahoreau, M. and Caisso, J. (1990). Dealumination of Y Zeolite with Ammonium Hexafluorosilicate: A SIM-XPS Study of the Aluminium Distribution. *Zeolites*, 10, 703-706.

[14] Wang, Q. L; Giannetto, G; Torreaaba, M; Perot, G; Kappenstein, C. and Guisnet, M. (1991). Dealumination of Zeolites: II. Kinetic Study of the Dealumination by Hydrothermal Treatment of a NH4NaY Zeolite. *Journal of Catalysis*, 130, 459-470.

[15] Panov, A. G; Gruver, V. and Fripiat, J. J. (1997). Fluorination of USY and Modification of Its Catalytic Properties. *Journal of Catalysis*, 168, 321-327.

[16] Wang, Q. L; Giannetto, G. and Guisnet, M. (1991). Dealumination of Zeolites: III. Effect of Extra-Framework Aluminum Species on the Activity, Selectivity, and Stability of Y Zeolites in *n*-Heptane Cracking. *Journal of Catalysis*, 130, 471-482.

[17] Remy, M. J; Stanica, D; Poncelet, G; Feijen, E. J. P; Grobet, P. J; Martens, J. A. and Jacobs, P. A. (1996). Dealuminated H-Y Zeolites: Relation between Physicochemical Properties and Catalytic Activity in Heptane and Decane Isomerization. *Journal of Physical Chemistry*, 100, 12440-12447.

[18] Hoets, J; Mesoporous Materials Web Page [Website]. Available from: <http://www.chm.bris.ac.uk/webprojects2001/hoets/mesoporouswebpagehome.htm > [Accessed: 9 September 2007].

[19] Guisnet, M. and Fouche V. (1991). Isomerization of *n*-Hexane on Platinum Dealuminated Mordenite Catalysts: III. Influence of Hydrocarbon Impurities. *Applied Catalysis*, 71, 307-317.

[20] Simon-Masseron, A; Marques, J. P; Lopes, J. M; Ribeiro, F. R; Gener, I. and Guisnet, M. (2007). Influence of the Si/Al Ratio and Crystal Size on the Acidity and Activity of HBEA Zeolites. *Applied Catalysis*, 316, 75-82.

[21] Roussel, M; Lemberton, J; Guisnet, M; Cseri, T. and Benazzi, E. (2003). Mechanisms of *n*-decane Hydrocracking on a Sulfided NiW on Silica-alumina Catalyst. *Journal of Catalysis*, 218, 427-437.

[22] Guerin, M; Kappenstein, C; Alvarez, F; Giannetto, G. and Guisnet, M. (1988). Preparation of PtHY Catalysts: Influence on the Catalytic Properties of the Complexes Used as Platinum Precursors. *Applied Catalysis*, 45, 325-333.

[23] Chao, K; Lin, C; Lin, C; Wu, H; Tseng, C. and Chen, S. (2002). *n*-Heptane Hydroconversion on Platinum-loaded Mordenite and Beta Zeolites: the Effect of Reaction Pressure. *Applied Catalysis A: General*, 203, 211-220.

[24] Perot, G. and Guisnet, M. (1990). Advantages and Disadvantages of Zeolites as Catalysts in Organic Chemistry. *Journal of Molecular Catalysis*, 61, 173-196.

[25] Ward, John W. (1993). Hydrocracking Processes and Catalysts. *Fuel Processing Technology*, 35, 55-85.

[26] Akhmedov, V. M. and Al-Khowaiter, S. H. (2007). Recent Advances and Future Aspects in the Selective Isomerization of High *n*-Alkanes. *Catalysis Reviews*, 49, 33-139.

[27] Marques, J. P; Gener, I; Ayrault, P; Bordado, J. C; Lopes, J. M; Ribeiro, F. R. and Guisnet, M. (2003). Infrared Spectroscopic Study of the Acid Properties of Dealuminated BEA Zeolites. *Microporous and Mesoporous Materials*, 60, 251-262.

[28] Burckle, E. C. (2000). *Comparison of One-, Two-, and Three- Dimensional Zeolites for the Alkylation of Isobutane with 2-Butene.* Masters' Thesis, University of Cincinnati, Cincinnati, Ohio.

[29] Bourdillon, G. and Gueguen, C. (1990). Characterization of Acid Catalysts by Means of Model Reactions: I. Acid Strength Necessary for the Catalysis of Various Hydrocarbon Reactions. *Applied Catalysis*, 61, 123-139.

[30] Maesen, T. L. M.; Calero, S; Schenk, M. and Smit, B. (2004). Alkane Hydrocracking: Shape Selectivity or Kinetics? *Journal of Catalysis*, 221, 241-251.

[31] Guisnet, M. and Magnoux, P. (1997). Deactivation by Coking of Zeolite Catalysts. Prevention of Deactivation. Optimal Conditions for Regeneration. *Catalysis Today*, 36, 477-483.

[32] Price, G. L; TU Chemical Engineering Zeolite Page [Website]. Available from: <www.personal.utulsa.edu/~geoffrey-price/zeolite/fau.htm> [Accessed: 17 July 2007].

[33] Baerlocher, Ch; Meier, W. M. and Olson, D. H. (2001). *Atlas of Zeolite Framework Types*. 5th Edition. Amsterdam: Elsevier.

[34] Tran, M. T; Gnep, N. S; Szabo, G. and Guisnet, M. (1998). Comparative Study of the Transformation of *n*-Butane, *n*-Hexane and *n*-Heptane over H-MOR Zeolites with Various Si/Al Ratios. *Applied Catalysis*, 170, 49-58.

[35] Guisnet, M. and Fouche V. (1991). Isomerization of *n*-Hexane on Platinum Dealuminated Mordenite Catalysts: I. Influence of the Silicon-to-aluminium Ratio of the Zeolite. *Applied Catalysis*, 71, 283-293.

[36] Chen, S; Yang, Y; Zhang, K. and Wang, J. (2006). Beta Zeolite Made from Mesoporous Material and its Hydrocracking Performance. *Catalysis Today*, 116, 2-5.

[37] Pérez-Pariente, J; Sanz, J; Fornés V. and Corma, A. (1990). ^{29}Si and ^{27}Al MAS NMR Study of Zeolite Beta with Different Si/Al Ratios. *Journal of Catalysis*, 124, 217-223.

[38] Wang, Z. B; Kamo, A; Yoneda, T; Komatsu, T. and Yashima, T. (1997). Isomerization of *n*-Heptane Over Pt-loaded Zeolite Beta Catalysts. *Applied Catalysis*, 159, 119-132.

CHAPTER THREE

LITERATURE REVIEW: PART 2:

PARAFFINS HYDROISOMERIZATION

3.1 Introduction

The isomerization process is typically used to upgrade the quality of the refinery naphtha stream in order to boost the research octane number (RON). In this process, normal paraffins that exist in the feed stream (typically light naphtha) are converted into their isomers, which have higher octane numbers than the normal paraffins [1]. This process is industrially favoured since the use of isoparaffinic products in the gasoline pool limits the addition of aromatics and oxygenates, which have maxima in terms of their allowed contents in gasoline due to environmental regulations [2,3]. An example of the stark contrast between the RON of an isoparaffin and that of its linear counterpart is demonstrated with iC_7, which has an octane number of 45, as opposed to nC_7, whose octane number is 0 [4].

Typically, hydroisomerization reactions require the presence of bifunctional catalysts. A bifunctional catalyst possesses both a hydrogenation/dehydrogenation function, usually provided by a noble metal, such as platinum; and a cracking function, provided by an acid site. From the thermodynamics of isomerization, the formation of isoparaffins is favoured at lower reaction temperatures and hence catalysts operating at low temperatures would typically be more selective to isomers than those that operate at high temperatures [5,6]. The thermodynamic distribution of C_7 isomers at different temperatures is shown in Figure 3-1 as an example.

Originally, platinum-loaded chlorinated alumina catalysts have been used at commercial isomerization units due to their high acidity and the low reaction temperature required, which is around 180 ^{o}C [5-7]. However, this type of catalyst has a number of drawbacks that limited its use. The presence of chlorine required in catalyst regeneration results in many corrosion and environmental problems [2,4]. In addition, this catalyst is prone to fast deactivation and requires a cautious feed pre-treatment due to its sensitivity to water and sulfur [6-9]. Zeolites, on the other hand, do not have these drawbacks and are

both stable and highly resistant to impurities, which make them ideal for use in hydroisomerization reactions [7]. For example, platinum-loaded Mordenite has been used commercially by Shell (Shell Hysomer Process) to hydroisomerize the C_5/C_6 stream of naphtha into a product rich in higher octane isomers with an overall octane of about 80. The octane number can even be further boosted to about 90 by combining a separation process (Isosiv Process of UOP) that involves recycling the normal alkanes from the product stream into the reactor [8]. In this process, Mordenite has shown to be stable in the presence of reasonable quantities of water and sulfur in the feed [10].

Figure 3-1. Thermodynamic distribution of C_7 isomers at different reaction temperatures and 1 atmosphere (modified from [6]).

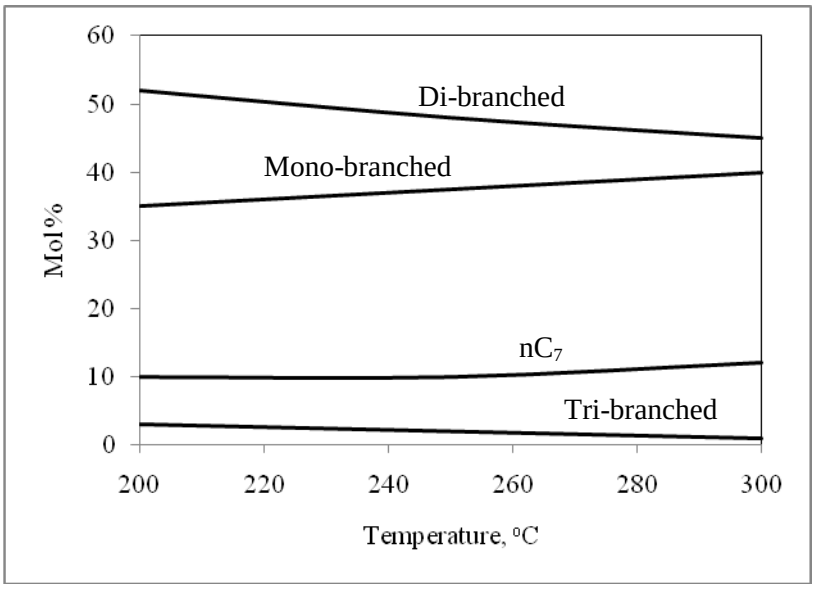

3.2 Normal Alkanes Reaction Mechanism

The hydroisomerization of normal alkanes over bifunctional catalysts proceeds normally through the monomolecular mechanism. In this mechanism, the dehydrogenation of the alkane molecule into its alkene takes place on the noble metal site of the catalyst. The alkenes then migrate from the metal site to an acidic site. This is followed by a protonation of the resulting alkene on the Brönsted acid site, transforming the alkene to an alkylcarbenium ion intermediate. After that, the formed alkylcarbenium ion undergoes either a structural rearrangement, followed by migration to and hydrogenation on a metal site to produce a structural isomer of the starting alkane, or a β-scission followed by hydrogenation on a metal site to produce cracked products [2,7,8,11-17]. However, this reaction mechanism requires that a proper balance exists between the catalyst acid and

metal functions in terms of the number of present Brönsted and metal sites [13,18]. If this balance, though, does not exist in the catalyst, this can lead to unwanted side reactions such as hydrogenolysis, which can take place on the metal sites and dimerization-cracking, which can occur on the acid sites [13]. The dimerization-cracking mechanism, which occurs when there is no good balance between acid and metal functions, proceeds via cracking of a long chain intermediate that forms by the dimerization of two alkylcarbenium ions [19]. Figure 3-2 provides a demonstration of the possible reaction pathways over a bifunctional catalyst with normal hexane as the reactant following the monomolecular reaction mechanism and Figure 3-3 shows the difference between the monomolecular and bimolecular mechanisms during the hydroisomerization of normal heptane.

Figure 3-2. Possible reaction pathways for the hydroisomerization of n-hexane over a bifunctional catalyst according to the classical unimolecular mechanism. 1 and 2 indicate two possible successive isomerization reactions, while 3 is a possible cracking reaction [2].

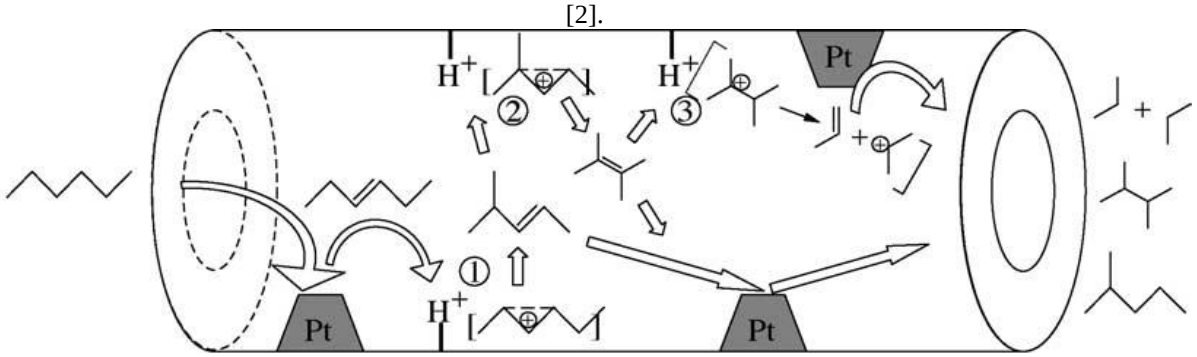

Figure 3-3. Monomolecular reaction mechanism against the bimolecular mechanism for the hydroisomerization of normal heptane (adapted from [19]).

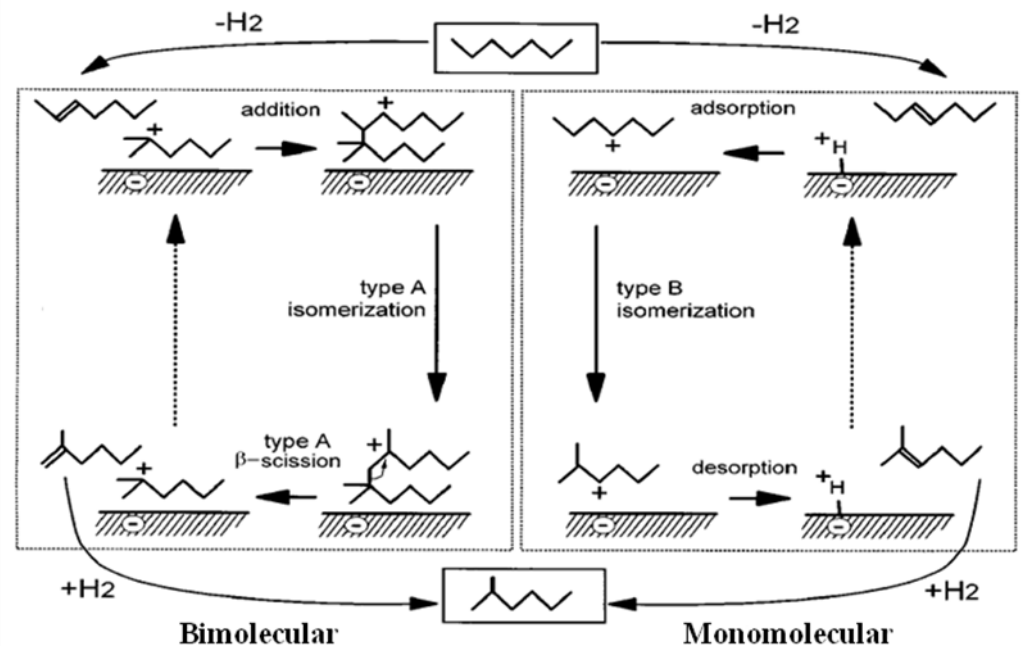

3.3 Zeolite Activity

The performance of zeolites during the hydroisomerization of paraffins depends on many factors that affect their activity, selectivity, and stability. These factors include alkane chain length, reaction temperature, reaction pressure, contact time, zeolite geometry, zeolite acidity, acid-metal balance, de-alumination, the presence of sulfur or other impurities in the feed, and the presence of coke in the catalyst. These factors are discussed in detail in the following sub-sections.

3.3.1 Effect of Alkane Chain Length

Weitkamp [11] has studied the effect of alkane chain length on the hydrocracking/hydroisomerization activity of zeolite. The experiments were performed on platinum-loaded zeolite Y in its calcium form and at a pressure of 39 bar. Normal alkanes with 6 to 12 carbon atoms were tested for reactivity. It was found that increasing the chain length results in an increase in the total conversion of the reactant, as shown in Figure 3-4. However, increasing the chain length decreases the hydroisomerization conversion versus that of cracking, as shown in Figure 3-5, which is due to the increasing tendency for cracking at longer chains. This increasing tendency to crack is, in turn, due to increasing reactivity of normal alkanes on zeolites as the chain length increases, caused by a lower Gibbs free energy of adsorption and higher Henry constants for longer alkanes, making them adsorb easily on the catalyst surface for longer times, raising the probability of cracking [20-23]. With regards to the product distribution, it was found that increasing the alkane chain length results in a considerably higher selectivity towards multi-branched isomers, which could be explained by the increase in the number of possible isomers at higher alkane chain lengths.

3.3.2 Effect of Reaction Temperature

Temperature has a big influence on the conversion of normal alkanes. Generally, an increase in temperature results in an increase in the total conversion (both hydrocracking and hydroisomerization) [4-6,24-28]. However, the hydroisomerization conversion of a normal alkane increases with temperature, peaks at a certain point, and then starts dropping until it vanishes completely as cracking becomes the predominant reaction. This can be clearly inferred from Figure 3-4. In addition, the selectivity towards hydroisomerization decreases with increasing temperature [4,29,30], and this phenomenon becomes more

pronounced as the feed alkane chain length increases [6]. This decrease in overall isomers selectivity is however opposed by an increase in the selectivity to multi-branched isomers [25].

Figure 3-4. Effect of increasing alkane chain length on the hydroisomerization conversion at different reaction temperatures (adapted from [11]).

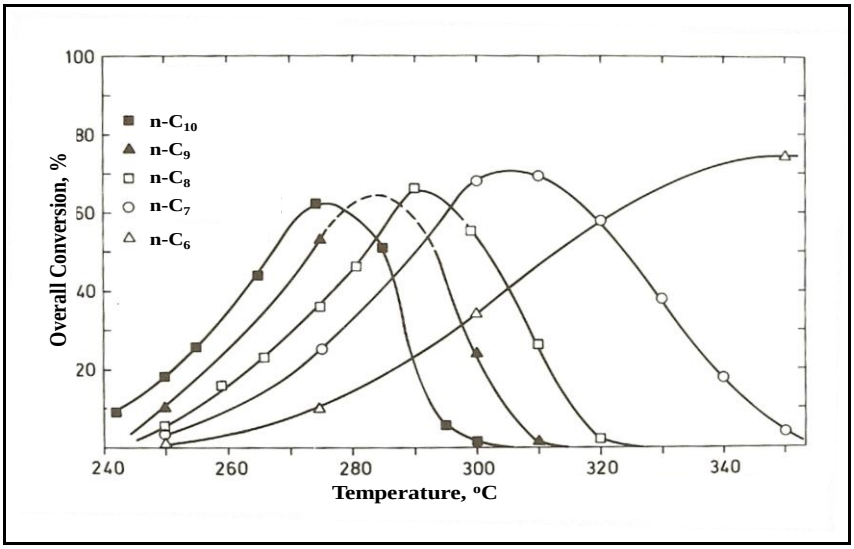

Figure 3-5. Effect of increasing alkane chain length on the hydrocracking conversion at different reaction temperatures (adapted from [11]).

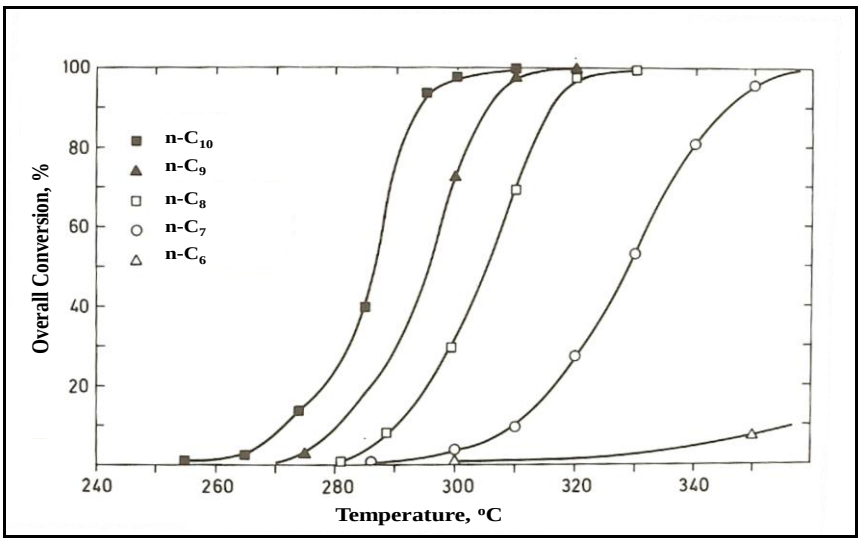

3.3.3 Effect of Reaction Pressure

Wang et al [24] have studied the effect of increasing the hydrogen partial pressure, and therefore the overall reaction pressure, on the hydroisomerization of normal heptane over platinum-loaded zeolite Beta. They have found that increasing the pressure results in a

decreased overall conversion and an increased selectivity to isomers, with the selectivity to multi-branched isomers being reduced. Similar findings were reported by Chao et al [31] when they tested the effect of varying the reaction pressure over the range 1 – 41.3 bar on zeolite Mordenite catalysts of different Si/Al ratios and zeolite Beta, with the addition that pressure reduced the cracking yield with all catalysts as well as improved the Mordenite catalyst stability. In addition, the increase of hydrogen pressure has been found to reduce the hydroisomerization reaction rate [32]. Clearly, the increase in reaction pressure has the exact contrary effect to that of reaction temperature, as seen in the previous section. A possible explanation of this pressure effect is an increase in the hydrogenation activity at a higher hydrogen pressure that results in the hydrogenation of more intermediate olefins, which can be due to a shorter intermediate olefin residence time inside the catalyst [33], and thus minimizing the cracking activity.

3.3.4 Effect of Contact Time

The variation of contact time, which represents the time reactants spend in order to pass through the catalyst bed during a reaction, has a similar effect to that of reaction temperature, as noticed by Wang et al [24]. They found that increasing the contact time results in an increased overall conversion of n-heptane at the constant temperature of 220^{o}C, and in a reduced selectivity to hydroisomerization versus cracking. A similar observation was found by Chica and Corma [6] when they tested the hydroisomerization of nC_5, nC_6 and nC_7 over platinum-loaded different zeolite supports. However, the decrease in selectivity to isomers was opposed by an increase in the overall yield of isomers at short contact times. It was also shown that with increasing contact times, the formation of multi-branched isomers increases, leading to a lower mono/multi-branched isomers ratio. This behaviour could be due to an initial formation of mono-branched isomers and their subsequent transformation into multi-branched isomers. Figure 3-6 shows the effect of contact time (W/F_o) on the conversion, selectivity and isomers yield for the hydroisomerization of n-heptane on platinum-loaded Beta catalyst at 220^{o}C [24].

Figure 3-6. Effect of contact time on the conversion, selectivity and isomers yield for the hydroisomerization of n-Heptane on platinum-loaded β catalyst at 220°C (adapted from [24]).

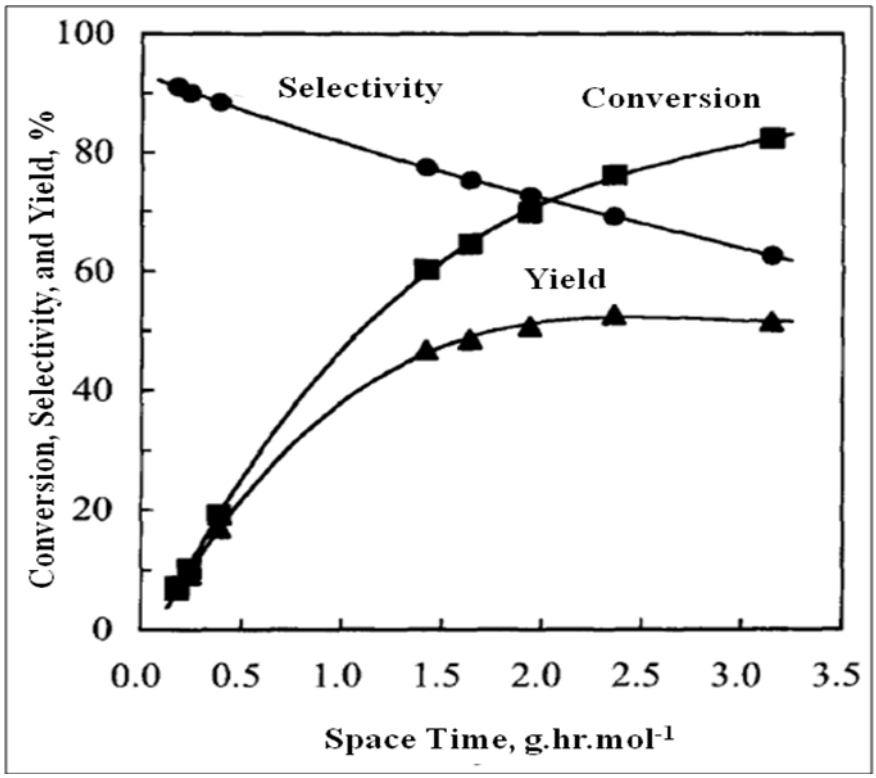

3.3.5 Effect of Time-on-stream

Time-on-stream is a measure of the stability of the zeolitic catalysts during reaction and how well the catalyst will maintain its original activity. This is dependent on the type of zeolite under investigation. For example, zeolite Beta has proven to be very stable with almost no change in activity when tested for almost 80 hours with normal heptane at 220°C [24]. On the contrary, Mordenite deactivates very quickly after considerably shorter times [32-36] due to coking [35]. However, the stability of Mordenite can be improved to a high extent upon de-alumination to Si/Al molar ratios above 60. Unfortunately, this improved stability is in the expense of hydroisomerization activity [29,32,33].

3.3.6 Effect of Zeolite Structure

Each zeolite type has its unique shape-selective properties that affect its performance during a catalytic reaction, as explained in the previous chapter. These properties, in turn, have an important role during the hydroisomerization of paraffins. For instance, zeolite Mordenite tends to produce more multi-branched isomers and cracking products than mono-branched isomers when compared with zeolite Y. This can be attributed to their effectively one-dimensional pore system and high acid sites density that

result in a rapid coking, and hence impose a diffusion limitation on formed olefins, which causes them to undergo further isomerization or cracking before reaching other hydrogenation sites [24,25,36,37]. Another possible explanation is that the strength of Mordenite acid sites, combined with its narrow pore structure, result in slow desorption of intermediate olefins, which increases the tendency to form cracking products [36]. Similarly, the yield of isomers over both ultra-stable zeolite Y and Beta, which possess 3-dimensional pore structures, was found to be considerably higher than that obtained over Mordenite, obviously for the same reason [24,37]. In order to further demonstrate the effect of zeolite structure and geometry on its performance, results of a study by Gopal [38] are presented. He studied the hydroisomerization of normal heptane over different zeolites of similar Si/Al ratios loaded with 0.5 wt% Pt at varying temperatures and at a pressure of 7.9 bar. Figure 3-7 shows the reported results for normal heptane conversion as a function of temperature over platinum-loaded zeolite ZSM-5, Beta, Mordenite, ZSM-12, and USY.

Figure 3-7. Heptane conversion as a function of temperature over different zeolites (adapted from [38]).

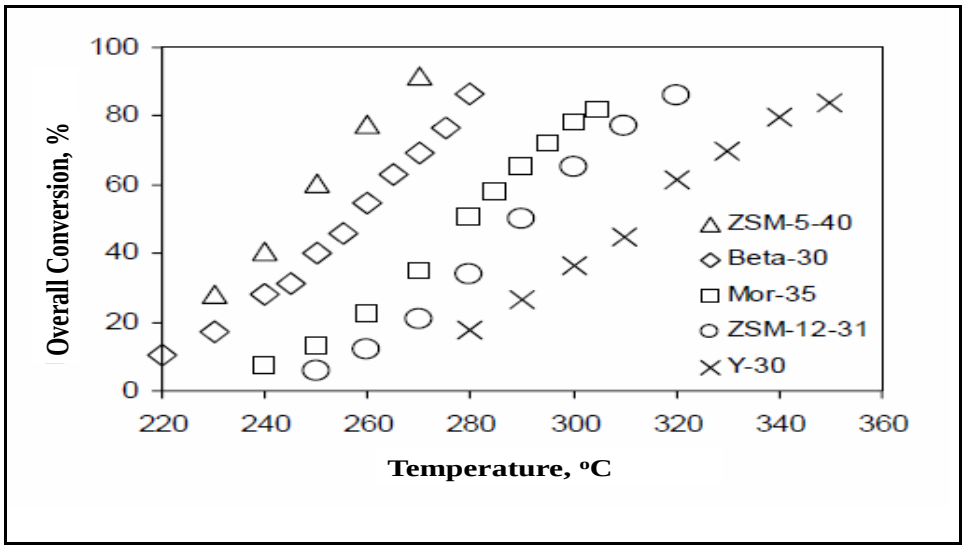

From Figure 3-7, there are big differences in zeolite activity when changing the type of zeolite, as apparent from the different temperatures required to achieve similar conversions of normal heptane, even though the Si/Al ratio for all catalysts tested ranges from 30 to 40. Shape selectivity plays a major role in contributing to this finding. Other studies have also demonstrated the difference zeolite structure makes on this reaction [39]. For example, Patrigeon et al [41] and Raybaud, Patrigeon, and Toulhoat [42] have proven that porosity of the zeolite plays a major role in influencing the selectivity of the catalyst to

multibranched isomers during the hydroisomerization of normal heptane. Patrigeon et al tested 1 wt% Pt-loaded zeolite Y and Beta, which have 3D pore structures, silica-alumina and pillared clay, which are mesoporous materials, and zeolite EU-1 and ZSM-22, which have one-dimensional structures at temperatures in the range 190 to 320^{o}C and atmospheric pressure.

Table 3-1. Kinetic diameter, boiling point and RON of heptane isomers [40].

Component	**Kinetic diameter, nm**	**Boiling point, ^{o}C**	**RON**
n-Heptane (nC7)	0.43	98.5	0.0
2-Methylhexane (2-MHx)	0.5	90.0	42.2
3-Methylhexane (3-MHx)	0.5	92.0	52.0
3-Ethylpentane (3-EP)	0.5	93.5	65.0
2,3-Dimethylpentane (2,3-DMP)	0.56	89.7	91.1
2,4-Dimethylpentane (2,4-DMP)	0.56	80.4	83.1
2,2-Dimethylpentane (2,2-DMP)	0.62	79.2	92.8
3,3-Dimethylpentane (3,3-DMP)	0.62	86.0	80.8
2,2,3-Trimethylbutane (2,2,3-TMB)	0.62	80.8	109.0

It was noticed that the ratio of 2-methylhexane to 3-methylhexane and that of 2,3-dimethylpentane plus 2,4-dimethylpentane to 2,2-dimethylpentane plus 3,3-dimethylpentane plus 2,2,3-trimethylbutane, designated by R, are almost constant at low numbers with various conversion levels for zeolite Y and Beta catalysts and pillared clay, whereas these ratios are larger for zeolite EU-1 and ZSM-22, with the difference between the two groups increasing at lower conversion levels as can be seen from Figures 3-8 and 3-9.

Figure 3-8. 2-MC_6/3-MC_6 ratio as a function of normal heptane conversion for different porous materials (adapted from [41]).

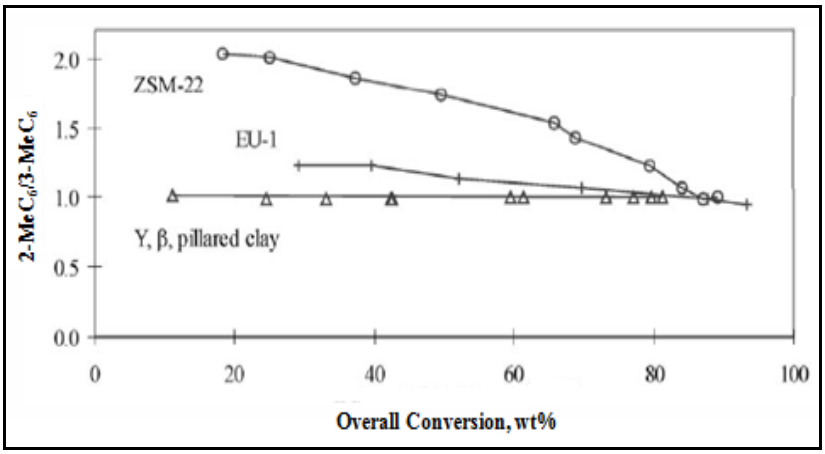

Figure 3-9. R ratio as a function of normal heptane conversion for different porous materials (adapted from [41]).

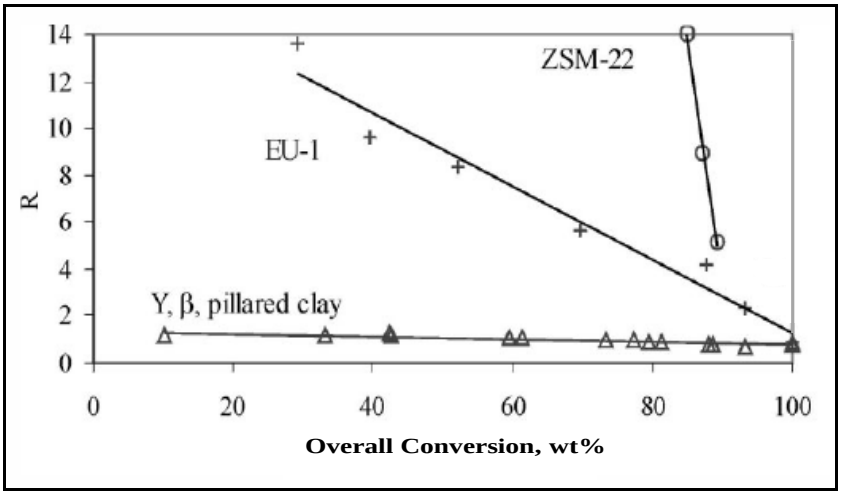

The observation from Figures 3-8 and 3-9 led to the conclusion that the more restricted structures of zeolite EU-1 and ZSM-22 and their lower porosities resulted in more bulky molecules (see Table 3-1) being either unable to form or to crack, resulting in more cracking and less isomer yield.

From another point of view, the zeolite crystal size has a pronounced effect on its selectivity for isomers. Chica and Corma [6] found that zeolite Beta with a nano-crystalline structure is more stable against coking and achieves a lower cracking yield when compared with the commercial zeolite Beta. This observation is explained by the shorter times it takes reactants and products to diffuse into and out of the smaller crystals in the structure, resulting in less cracking.

3.3.7 Effect of Acidity

The acidity of a given zeolite support is mainly dependent on the Si/Al ratio, which influences the Brönsted acidity as discussed in chapter 2. During the hydroisomerization of normal alkanes, a lower Si/Al ratio, therefore higher acidity resulting from a higher number and strength of acid sites, of a zeolite catalyst is found to increase conversion at fixed reaction conditions, having a similar effect to raising temperature [43]. The same observation is found with the selectivity to isomerization versus cracking and the selectivity to multi-branched versus mono-branched isomers, the former being decreased with increasing acidity and the latter increased with increasing acidity. However, Mordenite is exempt from this behaviour because of the very fast deactivation its highly acidic form undergoes, which decreases conversion and leads to an opposite effect on selectivity [2,4,6]. Figure 3-10 gives an illustration of the loss in activity of zeolite Mordenite at high acid site densities during the hydroisomerization of n-hexane [33].

Figure 3-10. The isomerization activity (A_o, 10^{-3} mol.g^{-1}.h^{-1}) as a function of the reciprocal to Si/Al ratio for n-hexane hydroisomerization over Mordenite at 250^oC and 30 bar (modified from [33]).

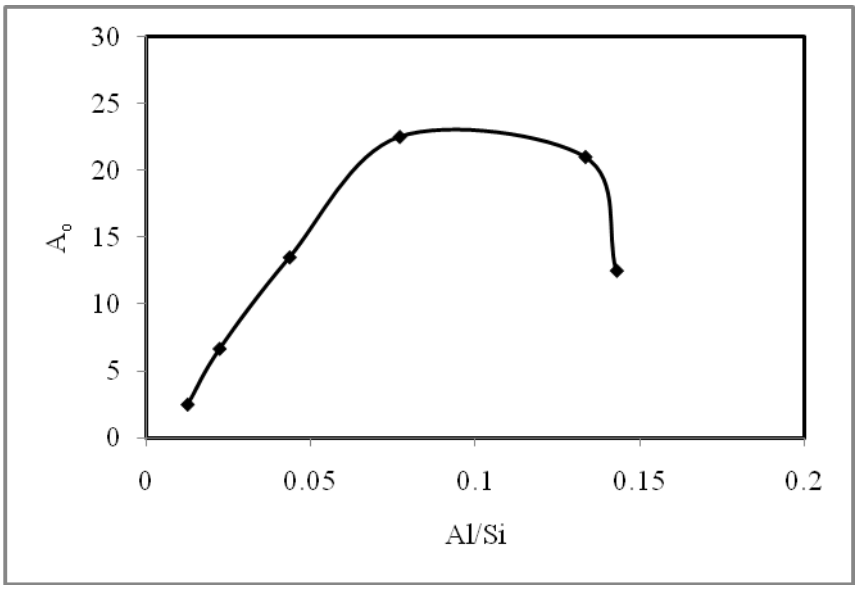

The high selectivity towards isomers at lower acidities (higher Si/Al ratios) is believed to be due to the lower chance that the reaction intermediate olefins meet consecutive acidic sites to either further isomerize them (to obtain multi-branched isomers) or to crack them into cracking products before being hydrogenated on platinum atoms [24]. This less cracking activity results in the zeolite having a higher stability against deactivation by coking, which is not the case for zeolites with low Si/Al ratios [36,44].

The noticed similarity between temperature and acidity in their influence on reaction selectivity is due to the fact that selectivity is only a function of the conversion level achieved and the catalyst pore geometry, which causes factors that alter conversion in a certain manner to change selectivities accordingly [2,13].

3.3.8 Effect of Acid-metal Balance

The acid-metal balance in a zeolitic catalyst has a strong impact on the extent of hydroisomerization versus cracking, i.e. the selectivity to isomers versus cracked products. This balance is expressed by the ratio of metallic sites to acidic sites in a given bifunctional catalyst, or by the percentage of metal (commonly platinum) loading on the catalyst [45-47].

Out of the many metals incorporated into zeolites and tested for the hydroisomerization of alkanes in the literature (Pt, Pd, Re, Ir, Ni, Co, Zn, Rh, Ru, and Fe), platinum produced the best results. Even though it has been argued that the reason for platinum's superior performance is its efficiency in hydrogen transfer, a possible explanation of its superiority could be the positive influence that platinum has on the acidity of the zeolite [43,48], in addition to it having the highest capacity for hydrogenation [49].

The platinum content in zeolite has been found to increase the selectivity to isomers as well as the total isomers yield during the hydroisomerization of normal heptane over a bifunctional Beta catalyst. However, the conversion was found to slightly drop as the platinum content increased. The enhanced selectivity to isomers could be due to the stronger hydrogenating function at higher platinum contents, which leads to the intermediate olefins being rapidly transformed into isomers before they see enough acidic sites on which they can crack [24]. Similar observations were found by Guisnet et al [36] when they studied the effect of changing the ratio of accessible platinum sites (n_{Pt}) to acidic sites (n_A), expressed by n_{Pt}/n_A on the hydroisomerization of normal heptane over zeolite Y. In addition, they found that the ratio of mono-branched to multi-branched isomers of C_7 increases as the ratio n_{Pt}/n_A increases, which is also the case for the ratio of isomers to cracked products yield, expressed by Isom/Crack or I/C. However, they surprisingly found that at higher densities of platinum ($n_{Pt}/n_A > 0.3$) the ratio I/C drops to

lower values, generating more cracked products. This means that at some point during increasing platinum site density, the number of available platinum sites causes the hydrogenolysis reaction (breaking the carbon-carbon single bond by the addition of hydrogen to both carbon atoms [50,51]) to occur, resulting in more cracked products on the expense of isomerized ones. Guisnet et al found that for values of n_{Pt}/n_A lower than 0.17 heptane transforms into its mono, multibranched isomers, and cracked products simultaneously, whereas at values higher than 0.17 for this ratio it forms those types of products in a successive manner, indicating an ideal bifunctional behaviour. This means that an optimum ratio for hydroisomerization of normal alkanes would be between 0.17 and 0.3. A later study by Alvarez et al [52] using the same catalysts but with normal decane as the reactant also found that optimum performance occurs at n_{Pt}/n_A values above 0.17.

Given that platinum content has a substantial impact on the activity of zeolite during alkanes hydroisomerization, Guerin et al studied whether the type of precursor used as a source for platinum loaded on zeolite Y has any effect by employing $[Pt(NH_3)_4]Cl_2 . H_2O$, $[Pt(NH_3)_2](H_2O)_2]^{2+}$, and $[Pt(H_2O)_4]^{2+}$ as platinum precursors. The results suggested that changing the source of platinum does not affect the activity of the zeolite, even though it influences the degree of dispersion of platinum in the catalyst [53].

3.3.9 Effect of Bimetal Loading

Loading another metal along with platinum over zeolites results in a bi-metallic catalyst that has a different performance during the hydroisomerization of normal alkanes. Blomsma et al [12] have studied the effect of Pd with Pt in bi-metallic zeolites Beta and USY during the hydroisomerization of normal C_7. They noticed that palladium positively influences the total heptane isomers yield and increases the yield of multi-branched isomers (i.e. increase in the octane number). In addition, they found that increasing palladium content decreases the contribution of hydrogenolysis in the formation of cracking products, until hydrogenolysis completely disappears at a palladium loading of 0.5 wt% with either 0.5 or 1.0 wt% platinum. Also, Liu et al [54] have found that adding Pd to Pt-loaded zeolite Beta reduces the aromatics yield above 250^oC. Furthermore, it was found that increasing palladium content results in a better acid/metal balance, which could

be observed through a decrease in the dimerization cracking usually caused by imbalanced acidic and metallic functions [12].

Pope et al [43] have investigated the effect of loading both 1% Ni with 0.5% Pt and 1% Zn with 0.5% Pt for the reaction of normal heptane over zeolite Y at 250^{o}C and 34.5 bar in an autoclave reactor. They have found that a 1% loading of any of Ni or Zn resulted in a better activity and selectivity relative to a sample with only 0.5% Pt. In addition, increasing the Ni loading to 3% caused the catalyst selectivity to drop. However, when the same formulations of Ni or Zn (1%) were used with 1% Pt, no improvement was found over a sample with only 1% Pt. This suggests that loading Ni or Zn is of benefit when using low Pt loadings. A recent study by Barsi and Cardoso [55] of the effect of varying the metal contents of both Pt and Ni in Zeolite USY with a framework Si/Al ratio of 4.6 during the hydroisomerization of normal hexane at 250^{o}C and atmospheric pressure has shown that a molar ratio of 1:1 Pt to Ni loading provides the best activity and stability for the catalyst. Figure 3-11 shows the performance they have reported of the catalysts with varying Pt-Ni loadings during deactivation tests, with the total metal loading being 180 μmol per gram of catalyst.

Figure 3-11. The isomerization activity (10^{-3} mol.g^{-1}.h^{-1}) as a function of time-on-stream (min) for n-Hexane hydroisomerization over Zeolite USY loaded with varying Pt-Ni levels (modified from [55]).

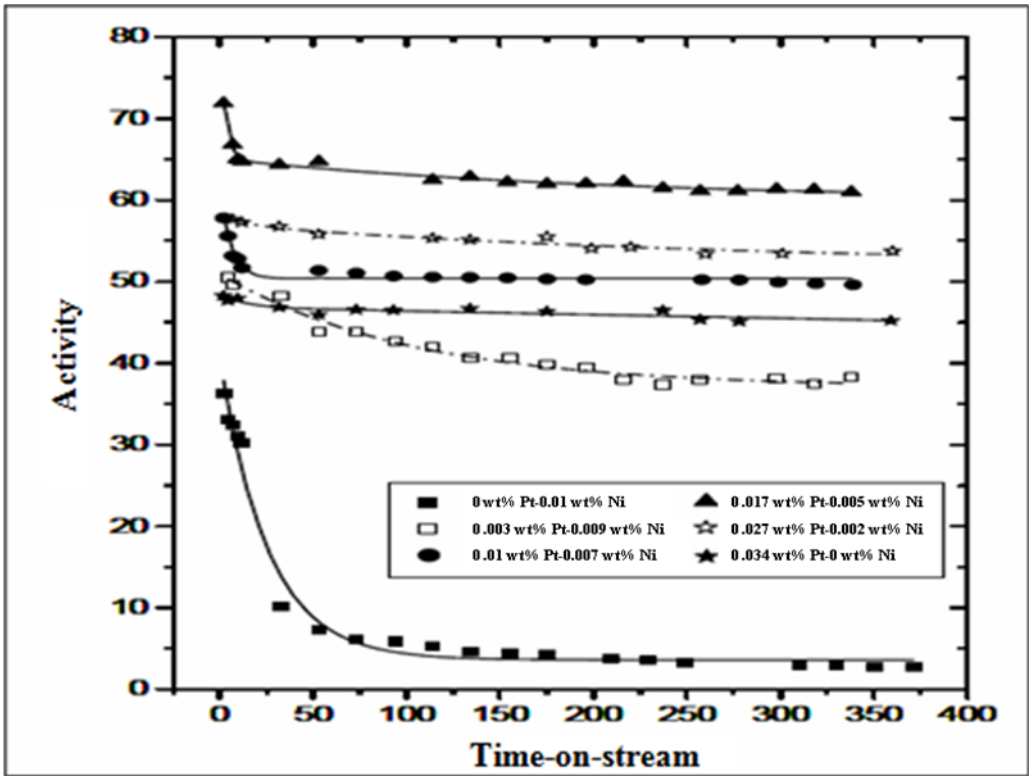

Figure 3-11 shows that the catalyst sample with only Ni had a very poor performance (reached an activity of less than 5 $mmol.h^{-1}.g^{-1}$ after 6 hours) versus that with pure Pt loading (around 45 $mmol.h^{-1}.g^{-1}$ after 6 hours). Therefore, one would expect the formulations of different Pt-Ni ratios to result in activities between 5 and 45 $mmol.h^{-1}.g^{-1}$ after the same period of reaction. However, surprisingly, most formulations resulted in a higher activity than that with pure Pt, with the formulation 50Pt-50Ni achieving an activity of more than 60 $mmol.h^{-1}.g^{-1}$ after the same period of reaction. The authors have attributed the positive effect the Ni addition to Pt causes versus catalysts with pure Ni or Pt to better metal dispersion and thus better hydrogenation/dehydrogenation function due to the formation of smaller metal particles during the reduction process, which disperse better. Another reason for this enhanced performance could be that Pt and Ni atoms interact in such a way that improves the catalysts properties. Experiments by Eswaramoorthi and Lingappan [56] showed very similar results when they varied the amount of Ni on 0.1 wt% Pt-loaded zeolite Y during the hydroisomerization of hexane and heptane over temperatures between 225 and 375^{o}C and at atmospheric pressure. They found that a Ni loading of 0.3 wt% (which results in a close to 1:1 molar ratio with Pt) gave the best conversion and isomerization to cracking yield for both feeds at all studied temperatures. They also found that increasing Ni loadings inhibits both the activity and selectivity of the catalyst. The reason for the drop in catalyst performance was argued to be the formation of larger particle sizes of bimetallic Ni-Pt particles at higher Ni loadings, resulting in some Ni content not being reduced, thus contributing to pore blockage of the catalyst.

Employing low loadings of Pt (0.4 wt%) on zeolite Beta, Liu et al [57] have recently studied the influence of a number of alkaline earth metals (namely, Magnesium, Calcium, Strontium, and Barium) on the performance of the zeolite during the hydroisomerization of normal heptane at 230^{o}C and atmospheric pressure. The amounts of alkali earth metals loaded were such that the molar ratio of each metal to platinum was 5. Their findings were that, at similar conversion levels, all the alkaline earth metals have substantially promoted the selectivity to isomers versus cracking products when compared to a platinum-only zeolite sample. The performace of zeolite plus metal was enhanced over that with only platinum in the order Mg < Ca < Sr < Ba. The high selectivity of Ba-loaded zeolite could be attributed to larger amounts of hydrogen taken up by the zeolite structure during reduction, since Ba ions interact the least with Pt, and also to the

introduction of additional strong acid sites. The ratio of mono to multi-branched isomers has been, however, found to be larger when using any of the alkaline earth metals. This could be possibly due to a faster desorption rate of intermediate carbenium ions from acid sites when alkaline earth metals are present, thus inhibiting cracking, but at the same time, preventing subsequent isomerisation steps from occurring.

The effect of introducing aluminium into the structure of 1 wt% platinum-loaded Zeolite Y catalysts has been studied by Le Van Mao and Saberi [58]. In their work, they examined the performance of catalysts with Al loadings of up to 7 wt%. They performed their experiments of normal heptane hydroisomerization at 225^{o}C and atmospheric pressure. They found that Al loadings up to 2 wt% almost did not change the acid site density of the catalyst, while product selectivity changed dramatically. The selectivity to isomers versus cracking products improved substantially upon introducing Al, and continued increasing until the Al loading reached 7 wt%. This was accompanied by a continual decrease in the amount of cracking products generated, though the yield of branched $C_5 - C_7$ products (having high RON values) reached a maximum around Al loadings of 1 – 1.5 wt%, and started decreasing thereafter. The authors suggested the presence of a third function in the catalyst brought by the loaded Al species, by which desorption of mono and multi-branched carbenium ion intermediates is facilitated from the acid sites, hence decreasing the cracking rate.

Using platinum-free bimetallic catalysts in the hydroisomerization of normal octane, Karthikeyan et al [48] tested the effect of changing the loading of Ni on 0.1 wt% Pd-loaded zeolite Y catalysts over temperatures ranging from 200 to 450^{o}C. It was found that the catalyst performance improved with increasing Ni loading, until it reached an optimum value of 0.3 wt%, beyond which both activity and selectivity of the catalyst drops. It was argued that the cause for this behaviour was the formation of bigger bimetallic particles at Ni loadings higher than 0.3 wt%, which leads to some Ni atoms not being reduced and possibly the blockage of some catalyst pores. In contrast to the effect of Ni addition on Pd-loaded zeolite Y, Henriques et al [59] have found out that adding Sn to Pd-loaded catalysts reduces their activity and selectivity to heptane isomers, while substantially improves their stability by minimizing coke formation. It was hypothesized

that Sn improves the hydrogenating activity of the catalyst, thus causing the coke precursors to be hydrogenated before they form coke.

The order of metal loading has been found to influence the performance of the resulting catalyst. For example, when platinum was loaded after nickel on zeolite Y, the catalyst showed better activity and selectivity than when platinum was loaded first. In addition, a better platinum dispersion was found in the former case. This can be explained by the occupation of the zeolite sodalite cages by Ni when it is first loaded, causing platinum to deposit in the zeolite supercages, which is a more favourable arrangement [43]. A similar finding has been reported by Roldán et al [60] when loading Pd before Pt on Beta catalysts. They have found that Pd when loaded and is reduced before loading Pt, bimetallic species that enhance the catalyst performance and improve metal dispersion are formed, a behaviour not seen when Pt is loaded first or even when the metals are loaded simultaneously. In Le Van Mao and Saberi's work (discussed above) [58], they found that loading Al simultaneously with Pt results in the best performance of the catalyst, when compared to loading either Pt or Al first. Similarly, Martins et al [61] found that loading Ni simultaneously with Pt on zeolite Beta gives better results over loading Ni prior to Pt during the hydroisomerization of hexane at 250^{o}C and atmospheric pressure. They attributed this behaviour to the better metal dispersion of the catalyst sample when metals were loaded simultaneously.

Gu et al [62] have tested the effect of adding a second metal salt instead of pure metal to 0.4 wt% platinum-loaded USY and 0.4 wt% platinum-loaded acid-leached USY zeolite during the hydroisomerization of normal heptane. They have used Cs salt of tungsophosphoric acid (PW) at different levels of Cs atoms per salt molecule (1.5, 2, and 2.5) and different percentages of salt in the zeolite (5 – 20 wt%). The reactions took place at temperatures ranging from 230 to 310^{o}C. It has been found that the used Cs salt of PW caused a drop in the activity of the USY sample, while considerably improved the activity and selectivity of acid-leached sample. Moreover, the optimum formulation of the Cs salt of PW, which gave even better performance, was 2 atoms of Cs in the salt molecule and a 10 wt% loading of the salt in the zeolite catalyst. The Cs salt of PW is known to be a very strong acid, even a superacid. However, this strong acidity is dispersed throughout the surface of dealuminated USY mesopores, and that is why the catalyst sample supported

with this salt performed better than the dealuminated USY sample, due to the introduced moderate acidity. A similar study by Wei eta l [63] using Cr and La doped tungstophosphoric acid (PW) supported on 0.4 wt% platinum-loaded USY zeolite during the hydroisomerization of normal heptane, and at the same reaction conditions has demonstrated similar findings. Pt-PW caused a drop in the activity of USY, but improved that of dealuminated USY sample, respectively. Similarly, doping Pt-PW with either La or Cr greatly improved both the dealuminated USY sample's activity and selectivity to isomers, with the best results obtained with a 5 to 1 molar ratio of Cr to Pt, and a 10 wt% loading of PW in the catalyst. The authors attributed the enhanced performance of catalyst, especially the suppression of cracking, due to doping with Cr to the introduction of desorption-transfer promoting sites, which help reduce the residence time of desired products, causing them to leave the catalyst structure before they crack.

3.3.10 Effect of De-alumination

As discussed in the previous chapter, de-alumination of zeolites causes their framework Si/Al ratio to increase, whether accomplished through acid leaching or steaming. The effect of changing the Si/Al ratio was reviewed in sub-section (3.3.7). Generally, when the zeolite is deeply dealuminated and acid-leached, it usually loses much of its activity due to loss of acidity [62], and hence the reduction in its capacity for alkane adsorption [21]. Another effect of dealumination is an improvement in isomerization selectivity [64]. However, the extra framework aluminium (EFAL) species that result from hydrothermal treatment have an additional effect on the performance of zeolites during the transformation of normal paraffins. Wang, Giannetto, and Guisnet [65] have studied the effect of EFAL species present in a series of hydrothermally de-aluminated zeolite Y catalysts on their performance during n-heptane isomerization and cracking in the absence of hydrogen. They noticed that an increase in the EFAL in the zeolite unit cell resulted in a higher cracking activity, and hence more rapid coking. However, the faster rate of coking is accompanied by an increase in isomerization activity. This behaviour of EFAL species can be attributed to their Lewis acidic sites, which have an inductive effect on Brönsted acidic site, resulting in the high activity.

Remy et al [66] have tested the effect of dealumination and deep dealumination on the activity of zeolite Y during the hydroisomerization of both normal heptane and normal

decane at a temperature of 185^{o}C and atmospheric pressure. They have found that the turnover frequency of heptane hydroisomerization (TOF), expressed by the rate of heptane hydroisomerization in mol per gram of catalyst per second divided by the catalyst framework tetrahedral aluminium content ($Al(IV)_F$) in mol per gram of catalyst, improves upon mild steaming and acid leaching of the zeolite (which causes a reduction of framework aluminium content per unit cell of zeolite Y) until it reaches a maximum value at a certain number of $Al(IV)_F$ atoms per unit cell (20 in the case of heptane and around 10 in the case of decane), and then starts decreasing sharply for catalysts that had been deeply dealuminated (steamed at more severe conditions and acid leached with a mineral acid), having low numbers of $Al(IV)_F$ per unit cell. This behaviour of TOF has been explained in that the acidity of sites increase as the amount of $Al(IV)_F$ in the unit cell is reduced, resulting in increasing TOF. However, at a certain point the removal of the EFAL species from the unit cell due to deep dealumination, thus removing the favourable inductive effect they have on the acidity of $Al(IV)_F$ sites, can cause the drop in TOF. The authors have studied the effect of the content of the EFAL species in the unit cell, whether in octahedral coordination or different coordinations, on the TOF of the reaction, and found that initially their removal from the unit cell does not affect the TOF, but at a certain level of removal the TOF starts decreasing, both in the case of heptane and decane. This latter observation does indeed suggest that there is an inductive effect of the EFAL species on $Al(IV)_F$ sites.

3.3.11 Effect of Sulfur and Impurities in the Feed

Sulfur species are commonly present in hydrocarbon feeds in the form of mercaptans or thiophenes, with thiophenes being the typical form [67]. These sulfur species cause faster deactivation rates of bifunctional catalysts by poisoning the hydrogenating metal sites through chemisorption [68], which lowers the interactions between the metal site and acid sites, thus causing a migration of metal atoms out of the catalyst pores and promoting metal sintering [69]. Therefore, these sulfur species are usually removed from feeds via hydrodesulfurization (HDS) through conversion into H_2S gas before the hydrocarbon feeds are further processed [67]. Ways to increase the sulfur-tolerance of a platinum-loaded catalysts were found to be increasing the acid site concentration (hence the acidity) of the catalyst support, thus enhancing the electron-deficiency of Pt, which promotes activity and sulfur-tolerance of the catalyst, and the fixation of Pt atoms inside the catalyst pores with the use of nickel [70,71].

The effect of sulfur on the performance of platinum-loaded Mordenite was studied by Romero et al [72] during the hydroisomerization of normal decane at a temperature of 350^{o}C and a system pressure of 30 atmospheres. They found that adding 1% by weight of dimethyldisulfide (DMDS) to the decane feed resulted in a substantial decrease in the catalyst activity, both for isomerization and cracking, when comparing it to the activity achieved with pure normal decane. Specifically, the isomerization activity is much more affected by sulfur than the cracking activity (three times the effect), due to the poisoning effect of sulfur on the metal sites are responsible for hydrogenation/dehydrogenation. However, the decrease in isomerization activity was found to be more reversible than the cracking activity, as 50% of the isomerization activity was restored upon the re-introduction of pure normal decane, whereas the cracking activity was only restored by 10%, resulting in a higher selectivity towards isomers. This observation suggests that not only does sulfur affect the metal sites, but it also has an effect on the Mordenite structure, causing the almost irreversible effect in the cracking activity.

Arribas, Márques, and Martínez [72] have studied the effect of adding 200 ppm sulfur to the feed during the simultaneous normal heptane hydroisomerization and benzene hydrogenation (75 wt% C_7 – 25 wt% benzene) over 1% platinum-loaded zeolite Beta at 220^{o}C and 30 bar. They reported that the hydroisomerization activity started dropping once sulfur was introduced into the feed, until it reached 75% of its original value after 400 minutes on-stream and remained thereafter. The selectivity to normal heptane isomers, however, decreased and reached a plateau of 62% of the starting selectivity in a faster manner, taking only 60 – 70 minutes on-stream. This means that the hydroisomerization activity was also more impacted here than that of cracking. When sulfur-free feed was reintroduced to the catalyst, a recovery of up to 93% of the starting hydroisomerization activity was achieved.

On the other hand, the effect of impurities presence in a feed of normal hexane was studied by Guisnet and Fouche [29] also over Mordenite but at a temperature of 250^{o}C and a pressure of 1 atmosphere. Two samples of Mordenite were tested; one with a Si/Al ratio of 8 and a de-aluminated one with a ratio of 68. The tested impurities were other alkanes, naphthenes, and aromatics added to normal hexane is small amounts (5% by weight). It

was found that a lighter alkane (normal pentane) does not influence either the activity or stability of the catalyst when added to normal hexane, whereas heavier alkanes (normal heptane and 2-methylhexane) affect the stability of the Mordenite with high acidity only. This is due to the less cracking tendency of pentane than hexane, which results in no deactivation arising from pentane. No effect on selectivity was observed with either of the alkanes. For naphthenes and aromatics, methylcyclohexane (MCH) and toluene were found to negatively affect both the activity and stability of Mordenite with high acidity and affect the activity of de-aluminated Mordenite. The reason why they do not affect the stability of the de-aluminated Mordenite is due to the present mesopores in this catalyst, which facilitate the movement of these molecules and prevent deactivation. 1-methylnaphthalene, however, had a negative effect on both the activity and stability when tested with either catalyst, probably due to its large molecular size. The decrease in activity for both catalysts is due to a competing effect between naphthenes and aromatics with intermediate olefins over acidic sites in the catalyst, which result in lower isomerization and cracking rates.

3.3.12 Effect of Coke in the Catalyst

Coke formation and deposition on the catalyst pores and poisoning of its active sites are of the main reasons for catalyst deactivation in hydrocarbon catalyzed reactions [74-76]. The nature of coke depends on the temperature at which the reaction takes place. At low reaction temperatures (below 200^{o}C), the type of coke depends on the reactant type and consists mainly of rearrangement and condensation products. However, at temperatures above 350^{o}C, polyaromatic compounds that do not dissolve easily tend to form in mesopores and supercages and block the catalyst pores [74,75], reducing the activity of catalyst, even when the concentration of coke is low, due to the large size of these compounds [77]. The ease at which coke can be removed from the zeolite catalyst during regeneration with air treatment depends on the structure of the zeolite and is shape-selective [78]. The effect of coke on the hydroisomerization of normal hexane over platinum-loaded zeolite Y was studied by Ribeiro et al [79] for the purpose of enhancing catalyst stability after determining the more affected catalytic function by coke, whether the acidic or the hydrogenating function. The experiments were run at temperatures of 250 and 270^{o}C, a pressure of 40 bar, and platinum contents of 0.03 and 6% by weight on both fresh and coked catalysts. Coke content on the deactivated 0.03 and 6 wt% platinum-loaded catalysts were 3.6 and 4.0% by weight, respectively. The isomerization activity of

the deactivated 6 wt% platinum zeolite catalyst was less than that with the deactivated 0.03 wt% platinum one, which is an opposite observation to what is noticed with the fresh catalysts. In addition, the selectivity to multi-branched isomers increased for the deactivated catalysts. This means that coke has the same effect as decreasing platinum content on the isomerization activity and the selectivity to multi-branched isomers, which leads to the conclusion that coke has a larger poisoning effect on the hydrogenating sites than on acidic sites.

3.4 Kinetics of Hydroisomerization

When the hydroisomerization reaction proceeds through the monomolecular mechanism, it can be described to possess an ideal bifunctional behaviour. Denayer et al [80] demonstrated the overall reaction mechanism involving diffusion of the reactant into the zeolite structure, adsorption on the surface of the catalyst, conversion on the acid/metal active sites, and desorption of products and their diffusion out of the catalyst. Figure 3-12 explains the sequence of events that takes place during the reaction.

Figure 3-12. Demonstration of the reaction mechanism within a bifunctional catalyst pore structure [80].

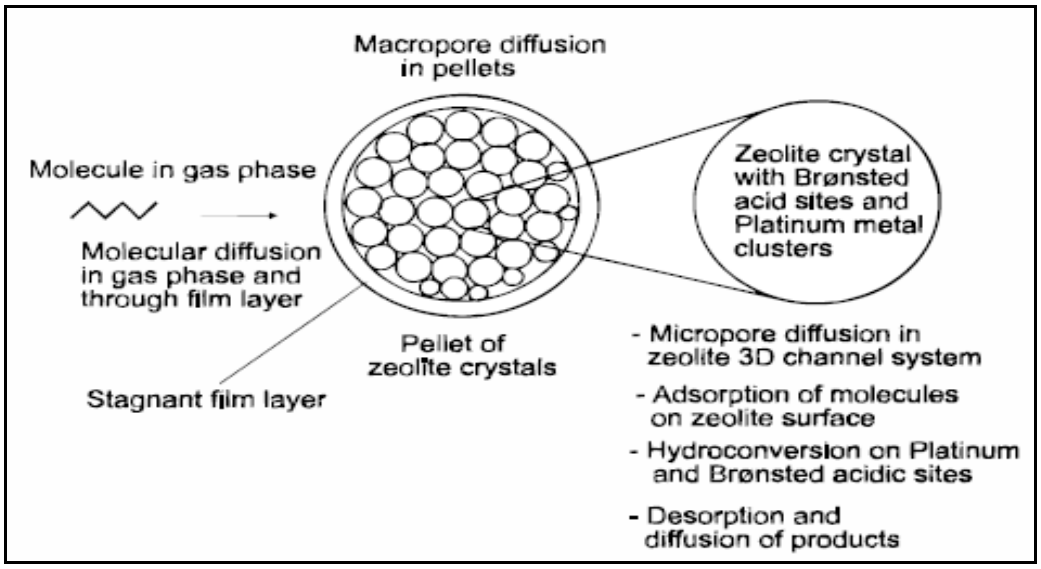

As shown previously in Figure 3-2 for normal hexane as the example alkane, upon adsorption of the alkane on the platinum site, it undergoes dehydrogenation to its corresponding alkene, which desorbs from the platinum site. The alkene then migrates to an acid site where it adsorbs prior to protonation to form a carbenium ion. The carbenium

ion undergoes rearrangement (isomerization) before deprotonation to form an isoalkene, which desorbs from the acid site and migrates to a platinum site where it is finally hydrogenated to an isoalkane. Van de Runstraat and co-workers [81] proposed that the overall isomerization reaction rate of normal hexane is described by the following equation when the carbenium ion rearrangement is the rate-determining step (ideal bifunctional behaviour):

$$R = k_{iso}\frac{K_{dehydr} \cdot K_{prot} \cdot \left(\frac{p_nC_6}{p_{H2}}\right)}{1 + K_{dehydr} \cdot K_{prot} \cdot \left(\frac{p_nC_6}{p_{H2}}\right)} \approx k_{iso}\left(K_{dehydr} \cdot K_{prot} \cdot \left(\frac{p_nC_6}{p_{H2}}\right)\right)^{\alpha} \qquad (1)$$

In this equation, R is the reaction rate, K_{dehydr} is the hexane dehydrogenation equilibrium constant, K_{prot} is the hexene protonation equilibrium constant, k_{iso} is the protonated hexene isomerization rate constant, p_{nC6} is the normal hexane partial pressure, p_{H2} is the hydrogen partial pressure, and α is the order of reaction and is smaller than or equal to 1. Equation (1) assumes no diffusion limitations inside the zeolite micropores (that there is equilibrium between the hydrocarbon concentrations and the gas phase). However, this equation is not valid for the cases of complete micropore filling (diffusion limitation), high pressure, or when using a long alkane molecule. Instead, the following equation is used at these conditions:

$$R = k_{iso}\frac{PAR(1) \cdot p_{n\text{-alkane}}}{p_{H2} + PAR(2) \cdot p_{H2} \cdot p_{n\text{-alkane}} + PAR(3) \cdot p_{n\text{-alkane}}} \qquad (2)$$

In this equation, PAR(1), PAR(2), and PAR(3) are parameters that consist of equilibrium and adsorption constants, which account for reactant diffusion into the catalyst pores, its adsorption on active sites, product desorption from active sites and diffusion from the catalyst pores. Langmuir adsorption of alkane products is given by the term $PAR(3).p_{n\text{-alkane}}$. This equation was found to work by Froment [82] for the hydroisomerization of normal decane over platinum-loaded USY zeolite. Van de Runstraat et al developed an equation that enables modelling of the intermediate region between the two extremes represented by equations (1) and (2):

$$E_{act,iso} = E_{act,app} + (1 - \theta_{n\text{-alkoxy}}) \cdot [-\Delta H_{prot,ads} - \Delta H_{ads,n=C6} + \Delta H_{dehydr}] \qquad (3)$$

Here, $E_{act,\ app}$ refers to the apparent activation energy, $E_{act,\ iso}$ refers to the n-alkoxy isomerization activation energy, ΔH_{dehydr} is the dehydrogenation enthalpy, $\Delta H_{prot,\ ads}$ is the enthalpy of protonation (alkoxy formation) from the alkene adsorbed state, and $\Delta H_{ads,\ n=6}$ is the enthalpy of adsorption of normal hexene. This equation assumes that the adsorption enthalpy of normal hexane equals that of normal hexene. Equation (3) is used to calculate the isomerization activation energy from experimental data [81].

Matsuda et al [83] have estimated the apparent activation energy and reaction order for the hydroisomerization of normal heptane over 0.5 wt% platinum-loaded zeolite Beta and USY at atmospheric pressure and hydrogen/hydrocarbon ratios from 3.33 to 18.6. The apparent activation energies were calculated over temperatures ranging from 200 to 300^{o}C and the order of reaction in hydrogen and nC_7 was calculated at 200^{o}C. Table 3-2 displays the results they have reported along with results found by Holló et al [84] for 0.4 wt% Pt-loaded Mordenite. The reason for the negative reaction orders in hydrogen was attributed to the lower concentration of carbenium ions at higher hydrogen pressures, which occurs because a high hydrogen concentration slows the formation of carbenium ions from intermediate alkenes, thus resulting in a reduced isomerization rate. Ribeiro, Marcilly and Guisnet [5] developed a rate equation which is valid at low levels of conversion and that takes into account the concentration of carbenium ions when they studied the hydroisomerization of normal hexane over zeolite Y catalysts at temperatures ranging from 230 to 325 ^{o}C and pressures from 30 – 40 bar:

$$r = k_3 C_m K_1 K_2 \frac{p_{nC6}}{p_{H2} + K_1 K_2 p_{nC6}} \qquad (4)$$

In the above equation, k_3 is the rate constant for isomerization, C_m is the Brönsted acid sites concentration of the catalyst, K_1 is the equilibrium constant of normal hexane dehydrogenation, K_2 is the equilibrium constant of carbenium ion formation (protonation), p_{nC6} is the partial pressure of normal hexane, and p_{H2} is the partial pressure of hydrogen. This equation proved that the bifunctional mechanism is valid for hydrogen to hydrocarbon ratios below 10. For ratios above 10, there is limitation in the concentration of the reactant (hexane), leading to a low concentration of intermediate hexane, which, in turn, invalidates the rate equation, since it assumes that the rate limiting step is the cabenium ion

rearrangement (there is an equilibrium between the concentration of intermediate olefins and protonated olefins).

Table 3-2. Activation energy and reaction order for nC_7 hydroisomerization over Pt-loaded zeolite Beta, Mordenite, and USY [83,84].

Catalyst	Apparent Activation Energy, kJ/mol	Reaction order in H_2	Reaction order in nC_7
Pt/Hβ	130	-0.8	0
Pt/USY	110	-0.6	0.5
Pt/MOR	118	-1.1	0.15

Several kinetic modelling techniques have been adopted in the literature to model and describe hydroconversion (hydroisomerization and hydrocracking) reactions of hydrocarbons using platinum-loaded zeolite supports (bifunctional catalysts). Table 3-3 summarizes the experimental conditions and the kinetic modelling techniques used by some researchers, as found from the literature, as well as the technique used in this work (initial rates), which is implemented in Chapter 6.

In general, the kinetic modelling techniques adopted in the literature can be classified into:

1. Ones that take into account the intrinsic reactivity of the feed alkane over the zeolite to determine activation energies, rates and order of the reaction, while ignoring diffusion and adsorption effects on the reaction pathway. These techniques are usually used when studying a single reactant on an open zeolite, such as USY. For example, in Ribeiro et al's study [5], they used the intrinsic reaction kinetics in calculating the isomerisation and cracking rates of reaction of normal hexane over USY catalysts with varying platinum contents in order to determine the optimum platinum loading that leads to a maximum isomerisation rate and minimum cracking rate. In addition, they found out that both the isomerisation and cracking activation energies of hexane conversion stay constant at platinum loadings equal to or higher than 0.5 wt%, which led to the conclusion that the bifunctional hydroisomerization mechanism exists at those platinum loadings. In the current work, the initial rates method is used to determine ratios of cracking and isomerisation rate constants for USY catalysts with varying acidic properties, with

the purpose of identifying the catalyst with the least cracking activity and the most isomerisation activity and the optimum reaction temperature and pressure that achieve the best performance.

2. Ones that include diffusion and adsorption effects to intrinsic kinetics. These are used generally when testing potentially restricted zeolite structures, when studying the effect of high pressure on the reaction mechanism, or when multiple reactants are introduced to the catalyst simulataneusly, in which case the impact of the competitive adsorption of longer chain alkanes is studied. For example, in Denayer et al studies [88,89], the effect of reacting a mixture of normal heptane and normal nonane over zeolite USY in both vapour and liquid phase conditions was studied using the adsorption-reaction approach. They found out that, even though the reactivity of normal nonane is much higher than that of normal heptane at vapour phase conditions due to its preferential adsorption and led to higher rates of cracking, the reactivity of normal nonane became almost equal to that of normal heptane at liquid phase conditions, eliminating excessive cracking and allowing for a higher isomer yield. This means that the competitive adsorption of differeing length alkanes is eliminated at liquid conditions and that their adsorption becomes non-selective, paving the way for their intrinsic reactivities to dictate the outcome of the reaction. Using the adsorption-reaction approach might be useful in determining whether any of the tested catalysts in the current work has any structural constraints that affect its product selectivity.

3. Ones that take into account all elementary steps of the reaction including all possible rearrangements (hydride shift, alkyl shift, protonated cyclopropane intermediate, etc) on the reaction scheme in order to obtain more detailed information about rate constants and activation energies of individual reaction steps. For example, in Fúnez et al's work [87], their use of a parallel/consecutive reaction scheme to study the conversion of normal octane on zeolite Mordenite, Beta, and USY enabled the calculation of rate constants of mono-branched and multi-branched isomers formation, cracking products formation from mono-branched isomers, and cracking products formation from multi-branched isomers, in addition to activation energies of all those steps for all three zeolite types. Results showed that Beta zeolite has the highest tendency to crack mono-branched isomers directly, due to its high acid site density, and that Mordenite forms the least

mono-branched isomers and generates the most cracked products from multi-branched isomers, due to its restricted structure (effectively one-dimensional). The use of such comprehensive and detailed models is suitable for predicting to a high certainty the product nature of reactions over catalysts with different formulations.

Table 3-3. Kinetic modelling techniques and experimental conditions for hydroconversion reactions on bifunctional zeolite catalysts as found from the literature.

Reference	Feed	Catalyst	P, bar	T, ^{o}C	WHSV, h^{-1}	H_2/HC, mol/mol	Kinetic Modelling Technique
[80]	n-C6 - n-C9 mixture	Pt/HY	4.5	233	-	13.1	Multicomponent adsorption-reaction model
[81]	n-C_6	Pt/MOR, Pt/BEA, Pt/ZSM-5, Pt/ZSM-22, Pt/TON	1.0	240	5.9 – 23.6	>20	Intrinsic & adsorption-reaction kinetics
[82]	n-C8, n-C10, n-C12	Pt/USY	5 - 100	130 - 250	-	10 - 150	Lumped adsorption-reaction model & Non-linear regression
[84]	nC_5, nC_6, nC_7, Cycl-C_6, and binary mix	Pt/MOR	5 - 40	180 - 220	1.26 – 1.88	1 - 20	Kinetics of skeletal rearrangement of hydrocarbons
[85]	nC_{16}	Pt/USY	35	300 - 320	0.47 – 2.05	6 - 11	Generalized mechanistic kinetic model
[86]	C_5 – C_9, C_{12}	Pt/HY, Pt/USY	4.5 - 15	233 - 290	0.185 – 460.8	4.23 - 250	Fundamental microkinetic model
[87]	Liquid n-C8	Pt/MOR, Pt/BEA, Pt/USY	50 - 90	250 - 290	-	-	parallel/consecutive reaction scheme model
[88,89]	Liquid C_7 & C_9 mixture	Pt/HY	4.5 - 100	230 - 270	-	0.5	Adsorption-reaction model
[90]	nC_7	Pt/HY, Pt-Zn/HY	1.0	195 - 240	0.909 – 6.25	-	Initial rates
[91]	nC_8	Pt/USY	4.5 - 7	230 - 310	1.58 – 118.75	13.1 - 250	Lumped adsorption-reaction model
[27]	nC_7	Pt/Al_2O_3-BEA	28	295 - 405	20	5.36	Simple dual-site model
[92]	nC_8 - nC_{12}	Pt/USY	5 - 50	220 - 260	0.6 – 10	30 - 300	Modified single-event model
[93]	VGO	Pt/USY	120	267	3.8 v/v	506 v/v	Partially relumped single-event kinetic equations
[94]	Cyclic C_7, C_8, and C_{10}	Pt/USY	10 - 50	220 - 300	0.14 – 1.19	50 - 300	Single-event model
[5]	nC_6	Pt/HY	30 - 40	230 - 325	8.6	26.1	Intrinsic reaction kinetics
[13]	nC_6 - nC_9 mixture	Pt/HY, Pt/USY	4.5	233	-	13.1	Intrinsic reaction kinetics
[95]	nC_6 - nC_9 mixture	Pt/ZSM-22, Pt/USY	4.5	233	-	13.1	Adsorption lumped-reaction scheme
This thesis	**nC_7**	**Pt/USY**	**1 - 15**	**170 - 310**	**2.565 – 10.26**	**9.0**	**Initial Rates**

3.5 Conclusion

The importance of the hydroisomerization of alkanes arises from their low octane numbers compared to their isomers. When bifunctional zeolites are used in the reaction, high yields of isomers are generated with great stability over that of chlorinated alumina catalysts. Two reaction mechanisms contribute to forming isomers, and their contribution to the reaction scheme depends on the acid-metal balance of the catalyst. Increasing reaction temperature, contact time, and zeolite acidity results in higher catalyst activity and, therefore, overall conversion, while increasing pressure has an opposite effect on activity. Selectivity and stability of catalysts can be promoted by using dealuminated catalysts (improved porosity), higher metal-loading (better acid-metal balance), and bimetal loading (less cracking yield). The metal function of the catalyst is of higher importance, as it can be considerably affected by the presence of sulfur or coke in the catalyst. When there is a good balance between the metal and acid functions of the catalyst, the rate-limiting step in the reaction becomes the carbenium ion rearrangement. Generally, the reaction can be modelled by the intrinsic kinetics of the reaction. However, when carrying the reaction out at very high pressures or using catalysts with a high level of constraint, one has to account for diffusional limitations and adsorption effects when building a kinetic model that successfully describes the reaction. Different kinetic modelling techniques have been reported in the literature in attempts to predict this reaction over bifunctional zeolites. They either look into the intrinsic kinetics of the reaction, while ignoring diffusion and adsorption effects, lump some of the elementary reaction steps and evaluate competitive adsorption in high pressure or multi-component reaction systems, or go into detail by modelling all simple reaction steps for the purpose of estimating properties of individual reaction steps.

3.6 References

[1] Gary, J. and Handwerk, G. (2001). *Petroleum Refining: Technology and Economics.* 4th edition. New York: Marcel Dekker, Inc. p. 204.

[2] Roldán R; Romero, F. J; Jiménez-Sanchidrián, C; Marinas, J. M. and Gómez, J. P. (2005). Influence of Acidity and Pore Geometry on the Product Distribution in the Hydroisomerization of Light Paraffins on Zeolites. *Applied Catalysis A: General*, 288, 104-115.

[3] Grau, J. M; Vera, C. R. and Parera, J. M. (2002). Preventing self-poisoning in [Pt/Al_2O_3 + SO_4^{2-}-ZrO_2] mixed catalysts for isomerization-cracking of heavy alkanes by prereduction of the acid function. *Applied Catalysis A: General*, 227, 217-230.

[4] Jiménez, C; Romero, F. J; Roldán, R; Marinas, J. M. and Gómez, J. P. (2003). Hydroisomerization of a Hydrocarbon Feed Containing *n*-Hexane, *n*-Heptane and Cyclohexane on Zeolite-supported Platinum Catalysts. *Applied Catalysis A: General*, 249, 175-185.

[5] Ribeiro, F. R; Marcilly, C. and Guisnet, M. (1982). Hydroisomerization of *n*-Hexane on Platinum Zeolites: I. Kinetic Study of the Reaction on Platinum/Y-Zeolite Catalysts: Influence of the Platinum Content. *Journal of Catalysis*, 78, 267-274.

[6] Chica, A. and Corma A. (1999). Hydroisomerization of Pentane, Hexane, and Heptane for Improving the Octane Number of Gasoline. *Journal of Catalysis*, 187**,** 167-176.

[7] Bekkum, H. V; Flanigen, E. M; Jacobs, P. A. and Jansen, J. C. (2001). *Introduction to Zeolite Science and Practice*. 2nd Edition. Amsterdam: Elsevier. p. 643-650, 756-760.

[8] Weitkamp, J. and Puppe, L. (1999). *Catalysis and Zeolites*. Berlin: Springer.

[9] Gopal, Srikant and Smirniotis, Panagiotis G. (2004). Factors Affecting Isomer Yield for *n*-heptane Hydroisomerization over As-synthesized and Dealuminated Zeolite Catalysts Loaded with Platinum. *Journal of Catalysis*, 225, 278-287.

[10] Jansen, J. C; Stöcker, M; Karge, H. G. and Weitkamp, J. (1994) *Advanced Zeolite Science and Applications*. Amsterdam: Elsevier.

[11] Ward, J. W. and Qader, S. A. (1975). *Hydrocracking and Hydrotreating*. Washigton D.C: American Chemical Society.

[12] Blomsma E; Martens, J. A. and Jacobs, P. A. (1997). Isomerization and Hydrocracking of Heptane over Bimetallic Bifunctional PtPd/H-Beta and PtPd/USY Zeolite Catalysts. *Journal of Catalysis*, 165, 241-248.

[13] Denayer, J. F; Baron, G. V; Vanbutsele, G; Jacobs P. A. and Martens J. A. (2000). Evidence for Alkylcarbenium Ion Reaction Intermediates from Intrinsic Reaction Kinetics of C_6–C_9 n-Alkane Hydroisomerization and Hydrocracking on Pt/H–Y and Pt/USY Zeolites. *Journal of Catalysis*, 190, 469-473.

[14] Martens, J. A; Jacobs, P. A. and Weitkamp, J. (1986). Attempts to Rationalize the Distribution of Hydrocracked Products: I. Qualitative Description of the Primary Hydrocracking Modes of Long Chain Paraffins in Open Zeolites. *Applied Catalysis*, 20, 239-281.

[15] Alvarez, F; Giannetto, G; Guisnet, M. and Perot, G. (1987). Hydroisomerization and Hydrocracking of *n*-Alkanes: 2. *n*-Heptane Transformation on a Pt-Dealuminated Y Zeolite – Comparison With a Pt-Y Zeolite. *Applied Catalysis*, 34, 353-365.

[16] Gauw, F. J. M. M. de. (2002). *Kinetic Studies of Alkane Hydroisomerization over Solid Acid Catalysts*. PhD Thesis, Eindhoven University of Technology, Eindhoven.

[17] Kuchar, P. J; Bricker, J. C; Reno, M. E. and Haizmann, R. S. (1993). Paraffin isomerization innovations. *Fuel Processing Technology*, 35, 183-200.

[18] Martens, J. A; Jacobs, P. A. and Weitkamp, J. (1986). Attempts to Rationalize the Distribution of Hydrocracked Products: II. Relative Rates of Primary Hydrocracking Modes of Long Chain Paraffins in Open Zeolites. *Applied Catalysis*, 20, 283-303.

[19] Blomsma E; Martens, J. A. and Jacobs, P. A. (1996). Mechanisms of Heptane Isomerization on Bifunctional Pd/H-Beta Zeolites. *Journal of Catalysis*, 159, 323-331.

[20] Maesen, T. L. M; Beerdsen, E; Calero, S; Dubbeldam, D. and Smit, B. (2006). Understanding Cage Effects in the *n*-alkane Conversion on Zeolites. *Journal of Catalysis*, 237, 278-290.

[21] Denayer, J. F. M. and Baron, G. V. (1997). Adsorption of Normal and Branched Paraffins in Faujasite Zeolites NaY, HY, Pt/NaY and USY. *Adsorption*, 3, 251-265.

[22] Denayer, J. F; Baron, G. V; Martens, J. A. and Jacobs, P. A. (1998). Chromatographic Study of Adsorption of *n*-Alkanes on Zeolites at High Temperatures. *Journal of Physical Chemistry B*, 102, 3077-3081.

[23] Pham-Huu, C; Del Gallo, P; Peschiera, E. and Ledoux, M. J. (1995). *n*-Hexane and *n*-heptane Isomerization at Atmospheric and Medium Pressure on MoO_3–carbon-modified Supported on SiC and γ-Al_2O_3. *Applied Catalysis A: General*, 132, 77-96.

[24] Wang, Z. B; Kamo, A; Yoneda, T; Komatsu, T. and Yashima, T. (1997). Isomerization of *n*-Heptane Over Pt-loaded Zeolite β Catalysts. *Applied Catalysis*, 159, 119-132.

[25] Ribeiro, F. R; Marcilly, C. and Guisnet, M. (1982). Hydroisomerization of *n*-Hexane on Platinum Zeolites: II. Comparison between the Reaction Mechanisms on Platinum/Y-Zeolite and on Platinum/Mordenite. *Journal of Catalysis*, 78, 275-280.

[26] AbouI-Gheit, A. K; Menoufy, M. F; EI-Morsi, A. K. and Abdel-Hamid, S. M. (1987). Hydroconversion and Diffusion of *n*-Heptane on Mordenite Catalysts. *Zeolites*, 1987, 7, 353-359.

[27] Degnan, T. F. and Kennedy, C. R. (1993). Impact of Catalyst Acid/Metal Balance in Hydroisornerization of Normal Paraffins. *AIChE Journal*, 39, 607-614.

[28] Henriques, C; Dufresne, P; Macilly, C. and Ribeiro, F. R. (1986). Influence of Tin on the Stability of Sn/Pd HY Zeolites in the Hydrocracking and Hydroisomerization of *n*-Heptane. *Applied Catalysis*, 21, 169-177.

[29] Guisnet, M. and Fouche V. (1991). Isomerization of *n*-Hexane on Platinum Dealuminated Mordenite Catalysts: III. Influence of Hydrocarbon Impurities. *Applied Catalysis*, 71, 307-317.

[30] Siliconfareast Web Page [Website]. Available from: <http://www.siliconfareast.com/edxwdx.htm> [Accessed: 1 September 2007].

[31] Chao, K; Lin, C; Lin, C; Wu, H; Tseng, C. and Chen, S. (2000). *n*-Heptane Hydroconversion on Platinum-loaded Mordenite and Beta Zeolites: the Effect of Reaction Pressure. *Applied Catalysis A: General*, 203, 211-220.

[32] Tran, M. T; Gnep, N. S; Szabo, G. and Guisnet, M. (1998). Isomerization of *n*-Butane over H-Mordenites under Nitrogen and Hydrogen: Influence of the Acid Site Density. *Journal of Catalysis*, 174, 185-190.

[33] Guisnet, M. and Fouche, V. (1991) Isomerization of *n*-Hexane on Platinum Dealuminated Mordenite Catalysts: I. Influence of the Silicon-to-Aluminium Ratio of the Zeolite. *Applied Catalysis*, 71, 283-293.

[34] Simon-Masseron, A; Marques, J. P; Lopes, J. M; Ribeiro, F. R; Gener, I. and Guisnet, M. (2007). Influence of the Si/Al Ratio and Crystal Size on the Acidity and Activity of HBEA Zeolites. *Applied Catalysis*, 316, 75-82.

[35] Tran, M. T; Gnep, N. S; Szabo, G. and Guisnet, M. (1998). Comparative Study of the Transformation of *n*-Butane, *n*-Hexane and *n*-Heptane over H-MOR Zeolites with Various Si/Al Ratios. *Applied Catalysis*, 170, 49-58.

[36] Guisnet, M; Alvarez, F. Giannetto, G. and Perot, G. (1987). Hydroisomerization and Hydrocracking of *n*-Heptane on PtH Zeolites: Effect of The Porosity and of The Distribution of Metallic and Acid Sites. *Catalysis Today*, l, 415-433.

[37] Ramos, M. J; Gómez, J. P; Dorado, F; Sánchez, P. and, Valverde J. L. (2007). Hydroisomerization of a Refinery Naphtha Stream over Platinum Zeolite-based Catalysts. *Chemical Engineering Journal*, 126, 13-21.

[38] Gopal, S. (2003). *Synthesis, Modification, Characterization and Catalytic Studies of Zeolite based Bifunctional Catalysts for Hydroisomerization Reactions*. PhD Dissertation, University of Cincinnati, Cincinnati, Ohio.

[39] Matsuda, T; Watanabe, K; Sakagami, H. and Takahashi, N. (2003). Catalytic Properties of H_2-reduced MoO_3 and Pt/zeolites for the Isomerization of Pentane, Hexane, and Heptane. *Applied Catalysis A: General*, 242, 267-274.

[40] Maloncy, M. L; Maschmeyer, Th. and Jansen, J. C. (2005). Technical and Economical Evaluation of a Zeolite Membrane Based Heptane Hydroisomerization Process. *Chemical Engineering Journal*, 106, 187-195.

[41] Patrigeon, A; Benazzi, E; Travers, Ch. and Bernhard, J. Y. (2001). Influence of the Zeolite Structure and Acidity on the Hydroisomerization of *n*-heptane. *Catalysis Today*, 65, 149-155.

[42] Raybaud, P; Patrigeon, A. and Toulhoat, H. (2001). The Origin of the C_7-Hydroconversion Selectivities on Y, *β*, ZSM-22, ZSM-23, and EU-1 Zeolites. *Journal of Catalysis*, 197, 98-112.

[43] Pope, T. D; Kriz, J. F; Stanciulescu, M. and Monnier, J. (2002). A Study of Catalyst Formulations for Isomerisation of C_7 Hydrocarbons. *Applied Catalysis A: General*, 233, 45-62.

[44] Simon-Masseron, A; Marques, J. P; Lopes, J. M; Ribeiro, F. R; Gener, I. and Guisnet, M. (2007). Influence of the Si/Al Ratio and Crystal Size on the Acidity and Activity of HBEA Zeolites. *Applied Catalysis*, 316, 75-82.

[45] Soualah, A; Lemberton, J. L; Pinard, L; Chater, M; Magnoux, P. and Moljord, K. (2008). Hydroisomerization of Long-chain *n*-alkanes on Bifunctional Pt/zeolite Catalysts: Effect of the Zeolite Structure on the Product Selectivity and on the Reaction Mechanism. *Applied Catalysis A: General*, 336, 23-28.

[46] Galperin, L. B; Bradley, S. A. and Mezza, T. M. (2001). Hydroisomerization of *n*-decane in the Presence of Sulfur: Effect of Metal–acid Balance and Metal Location. *Applied Catalysis A: General*, 219, 79-88.

[47] Soualah, A; Lemberton, J; Chater, M; Magnoux, P. and Moljord, K. (2007). Hydroisomerization of *n*-Decane over Bifunctional Pt- HBEA Zeolite. Effect of the Proximity between the Acidic and Hydrogenating Sites. *Reaction Kinetics and Catalysis Letters*, 91, 2, 307-313.

[48] Karthikeyan, D; Lingappan, N. and Sivasankar, B. (2008). Hydroisomerization of *n*-Octane over Bifunctional Ni-Pd/HY Zeolite Catalysts. *Industrial & Engineering Chemistry Research*, 47, 6538-6546.

[49] Sánchez, P; Dorado, F; Ramos, M. J; Romero, R; Jiménez, V. and Valverde, J. L. (2006). Hydroisomerization of C_6–C_8 *n*-alkanes, Cyclohexane and Benzene over Palladium and Platinum Beta Catalysts Agglomerated with Bentonite. *Applied Catalysis A: General*, 314, 248-255.

[50] International Union of Pure and Applied Chemistry [Website]. Available from: <www.iupac.org/goldbook/C00897.pdf> [Accessed: 7 September 2007].

[51] Sinfelt, J. H. (1973). Catalyst Specificity. *AIChE Journal*, 19:4, 673-683.

[52] Alvarez, F; Rebeiro, F. R; Perot, G. Thomazeau, C. and Guisnet, M. (1996). Hydroisomerization and Hydrocracking of Alkanes: 7. Influence of the Balance

between Acid and Hydrogenating Functions on the Transformation of *n*-Decane on PtHY Catalysts. *Journal of Catalysis*, 162, 179-189.

[53] Guerin, M; Kappenstein, C; Alvarez, F; Giannetto, G. and Guisnet, M. (1988). Preparation of PtHY Catalysts: Influence on the Catalytic Properties of the Complexes Used as Platinum Precursors. *Applied Catalysis*, 45, 325-333.

[54] Liu, Y; Guo, W; Zhao, X. S; Lian, J; Dou, J. and Kooli, F. (2006). Zeolite Beta Catalysts for *n*-C_7 Hydroisomerization. *Journal of Porous Materials*, 13, 359-364.

[55] Barsi, F. V. and Cardoso, D. (2009). Bimetallic Pt-Ni Catalysts Supported on USY Zeolite for n-Hexane Isomerization. *Brazilian Journal of Chemical Engineering*, 26:2, 353-360.

[56] Eswaramoorthi, I. and Lingappan, N. (2003). Ni–Pt/H-Y Zeolite Catalysts for Hydroisomerization of *n*-hexane and *n*-heptane. *Catalysis Letters*, 87, 3-4, 133-142.

[57] Liu, P; Zhang, X; Yao, Y. and Wang, J. (2010). Alkaline Earth Metal Ion-exchanged β Zeolite Supported Pt Catalysts for Hydroisomerization of *n*-heptane. *Reaction Kinetics, Mechanisms and Catalysis*, 100, 217-226.

[58] Le Van Mao, R. and Saberi, M. A. (2000). Catalysts for the Hydroisomerization of *n*-heptane, Prepared According to the Concept of 'Triangular' Site Configuration (Acid/metal/desorption-transfer Promoting Sites). *Applied Catalysis A: General*, 199, 99-107.

[59] Henriques, C; Dufresne, P; Marcilly, C. and Ribeiro, R. (1986). Influence of Tin on the Stability of Sn/Pd HY Zeolites in the Hydrocracking and Hydroisomerization of *n*-Heptane. *Applied Catalysis*, 21, 169-177.

[60] Roldán, R; Beale, A. M; Sánchez-Sánchez, M; Romero-Salguero, F. J; Jiménez-Sanchidrián, C; Gómez, J. P. and Sankar, G. (2008). Effect of the Impregnation Order on the Nature of Metal Particles of Bi-functional Pt/Pd-supported Zeolite

Beta Materials and on Their Catalytic Activity for the Hydroisomerization of Alkanes. *Journal of Catalysis*, 254, 12-26.

[61] Martins, A; Silva, J. M; Ribeiro, F. R. and Ribeiro, M. F. (2006). Hydroisomerization of *n*-hexane over Pt–Ni/HBEA Using Catalysts Prepared by Different Methods. *Catalysis Letters*, 109, 1-2, 83-87.

[62] Gu, Y; Wei, R; Ren, X. and Wang, J. (2007). Cs Salts of 12-tungstophosphoric Acid Supported on Dealuminated USY as Catalysts for Hydroisomerization of *n*-heptane. *Catalysis Letters*, 113, 1-2, 41-45.

[63] Wei, R; Wang, J. and Xiao, G. (2009). Hydroisomerization of *n*-Heptane Over Cr Promoted Pt-bearing $H_3PW_{12}O_{40}$ Catalysts Supported on Dealuminated USY Zeolite. *Catalysis Letters*, 127, 360-367.

[64] Talebi, G; Sohrabi, M; Royaee, S. J; Keiski, R. L; Huuhtanen, M. and Imamverdizadeh, H. (2008). Synthesis and Activity Measurement of the Some Bifunctional Platinum Loaded Beta Zeolite Catalysts for *n*-heptane Hydroisomerization. *Journal of Industrial and Engineering Chemistry*, 14, 614-621.

[65] Wang, Q. L; Giannetto, G. and Guisnet, M. (1991). Dealumination of Zeolites: III. Effect of Extra-Framework Aluminum Species on the Activity, Selectivity, and Stability of Y Zeolites in *n*-Heptane Cracking. *Journal of Catalysis*, 130, 471-482.

[66] Remy, M. J; Stanica, D; Poncelet, G; Feijen, E. J. P; Grobet, P. J; Martens, J. A. and Jacobs, P. A. (1996). Dealuminated H-Y Zeolites: Relation between Physicochemical Properties and Catalytic Activity in Heptane and Decane Isomerization. *Journal of Physical Chemistry*, 100, 12440-12447.

[67] Vaarkamp, M; Reesink, B. H. and Berben, P. (1998). *Process for Hydrogenation, Hydroisomerization and/or Hydrodesulfurization of a Sulfur Contaminant Containing Feedstock*. International Patent, WO 98/35754.

[68] Smith, J. M. (1981). *Chemical Engineering Kinetics.* 3rd edition. Singapore: McGraw-Hill, Inc. p. 355.

[69] Simon, L. J; van Ommen, J. G; Jentys, A. and Lercher, J. A. (2002). Sulfur Tolerance of Pt/mordenites for Benzene Hydrogenation: Do Brønsted Acid Sites Participate in Hydrogenation? *Catalysis Today*, 73, 105-112.

[70] Simon, L. J; van Ommen, J. G; Jentys, A. and Lercher, J. A. (2001). Sulfur-Tolerant Pt-Supported Zeolite Catalysts for Benzene Hydrogenation: I. Influence of the Support. *Journal of Catalysis*, 201, 60-69.

[71] Simon, L. J; van Ommen, J. G; Jentys, A. and Lercher, J. A. (2001). Sulfur-Tolerant Pt-Supported Zeolite Catalysts for Benzene Hydrogenation: II. Influence of Cation Exchange Level for Pt/MOR-Based Catalysts. *Journal of Catalysis*, 203, 434-442.

[72] Romero, M; Perot, G; Gueguen, C. and Guisnet, M. (1981). Improvement by Sulphur of the Hydroisomerization Selectivity of Platinum-Mordenite Catalysts. *Applied Catalysis*, 1, 273-275.

[73] Arribas, M. A; Márquez, F. and Martínez, A. (2000). Activity, Selectivity, and Sulfur Resistance of $Pt/WO_x–ZrO_2$ and Pt/Beta Catalysts for the Simultaneous Hydroisomerization of *n*-Heptane and Hydrogenation of Benzene. *Journal of Catalysis*, 190, 309-319.

[74] Guisnet, M. and Magnoux, P. (2001). Organic Chemistry of Coke Formation. *Applied Catalysis A: General*, 212, 83-96.

[75] Gallezot, P; Leclercq, C; Guisnet, M. and Magnoux, P. (1988). Coking, Aging, and Regeneration of Zeolites: VII. Electron Microscopy and EELS Studies of External Coke Deposits on UHSY, H-OFF, and H-ZSM-5 Zeolites. *Journal of Catalysis*, 114, 100-111.

[76] Guisnet, M; Costa, L. and Ribeiro, F. R. (2009). Prevention of Zeolite Deactivation by Coking. *Journal of Molecular Catalysis A: Chemical*, 305, 69-83.

[77] Magnoux, P; Cartraud, P; Mignard, S. and Guisnet, M. (1987). Coking, Aging, and Regeneration of Zeolites: II. Deactivation of HY Zeolite During *n*-Heptane Cracking. *Journal of Catalysis*, 106, 235-241.

[78] Magnoux, P. and Guisnet, M. (1988). Coking, Aging, and Regeneration of Zeolites: VI. Comparison of the Rates of Coke Oxidation of HY, H-Mordenite, and HZSM-5. *Applied Catalysis*, 38, 341-352.

[79] Ribeiro, F. R; Guisnet, M. and Marcilly, C. (1985). Influence of Coke on the Kinetics of *n*-Hexane Hydroisomerization on Platinum HY Catalysts. *Applied Catalysis*, 13, 281-288.

[80] Denayer, J. F; Baron, G. V; Souverijns, W; Martens, J. A. and Jacobs, P. A. (1997). Hydrocracking of *n*-Alkane Mixtures on Pt/H-Y Zeolite: Chain Length Dependence of the Adsorption and the Kinetic Constants. *Industrial & Engineering Chemistry Research*, 36, 3242-3247.

[81] Van de Runstraat, A; Kamp, J. A; Stobbelaar, P. J; Van Grondelle, J; Krijnen, S. and Van Santen, A. (1997). Kinetics of Hydro-isomerization of *n*-Hexane over Platinum Containing Zeolites. *Journal of Catalysis*, 171, 78-84.

[82] Froment, G. F. (1987). Kinetics of the Hydroisomerization and Hydrocracking of Paraffins on a Platinum Containing Bifunctional Y-Zeolite. *Catalysis Today*, 1, 455-473.

[83] Matsuda, T; Kodama, H; Sakagami, H. and Takahashi, N. (2003). Comparison of the Catalytic Properties of H_2-reduced Pt/MoO_3 and of Pt/zeolites for the Conversions of Pentane and Heptane. *Applied Catalysis A: General*, 248, 269-278.

[84] Holló, A; Hancsók, J. And Kalló, D. (2002). Kinetics of Hydroisomerization of C_5-C_7 Alkanes and Their Mixtures over Platinum Containing Mordenite. *Applied Catalysis A: General*, 229, 93-102.

[85] Kumar, H. and Froment, G. F. (2007). A Generalized Mechanistic Kinetic Model for the Hydroisomerization and Hydrocracking of Long-Chain Paraffins. *Industrial & Engineering Chemistry Research*, 46, 4075-4090.

[86] Thybaut, J. W; Marin, G. B; Baron, G. V; Jacobs, P. A. and Martens, J. A. (2001). Alkene Protonation Enthalpy Determination from Fundamental Kinetic Modeling of Alkane Hydroconversion on Pt/H–(US)Y-Zeolite. *Journal of Catalysis*, 202, 324-339.

[87] Fúnez, A; Thybaut, J. W; Marin, G. B; Sánchez, P; De Lucas, A. and Valverde, J. L. (2008). Assessment of Dominant Factors Affecting Liquid Phase Hydroisomerization on Bifunctional Zeolites. *Applied Catalysis A: General*, 349, 29-39.

[88] Denayer, J. F. M; Ocakoglu, R. A; Huybrechts, W; Dejonckheere, B; Jacobs, P; Calero, S; Krishna, R; Smit, B; Baron, G. V. and Martens, J. A. (2003). High-pressure Liquid Phase Hydroconversion of Heptane/nonane Mixtures on Pt/H-Y Zeolite Catalyst. *Journal of Catalysis*, 220, 66-73.

[89] Denayer, J. F. M; De Jonckheere, B; Hloch, M; Marin, G. B; Vanbutsele, G; Martens, J. A. and B., Gino V. (2002). Molecular Competition of C_7 and C_9 *n*-Alkanes in Vapour- and Liquid-Phase Hydroconversion over Bifunctional Pt–USY Zeolite Catalysts. *Journal of Catalysis*, 210, 445-452.

[90] Saberi, M. A. and Le Van Mao, R. (2003). Comparative Study of Kinetic Behaviour of the Bifunctional and Trifunctional Catalysts in the Hydroisomerization of *n*-Heptane. *Applied Catalysis A: General*, 242, 139-150.

[91] Denayer, J. F. M; Martens, J. A; Jacobs, P. A; Thybaut, J. W; Marin, G. B. and Baron, G. V. (2003). Influence of the Zeolite Composition on the Hydro-

isomerisation and Hydrocracking of Alkanes on Pt/USY Zeolites: Modelling of the Reaction Kinetics Using an Adsorption-reaction Approach. *Applied Catalysis A: General*, 246, 17-28.

[92] Martens, G. G; Marin, G. B; Martens, J. A; Jacobs, P. A. and Baron, G. V. (2000). A Fundamental Kinetic Model for Hydrocracking of C_8 to C_{12} Alkanes on Pt/US-Y Zeolites. *Journal of Catalysis*, 195, 253-267.

[93] Martens, G. G. and Marin, G. B. (2001). Kinetics for Hydrocracking Based on Structural Classes: Model Development and Application. *AIChE Journal*, 47:7, 1607-1622.

[94] Martens, G. G; Thybaut, J. W. and Marin, G. B. (2001). Single-Event Rate Parameters for the Hydrocracking of Cycloalkanes on Pt/US-Y Zeolites. *Industrial & Engineering Chemistry Research*, 40, 1832-1844.

[95] Denayer, J. F; Baron, G. V; Vanbutsele, G; Jacobs, P. A. and Martens, J. A. (1999). Modeling of Adsorption and Bifunctional Conversion of *n*-alkanes on Pt/H-ZSM-22 Zeolite Catalyst. *Chemical Engineering Science*, 54, 3553-3561.

CHAPTER FOUR
EXPERIMENTAL

4.1 Introduction

The objective of hydroisomerizing n-heptane is to maximize the production of octane boosting isomers, which results in an increased octane number of the output stream, enabling the blending of more heavy naphtha into the gasoline pool at refineries. The utilization of more heavy naphtha into the gasoline pool increases the refinery's profitability margin due to the high price of gasoline. The research octane numbers (RON) of the nine heptane isomers are listed in Table 3-1. From the table, it can be seen that increasing the branching in n-heptane isomers contributes to an increased RON.

Initially, hydroisomerization runs at a readily-available glass-pyrex atmospheric reactor were started in year 1 of the PhD program. To enable testing at higher pressures, a stainless-steel hydroisomerization unit with the capability of operating at up to 20 bars was planned, built, troubleshooted, and commissioned through year 2 of the program. In the following sections, an overview about the atmospheric and pressure units is given, in addition to experimental procedures and product analysis techniques.

4.2 Atmospheric Hydroisomerization Unit

A piping and instrumentation diagram (P&ID) of the atmospheric reaction rig is shown in Figure 4-1. The design specifications for the hydroisomerization unit are shown in Table 4-1.

Table 4-1. Design specifications for the atmospheric hydroisomerization unit.

Design Parameter	**Specification**
Design/Operating Pressure	1 bar
Design Temperature	600^{o}C
Operating Temperature	170 – 500^{o}C
nC_7 Flow Rate	0.125 – 0.5 ml/min
H_2/N_2 Flow Rate	100 – 1000 ml/min
Air Flow Rate	0 – 200 ml/min

Figure 4-1. Piping & Instrumentation Diagram (P&ID) of the atmospheric hydroisomerization unit.

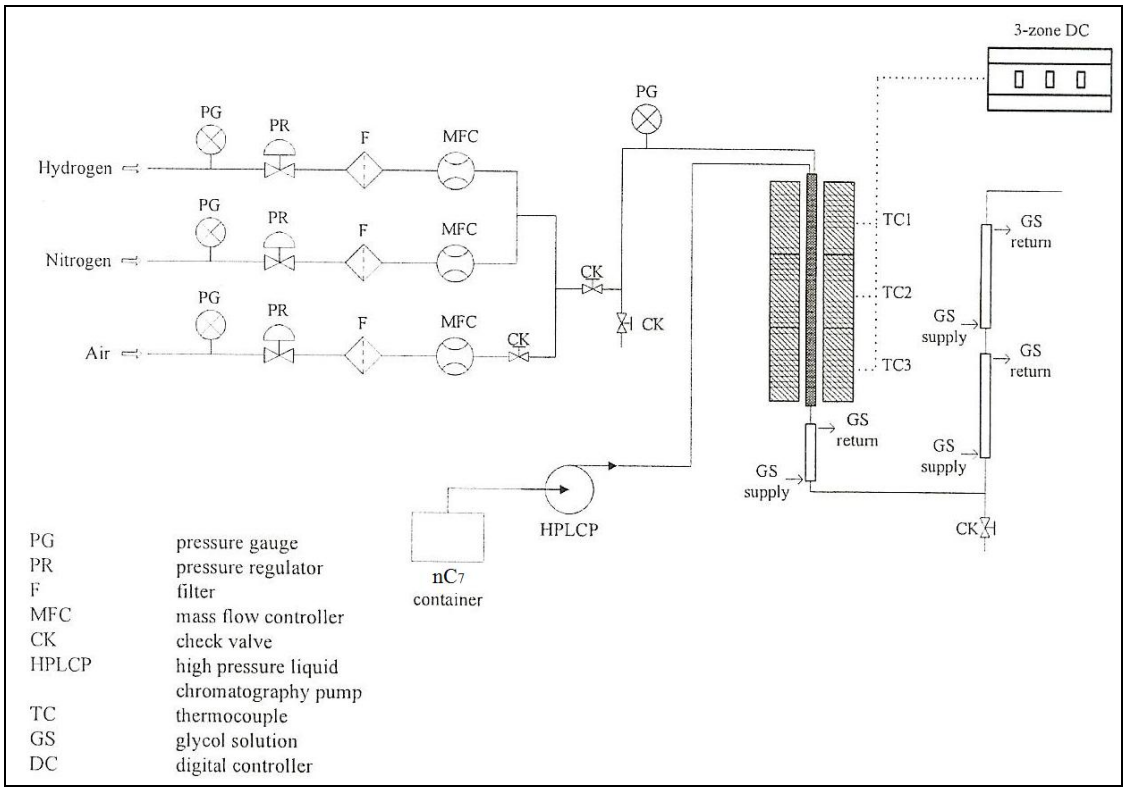

The design of the unit micro-reactor and its specifications are shown in Table 4-2 and Figure 4-2, respectively.

Table 4-2. Specifications of the atmospheric reactor.

Description	Specification
Material	Glass-pyrex
Reactor Total Length	60 cm
External Diameter	15.1 mm
Internal Diameter	11.2 mm
Thermowell Length	55 cm
Thermowell External Diameter	4 mm
Thermowell Internal Diameter	2 mm
Reactor Cross-sectional Area	0.825 cm^2
Reactor Total Volume	49.5 cm^3
Maximum Operating Temperature	550^oC
Acceptable Working Pressure at 550^oC	14.6 psi

Figure 4-2. Design of the hydroisomerization atmospheric reactor.

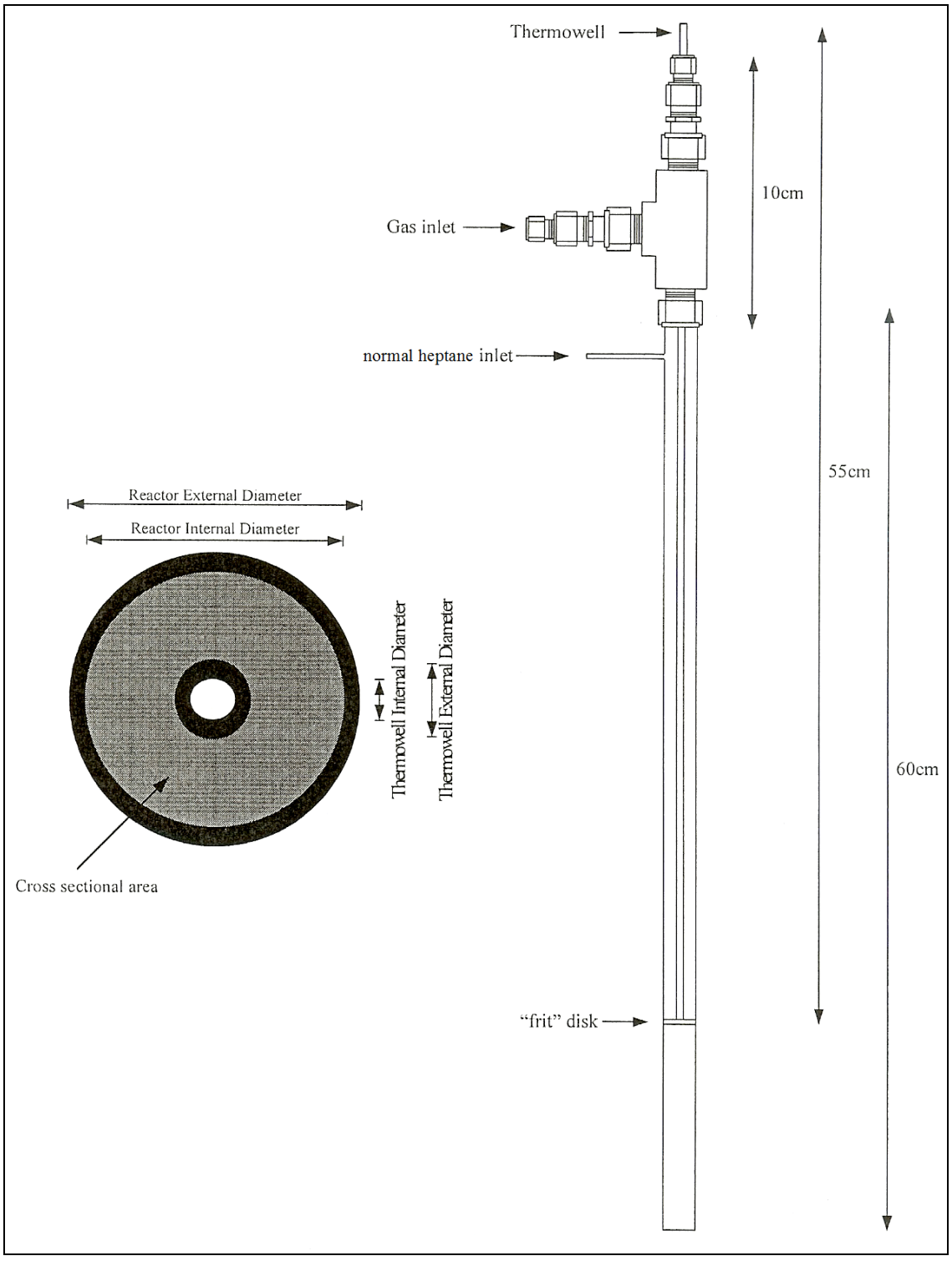

The gas-liquid separation section of the unit is shown in Figure 4-3. The purpose of this section is to separate the light ends from the product stream and recover heptane and its isomers with the liquid product. This is accomplished by circulating a cooled solution of water and ethylene glycol around the double-wall condenser tube.

Figure 4-3. Liquid-gas separation section.

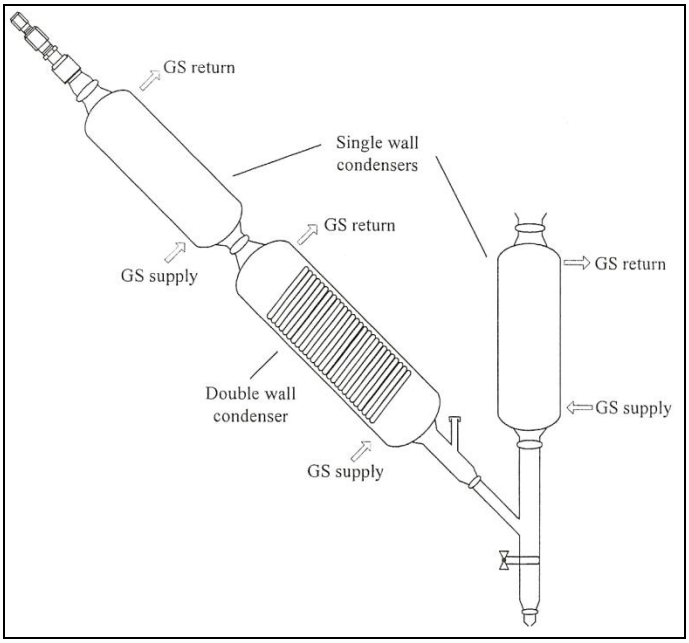

4.3 Pressure Hydroisomerization Unit

The specifications of the hydroisomerization pressure unit are as follows:

Table 4-3. Specifications of the pressure hydroisomerization unit.

Design Parameter	**Specification**
Design Pressure	50 bar
Design Temperature	650ºC
Operating Pressure	1-20 bar
Operating Temperature	170-500ºC
nC_7 Flow Rate	0.125-0.5 ml/min
H_2 Flow rate	100-1000 ml/min
N_2/Air Flow rate	50-500 ml/min
Reactor Total Volume	43.7 ml

Figure 4-4 shows the Piping & Instrumentation Diagram (P&ID) of the hydroisomerization pressure unit.

Figure 4-4. Piping & Instrumentation Diagram (P&ID) for the hydroisomerization pressure unit.

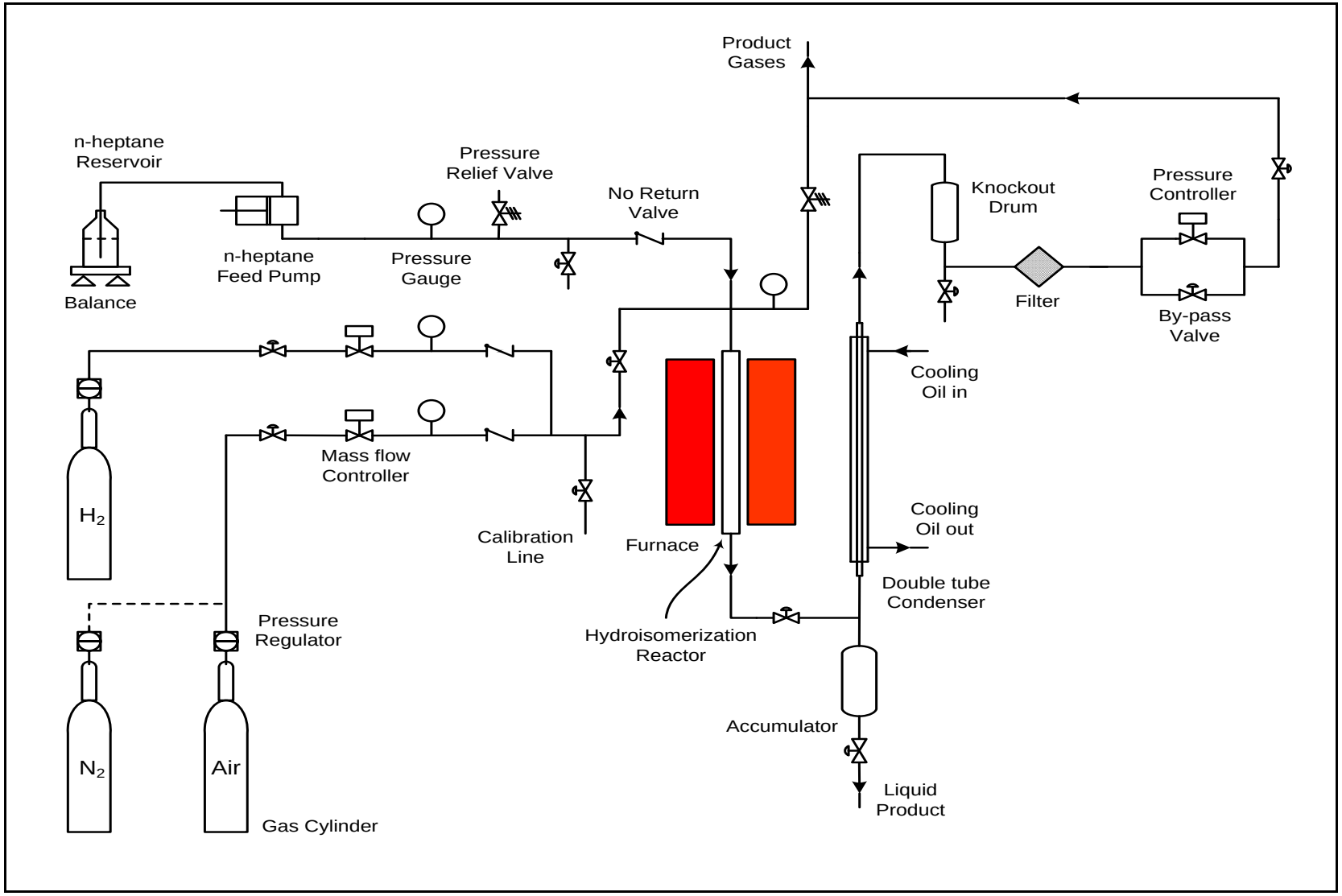

The unit consists of five modules: gas supply module, normal heptane feeding module, reactor module, separation module, and pressure controlling module. Detailed information about part specifications and manufacturers as well as the total cost estimation of the unit are given in the bill of materials in Appendix A.

The gas supply module provides the unit with highly pressurized hydrogen, nitrogen, or air. The three gases are delivered to the unit from highly pressurized gas cylinders (typically 150 bar). Each gas pressure is decreased to the desired pressure by using a pressure regulator while the flow rate is controlled by a mass flow controller. At the end of each gas line, a check valve is located to prevent any by-product gases from contaminating the gas supply module.

The normal heptane feeding module primarily consists of a feed tank, a balance, and an HPLC pump. The feed tank has a capacity of 1.0 L and is placed on the balance (accurate to 0.01 g) to monitor the feed flow rate. Normal heptane is pumped into the reactor module by an HPLC pump (Gilson 305 piston pump) that is capable of handling the pressure required (up to 15 bar).

The reactor module is the most critical zone in the unit. The feed (normal heptane, purity 99+ wt%) and the hydrogen (BOC, purity 99.99%) are mixed before the reactor inlet. The hydrogen and nC_7 mixture passes through the reactor in a down co-current flow mode. The reactor is made of stainless steel (SS-316) and its design specifications are shown in Table 4-4 and Figure 4-5. The reactor module is equipped with a built-in furnace that consists of three independently controlled heating zones. Each heating zone has an independent K-type thermocouple to measure the reactor skin temperature. A fourth thermocouple, connected to a power cut-off policeman, is installed in order to set a temperature limit after which the policeman cuts the power off the oven to prevent any temperature run away. The catalyst bed temperature is monitored by a thermocouple that is inserted into the reactor through a ceramic thermowell.

Table 4-4. Specifications of the pressure reactor.

Description	Specification
Body Material	SS-316
Reactor Total Length	64.5 cm
Reactor Bed Length	53.5 cm
External Diameter	1.27 cm
Internal Diameter	1.02 cm
Wall Thickness	0.1245 cm
Thermowell Diameter	0.3175 cm
Reactor Total Volume	43.70 ml
Reactor Bed Volume (Total Vol. – Themowell Vol.)	39.92 ml
Maximum Operating Temperature	550ºC
Allowable Working Pressure @ 550ºC	30 bar

The separation module is designed to achieve an efficient separation of hydrogen from the liquid products, taking into account the poor solubility of hydrogen in the liquid phase. The module starts with a high-pressure separator above which a double-tube co-current-flow heat exchanger is located to condense the vapour that might escape from the separator. The degree of cooling in the heat exchanger is controlled by the temperature of a cooling bath that circulates sub-cooled silicon oil from and to the the shell of the double-tube heat exchanger in a counter-current configuration to the product stream. The high-pressure separator is equipped with two valves in series for sampling.

The pressure controlling module starts with a knock-out vessel and an inline filter (with 7 micron mesh) to condense any traces of vapour that might escape from the heat exchanger. An automated pressure control valve and a pressure gauge are located afterwards to control and to monitor the system pressure. The pressure controlling module is equipped with a by-pass line (connected to vent) for emergency cases. In addition, for operational safety two relief valves set at 30 bar were installed; one connected to the liquid flow line and the other connected to the outlet of the pressure control valve.

Figure 4-5. Pressure reactor design.

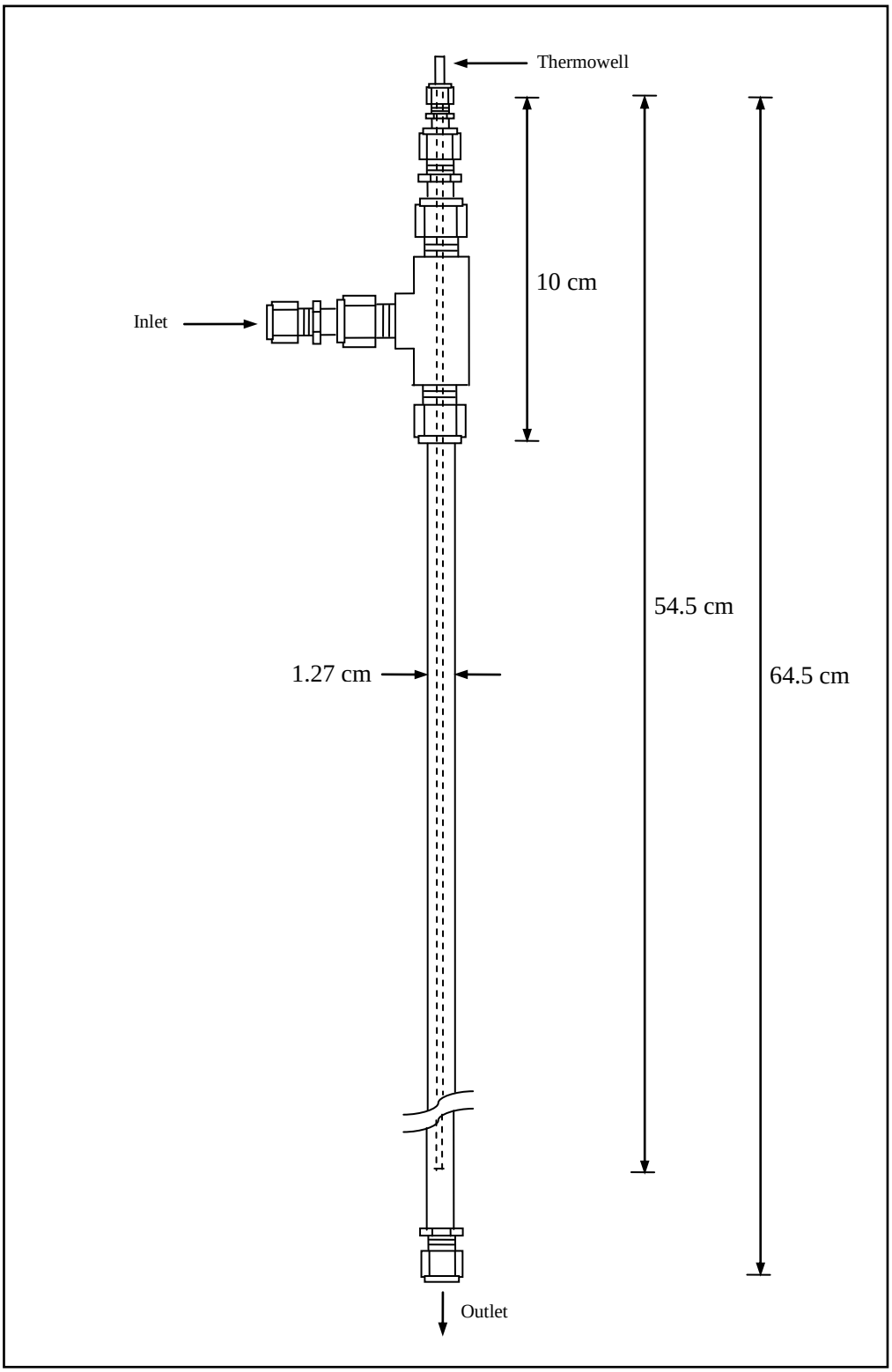

4.4 Pressure Unit Calibration & Commissioning

Before operating the unit, it has been commissioned by calibrating the mass flow controllers, the HPLC pump, and the thermocouple. In addition, the furnace stability has been checked and several leak tests were conducted.

4.4.1 Mass Flow Controllers

The calibration of the hydrogen mass flow controller is shown in Table 4-5 and Figure 4-6. The actual flow was measured by connecting a glass bubble meter of 0 – 100 ml capacity to the gas outlet and taking the average of 3 readings of the flow using a stopwatch. The same procedure was performed for the air/nitrogen mass flow controller and the results are shown in Tables 4-6 and 4-7 and Figures 4-7 and 4-8. It can be noticed from the figures that the response of mass flow to the valve opening is linear, as the R^2 values are very close to 1. In addition, without calibration considerable error in flows would have occurred, since the used mass flow controllers were not brand new and have been used before. Upon calibration, the required openings to achieve the desired flows were determined and verified using the bubble meter.

Table 4-5. Calibration of H_2 mass flow controller (range: 0 – 1000 ml/min).

H_2 Desired Flow (ml/min)	Valve Opening (%)	Actual flow (ml/min)	% Error	Required Opening to Achieve Desired Flow (%)
0	0	0	0.0	0.3
100	10	126.72	26.7	8.2
200	20	249.48	24.7	16.1
300	30	373.83	24.6	24.0
400	40	495.87	24.0	31.9
500	50	628.27	25.7	39.7
600	60	769.23	28.2	47.6
700	70	869.57	24.2	55.5
800	80	1008.4	26.1	63.4
900	90	1132.08	25.8	71.3
1000	100	1276.6	27.7	79.2
187.5				**15.1**
375				**29.9**
750				**59.5**

Figure 4-6. Calibration of H_2 mass flow controller (range: 0 – 1000 ml/min).

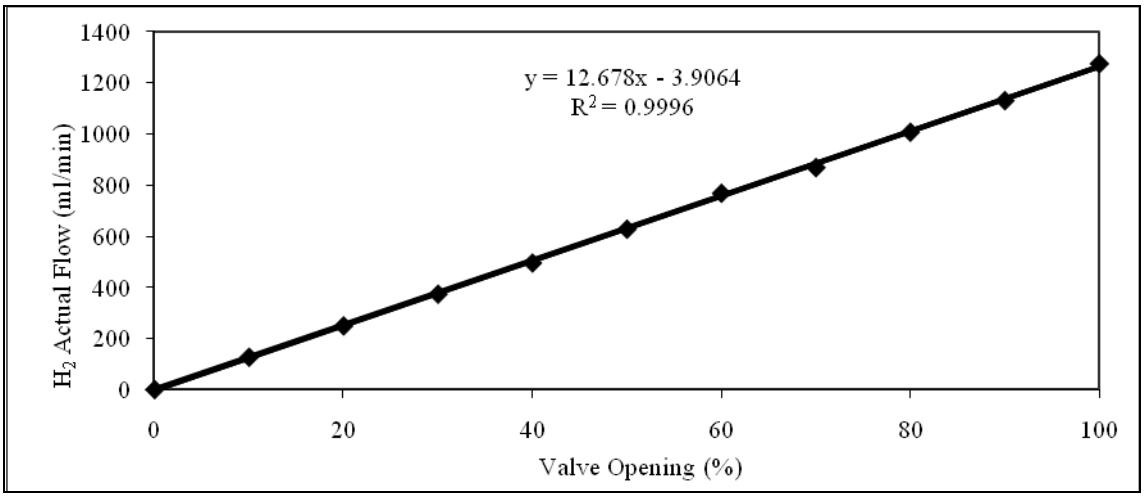

Table 4-6 Calibration of N_2 mass flow controller (range: 0 – 500 ml/min).

N_2 Desired Flow (ml/min)	Valve Opening (%)	Actual flow (ml/min)	% Error	Required Opening to Achieve Desired Flow (%)
0	0	0	0.0	-0.6
50	10	58.94	17.9	8.0
100	20	117.5	17.5	16.6
150	30	181.27	20.8	25.2
200	40	235.29	17.6	33.8
250	50	295.56	18.2	42.5
300	60	358.21	19.4	51.1
350	70	416.67	19.0	59.7
400	80	466.93	16.7	68.3
450	90	526.32	17.0	76.9
500	100	574.16	14.8	85.6

Figure 4-7. Calibration of N_2 mass flow controller (range: 0 – 500 ml/min).

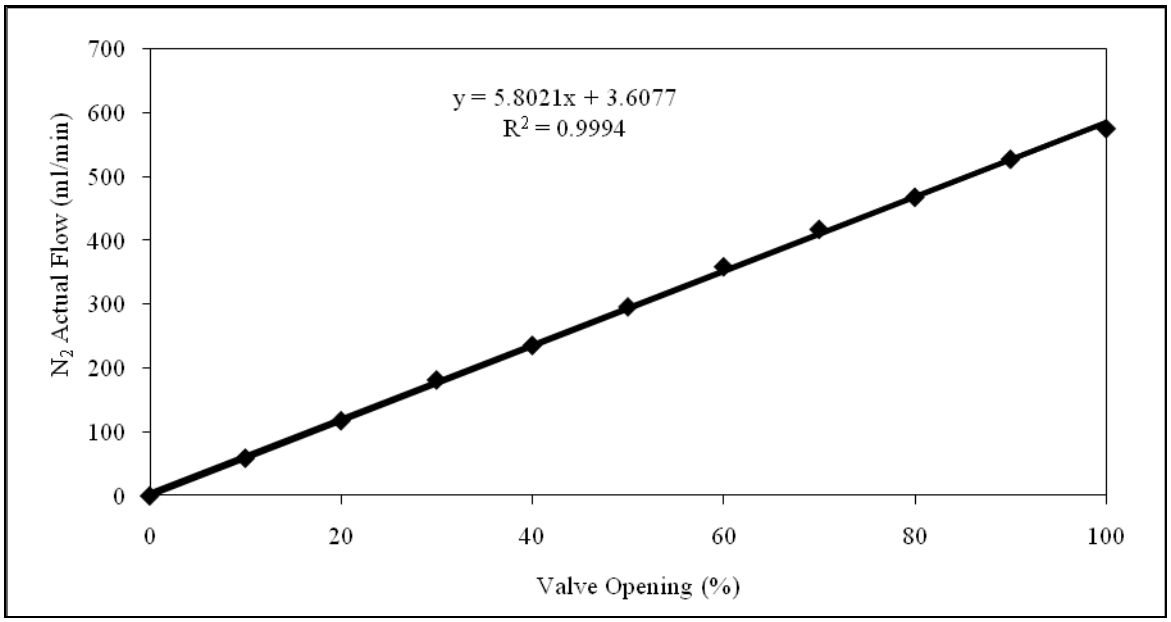

Table 4-7. Calibration of air mass flow controller (range: 0 – 500 ml/min).

N_2 Desired Flow (ml/min)	Valve Opening (%)	Actual flow (ml/min)	% Error	Required Opening to Achieve Desired Flow (%)
0	0	0	0.0	0.0
50	10	59.55	19.1	8.3
100	20	120.97	21.0	16.6
150	30	181.00	20.7	24.9
200	40	239.04	19.5	33.3
250	50	301.13	20.5	41.6
300	60	360.36	20.1	49.9
350	70	422.54	20.7	58.2
400	80	480.00	20.0	66.6
450	90	540.54	20.1	74.9
500	100	600.00	20.0	83.2

Figure 4-8. Calibration of air mass flow controller (range: 0 – 500 ml/min).

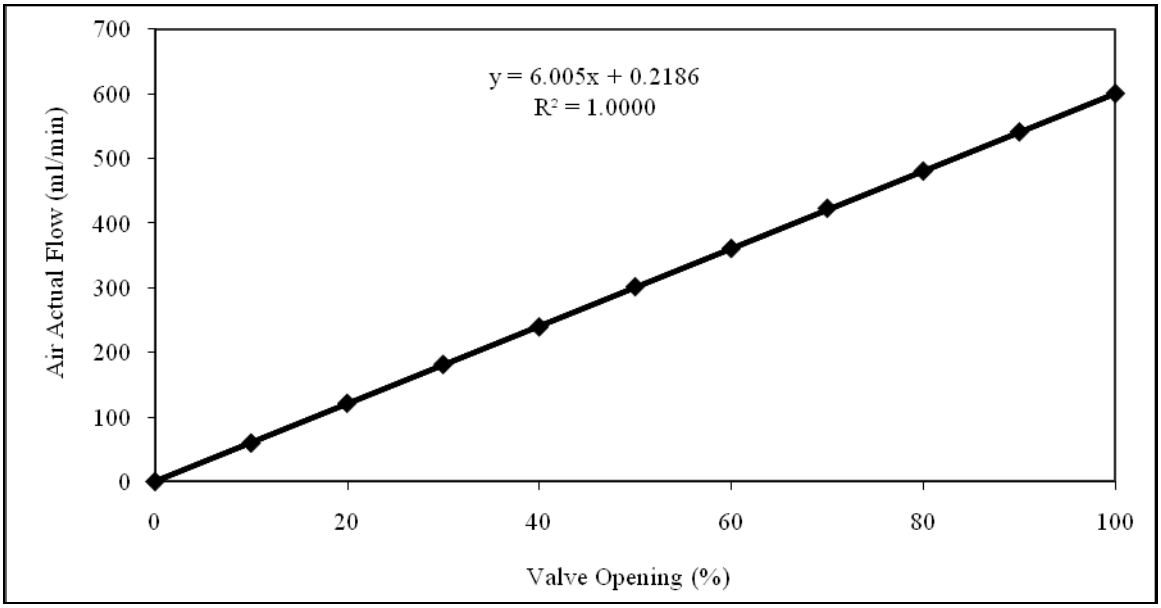

4.4.2 HPLC Pump

For the calibration of the HPLC pump, which was used to feed nC_7 into the reactor at pressures of 1 – 15 bar, the pump was operated at each sitting for the duration of one hour, and the variation in the weight of the feed tank was used to calculate the actual volume pumped. Table 4-8 and Figure 4-9 show the results of this calibration. Despite the large error found with the pump setting of 0.3325 ml/min, errors from the other settings were minimal and conformed to a large degree to the trendline in Figure 4-9. Therefore, the trendline equation was utilized to predict pump settings equivalent to the desired flows 7.5, 15, and 30 ml/hr.

Table 4-8. Calibration of nC_7 HPLC Pump.

nC_7 Desired Flow (ml/hr)	Pump Setting (ml/min)	Actual flow (ml/hr)	% Error	Required Setting to Achieve Desired Flow (ml/min)
2.55	0.0425	2.545	0.2	0.0330
5.1	0.085	5.263	3.2	0.0761
7.5	0.125	7.753	3.4	**0.1167**
10.05	0.1675	10.336	2.8	0.1598
15	0.25	15.702	4.7	**0.2435**
19.95	0.3325	23.757	19.1	0.3273
25.05	0.4175	23.945	4.4	0.4135
30	0.5	29.02	3.3	**0.4973**

Figure 4-9. Calibration of nC_7 HPLC Pump.

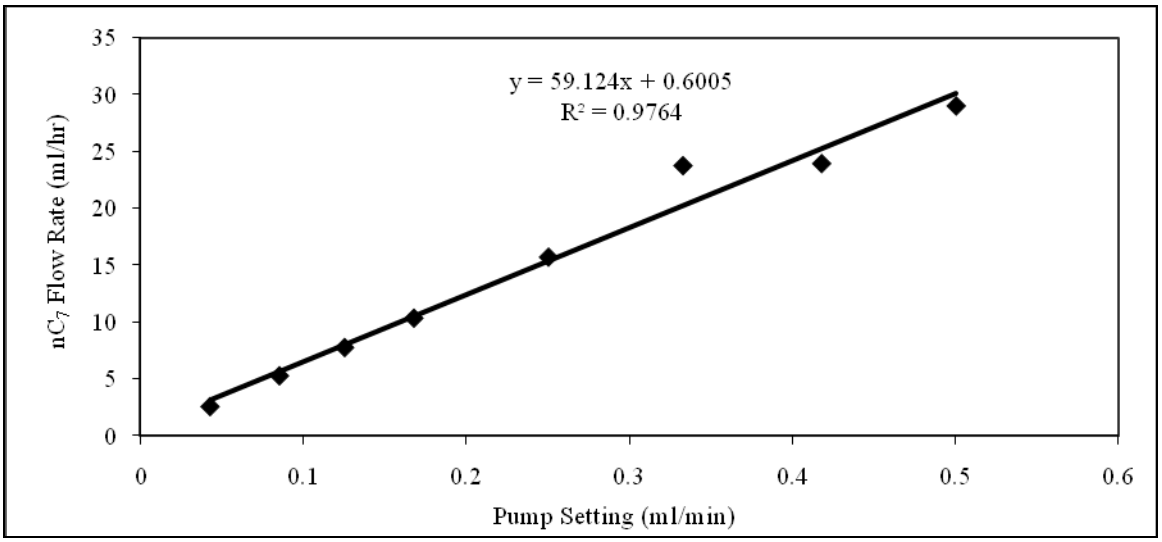

4.4.3 Oven

The temperature profiles were measured across the oven length (35 cm) from the reactor inside at temperature settings of 100, 150, 200, 250, 300, 400, and 500°C in order to determine the oven stable zone, so that the catalysts are packed in that zone during experimental runs. Figure 4-10 shows the temperature profiles during the oven calibration. The stable zone was found to be approximately 5 cm long (between 15 and 20 cm down the oven).

Figure 4-10. Temperature profiles during the oven calibration.

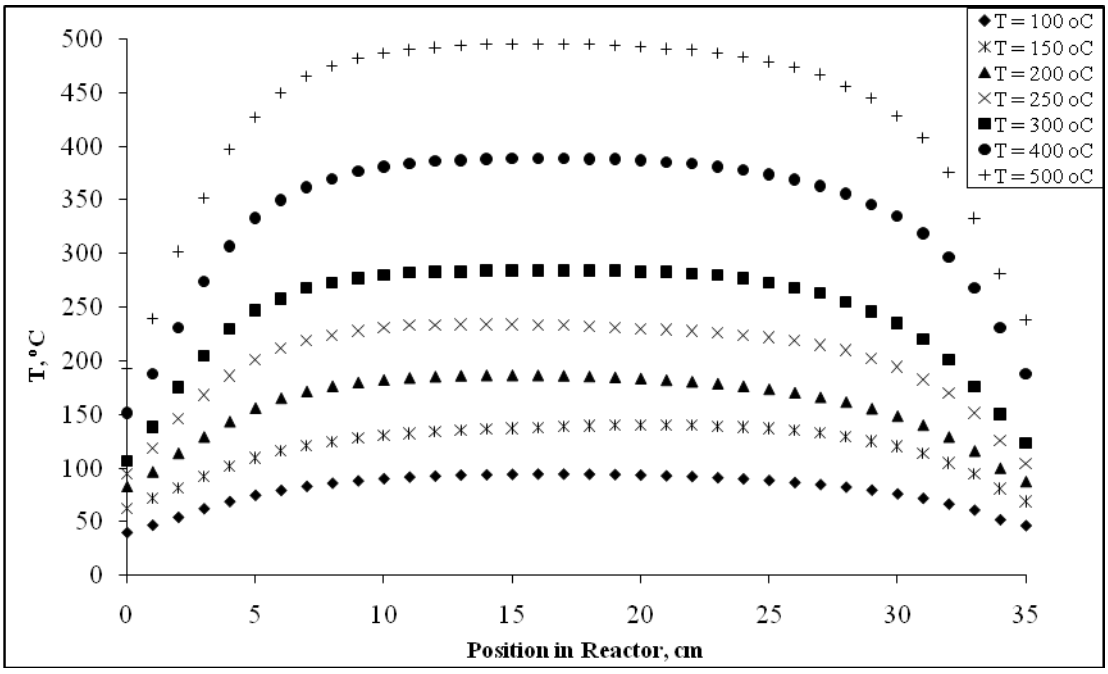

Afterwards, blank experimental runs were performed over inert glass beads that were loaded into the reactor. Normal heptane and hydrogen gas were introduced at 3 different space times (35.14, 70.6, and 140.6 kg.s/mol) chosen for real experiments, and temperature measurement were taken across the oven stable zone at different temperature control sittings in order to determine the optimum sittings which result in uniform temperature profiles in the reactor catalyst zone during experiments at temperatures from 170 to 310^{o}C and pressures of 1, 8, and 15 bar.

4.4.4 Thermocouple

The used thermocouple in taking experimental readings was a grounded 1.0 mm in diameter type K thermocouple. It was calibrated using a Varian 3400 GC oven set temperatures from 35 to 299^{o}C, while recording the thermocouple readings. Table 4-9 shows the data for the calibration along with corrected values of actual readings after using the equation generated from Figure 4-11.

Table 4-9. Thermocouple calibration data and corrected reactor temperature values of experimental readings.

Set T, ^{o}C	Thermocouple Reading, ^{o}C	Experimental Reading, ^{o}C	Corrected Reactor Value, ^{o}C
35	31.9	40	41.5
40	38	50	51.5
50	47.5	60	61.5
60	57.8	70	71.4
70	68.1	80	81.4
80	78.3	90	91.3
90	88.7	100	101.3
100	99	110	111.2
110	109.6	120	121.2
120	119.8	130	131.2
130	130	140	141.1
140	140	150	151.1
150	150	160	161.0
160	160	170	171.0
170	169.7	180	180.9
180	179.3	190	190.9
190	189.2	200	200.9
200	198.8	210	210.8
210	210	220	220.8
220	219	230	230.7
230	229	240	240.7
240	239	250	250.7
250	249	260	260.6
260	259	270	270.6
270	269	280	280.5
280	279	290	290.5
290	289	300	300.4
299	298	310	310.4

Figure 4-11. Calibration of thermocouple.

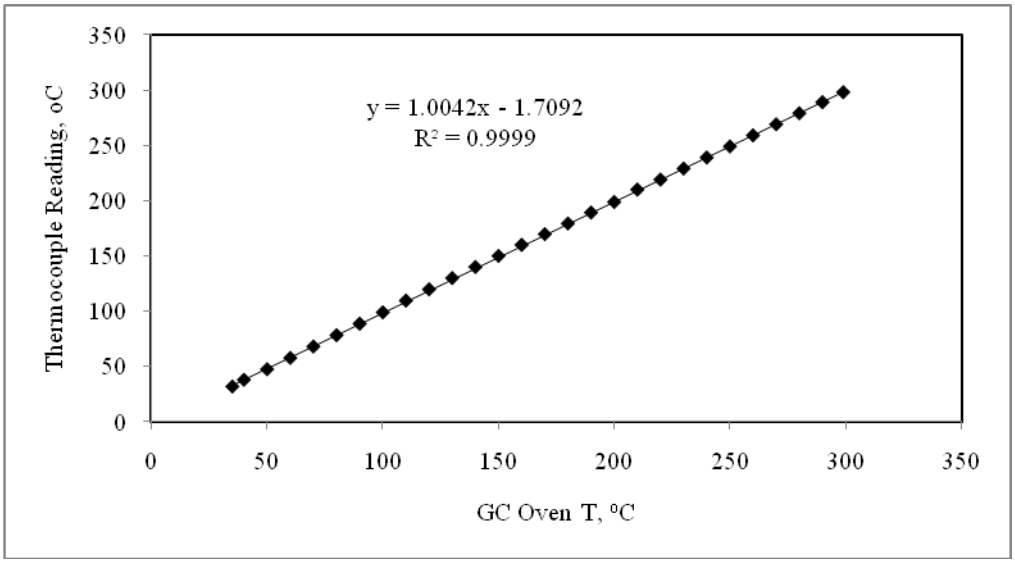

4.5 Catalyst Loading & Activation

After performing the ion-exchange, each platinum-loaded zeolite sample was pelletized and sieved in a mesh of size 40 – 60 and 2 grams were loaded into the reactor according to Figure 4-12. During the catalyst loading, glass beads of 1 – 1.3 mm in diameter were used to fill the top and bottom of the reactor, with the catalyst bed in between. Fine glass wool was used as layers separating the catalyst from the glass beads. The purpose of using glass beads is to uniformly distribute the flow over the catalytic bed and to avoid channelling. This packing procedure resulted in a catalyst bed length of 3-4 cm. After loading, the activation of the catalyst was performed in-situ by first removing ammonium from the catalyst by heating in air at 500^{o}C. Following the removal of ammonium, the catalyst was then reduced in a hydrogen atmosphere at 450^{o}C, which resulted in the conversion of platinum ions into their elemental form. The procedure undertaken to perform both calcination and reduction of the catalyst is summarized in Table 4-10. During air heating stages, a slow temperature ramping rate was used (1^{o}C/min) as fast heating rates can cause steaming and agglomeration of platinum ions, leading to poor catalyst performance [1-3].

Figure 4-12. Reactor loading.

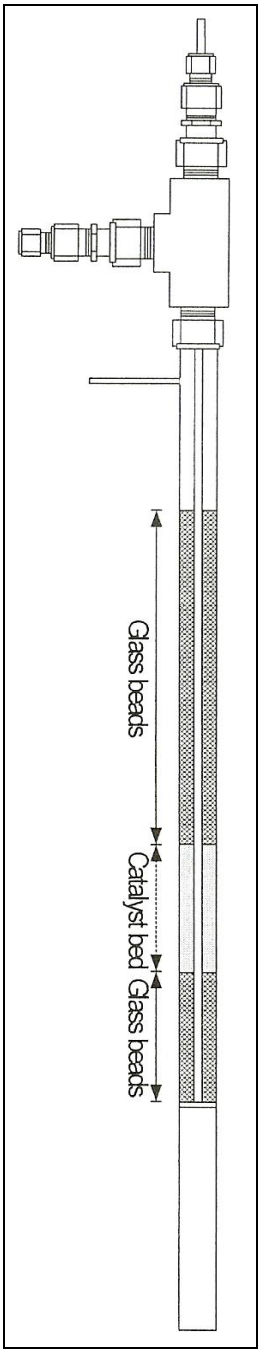

Table 4-10. Calcination and reduction conditions for the activation of the zeolite catalyst.

Gas	Air	Air	Air	H_2	H_2
T (^oC)	25 - 500	500	500 - 450	450	450 - 170
Rate/Time	1^oC/min	120 min	2^oC/min	240 min	2^oC/min
Process	Removal of NH_3 and H_2O, Pt oxide state Pt^{2+}			Reduction into elemental Pt, $Pt^{2+} \longrightarrow Pt^{(0)}$	

4.6 Experimental Procedure

The feedstock used for analysis was n-heptane with a purity of 99.33 wt% obtained from Sigma-Aldrich. The impurities present in the feedstock are mostly heptane isomers. Some physical properties of normal heptane are shown in Table 4-11.

Table 4-11. Physical properties of normal heptane.

Boiling point, ^oC	98.4
Specific gravity	0.684
Vapour pressure @ 20^oC, mmHg	4
k-value @ 1 bar	0.016
Viscosity @ 25^oC, cP	0.386
Volatility, g/l voc (w/v)	696
Total sulfur content, ppm	4.6

The optimum experimental conditions were selected after carefully reviewing the literature and determining the suitable conditions for normal heptane hydroisomerization. Table 3-3 in the previous chapter lists the common experimental conditions used in the literature for the hydroisomerization of normal alkanes. The literature indicates a useful starting point for the research for nC_7 at temperatures between 170 – 310^oC and pressures of 1 – 15 bar.

In each experiment, the required hydrogen flow was set and the temperature profile across the bed was recorded after stabilizing at the required temperature using the identified optimal oven settings. Then, nC_7 was introduced to the reactor by starting the HPLC pump at the required flow rate. For runs using the stainless-steel reactor, the system pressure was controlled using the readout and control unit.

During stability testing (or deactivation) runs, both liquid and gas product samples were taken regularly to check for deactivation until conversion was almost constant or for up to 4 days. For activity and selectivity test runs at specific temperatures, samples were first taken at one space time (W/F_o) value, then again at another after changing flow rate settings and waiting for steady state operation, then at a third, and finally at the original space time to check for short-term deactivation and repeatability. The three space times used in experiments were 35.14, 70.61, and 140.6 kg.s/mol (their calculations are shown in

Appendix C). The temperature profile across the bed was taken prior to each sample collection. Gas samples were collected through inert flexible tubing connected to the gas vent in a one-litre gas bag while the temperature profile was taken, while liquid samples were collected in a vial, had their weight checked, and then transferred into GC vials. The gas outlet flow rate was measured regularly using a bubble meter in order to perform a mass balance on the unit. The collected liquid samples were analyzed by injecting 0.2 μL into a Varian 3400 gas chromatograph (GC) with a capillary column type a 50m x 0.25mm i.d. BP-5 fitted to a flame ionization detector (FID) for experiments in the glass reactor and a CP-Sil PONA CB optimized gasoline column for experiments in the stainless-steel reactor to improve peak identification and separation. The gas analysis was performed on a Varian 3400 GC fitted with a 50m x 0.32mm i.d. PLOT Al_2O_3/KCl capillary column fitted to an FID detector. Overall hydrocarbon mass balance was always 90 ± 5%. It approached 95% mostly for runs with the highest flow rates and 85% for runs with the lowest flow rates. A number of factors could have influenced the mass balance: slight n-heptane leakage from the feed vessel, resulting in an exaggeration in the amount fed to the reactor – vapour escaping while collecting the liquid samples – liquid not draining properly from the sampling bomb upon collection – slight evaporation of the liquid sample prior to recording its weight – not accounting for the weight of coke accumulated on the catalyst during the run, since it is burnt off in between runs – error in GC analysis for both liquid and gas samples.

Catalysts USY-B, USY-C, and USY-D were tested using the atmospheric hydroisomerization unit and catalyst USY-A, USY-C, USY-D, in addition to CBV-712 and CBV-760 (obtained from Zeolyst) were tested using the purpose-built pressure unit. Properties and characterization of these catalysts are discussed in the next chapter. Overall, a total of 305 runs were conducted, including tests in which 1 wt% and 100 ppm of dimethyldisulfide (DMDS) were added to the normal heptane feed were performed on catalysts USY-D and CBV-712, respectively to study the effect of sulfur poisoning on the catalysts. On all catalysts, 1 wt% Pt loading was used.

4.7 GC Calibration

The calibration of the gas GC was done using a standard gas mixture containing 1% by volume of C_1, C_2, C_3, nC_4, iC_4, nC_5, and iC_5. Three injections of standard were made into the GC column to determine elution times of its component and their average peak area counts. Then, response factors (RFs) of each component were calculated by dividing

its mole % by its average peak area count, and are shown in Table 4-12. The RFs were used in calculating gas yields during experimental runs. Calculations of gas and liquid yields in addition to mass balance conducton are shown in Appendix C. Consequently, RFs were plotted against the carbon number of standard gas components in a log-log scale, which generated a straight trendline, as shown in Figure 4-13. Using the trendline equation from the figure, estimation of RFs for higher carbon number hydrocarbons was done and their values are shown in Table 4-12.

Table 4-12. Gas RF values for $C_1 - C_{10}$ hydrocarbons.

Component	Mol%	Peak Time, min	Average Area Count	RF
C_1	1	1.15	75380	1.3266E-05
C_2	1	1.18	139660	7.1602E-06
C_3	1	1.29	204980	4.8785E-06
iC_4	1	1.57	266300	3.7552E-06
nC_4	1	1.62	271840	3.6786E-06
iC_5	1	2.55	338660	2.9528E-06
nC_5	1	2.73	337900	2.9595E-06
C_6	1	-	-	2.5269E-06
C_7	1	-	-	2.1883E-06
C_8	1	-	-	1.9318E-06
C_9	1	-	-	1.7307E-06
C_{10}	1	-	-	1.5686E-06

Figure 4-13. A log-log scale plot of RF values versus carbon number of standard mixture components.

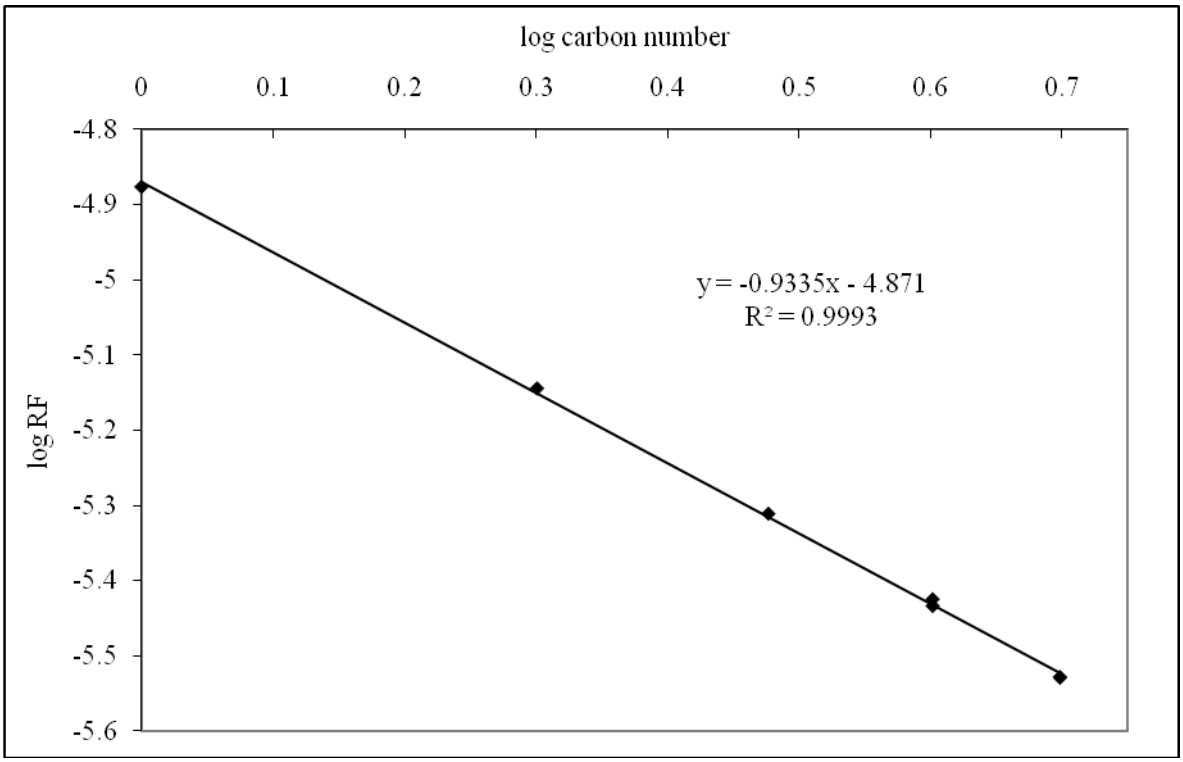

The temperature run program for the gas GC was set as follows: initial column temperature was held at 110°C for 5 minutes. Then, it was raised to 225°C using a ramp rate of 7.5°C/min. Finally, it was held at 225°C for 10 minutes. The PONA column of the liquid GC was programmed with a longer program to allow for separation of the wider range of products in the liquid phase. Its initial temperature was held at 30°C for 16 minutes. Then, it was raised to 200°C using a ramp rate of 5°C/min. Finally, it was held at 200°C for 2 minutes. Temperature programs used for both GCs are demonstrated in Figure 4-14.

Figure 4-14. Gas and liquid GC column temperature programs.

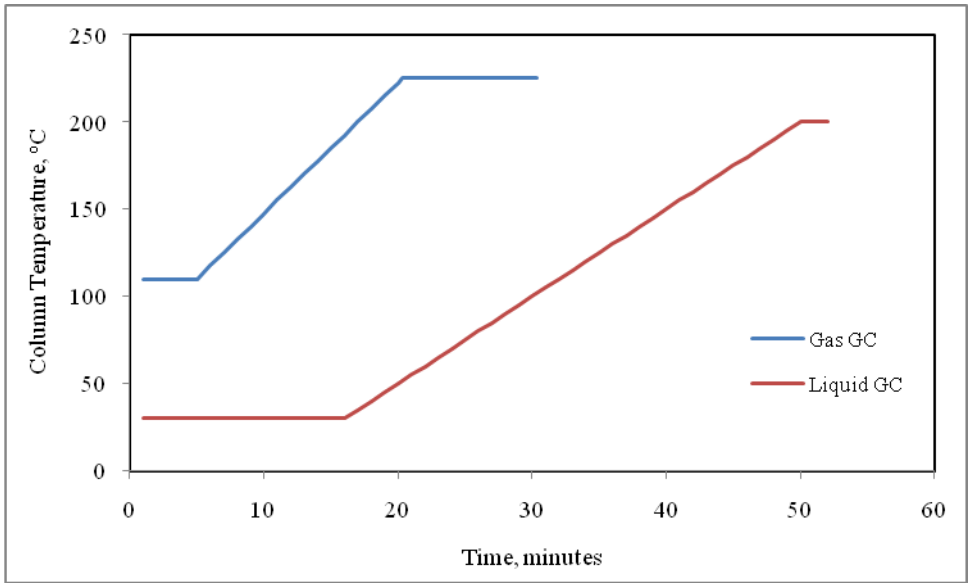

4.8 Discussion

The purpose-built stainless-steel pressure rig had a combination of newly procured parts and old used ones. Commissioning of old parts such as the mass flow controllers and the HPLC pump showed underlying errors in their settings. However, these errors were rectified during the calibration processes. On the other hand, the gas and liquid GC analysis, performed by old instruments, are possible sources of error. This is because their calibrations were done by the ESTD (External Standard) analysis method [4], which typically gives an uncertainty of 5% to the measurements. Therefore, on all conversion and yield results reported in Chapter 6 a ±5% confidence level should be assumed. For example, an overall conversion reading of 60 mol% should be regarded as 60 ± 3 mol%.

4.9 Conclusion

The availability of the glass atmospheric rig enabled carrying out experiments while the pressure rig was planned, built and commissioned. Commissioning of the pressure rig showed how some errors in readings in some parts were present, and these were avoided upon calibration of various parts. Experimantal setup and procedures were planned in such a way that ensures meaningful experimental data are generated, which allowed for a proper comparison of properties of different catalysts under various reaction conditions.

4.10 References

[1] Englen, C. W. R; Wolthuizen, J. P; van Hoof, J. H. C. and Zanbergen, H. W. in Murakima, Y; Lijima, A. and Ward. J. W. (Eds). (1986). *Studies in Surface Science and Catalysis: New Developments in Zeolite Science and Technology, Proceedings to the 7th International Zeolite Conference*, 28, 709.

[2] Reagan, W. J; Chester, A. W. and Kerr, G. T. (1991). Studies of the Thermal Decomposition and Catalytic Properties of Some Platinum and Palladium Ammine Zeolites. *Journal of Catalysis*, 69, 89-100.

[3] Holmes, S. M. (1994). *The formation of coke during hydrocarbon conversion over ZSM-5 catalysts*. PhD Thesis, UMIST, Manchester.

[4] Naddaf, A. and Bella, J. (2000). Comparison of Quantitative Analytical Methods in Headspace Gas Chromatography of Residual Solvents. *Chromatographia Supplement*, 51, 241-248.

CHAPTER FIVE

CATALYST CHARACTERIZATION & PREPARATION

5.1 Introduction

In this chapter, the commercial and in-house USY catalysts used are characterized and the catalyst preparation for reaction is covered as well as the synthesis of zeolite Y catalyst samples in their sodium form. Characterization performed in-house is discussed in section 5.4 with a brief description of the characterization techniques and their instruments.

5.2 Properties of Available in-house & Commercial USY Catalysts

The in-house ultrastable zeolite Y catalysts were generated previously using a pilot steaming rig at Crosfield as shown in Figure 5-1. Ion exchange conditions were as follows: 1 gram of zeolite was ion exchanged with 20 ml of a 1.5 molar solution of $(NH_4)SO_4$. USY-A was prepared by ion exchanging an originally steamed at 425^{o}C zeolite Y parent sample (Y-1) to reduce its soda content from 2.5 to 0.57 wt%, followed by steaming. USY-B, USY-C, and USY-D were generated by further ion exchanging the 0.57 wt% soda sample with MNH_4NO_3 down to 0.1 wt% soda, followed by mild, medium, and severe steaming, respectively. All four samples were ion exchanged into their ammonium form after steaming. The full procedures for synthesis, steaming, and ion-exchange of these materials have been reported previously by Crosfield [1]. Commercial samples CBV-712 and CBV-760 were obtained from Zeolyst International during the course of this thesis.

Characterization was checked against literature and externally to confirm previously reported data for in-house catalysts USY-A to USY-D. Where possible, the characterized catalysts were cross-checked with supplier's information, reported literature, and commercial laboratories. Properties of in-house catalysts and commercial ones determined by outside laboratories, and by MCA and SABIC in 2009, and reported previously are displayed in Table 5-1. Properties of pure NaY zeolite were also included for comparison. As expected, the steaming treatment of the four in-house catalysts caused shrinkage of the unit cell and increasingly reduced the crystallinity of the catalyst structure

with increasing severity of steaming. Overall bulk Si/Al ratio did not change much as expected, since Al atoms once knocked out of the framework remain in the structure. This is in agreement with the calculated values for extra framework aluminium atoms per unit cell, being the highest for USY-D. The steaming treatment also resulted in a reduced surface area of the catalysts and a greater presence of mesopores, which can be inferred from the increasing average pore diameters determined by N_2 isotherms. Catalysts CBV-712 and CBV-760, both acid-leached after steaming treatments, have higher bulk Si/Al ratios and a much lower calculated extra framework Al species per unit cell, indicating the removal of Al species from the unit cell. However, CBV-712, having a similar framework Si/Al ratio to that of USY-D, has a similar level of crystallinity and surface area to USY-D, although the method of determining the crystallinity on the CBV-712 sample is unknown. In addition, the low average pore diameter of CBV-760 in spite of the high degree of dealumination it underwent suggests that most of the framework dealumination occurred by acid leaching, since the steaming would increase the average pore diameter in a pronounced way, as can be noticed with the four USY in-house catalysts.

Figure 5-1. Generation procedure used for in-house USY samples [1].

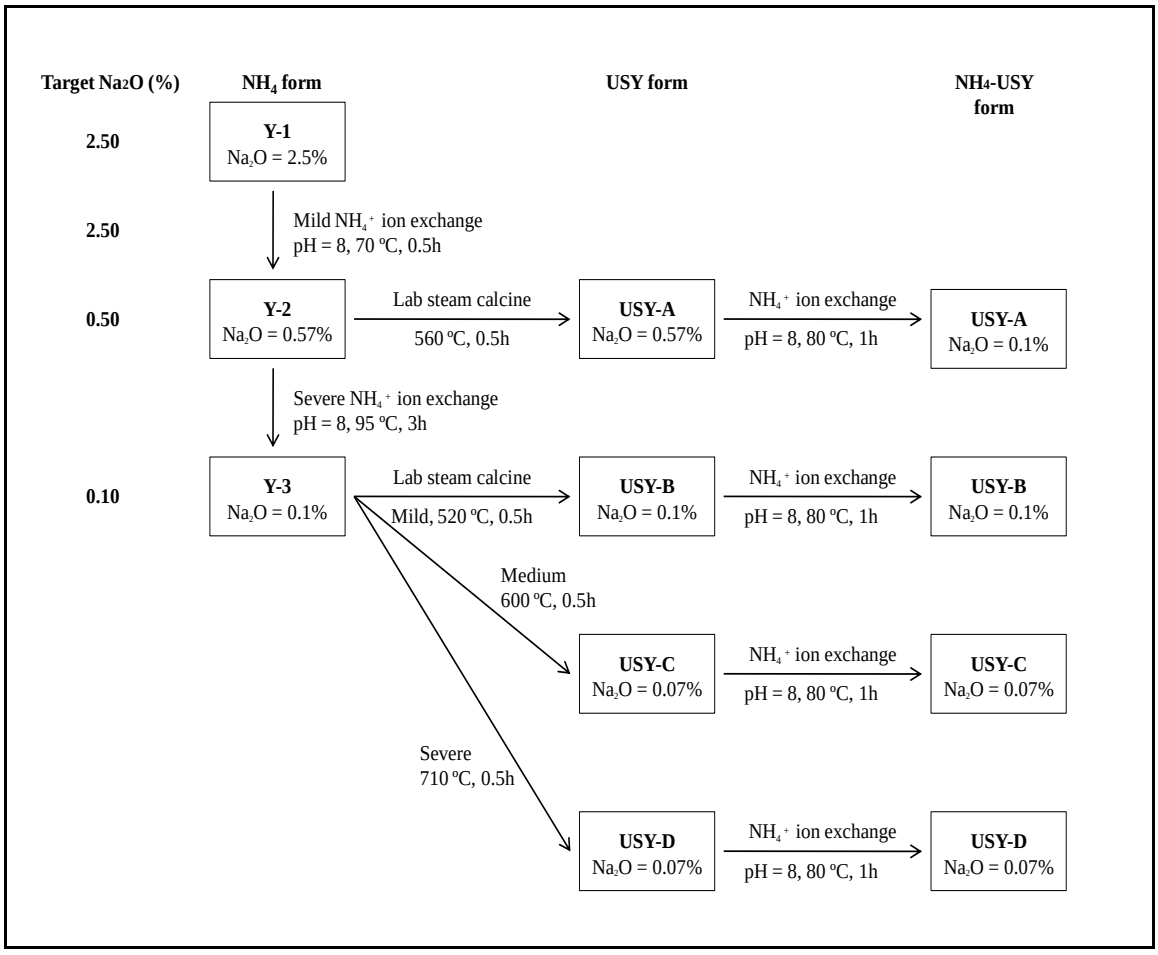

Table 5-1. Characterization of zeolite USY samples determined by outside laboratories and reported in the literature. Letters denote laboratories from: C (Crosfield), U (University of Manchester), M (University of Mullhouse), MC (MCA services), S (SABIC), and Z (Zeolyst) and numbers denote references from the literature.

	XRD Analysis		Chemical Analysis				NMR Spectroscopy			BET**		
Sample	Crystallinity, %*	Unit cell parameter, Å	Al_2O_3, wt%, theoriticaly ≈ 25%	SiO_2, wt%, theoretically ≈ 75%	Na_2O, wt%	Bulk Si/Al ratio	Extra framework Al atoms per unit cell***	Total Al atoms per unit cell***	Framework Si/Al ratio	Surface area, m^2/g	Pore volume, cm^3/g	Average pore diameter, Å
Pure NaY	100.0	24.65 [2]	-	-	13.0 [2]	2.60 [2]	0	53.0 - 58.0	2.60 [2]	828.8 [3]	0.32 [3]	5.6 [4]
USY-A	80.6 (U) 80.0 (C)	24.51 (M) 24.50 (U) 24.52 (C)	21.7 (M) 17.0 (U)	75.3 (M) 83.0 (U)	0.08 (M) <0.09 (U) 0.10 (C)	2.95 (M) 3.06 (U) 2.75 [5]	24.9 (M) 36.7 [5]	54.9 (M) 61.0 [5]	5.4 (M) 6.9 [5]	646.2 (S) 780 (C)	0.477 (S)	29.53 (S)
USY-B	78.9 (U) 83.0 (C)	24.52 (M) 24.53 (U,C)	22.6 (M) 17.1 (U)	77.7 (M) 82.8 (U)	0.09 (M,U) 0.10 (C)	2.90 (M) 3.00 (U)	23.2 (M)	55.1 (M)	5.0 (M)	588.8 (S) 772 (C)	0.4856 (S)	32.99 (S)
USY-C	79.1 (U) 73.0 (C)	24.45 (M,C) 24.46 (U)	22.5 (M) 18.3 (U)	76.4 (M) 81.6 (U)	0.09 (M,U) 0.07 (C)	2.90 (M) 2.80 (U) 2.47 [5]	40.4 (M) 44.9 [5]	59.6 (M) 68.3 [5]	9.0 (M) 7.21 [5]	576.7 (S) 729 (C)	0.5059 (S)	35.09 (S)
USY-D	71.8 (U) 70.0 (C)	24.38 (M) 24.37 (U) 24.39 (C)	23.0 (M) 18.4 (U)	77.2 (M) 81.6 (U)	0.09 (M,U) 0.07 (C)	2.85 (M) 2.80 (U)	43.8 (M)	61.2 (M)	10.0 (M) 9.0 (U)	456.8 (S) 681 (C)	0.4573 (S)	40.04 (S)
CBV-712	81.0 [6]	24.36 [7] 24.35 (Z)	-	-	0.05 (Z)	6.0 [6,8] 5.8 [9]	13.2 [8]	28 [7]	12.0 [8] 12.0 (Z)	730 (Z), 816.3 (MC)	0.4515 (MC)	42.75 (MC)
CBV-760	72.0 [6,10]	24.25 [7,11] 24.24 [12] 24.24 (Z)	-	-	0.03 [12] 0.03 (Z)	30.0 [6-10,13,14] 27.2 [11]	3.1 [8,13] 4.9 [11]	6.2 [7] 6.8 [11]	60.0 [8,13] 60.0 (Z) 55.0 [15]	746 [16] 720 (Z) 551 [12] 814.0 (MC)	0.44 [14,17] 0.41 [12] 0.4487 (MC)	21.0 [12] 24.38 (MC)

*The crystallinities of USY-A through USY-D are comparable as they were calculated at the same time and cross-referenced with Crosfield and the University of Manchester using the same method (8 most intense 2th XRD peaks using a Si standard). The technique used for Zeolyst CBV-712 and CBV-760 samples is unknown and values quoted are from literature sources that have carried out work on the catalysts. **Determined with degassing performed at 540°C for (C), at 300°C for (S) and [16], and 350°C for (MC). ***Based on a unit cell of 192 Al + Si and assuming 100% crystallinity.

Details of the acidic properties of the catalysts determined either in outside laboratories or reported in the literature are shown in Table 5-2. Again, a variety of methods have been used and the aim of the table is to put together commercial and literature data to allow some general consideration of acid properties to be discussed. As expected, the steaming of USY-A to USY-D samples showed a drop in the number of Brönsted/Lewis sites using pyridine adsorption FTIR results. The B/L ratio fell from 4.5 to 1.6. Steaming also caused the total acidity, expressed by the summation of Brönsted and Lewis acidities, to drop when comparing the total acidity of USY-A and USY-C (reported in [1]) or that of USY-B and USY-D (reported by Crosfield). The change is less clear on the CBV-712 and CBV-760 samples, where differing methods appear to show a slight difference (0.625 ± 0.005 and 0.57 ± 0.03). For catalysts CBV-712 and CBV-760, the higher degree of acid leaching done to CBV-760 did not result in a substantial drop in the ratio of Brönsted to Lewis acid sites (reported in [5,8]), suggesting both the removal of Al from the catalyst framework and the extra framework Al in almost equal proportions. This observation is also evident from the total acidity determined by ammonia TPD for the two catalysts, with the acidity of CBV-760 being almost half that of CBV-712. It is worth noting that the change in methodology performing the adsorption at 150^{o}C and 250^{o}C had a profound effect on the observed Brönsted and Lewis acidities, the higher temperature yielding much lower numbers of Lewis sites. This might be expected as Lewis sites are weaker and tests done at higher temperatures would lead to much less adsorption. Similarly, the results obtained for Brönsted sites are also much lower than at 150^{o}C. Figures 5-2 and 5-3 show the relationship between the Brönsted to Lewis ratio and the framework Si/Al ratio and the sample unit cell parameter, respectively. They demonstrate how the removal of Al from the framework upon dealumination results in lower Brönsted acid sites and shrinkage in the zeolite unit cell.

Figure 5-2. B/L ratio versus framework Si/Al ratio for USY samples.

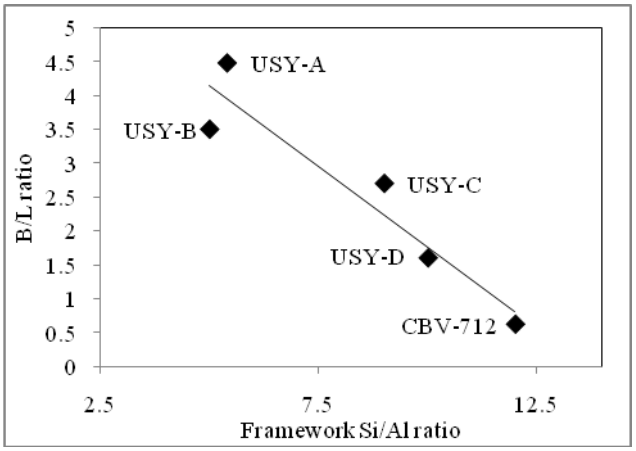

Figure 5-3. B/L ratio versus unit cell parameter for USY samples.

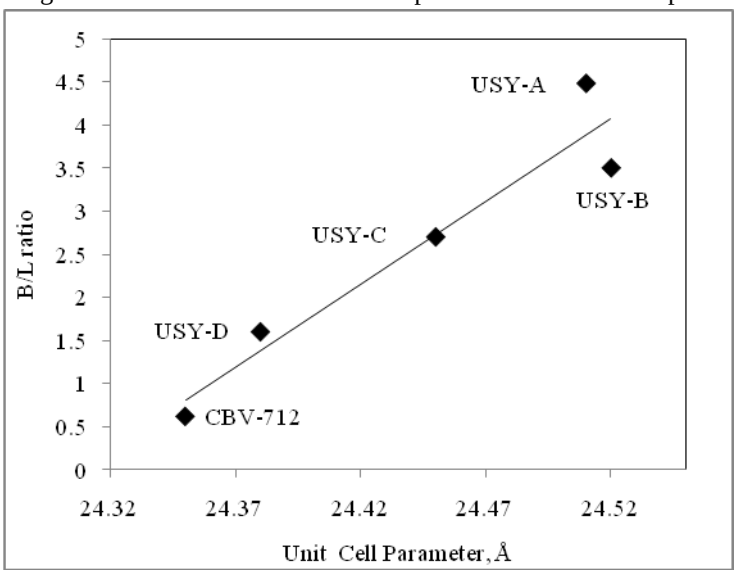

Table 5-2. Acidic properties of zeolite USY samples determined by outside laboratories and reported in the literature. C (Crosfield).

	Pyridine FTIR Analysis*			TPD Analysis**		
Sample	Brönsted sites, mmol/g	Lewis sites, mmol/g	Brönsted/Lewis sites	Total acidity, mmol/g	Strong acidity, mmol/g	Weak acidity, mmol/g
USY-A	0.972 [5]	0.217 [5]	4.48 [5]	-	-	-
USY-B	3.5 (C)	1.0 (C)	3.5 (C)	-	-	-
USY-C	0.754 [5]	0.279 [5]	2.70 [5]	-	-	-
USY-D	2.4 (C)	1.5 (C)	1.6 (C)	-	-	-
CBV-712	0.31 [6,9]	0.49 [6] 0.50 [9]	0.63 [6] 0.62 [9]	0.80 [6] 0.81 [9]	-	-
CBV-760	0.15 [6] 0.14 [9] 0.037 [12] 0.014 [15]	0.25 [6] 0.26 [9] 0.02 [12] 0.01 [15]	0.60 [6] 0.54 [9] 1.85 [12] 1.4 [15]	0.235 [13] 0.4 [6,9,10] 0.24 [14,17] 0.254 [16,18]	0.189 [13] 0.19 [14,17] 0.132 [18]	0.046 [13] 0.05 [14,17] 0.02 [18]

*Performed at 150°C for [5,6,9] and (C) and at 250°C for [12,15]. **Ammonia TPD: weak sites (ΔH_{ads} = 90 – 95 kJ/mol) and strong sites (ΔH_{ads} = 115 – 127 kJ/mol) for [13,14,17] and pyridine TPD for [16,18].

As seen from Tables 5-1 and 5-2, the tested catalysts in this work vary to a large degree in their:

- physicochemical properties: this is obvious from the framework Si/Al ratios
- structural properties: this can be inferred from BET results
- acidic properties: this is emphasized through the changing B/L ratio for steamed-only samples and total acidity for acid-leached samples.

Therefore, catalytic performance is expected to vary greatly among these samples when they are employed in studying the hydroisomerization of normal heptane.

5.3 Zeolite Y Synthesis

5.3.1 Recipe

The recipe of zeolite Y was obtained from a verified zeolite syntheses handbook [19]. The synthesis involved the use of a seeding agent. Gel calculations to determine the required weights of each reactant were performed and are listed in Appendix B. The recipe used to attempt the synthesis was as follows:

Zeolite-Y feed stock gel: (4.3 Na_2O: Al_2O_3: 10 SiO_2: 180 H_2O)

Zeolite-Y seed gel: (10.67 Na_2O: Al_2O_3: 10 SiO_2: 180 H_2O)

Typically, the synthesis of zeolite Y can be targeted by having the appropriate amounts of alumina, silica, and soda in solution. The following ternary phase diagram for these reactants demonstrates the proportions by which zeolite Y can be targeted, as well as other common zeolite phases:

Figure 5-4. Ternary diagram of alumina, soda, and silica for the synthesis of some zeolite phases [20].

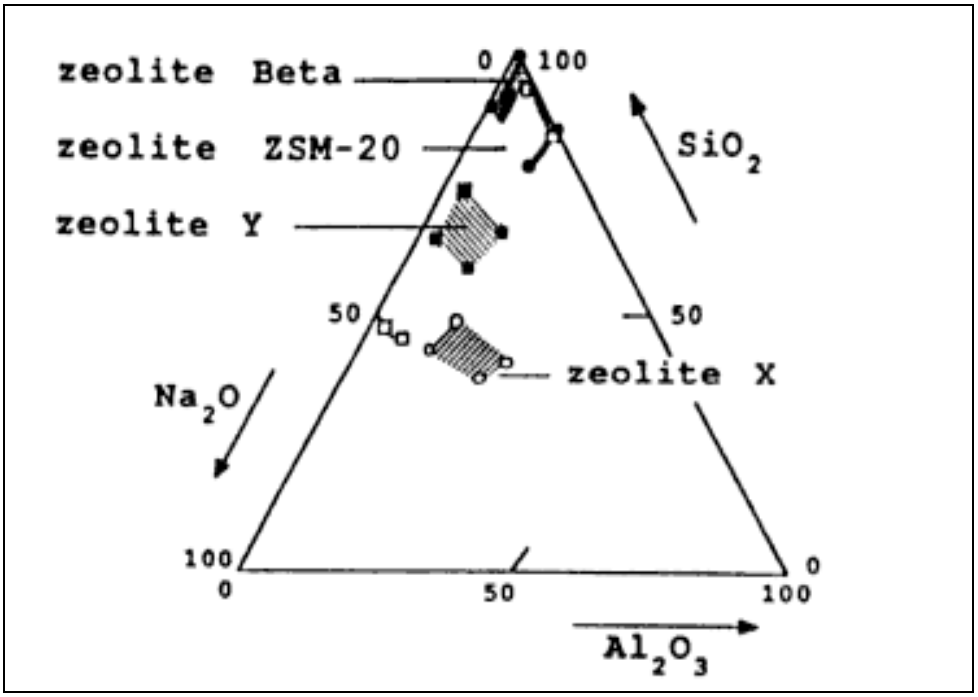

5.3.2 Tools, Equipment & Chemicals Used

The tools, equipment, and chemicals that were used during the synthesis are listed in Table 5-3 below:

Table 5-3. Tool, equipment, and chemicals used in zeolite Y synthesis and their suppliers.

Tools	Equipment	Chemicals
Plastic pipettes - Fisher	Weighing scales – Fisher PS-60	Ludox AS-40 colloidal silica (40 wt% silica & 60 wt% water) – Sigma-Aldrich
pH paper - Fisher	Magnetic stirrer & magnet	Anhydrous sodium aluminate (50.9 wt% Al_2O_3, 31.2 wt% Na_2O, 17.9 wt% H_2O) – Sigma-Aldrich
Mortar & pestle	Centrifuge – MSE Centaur 2	Sodium hydroxide (99 wt% NaOH) – Merck
Test tubes - Fisher	Oven – Varian 3400	de-ionized water (100% purity)
Plastic bottles - Fisher	-	-
Safety goggles - Fisher	-	-
Disposable gloves - Fisher	-	-
Sample vials - Fisher	-	-
Weighing paper - Fisher	-	-
Spatula - Fisher	-	-

5.3.3 Preparation Procedure

For the synthesis of zeolite Y, the seeding gel was first prepared as follows: calculated weights of de-ionized water, sodium hydroxide, and sodium aluminate were mixed in a plastic bottle until they were completely dissolved. Then, the required amount of silica solution (Ludox AS-40) was added to the solution and all were stirred using a magnetic stirrer for 10 minutes. After that, the solution was left at room temperature to age for one day. For the feedstock gel, calculated weights of de-ionized water, sodium

hydroxide, and sodium aluminate were mixed in another plastic bottle until they were completely dissolved. Then, the required amount of Ludox AS-40 was added to the solution and all were stirred using a magnetic stirrer for 10 minutes. The calculations for both the seeding and feedstock gels are demonstrated in Appendix B. Then, the required amount of the seeding gel was added to the feedstock gel and the overall mixture was mixed vigorously for 20 minutes. After that, the mixture was poured into three containers and all were heated in an oven at 100^{o}C for crystallization. After the selected crystallization times (20, 24, and 72 hours), each sample was taken out of the oven, decanted, and centrifuged several times while washing with de-ionized water after each centrifugation until the pH of the decanted solution dropped below 9. Finally, the samples were dried at 110^{o}C overnight until they were ready for characterization.

5.4 Characterization Techniques

In order to determine whether the attempted zeolite synthesis was successful or not, catalyst samples were analyzed by the scanning electron microscopy (SEM) in order to study their surfaces, energy dispersive X-ray (EDAX) to determine their Si/Al ratios, and the X-ray diffraction (XRD) in order to determine if they formed any crystals and the type of crystals formed.

5.4.1 SEM and EDAX Analyses

In scanning electron microscopy, the sample or specimen is viewed by an electronic map instead of displaying a direct image of it. The electronic map of the specimen is displayed as an output on a cathode ray tube (CRT). Figure 5-5 shows components of a typical SEM instrument. Electrons from a filament inside an electron gun are emitted to the specimen inside a vacuum chamber in the form of a line. This electron line hits the sample continuously, causing it to enlighten and in turn generate a signal. The resulting signal can be an X-ray fluorescence, secondary electrons, or backscattered electrons. In SEM, a detector is used to transfer the secondary electrons signal to the CRT. Viewing the image in 3D format can be achieved by increasing the scan rate of the electron beam. In addition, magnification of the sample is done through narrowing the electron beam, since magnification is expressed in the following formula:

$$\text{Magnification} = \text{Width of the CRT}/\text{Width of the electron beam} \quad (5)$$

As the width of the CRT is fixed, increasing the magnification can be done by decreasing the width of the electron beam. In order to prepare a specimen for analysis, it is crucial that any non-conductive samples be coated with a conductive material, such as gold, since the excessive charging from the electrons can damage the specimen. Sample coating is done through a sample sputter, which coats samples with a nanometer thickness of gold using a cold plasma process in which the specimen retains its dimensions. After the specimen has been coated, it is placed inside the SEM vacuum chamber and the electron gun is then switched on [21].

Figure 5-5. Components of a typical SEM instrument [21].

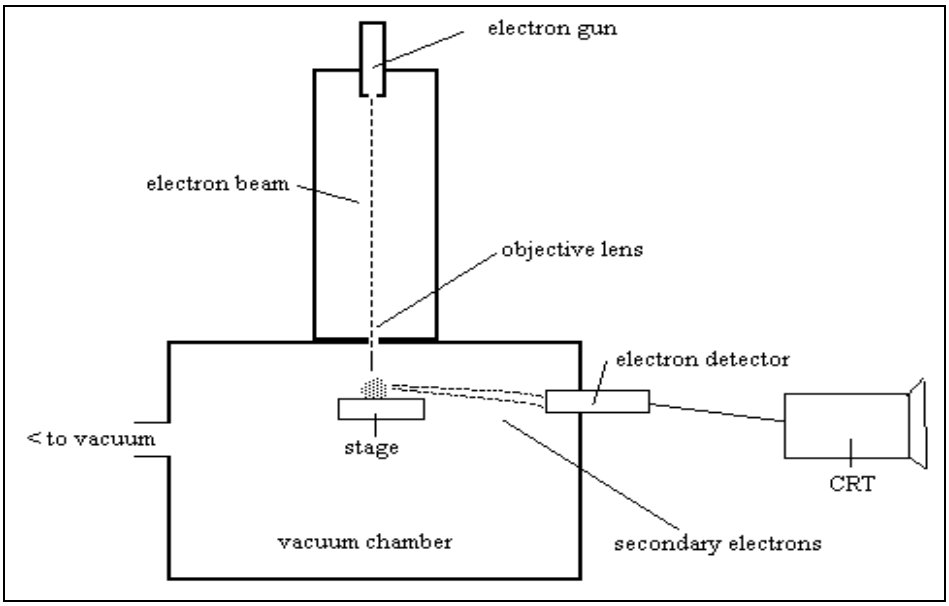

In EDAX (energy dispersive X-ray) analysis, in which elemental analysis is performed to quantify percentages by weight of different elements in a specimen, the same SEM instrument is usually used to carry out the analysis by having additional components. These components are an X-ray detector (spectrometer), a pulse detector, and an analyzer. EDAX works by having the electron beam hit the specimen, which causes electrons inside atoms of the specimen to be removed from the atoms, resulting in a void inside the atoms. This void in the atoms is then filled by higher energy electrons from an outer shell. When these higher energy electrons transfer to a lower energy shell, they emit some of their energy in the form of X-rays. The amount of energy the emitted X-ray has depends on the type of atom present in the specimen. Hence, each atom will have a characteristic peak in the EDAX spectrum, the height of which is corresponding to it concentration in the specimen [22]. Figure 5-6 shows an example of an EDAX spectrum.

Figure 5-6. Diagram of a typical EDAX spectrum.

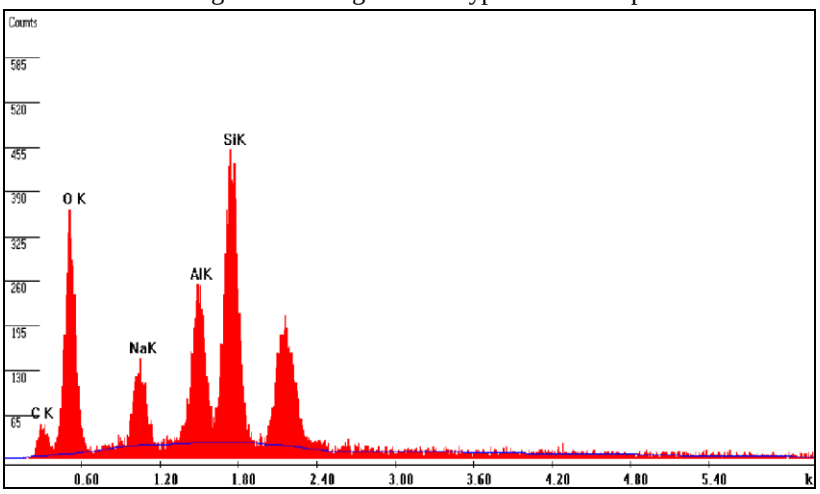

The synthesized catalyst samples were analyzed by an FEI Quanta 200 SEM after coating the specimens with gold particles to reduce the effect of charging in the SEM images. Figure 5-7 shows images of synthesized zeolite Y samples magnified 12000 times. It can be seen in the first two images that crystals with sharp edges are formed and that the two samples are similar. However, the third image (after 72 hours) shows some differences from the others. The edges in the small objects seem to be smoother and are almost round-shaped. In addition, larger objects can be seen in the upper right corner of the image, which were not present after 24 hours of crystallization time. These two observations indicate that formed crystals after 20 and 24 hours have either started to dissolve or to form a new phase. However, final conclusions in this regard can be made from the XRD analysis of the samples. EDAX analysis done on the SEM machine using Genesis EDS X-ray for the elemental analysis of the three samples showed that the molar Si/Al ratio was 2.18, 2.26, and 2.23 for the 20, 24, and 72-hour samples, respectively.

The SEM images of the catalysts studied for the hydroisomerization of normal heptane in their ammonium form are shown in Figures 5-8 to 5-13. It can be noticed from the figures that as the degree of steaming to which the in-house catalysts were subjected increases, the morphology of the surface is rougher with finer more angular-shaped “hair-like” crystals. This was not observed for the CBV acid-leached catalysts. The surface for CBV-760 does show more features than that of CBV-712.

Figure 5-7. Zeolite Y (20, 24, 72 hours magnified to 5 μm).

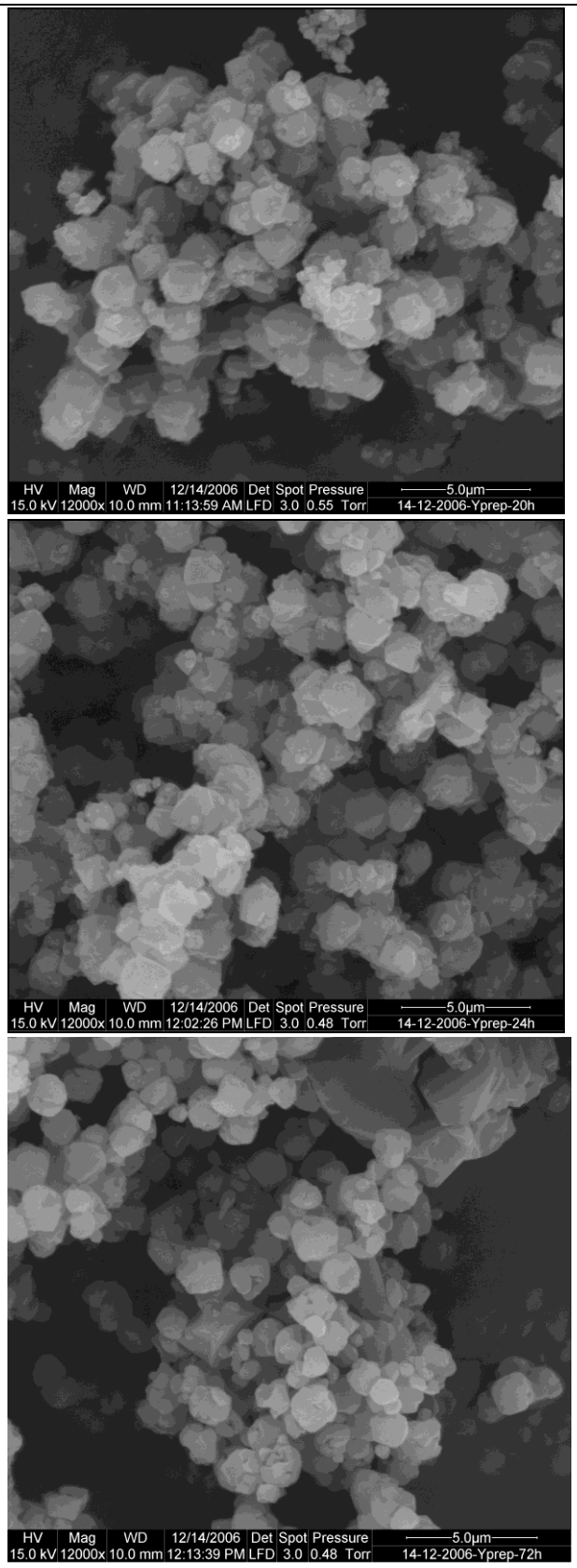

Figure 5-8. USY-A magnified to 5 µm.

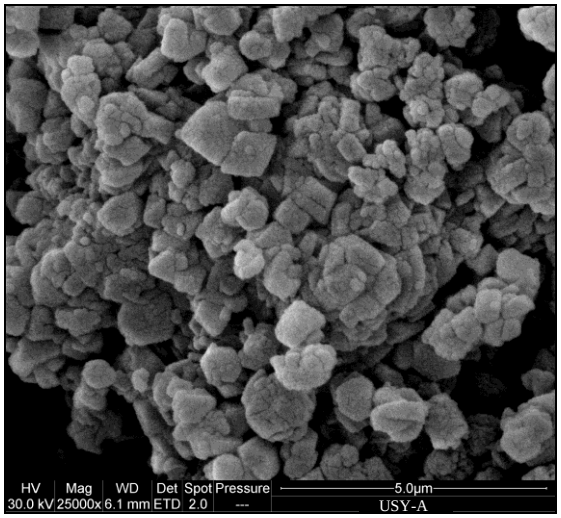

Figure 5-9. USY-B magnified to 2 µm.

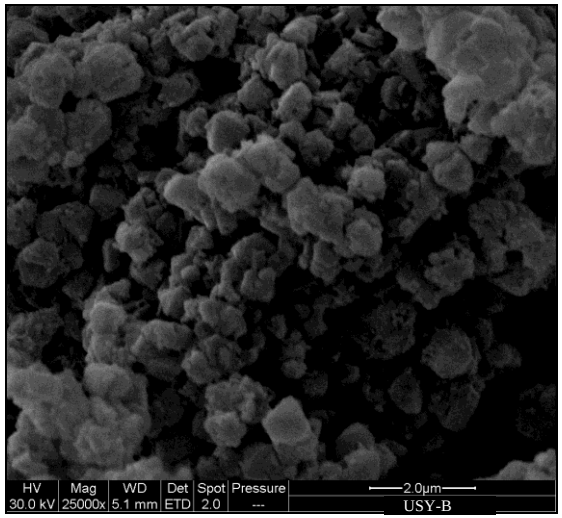

Figure 5-10. USY-C magnified to 2 µm.

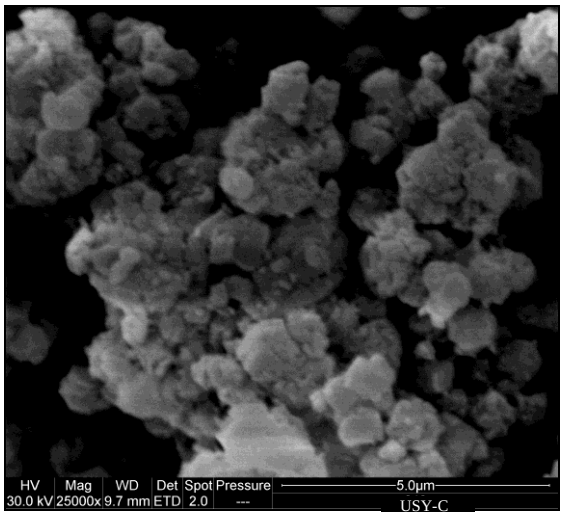

Figure 5-11. USY-D magnified to 5 µm.

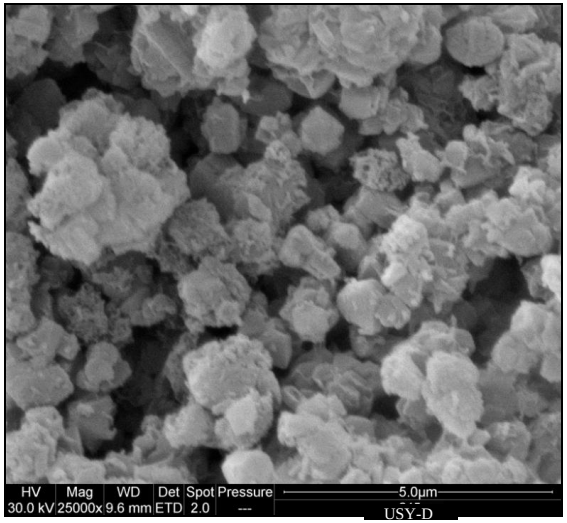

Figure 5-12. CBV-712 magnified to 5 µm.

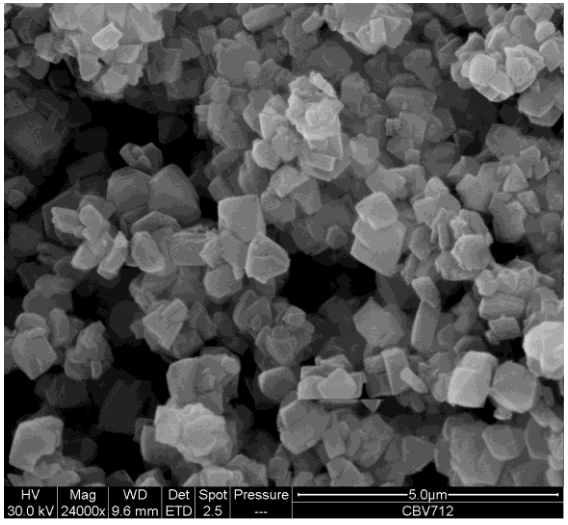

Figure 5-13. CBV-760 magnified to 5 µm.

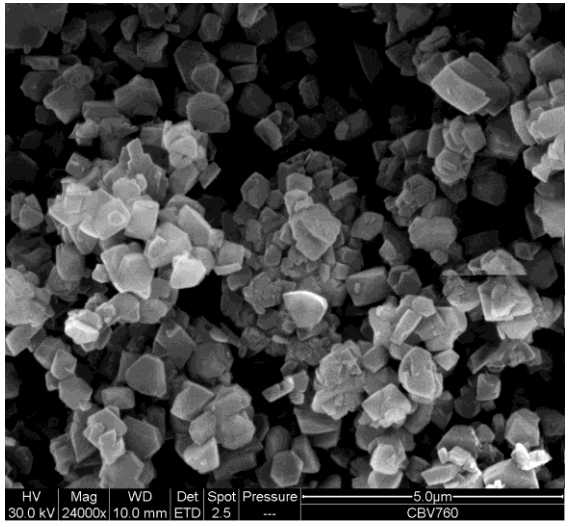

5.4.2 XRD Analysis Introduction

In X-ray diffraction analysis, X-rays are used to penetrate the material to be analyzed and provide information about it. X-rays are used because of the small wavelengths they possess (0.1 to a few angstroms), are similar to the size of atoms. The production of X-rays in this method is the same as that used in EDAX, but the purpose of X-rays here is different. When the X-rays hit the specimen, some of their electrons collide with atoms and deflect to another direction, while retaining their energy and wavelength. These diffracted X-rays give information about the electronic distribution of atoms in the specimen. When atoms are arranged in periodic fashion, as in crystals, the diffracted X-rays will have higher intensities at certain angles of diffraction, which enables the measurement of crystallinity in a sample by measuring its diffraction pattern. Bragg's law (Figure 5-14) relates the distance between two planes of atoms and the X-ray scattering angle to the X-ray wavelength by the following formula:

$$2d\sin\theta = n\lambda \tag{6}$$

In Bragg's law, d is the distance between two planes of atoms, θ is the scattering angle, λ is the wavelength of the X-ray, and n is an integer that represents the diffraction peak's order. This law is used for the interpretation of XRD data [19]. During the XRD analysis, the scattering angle θ at which the electron beam is generated is increased over a big range while patterns of the diffracted X-rays are measured. Then, the diffraction pattern is plotted by the XRD machine by generating a scan of scattering intensities or diffraction counts versus 2θ. The instrument used in this work was a Philips X'pert Pro PW3719 X-ray diffractometer.

Figure 5-14. Bragg's law [23].

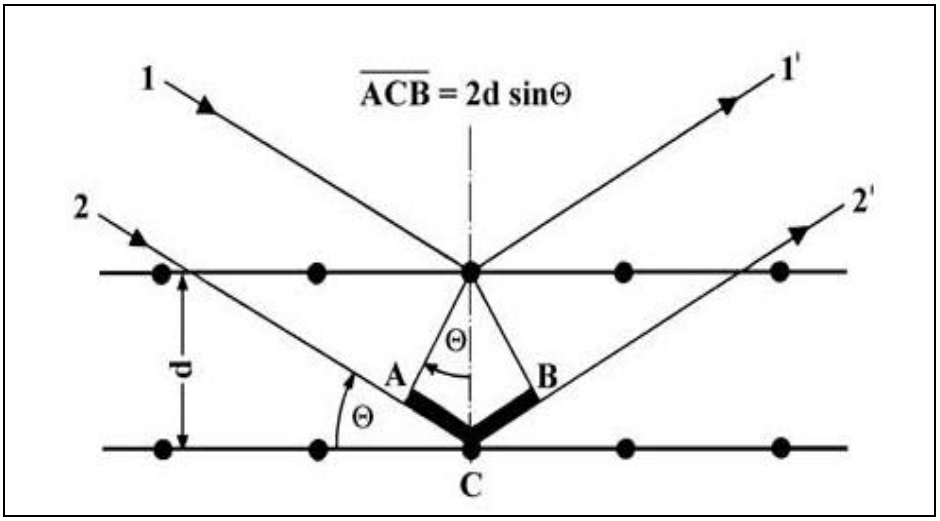

5.4.2.1 XRD Analysis of Synthesized Zeolite Y

Figure 5-15 shows the XRD pattern for zeolite Y samples. It can be noticed from the figure that the patterns for the 20 and 24-hour samples are almost identical. In addition, they are both very similar to the pattern of a typical Faujasite (Figure 5-16). This means that zeolite Y synthesis was successful and that one day of crystallization time is sufficient to prepare it. However, longer crystallization times can alter the present zeolite phase and start forming additional phases. This was obvious after 72 hours of crystallization, as noticed from the additional peaks formed around 2θ readings of 12, 17, 22, 28, and 34 for the 72-hour sample, which are characteristic of zeolite P (Figure 5-16). The presence of these additional peaks means that the zeolite P structure started forming and that of zeolite Y (which is meta-stable to zeolite P) started dissolving. This observation is in agreement with the SEM analysis, where a possibly new phase was noticed to have started forming after 72 hours of crystallization. Furthermore, the crystallinity of the 72-hour sample was calculated to be about 96% of that of the 24-hour sample, suggesting dissolving crystals. Hence, when synthesizing zeolite Y using the attempted recipe and reaction conditions, the reactions has to be terminated around 20 – 24 hours in order to prevent the transformation of the zeolite Y phase to that of zeolite P.

Figure 5-15. XRD pattern for Faujasite samples after 20, 24 and 72 hours of crystallization (zeolite P peaks were denoted by asterisks).

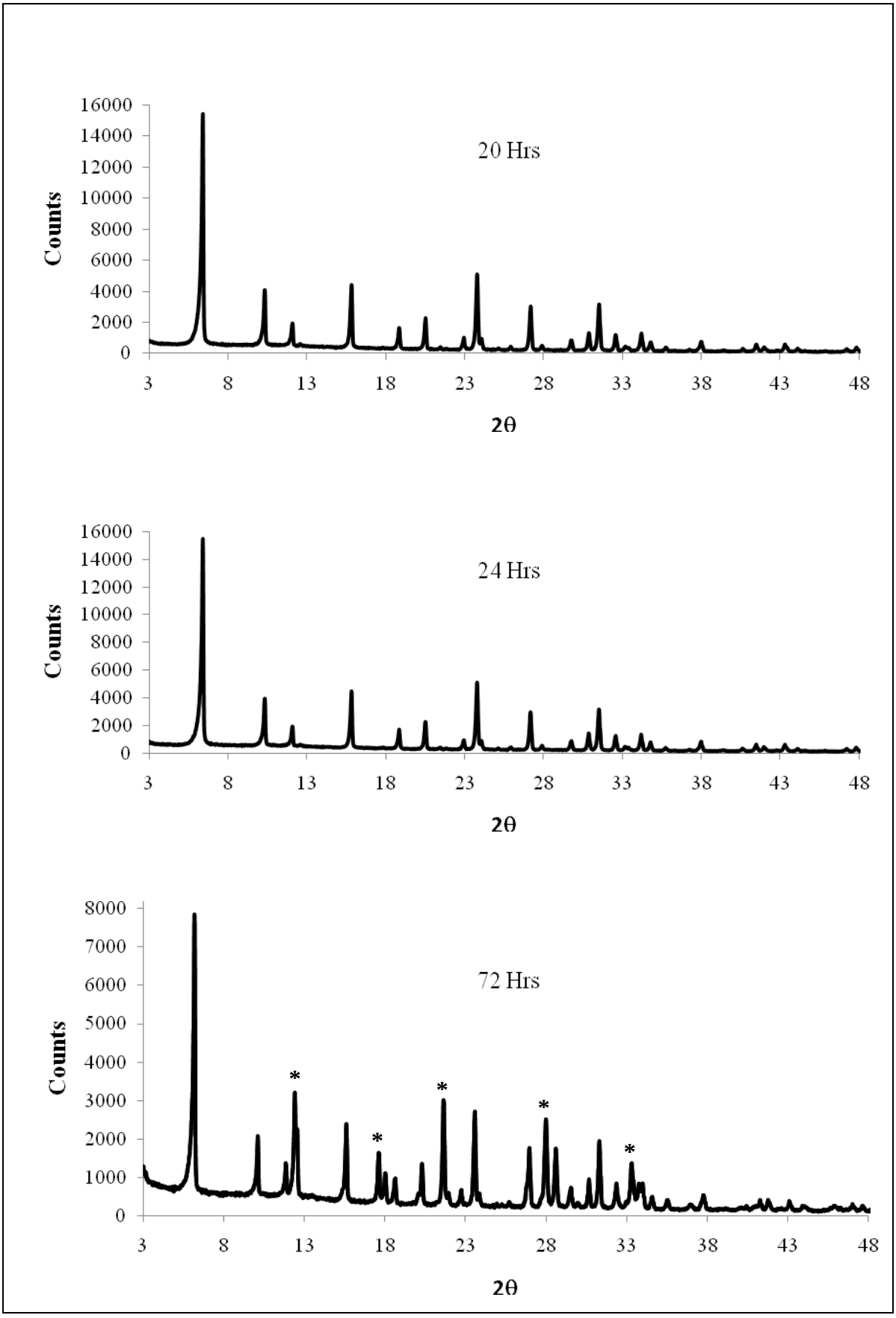

Figure 5-16. Comparison between XRD patterns for zeolite Y after 72 hours, typical Faujasite and zeolite P [24].

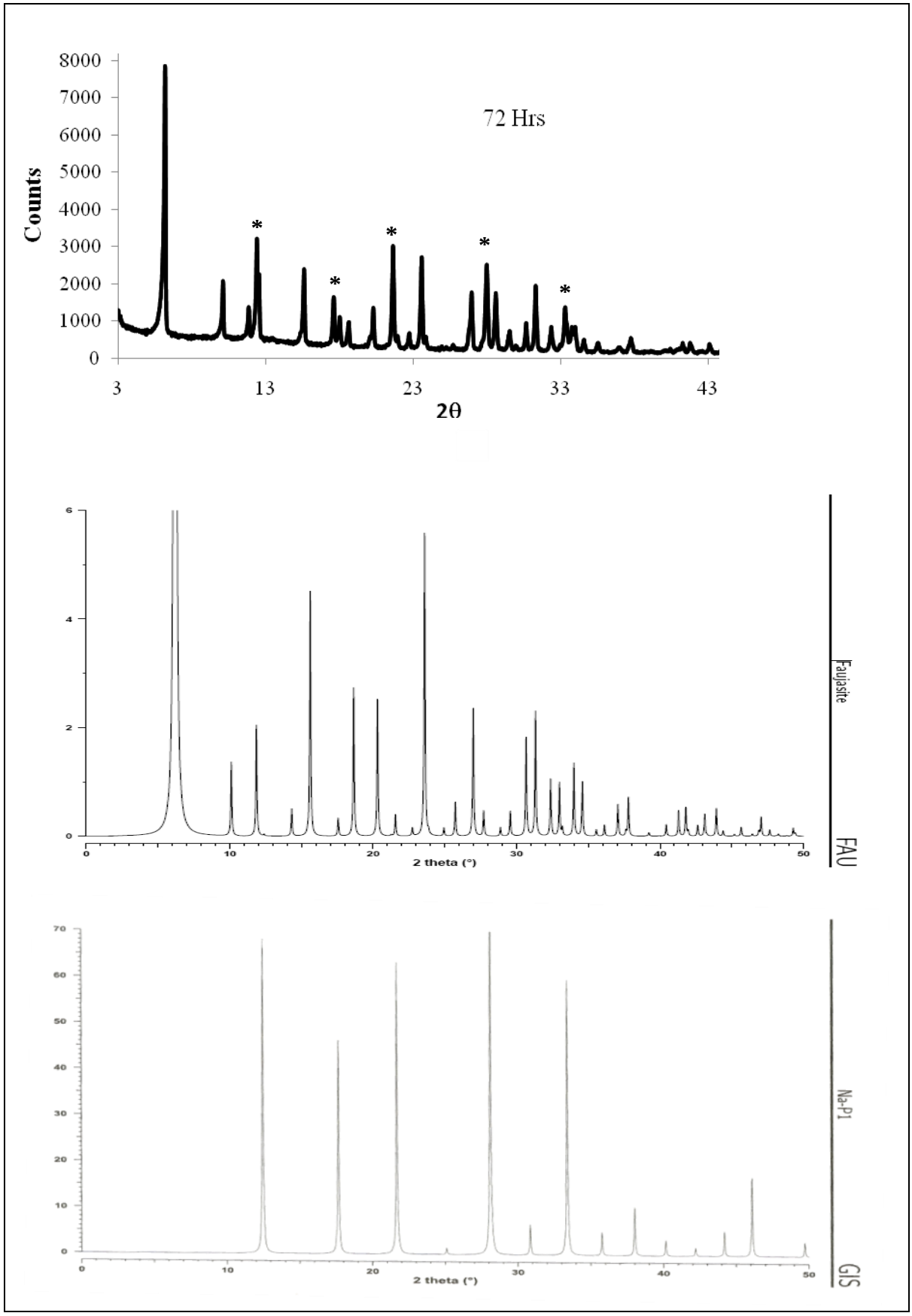

5.4.2.2 XRD Analysis of USY Samples Used in nC_7 Hydroisomerization

XRD analysis of spent catalysts that were experimentally studied in this thesis was performed to determine the loss of crystallinity of spent samples when compared to fresh ones. The loss of crystallinity was calculated by dividing the sum of all peak counts from the XRD pattern of the spent sample by the sum for the fresh sample and multiplying the result by 100. Table 5-4 presents the results for spent catalysts' crystallinities for catalysts tested in the atmospheric reactor as well those tested in the pressure reactor. It appears that the more severely steamed a sample the more the sample loses crystallinity during catalysis. However, catalysts that were acid-leached retained a much higher degree of crystallinity upon testing versus steamed ones. It is possible that the high presence of EFAL species in steamed-only samples resulted in higher coke contents, which, in turn, caused a greater reduction in the crystallinity of samples, since coke is amorphous.

Table 5-4. Crystallinity of spent catalysts used in both atmospheric and pressure reactors.

Reactor	Catalyst	Crystallinity, % before	Crystallinity, % after
Atmospheric	USY-B	100	53.11
	USY-C	100	52.03
	USY-D	100	51.21
Pressure	USY-A	100	"80.25"
	USY-C	100	52.2
	USY-D	100	49.85
	CBV-712	100	67.33
	CBV-760	100	72.77

5.4.3 Thermogravimetric Analysis

Thermogravimetric Analysis (TGA) is a technique in which the weight of a given sample is monitored continuously as a function of time and/or temperature, while under flowing air or an inert gas [25-28]. It is used in many applications such as studies of the thermal degradation of polymer and solvent evaporation, the transportation industry, and

minerals and metals studies [27-29]. Figure 5-17 provides a demonstration of the various parts of a typical TGA instrument.

Figure 5-17. Demonstration of the components of a typical TGA instrument [29].

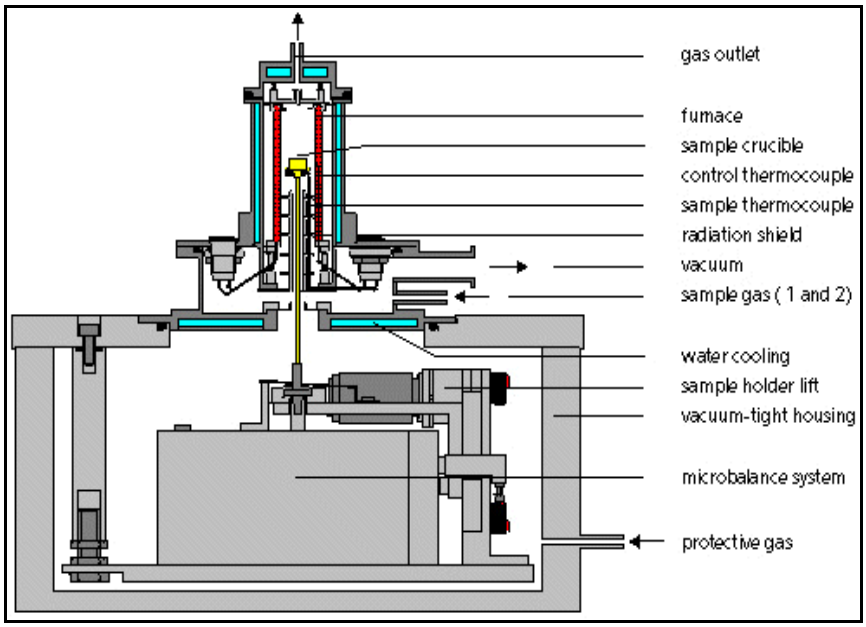

In this work, TGA was performed on spent catalyst samples in order to determine the coke content. Catalysts were separated into 3 parts based on their location inside the reactor: top, middle, and bottom samples, where about 10 mg of each sample was placed in a ceramic pan. The instrument used for this analysis was a TA instruments Q5000IR with a sensitivity of 0.1 μg. During sample analysis, nitrogen gas (BOC, white spot, 50 ml/min) was first introduced while the temperature was being ramped to ensure the removal of any water or condensates. Later, air flow (BOC, 50 ml/min) was switched on to burn the coke off the catalyst and allow recording the weight loss due to coke removal, thus enabling the calculation of coke content in the catalyst.

As an example, Figure 5-18 shows the TGA results for catalyst USY-B top, middle, and bottom parts, respectively after unloading the spent catalyst from the atmospheric glass reactor. The results for all catalysts used in both the atmospheric and pressure reactors are listed in Table 5-5. It is obvious that for USY-B the top section had the highest coke content in the catalyst bed (0.7902 wt%), whereas there was hardly any coke in the middle and bottom sections. This probably suggests that the top section of the catalyst bed was contributing the most activity and where the reaction was taking place. In addition, the somewhat high coke content in the top section is indicative of the high acidity of this catalyst, which caused low catalyst stability and thus fast deactivation and coking rate

during experiments using the glass atmospheric reactor. Catalyst USY-C possessed low coke contents in all three zones, which is attributed to its lower acidity than USY-B and thus higher stability. Catalyst USY-D contained virtually no coke in it. This is due to the catalyst having yet lower acidity and higher stability than USY-C.

Results differ, however, for results obtained with experiments in the pressure reactor, since catalysts were tested for longer periods of time, except for USY-A, which has a high coke content despite its short time on-stream. Catalysts USY-C and USY-D had high coke contents at the end of experiments, with USY-C's coke primarily located in the top section of the catalyst bed. The uniform distribution of USY-D's coke content implies that no diffusion limitations are encountered with this catalyst, since diffusion limitations would result in coking once reactants enter the catalyst structure, causing the top section of the bed to be coke-rich. The coke content of acid-leached catalysts is much less than steamed ones, with CBV-712 being almost free of coke. This implies that EFAL species might be responsible for higher coking rates seen with steamed catalysts. However, coke content of CBV-760 was a lot higher than CBV-712, which could be due to its smaller pores causing higher levels of cracking.

Table 5-5. Coke content in the top, middle, and bottom parts of spent catalyst bed for all catalysts.

Reactor	Si/Al	Catalyst	Coke Content, wt%		
			Top	Middle	Bottom
Atmospheric	5	USY-B	0.790	0.043	0.031
	7-9	USY-C	0.018	0.026	0.041
	9-10	USY-D	0.022	0.003	0.016
Pressure	5	USY-A	1.903	1.204	0.804
	7-9	USY-C	2.078	0.723	0.219
	9-10	USY-D	0.991	1.088	1.096
	12	CBV-712	0.083	0.022	0.061
	60	CBV-760	0.252	0.136	0.137

Figure 5-18. TGA for USY-B's top, middle, and bottom sections after experiments using the atmospheric unit.

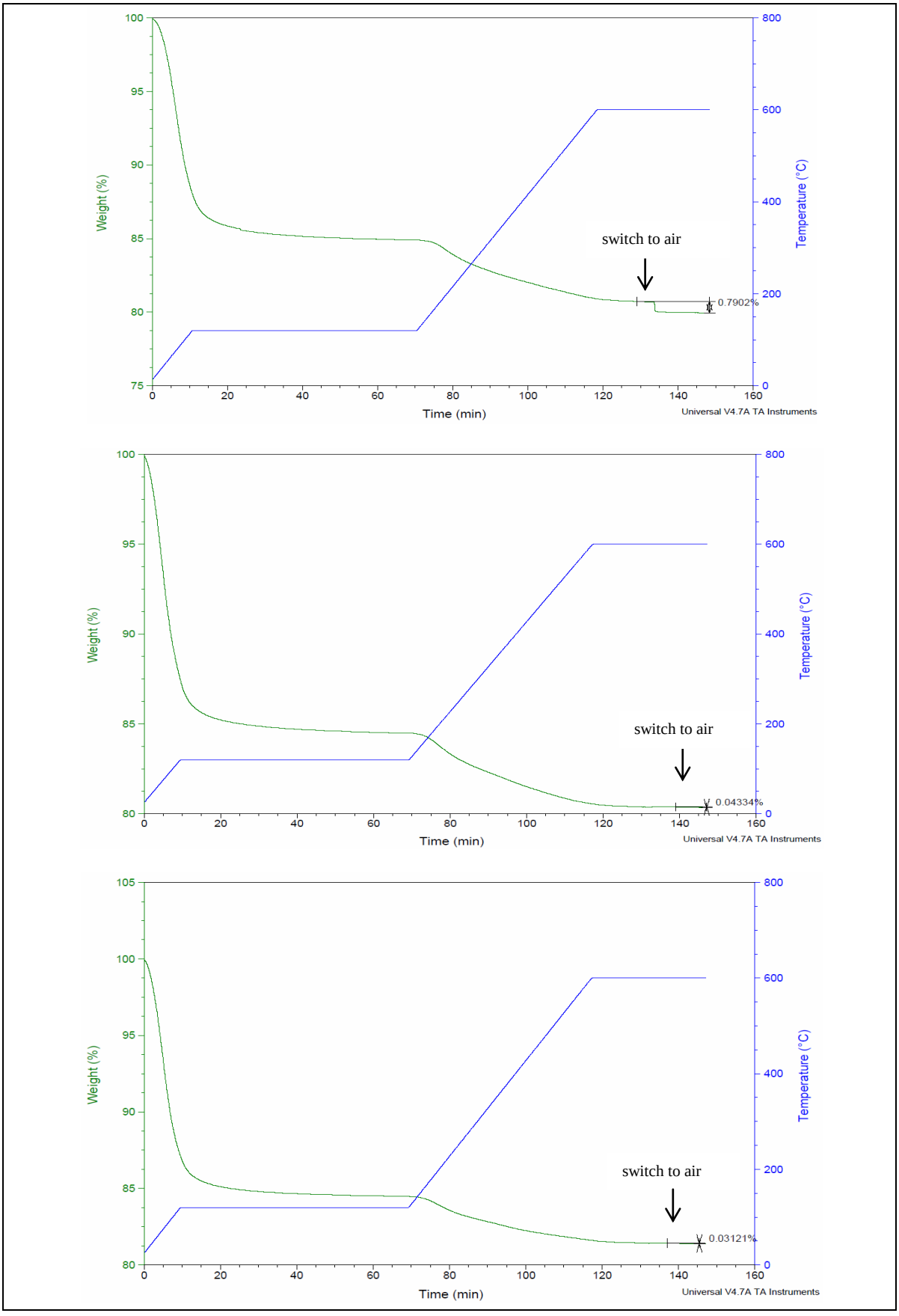

5.5 Metal-loading of USY Catalysts

Each of the tested catalyst samples was loaded with 1 wt% platinum by using an ion-exchange method that was previously used for loading platinum into zeolite A, Y, and ZSM-5 [30-33]. In this method, the ammonium form of the catalyst was added to a 5 x 10^{-3} molar aqueous solution of tetra-ammine platinum (II) chloride ($Pt(NH_3)_4Cl_2$) (98 wt% purity, Sigma-Aldrich), whose amount was calculated such that it results in 1 wt% platinum loading on the zeolite sample (calculation is shown in Appendix B), assuming a complete uptake of platinum in the catalyst. The mixture was left stirring at room temperature for 24 hours. After that, the mixture was centrifuged and washed with 10 times of its volume of de-ionized water in order to ensure that the catalyst is free of chloride ions, and the supernatant of the first wash was analyzed by chemical analysis to ensure the complete uptake of platinum in the structure. The washed catalyst was then dried overnight at 110^{o}C. Ion-exchange of the zeolite with the platinum salt proceeds according to the following chemical equation:

$$Pt(NH_3)_4^{2+}{}_{(aq)} + 2Cl^-{}_{(aq)} + 2M^-{}_{(zeol)} \rightarrow Pt(NH_3)_4M_2{}_{(zeol)} + 2Cl^-{}_{(aq)} \quad (7)$$

In this chemical equation, M^- denotes a zeolite ion.

5.6 Conclusion

After a successful synthesis of zeolite Y, where a crystallization time of 20 – 24 hours was sufficient for the formation of the Y phase, in-house steamed USY as well as commercial acid-leached USY catalysts were characterized in-house by SEM, EDAX, XRD, and TGA analyses (spent catalysts only). In addition, some characterizations were made at outside laboratories. There is a broad range of Si/Al and the very differing acidic properties (B/L and total acid sites) among these samples, making them of great interest for studying the hydroisomerization of normal heptane reaction. The varied structural defects caused by steaming to varying degrees and the types of dealumination (acid leaching or steaming) used also yield differing pore structures and different catalytic properties that are expected to show differences among catalysts in activity, selectivity and stability.

5.7 References

[1] Rawlence, D. J. and Earl, G. J. (1993). *Materials Having Novel Structure Factors for Catalysis of Hydrocarbon Transformation and Development of Selective Processes. BRITE – EURAM 4633, 5th Meeting Report*, Elf Solaize.

[2] Halasz, I; Agarwal, M; Marcus, B. and Cormier W.E. (2005). Molecular Spectra and Polarity Sieving of Aluminum Dificient Hydrophobic H-Y Zeolites. *Microporous and Mesoporous Materials,* 84 (23), 318-331.

[3] Romero, A; Garrido, A; Nieto-Márquez, A; De La Osa, A.R; De Lucas, A. and Valverde, J.L. (2007). The Influence of Operating Conditions on the Growth of Carbon Nanofibers on Carbon Nanofiber-supported Nickel Catalysts. *Applied Catalysis A: General*, 319, 246-258.

[4] Güleç, H. (2005). *Liquid Phase Hydrogenation of Citral on Zeolite Supported Monometallic (Ni, Pt) and Bimetallic (Ni-Sn, Pt-Sn) Catalysts*. MSc. Thesis, İzmir Institute of Technology, İzmir, Turkey.

[5] Alotaibi, F. M. (2009). *Deactivation Behaviour of Metal-loaded Zeolite Catalysts during High n-Alkane Selective Hydroisomerisation. 1st Year PhD Transfer Report,* University of Manchester.

[6] Burckle, E. C. (2000). *Comparison of One-, Two-, and Three- Dimensional Zeolites for the Alkylation of Isobutane with 2-Butene.* Masters' Thesis, University of Cincinnati, Cincinnati, Ohio.

[7] Remy, M. J; Stanica, D; Poncelet, G; Feijen, E. J. P; Grobet, P. J; Martens, J. A. and Jacobs, P. A. (1996). Dealuminated H-Y Zeolites: Relation between Physicochemical Properties and Catalytic Activity in Heptane and Decane Isomerization. *Journal of Physical Chemistry*, 100, 12440-12447.

[8] Pope, T. D; Kriz, J. F; Stanciulescu, M. and Monnier, J. (2002). A Study of Catalyst Formulations for Isomerisation of C_7 Hydrocarbons. *Applied Catalysis A: General*, 233, 45-62.

[9] Gopal, S. (2003). *Synthesis, Modification, Characterization and Catalytic Studies of Zeolite based Bifunctional Catalysts for Hydroisomerization Reactions*. PhD Dissertation, University of Cincinnati, Cincinnati, Ohio.

[10] Gopal, S. and Smirniotis, P. G. (2004). Factors Affecting Isomer Yield for *n*-heptane Hydroisomerization over As-synthesized and Dealuminated Zeolite Catalysts Loaded with Platinum. *Journal of Catalysis*, 225, 278-287.

[11] Handy, B. E; Jacobo, A; Galindo, Ma. G. C; González, M; Llanos, Ma. E; Gúzman, Ma. de L. and Hernández, F. (2002). Combined Thermometric Analysis of a Series of Highly Dealuminated USY zeolites. *Topics in Catalysis*, 19, 3-4, 249-258.

[12] Corma, A; Martínez, A; Martínez-Soria, V. and Montón, J. B. (1995). Hydrocracking of Vacuum Gas Oil on the Novel Mesoporous MCM-41 Aluminosilicate Catalyst. *Journal of Catalysis*, 153, 25-31.

[13] Thybaut, J. W; Marin, G. B; Baron, G. V; Jacobs, P. A. and Martens, J. A. (2001). Alkene Protonation Enthalpy Determination from Fundamental Kinetic Modeling of Alkane Hydroconversion on Pt/H–(US)Y-Zeolite. *Journal of Catalysis*, 202, 324-339.

[14] Denayer, J. F; Baron, G. V; Vanbutsele, G; Jacobs P. A. and Martens J. A. (2000). Evidence for Alkylcarbenium Ion Reaction Intermediates from Intrinsic Reaction Kinetics of C_6–C_9 *n*-Alkane Hydroisomerization and Hydrocracking on Pt/H–Y and Pt/USY Zeolites. *Journal of Catalysis*, 190, 469-473.

[15] Chica, A. and Corma A. (1999). Hydroisomerization of Pentane, Hexane, and Heptane for Improving the Octane Number of Gasoline. *Journal of Catalysis*, 187**,** 167-176.

[16] Jiménez, C; Romero, F. J; Roldán, R; Marinas, J. M. and Gómez, J. P. (2003). Hydroisomerization of a Hydrocarbon Feed Containing *n*-Hexane, *n*-Heptane and Cyclohexane on Zeolite-supported Platinum Catalysts. *Applied Catalysis A: General*, 249, 175-185.

[17] Denayer, J. F. M; Martens, J. A; Jacobs, P. A; Thybaut, J. W; Marin, G. B. and Baron, G. V. (2003). Influence of the Zeolite Composition on the Hydro-isomerisation and Hydrocracking of Alkanes on Pt/USY Zeolites: Modelling of the

Reaction Kinetics Using an Adsorption-reaction Approach. *Applied Catalysis A: General*, 246, 17-28.

[18] Roldán R; Romero, F. J; Jiménez-Sanchidrián, C; Marinas, J. M. and Gómez, J. P. (2005). Influence of Acidity and Pore Geometry on the Product Distribution in the Hydroisomerization of Light Paraffins on Zeolites. *Applied Catalysis A: General*, 288, 104-115.

[19] Robson, H. and Lillerud, K.P. (2001). *Verified Syntheses of Zeolitic Materials*. 2nd Edition. Amsterdam: Elsevier.

[20] Szostak, Rosemarie (1998). *Molecular Sieves: Principles of Synthesis and Identification*. 2nd Edition. London: Blackie Academic & Professional. p. 85.

[21] George Mason University, Scanning Electron Microscopy [Website]. Available from: <http://www.gmu.edu/departments/SRIF/tutorial/sem/sem.htm> [Accessed: 1 September 2007].

[22] Siliconfareast Web Page [Website]. Available from: <http://www.siliconfareast.com/edxwdx.htm> [Accessed: 1 September 2007].

[23] Bruker AXS Home Page [Website]. Available from: <http://www.bruker-axs.de/fileadmin/user_upload/xrfintro/sec1_8.html> [Accessed: 12 December 2010].

[24] Treacy, M. M. J. and Higgins, J. B. (2001). *Collection of Simulated XRD Powder Patterns for Zeolites*. Amsterdam: Elsevier.

[25] Wieboldt, R. C; Lowry, S. R. and Rosenthal, R. J. (1988). TGA/FT-IR: Thermogravimetric Analysis with Fourier Transform Infrared Detection of Evolved Gases. *Mickrochim. Acta [Wien]*, I, 179-182.

[26] Chandrasekhar, P. (1999). *Conducting Polymers, Fundamentals and Applications: A Practical Approach*. Netherlands: Springer. p. 297.

[27] Alger, Mark S. M. (1989). *Polymer Science Dictionary*. 2nd edition. London: Chapman & Hall. p. 565.

[28] Naya, S; Cao, R; Artiaga, R. and García, A. (2006). New Method for Material Classification from TGA Data by Nonparametric Regression. *Material Science Forum*, 514-516, 1452-1456.

[29] Gideon Analytical Labs, Inc. [Website]. Available from: <http://www.gideonlabs.com/thermal.htm> [Accessed: 7 October 2010].

[30] Weisz, P. B. and Frilette, V. J. (1960). Intracrystalline and Molecular-Shape-Selective Catalysis by Zeolite Salts. *Journal of Physical Chemistry*, 64, 382.

[31] Rabo, J. A; Schomaker, V. and Pickert, P. E. (1964). In: *Proceedings, 3rd International Congress on Catalysis, Amsterdam,* 2, Wiley, New York (1965), p. 1264.

[32] Englen, C. W. R; Wolthuizen, J. P; van Hoof, J. H.C. and Zanbergen, H. W. in Murakima, Y; Lijima, A. and Ward. J. W. (Eds*)*. (1986). *Studies in Surface Science and Catalysis: New Developments in Zeolite Science and Technology, Proceedings to the 7th International Zeolite Conference*, 28, 709.

[33] Kampers, F. W. H.; Engelen. C. W. R.; van Hoof, J. H. C and Konigsberger, D. C. (1990). Influence of Preparation Method on the Metal Cluster Size of Platinum/ZSM-5 Catalysts as Studied with EXAFS. *Journal of Physical Chemistry*, 94 (23), 8574-8578.

CHAPTER SIX

RESULTS & DISCUSSION

6.1 Introduction

The results of the catalytic experimental runs are discussed in this chapter in order to evaluate the catalysts' performance. First, the results of runs performed earlier in the atmospheric hydroisomerization unit are discussed. After that, discussion and analysis of the runs performed on the purpose-built pressure hydroisomerization unit follow. The purpose of the research is to choose the best catalyst among the ones tested for hydroisomerization of normal heptane and to determine the optimal experimental conditions that most enhance the catalyst stability and product octane number.

6.2 Atmospheric Unit Experiments

In this glass unit, catalysts USY-B, USY-C, and USY-D, all loaded with 1wt% platinum, were tested at temperatures ranging from 170 to 250^{o}C and at a space time of 140.6 kg.s/mol. At each temperature, products of the reaction were collected once steady-state conditions were achieved. Catalysts were regenerated by calcination and re-reduction in H_2 overnight before going to the next temperature. Products in the range of C_1 to C_6 were summed and labelled as cracking products, whereas all C_7s excluding normal heptane were summed and labelled isomerization products.

6.2.1 Effect of Reaction Temperature

Figures 6-1, 6-2, and 6-3 show the cracking and isomerization product yields as a function of reaction temperature for experiments with USY-B, USY-C, and USY-D, respectively. Up to 190^{o}C, hydroisomerization is the dominant reaction with almost no cracking present for all catalysts. However, for USY-B and USY-C, as the temperature rises to 210^{o}C hydroisomerization reaches a peak and cracking begins to take over, an observation that occurs at 230^{o}C for USY-D. The catalysts behave differently beyond their hydroisomerization yield peaks, as USY-B cracks normal heptane at a faster rate than hydroisomerize it, reaching almost 100% cracking at 250^{o}C. USY-C maintains its peak hydroisomerization rate at around 55% up to 230^{o}C and it falls to around 30% at 250^{o}C.

USY-D drops its hydroisomerization rate moderately to 42% from a peak of around 52%, without having a crossover from hydroisomerization to cracking up to 250°C. The behaviour of USY-B is possibly due to its higher acidity over that of USY-C and USY-D, indicated by its lower framework Si/Al ratio, and its lower average pore size (Table 5-1), which resulted in the higher selectivity towards cracking. USY-D, on the other hand, has a lower acidity and bigger average pore size than both USY-B and USY-C, resulting in a lesser degree of activity and higher selectivity to isomers. The activity of the three catalysts dropped in the order USY-B > USY-C > USY-D.

Figure 6-1. Hydroisomerization and cracking yields as functions of reaction temperature for USY-B.

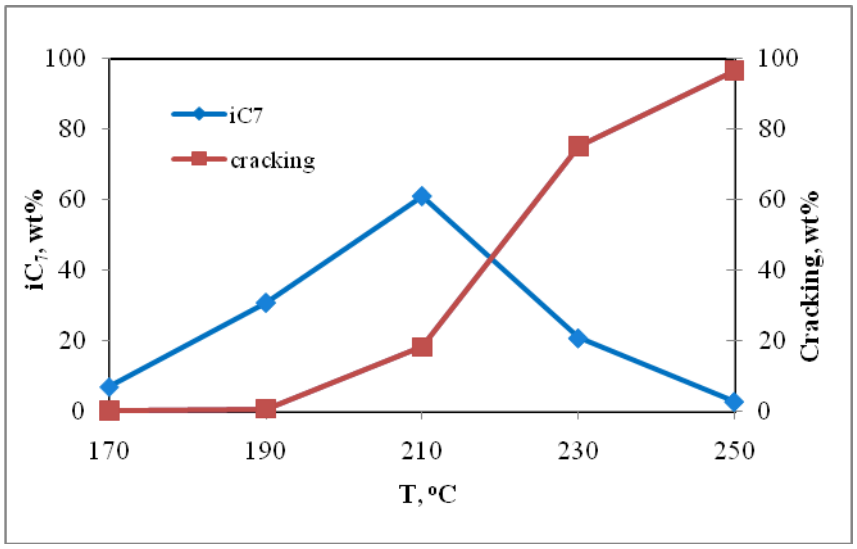

Figure 6-2. Hydroisomerization and cracking yields as functions of reaction temperature for USY-C.

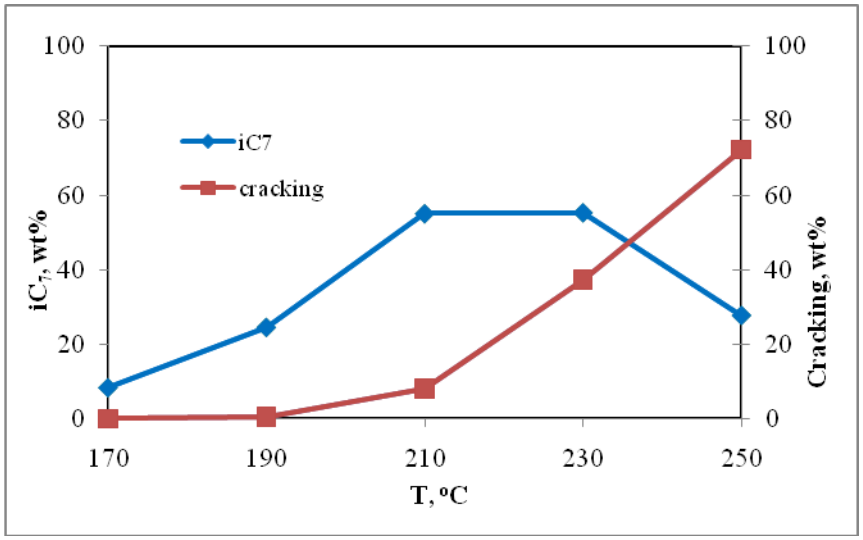

Figure 6-3. Hydroisomerization and cracking yields as functions of reaction temperature for USY-D.

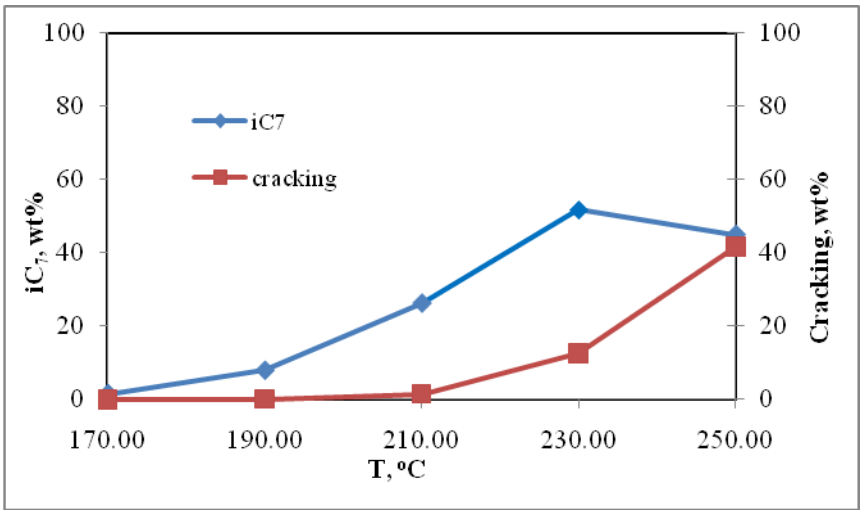

Figures 6-4, 6-5, and 6-6 show the hydroisomerization yield, cracking yield, and overall conversion, respectively for the three catalysts as a function of reaction temperature. These figures show clearly that catalyst USY-B is the most active among the three, but this high activity, due to its high acidity, comes with a lower selectivity to isomers. Isomers selectivity drops substantially above the temperature of 210^{o}C. On the other hand, USY-D is the least active but has a high selectivity to isomers. The behaviour of the three catalysts as a function of temperature is in good agreement with literature discussed in sub-section 3.3.2.

Figure 6-4. Hydroisomerization yield as a function of temperature for the three catalysts.

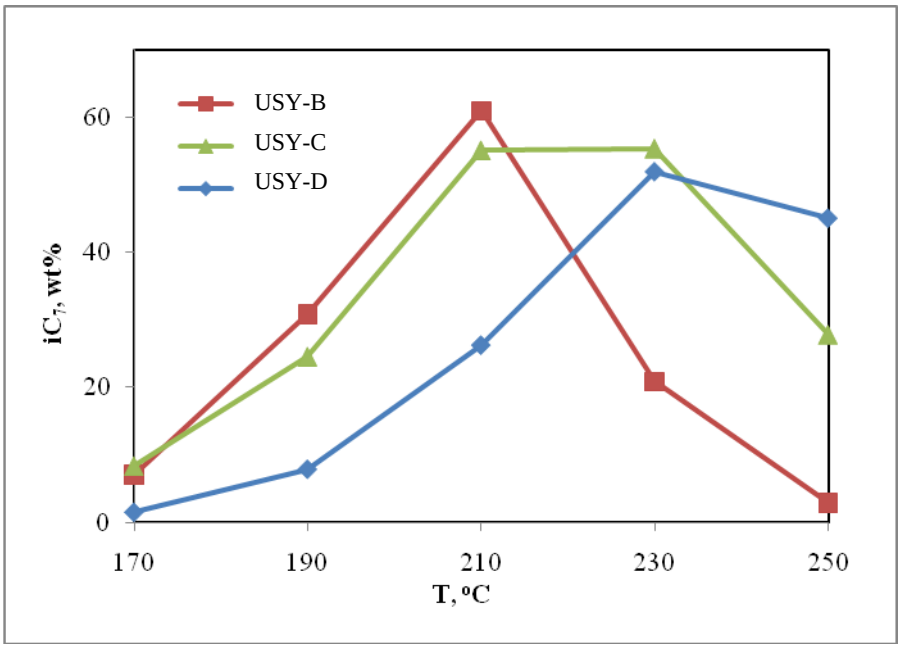

Figure 6-5. Cracking yield as a function of temperature for the three catalysts.

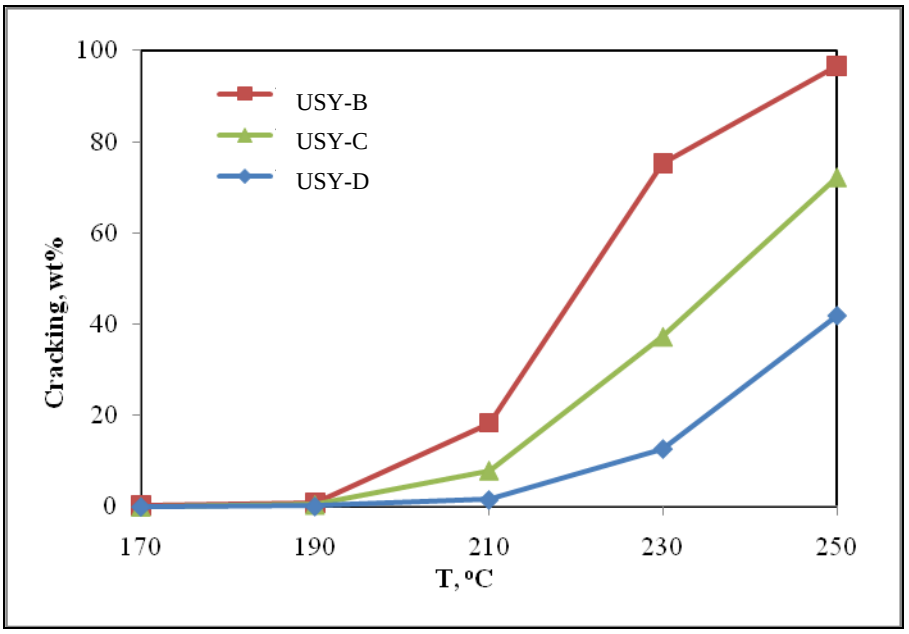

Figure 6-6. Overall conversion as a function of temperature for the three catalysts.

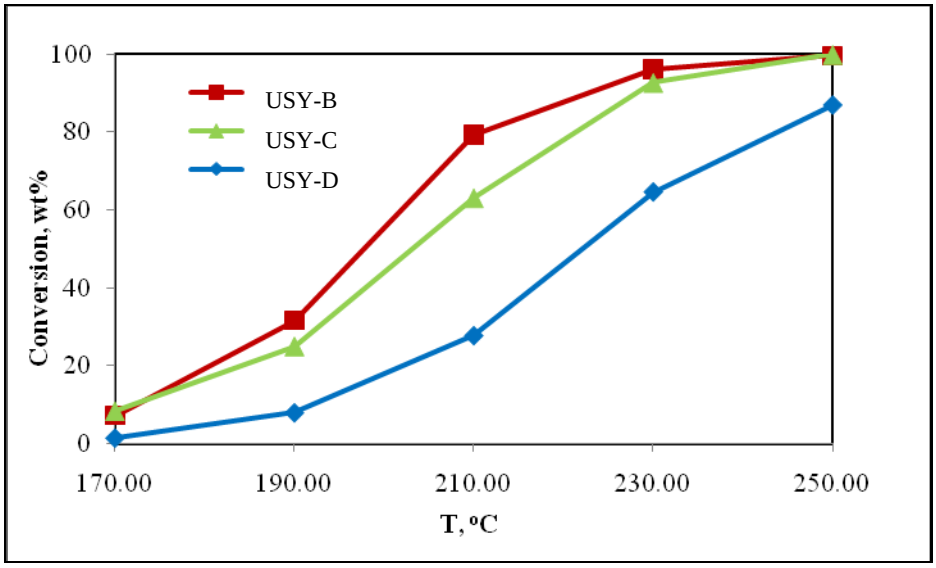

6.2.2 Effect of Overall Conversion

The selectivity of hydroisomerization and cracking products plotted versus overall conversion for the three catalysts is shown in Figures 6-7, 6-8, and 6-9. As expected, as the overall conversion increased, it can be seen clearly that the yield of hydroisomerization products decreased in the favour of cracked products for all catalysts. A higher selectivity to heptane isomers was noticed in the order USY-B > USY-C > USY-D at a given conversion. For example, at 80 wt% conversion, the selectivity for USY-B, USY-C, and USY-D was approximately 78, 75, and 62, respectively. The unit cells for USY-B, USY-C,

and USY-D are shrinking from USY-B (24.53 Å) to USY-D (24.38 Å) due to varying degrees of dealumination. This implies smaller pore openings. Having a larger pore size might have helped an easy movement (diffusion) of the larger transition-state molecules within the structure of USY-B, resulting in a slower rate of cracking at both low and moderate overall conversion levels. This correlation between the zeolite pore size and its selectivity towards hydroisomerization has been reported in the literature [1]. Another possible explanation for the argument of a higher diffusion rate in USY-B is the presence of an increasing amount of extra framework aluminium species in USY-C and USY-D's structures arising from the higher ratio of Lewis to Brönsted due to steaming, which might have induced a limitation and restriction of the movement of bulky intermediates within their structures.

Figure 6-7. Selectivity to hydroisomerization and cracking products as functions of overall conversion for USY-B.

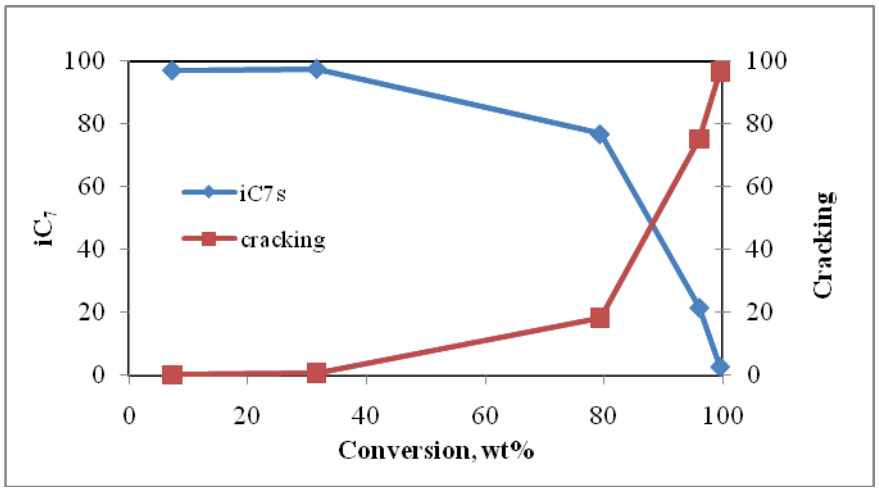

Figure 6-8. Selectivity to hydroisomerization and cracking products as functions of overall conversion for USY-C.

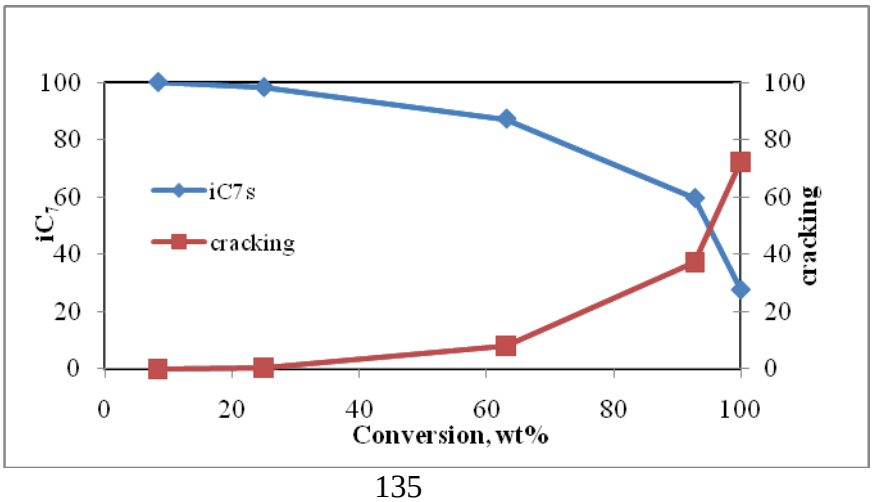

Figure 6-9. Selectivity to hydroisomerization and cracking products as functions of overall conversion for USY-D.

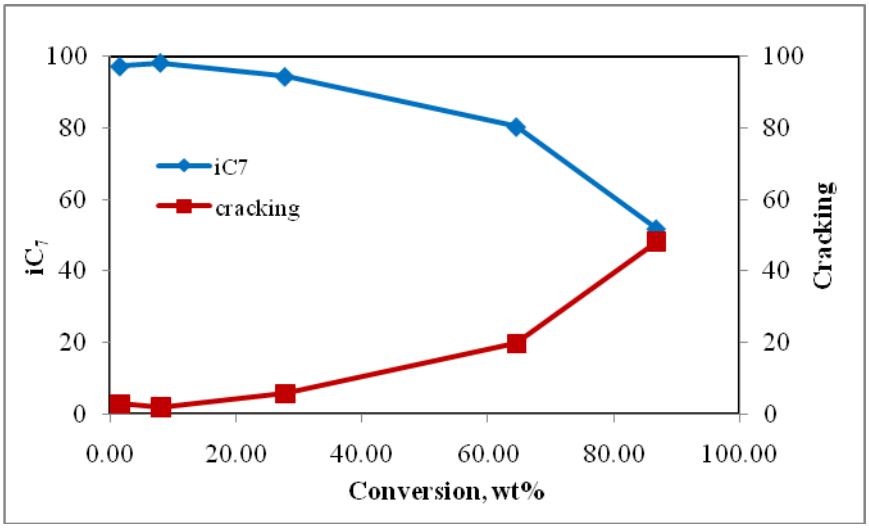

6.3 Pressure Unit Experiments

In this stainless-steel higher pressure unit discussed in section 4.3, catalysts USY-A, USY-C, USY-D, and CBV-712, all loaded with 1 wt% platinum, were tested at temperatures ranging from 210 to 250°C, space times of 140.6, 70.6, and 35.2 kg.s/mol, and pressures of 1, 8, and 15 bar. Catalyst CBV-760, due to its very low activity, was tested at temperatures from 250 to 310°C. Two poisoning experiments were performed to test the effect of poisons on the performance of catalysts: one with catalyst USY-D in which 1 wt% of dimethyldisulfide (DMDS) was added to the normal heptane feed, and another with catalyst CBV-712 in which 100 ppmw of DMDS was added to the feed. At each temperature, products of the reaction were collected once steady-state conditions were achieved. Catalysts were calcined and then re-reduced before going to the next temperature.

6.3.1 Effect of Time-on-stream

The deactivation behaviour of all catalysts was tested at a space time of 140.6 kg.s/mol and atmospheric pressure. Experiments with USY-A and USY-C were quickly terminated after one day due to deactivation. Results for these catalysts, reported elsewhere [2], were carried out in the glass atmospheric reactor at 250°C and a space time of 70.6 kg.s/mol and are shown in Figure 6-10 and 6-11, respectively. As can be seen in Figure 6-10, USY-A deactivated considerably despite its initial higher conversion rate than USY-C. The high acidity of USY-A is probably responsible for this poor performance. For

this reason further study of the performance of this catalyst was discontinued. Catalyst USY-C had a very good stability after a moderate drop in activity, stabilizing around 50 wt% conversion, as shown in Figure 6-11. This superior performance over USY-A is most probably due to its lower total acidity (Table 5-2) and larger average pore size (Table 5-1), causing a reduction in the coking rate responsible for pore blockage.

Figure 6-10. Overall conversion as a function of time-on-stream at 230°C for catalyst USY-A (adapted from [2]).

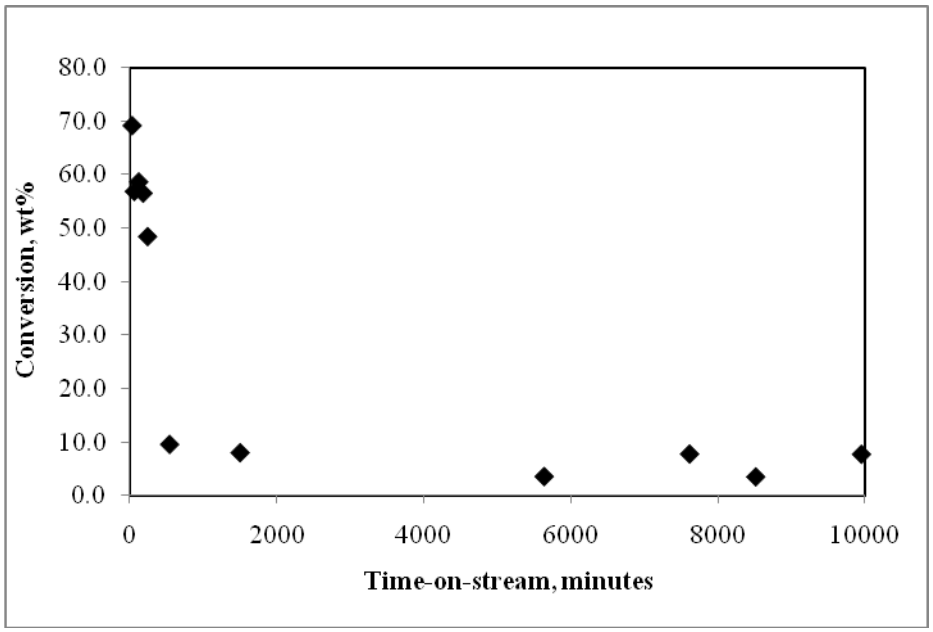

Figure 6-11. Overall conversion as a function of time-on-stream at 230°C for catalyst USY-C (adapted from [2]).

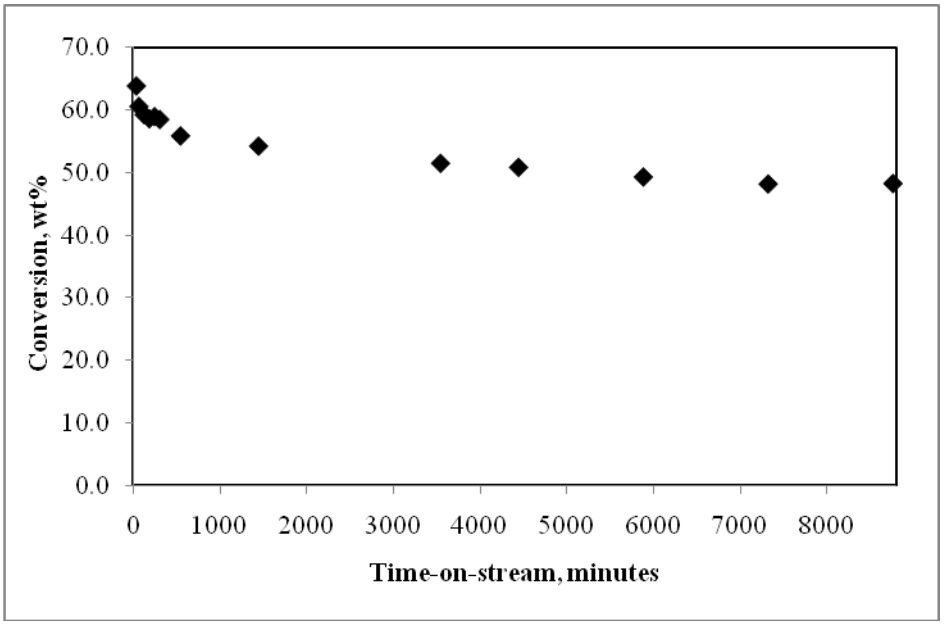

The deactivation behaviour for catalysts USY-D, CBV-712, and CBV-760 was studied at various temperatures and atmospheric pressure and at a space time of 140.6 kg.s/mol. Figure 6-12 shows the conversion in mol% for normal heptane over USY-D versus time-on-stream. Conversion in mol% was calculated as follows: $X = [(n_{C7})_0 - (n_{C7})_f]/(n_{C7})_0 \times 100$, where $(n_{C7})_0$ and $(n_{C7})_f$ are the initial and final concentrations of normal heptane in moles, respectively. It can be seen that the activity of this catalyst remained almost constant with time for temperatures of 210 and 230°C. However, a loss of conversion of almost 20 mol% over the course of three days is seen at 250°C. This drop in activity suggests deactivation due to coking at this temperature. In order to check for repeatability, the deactivation run at 210°C was repeated after the catalyst was calcined in-situ and the conversion levels obtained for the repeat experiment were very similar to the original test.

Figure 6-12. Overall conversion as a function of time-on-stream at different temperatures for catalyst USY-D.

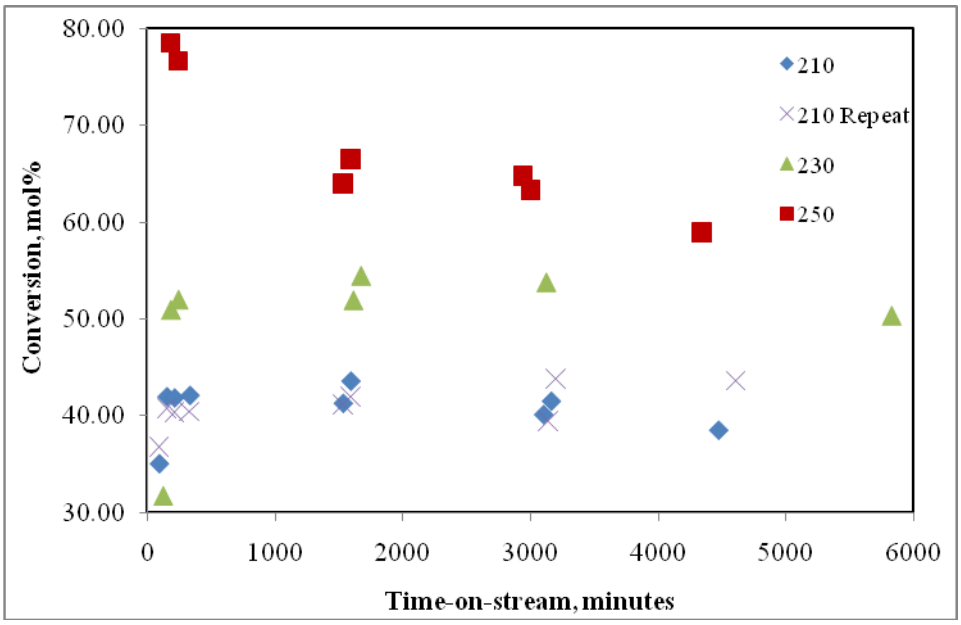

Catalyst CBV-712, which has a comparable framework Si/Al ratio, showed a higher activity than USY-D at 230°C, with conversion stabilizing around 60 mol% versus a percentage conversion in the low 50s for USY-D, as seen from Figure 6-13. This higher activity, though, comes at the expense of stability, as the activity of CBV-712 seems to be steadily decreasing at 230°C, while it was stable at this temperature for USY-D. Conversion was not enhanced at 250°C than it was at 230°C, with deactivation being steeper at 250°C. An explanation of this lower stability of CBV-712, even though it had

been acid-leached and its bulk aluminium content lowered, might be the presence of strong Lewis acid sites, which can occur in acid-leached samples (see sub-section 2.4.1). Another possibility is that the higher crystallinity of CBV-712 (Table 5-1) caused the stronger acidity that, in turn, resulted in the weaker stability of the catalyst (See sub-section 2.4.1). Both explanations fit well with the observation of a higher activity and lower stability of CBV-712 versus those of USY-D.

Figure 6-13. Overall conversion as a function of time-on-stream at different temperatures for catalyst CBV-712.

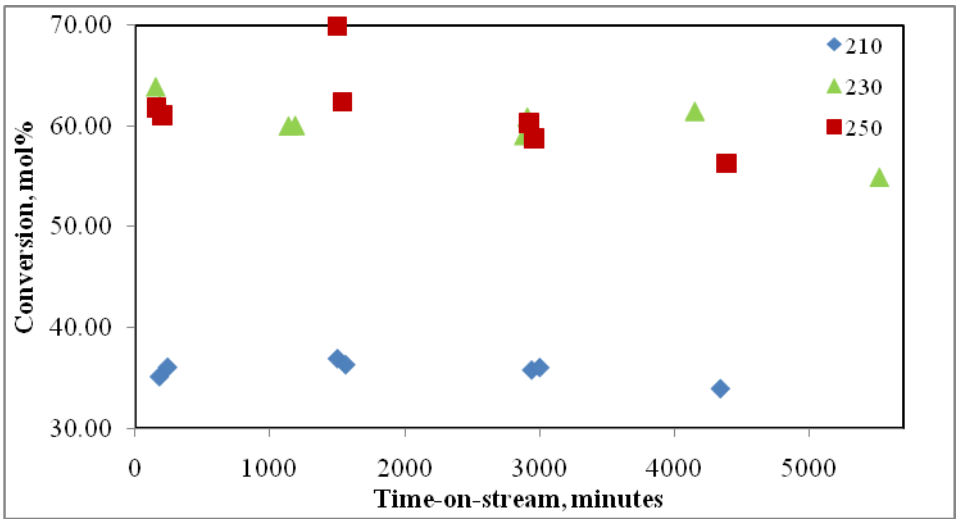

Figure 6-14 shows the deactivation behaviour of the deeply acid-leached catalyst CBV-760 at temperatures from 250 to 310°C. At 250 and 270°C, the conversion over this catalyst was stable at very low values during the first day on-stream; therefore the temperature was increased to 290°C. There, the conversion was higher, starting at around 50 mol%, but dropped to around 35 mol% by the third day, where it stabilized. At 310°C, the conversion was slightly lower than at 290°C and the catalyst was deactivating slowly with time. The poor performance of this catalyst compared to CBV-712 and USY-D despite its high degree of dealumination (supposed to enhance stability) is possibly due to its lower average pore diameter (Table 5-1), which could have arisen due to a partial collapse of its structure upon deep dealumination, evident from its lower crystallinity than the less severely acid-leached CBV-712. For comparison, the same catalyst was tested at 15 bar and the activity was increasing up to 6 hours. However, the reaction rig could not operate overnight at hight pressures, so deactivation behaviour could not be properly studied at pressure.

Figure 6-14. Overall conversion as a function of time-on-stream at different temperatures for catalyst CBV-760.

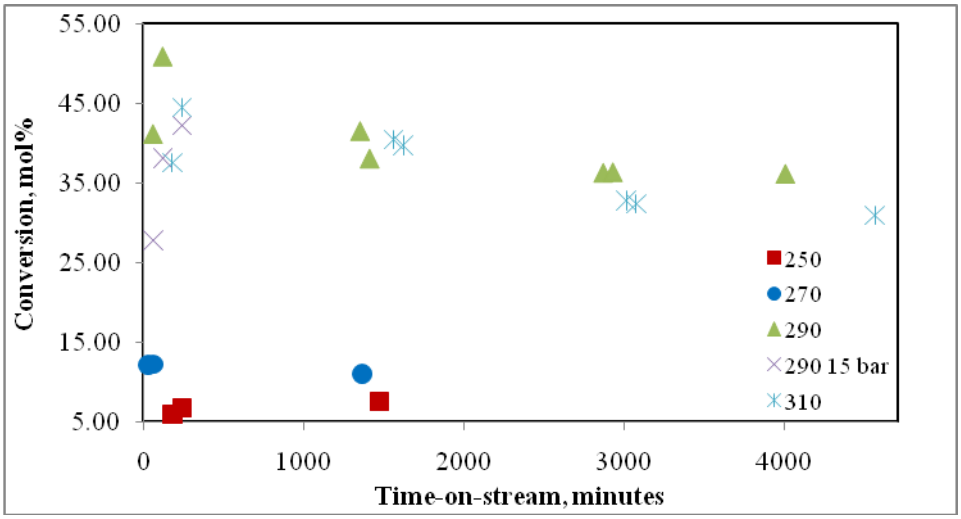

Figure 6-15 shows a comparison of the deactivation behaviour of catalysts USY-C, USY-D, CBV-712, and CBV-760 at 250°C. Both catalysts USY-C and CBV-760 are stable during the first day. CBV-712 is also stable for the first 24 hours but loses about 5 - 10% of its conversion over the next 2 days. USY-D is comparable in its performance to CBV-712 but it loses a lot of activity in the first day and then slowly thereafter with a meagre drop of 5 mol% over the next 48 hours, suggesting that it would be more stable than CBV-712 over a longer period.

Figure 6-15. Overall conversion as a function of time-on-stream at 250°C for all catalysts.

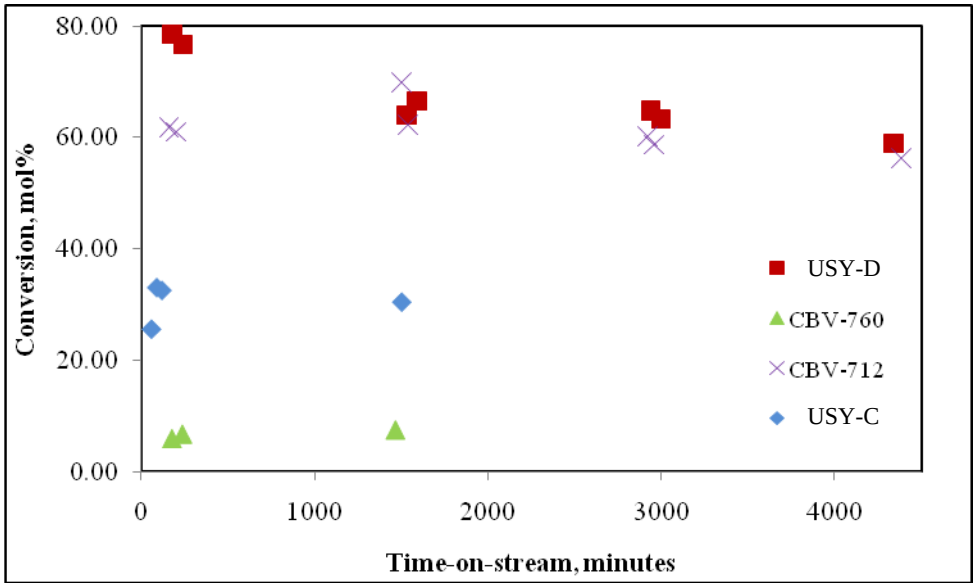

In order to test the effect of deactivation on the catalysts acid and hydrogenation/dehydrogenation functions, a ratio of the total isomers yield divided by the cracking products yield has been plotted versus time-on-stream in Figure 6-16. Aside from an initial drop in the I/C ratio for CBV-760, it and USY-C both see a rise of the ratio after one day on-stream (1440 minutes), which means that the selectivity has been switching from cracking to hydroisomerization for both catalysts, since conversion was almost constant during this time. This could have been caused by a minor deactivation of the acid sites, leading the intermediate olefins to have a less chance of rearranging further or crack on another acid site before they hydrogenate on a metal site. This perhaps explains why in Figure 6-17 the ratio of the mono to multi-branched isomers increased for these two catalysts. The I/C ratio for catalysts USY-D and CBV-712 is almost constant for the entire duration of the experiment, despite their observed deactivation over the period. This implies that both acid and metal functions have been equally deactivating. The Mono/Multi ratio is also almost constant for these catalysts, which adds to the conclusion that deactivation targeted both acid and hydrogenation functions. Identification for all the normal heptane isomers by GC that was necessary to calculate the Mono/Multi ratio is shown in Appendix D.

Figure 6-16. Isomer to cracking products ratio as a function of time-on-stream at 250°C for all catalysts.

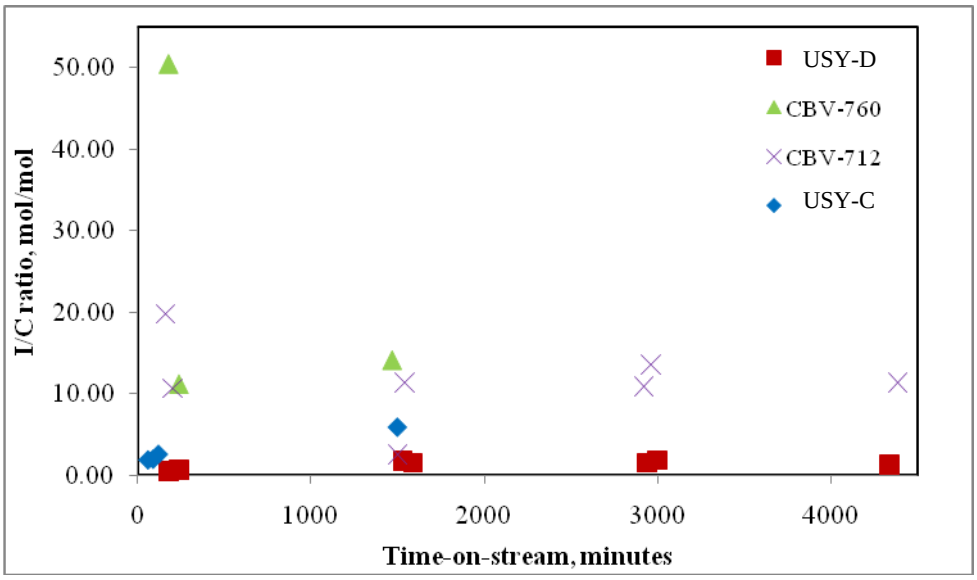

Figure 6-17. Mono to multi-branched isomers ratio as a function of time-on-stream at 250°C for all catalysts.

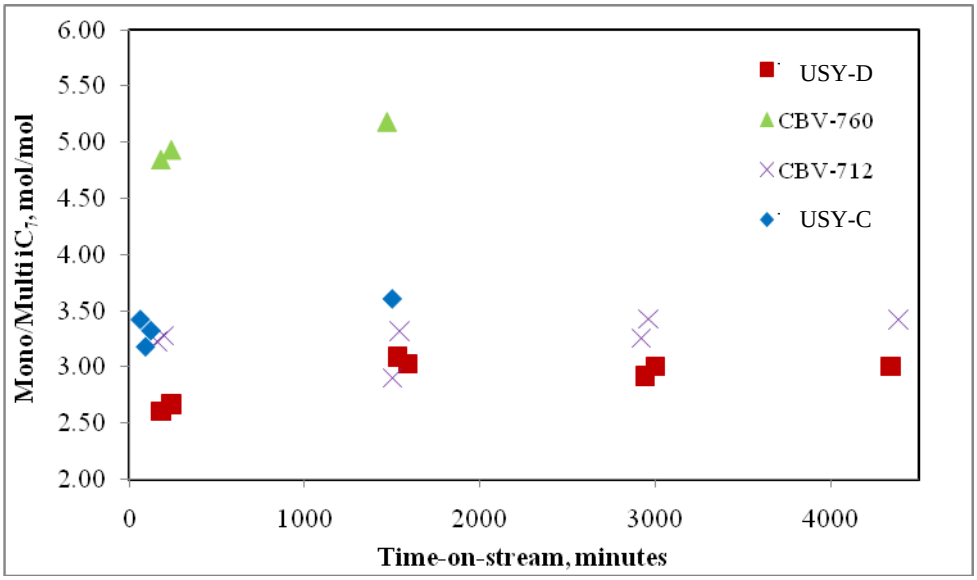

6.3.2 Effect of Reaction Temperature

The yield of heptane isomers versus overall conversion is shown in Figure 6-18 for USY-C at different temperatures. As can be seen from the figure, the yield increases with increasing conversion and, at some point, starts declining. However, 230°C seems to be the optimum temperature for operation for this catalyst, as a higher reaction temperature does not contribute to a higher yield of isomers. USY-D is able to carry the isomer yield higher than is USY-C at 250°C, as indicated from Figure 6-19. CBV-712 shows superiority in that its yield of isomers does not diverge from the straight line except for one point at 250°C, suggesting that its cracking activity is minimal, as seen from Figure 6-20. Its optimum temperature of operation is at 230°C, where the yield of isomers exceeds 60 mol%. CBV-760 yields the lowest amount of isomers among these catalysts, with a best performance at 290°C, as shown in Figure 6-21.

Figure 6-18. Heptane isomers yield as a function of overall conversion at different temperatures for USY-C.

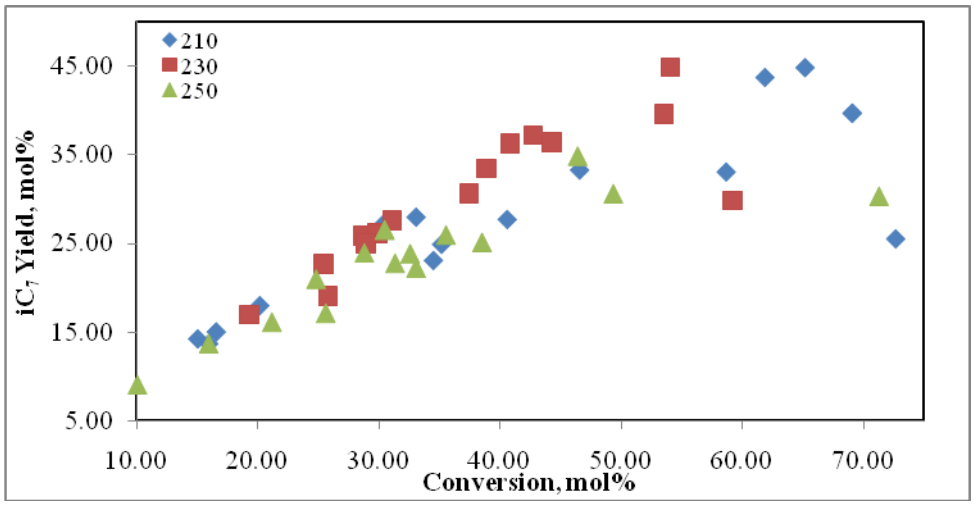

Figure 6-19. Heptane isomers yield as a function of overall conversion at different temperatures for USY-D.

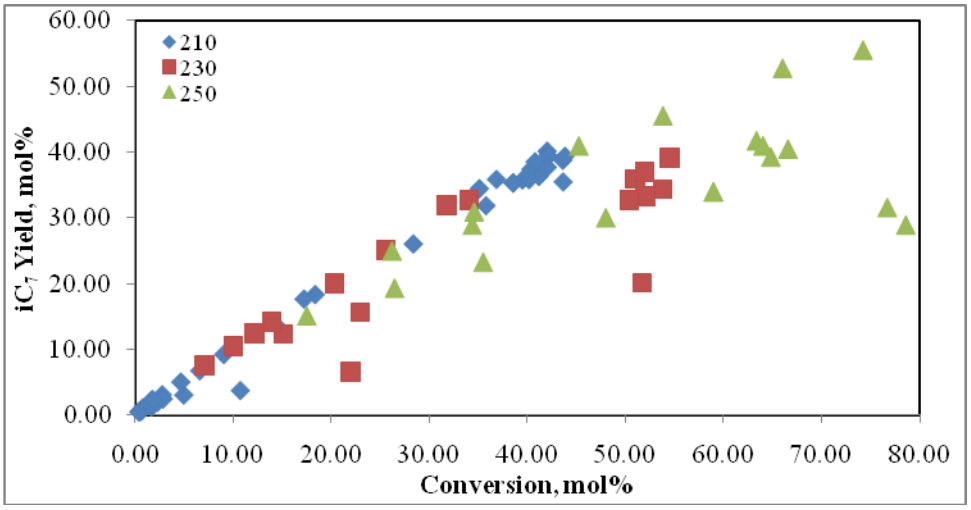

Figure 6-20. Heptane isomers yield as a function of overall conversion at different temperatures for CBV-712.

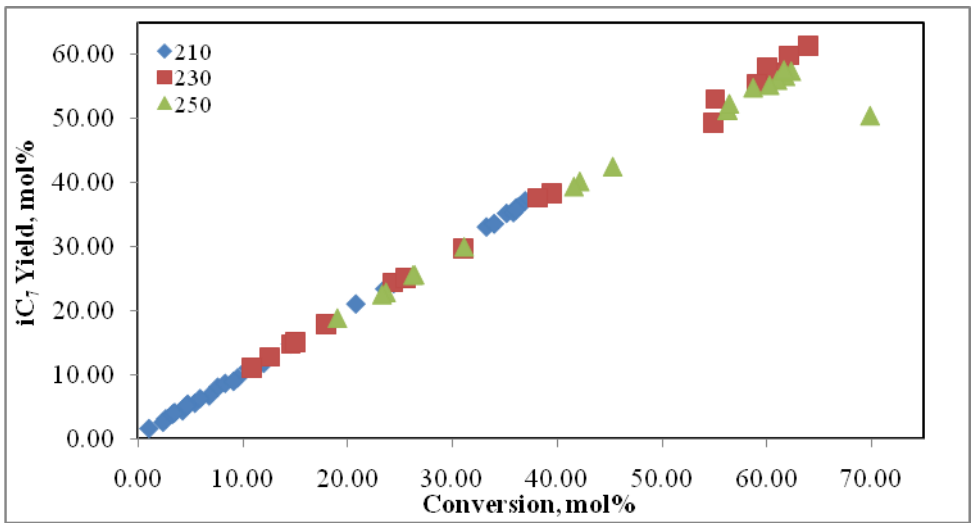

Figure 6-21. Heptane isomers yield as a function of overall conversion at different temperatures for CBV-760.

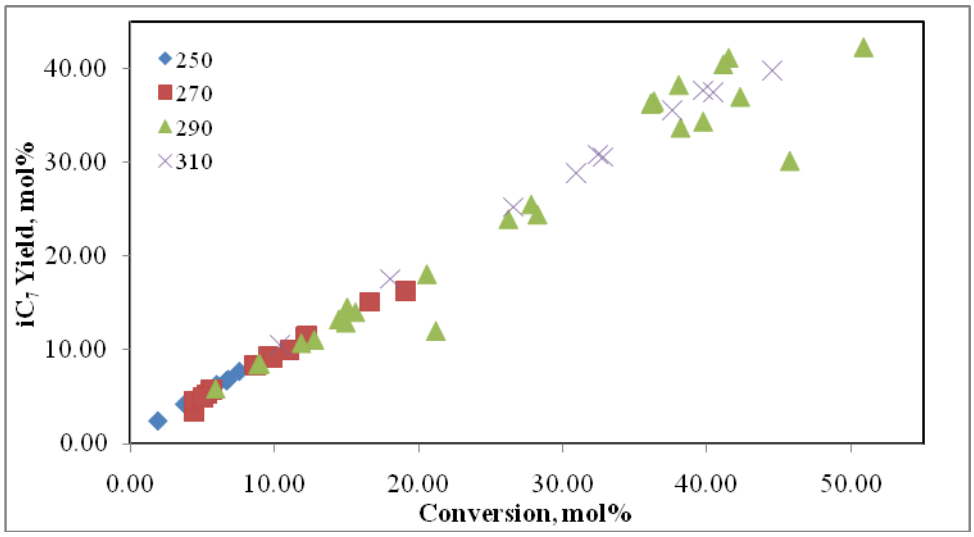

The isomer yield obtained with all catalysts tested at 210°C as a function of overall conversion is shown in Figure 6-22. USY-C is obviously poorer in performance than USY-D and CBV-712, due probably to its small pore structure and higher Brönsted/Lewis site ratio (Tables 5-1 and 5-2). This is evident by the clear diversion from the straight line Y=X above 30 mol% conversion, due to the increasing presence of cracking. The divergence from the straight line occurs for USY-D at 230 and 250°C (Figures 6-23 & 6-24). It is safe here to assume that CBV-712 does not generate much cracking products because of the moderate acid-leaching treatment subsequent to steaming which removed enough EFAL species responsible for increased cracking tendencies, but was not deep enough to the extent where it can cause a partial collapse of the structure and, hence, a loss of activity, as noticed with CBV-760.

Figure 6-22. Heptane isomers yield as a function of overall conversion at 210°C for all catalysts.

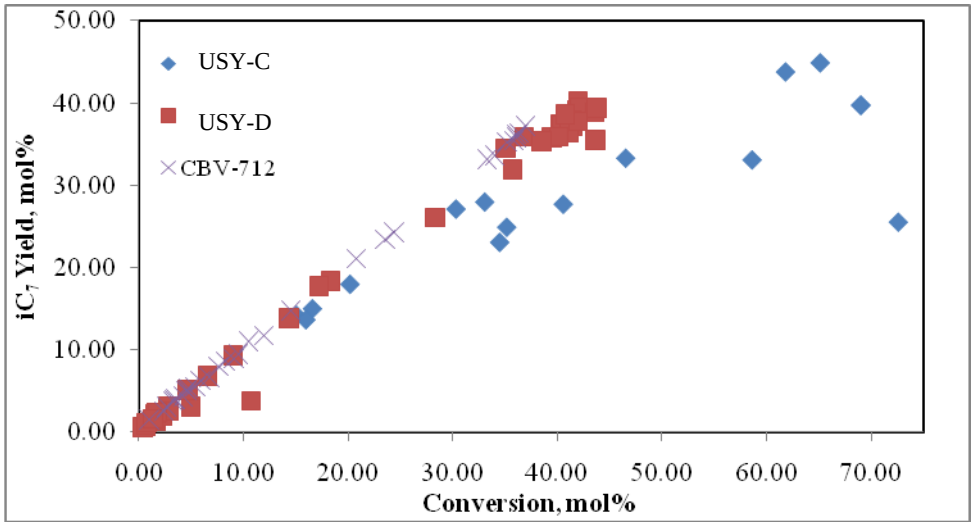

Figure 6-23. Heptane isomers yield as a function of overall conversion at 230°C for all catalysts.

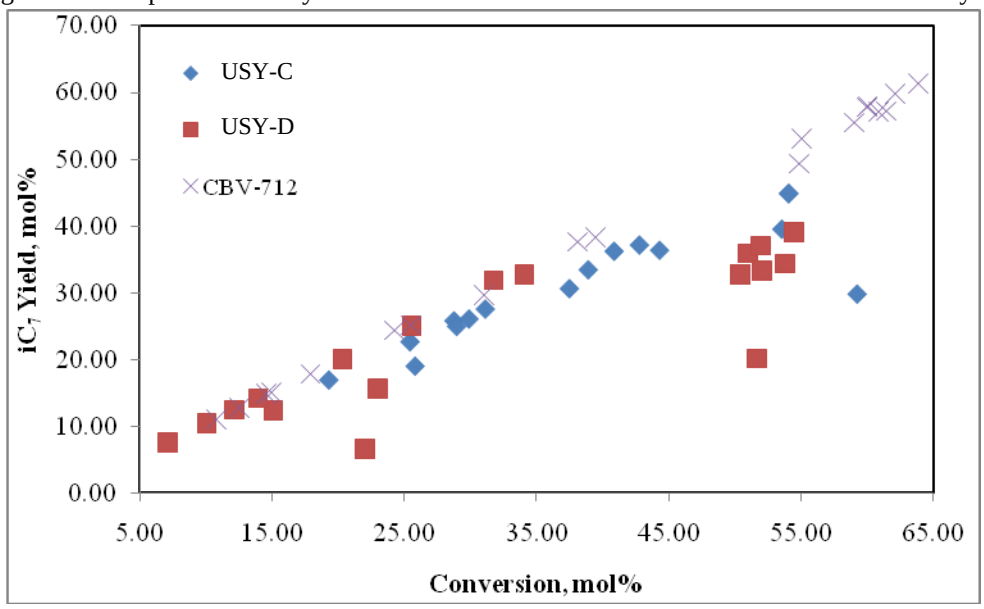

Figure 6-24. Heptane isomers yield as a function of overall conversion at 250°C for all catalysts.

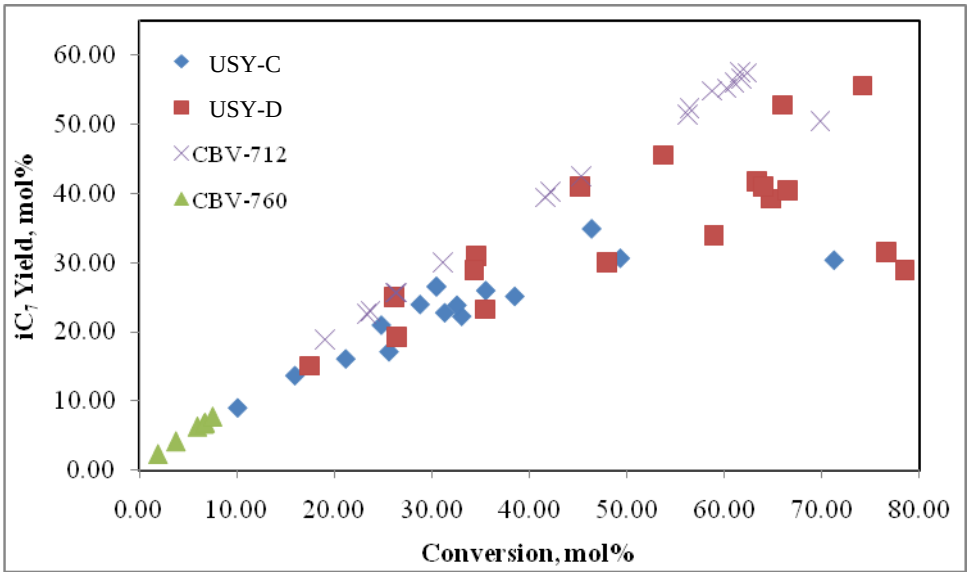

6.3.3 Effect of Reaction Pressure

The effect of system overall pressure on the yield of heptane isomers was not clear for catalysts USY-C, as it behaved in an unpredictable way with pressure as can be seen from Figure 6-25. By contrast, higher pressures were found to greatly enhance the performance of USY-D above conversions of 45 mol% (Figure 6-26), pushing the isomer yield to levels close to those achieved by CBV-712 (Figure 6-27). The reason for the better performance of USY-D and CBV-712 under higher pressures than USY-C and CBV-760 (Figure 6-28) could be the higher average pore diameters of the former two catalysts versus the latter ones (Table 5-1). Lower average pore diameters catalysts might have imposed

diffusion limitations on the bulky transition-state molecules, shifting the equilibrium to the generation of smaller cracked products, which could have resulted in a lower isomer yield.

Figure 6-25. Heptane isomers yield as a function of overall conversion at different pressures for USY-C.

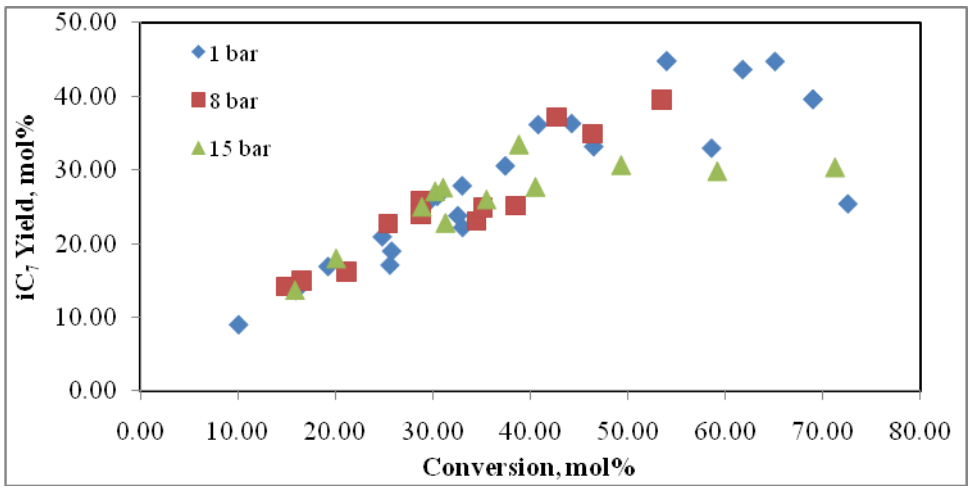

Figure 6-26. Heptane isomers yield as a function of overall conversion at different pressures for USY-D.

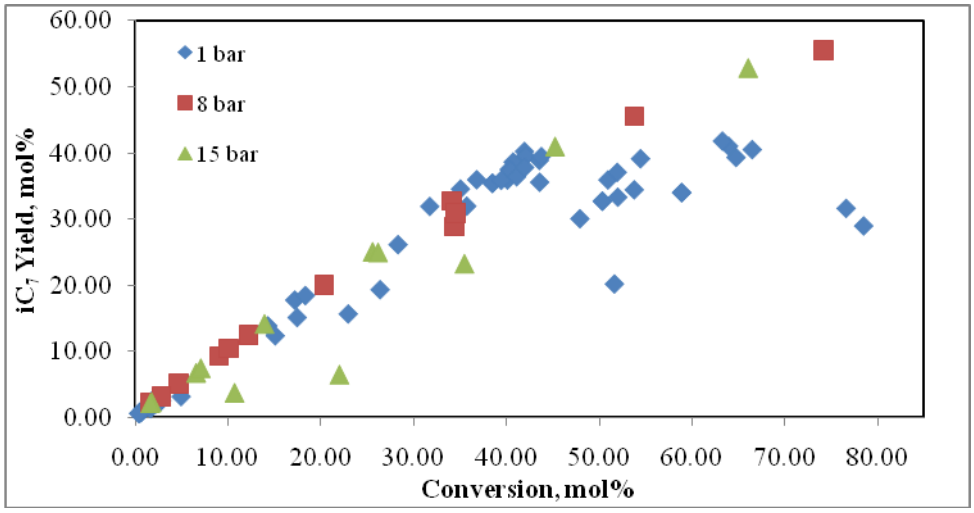

Figure 6-27. Heptane isomers yield as a function of overall conversion at different pressures for CBV-712.

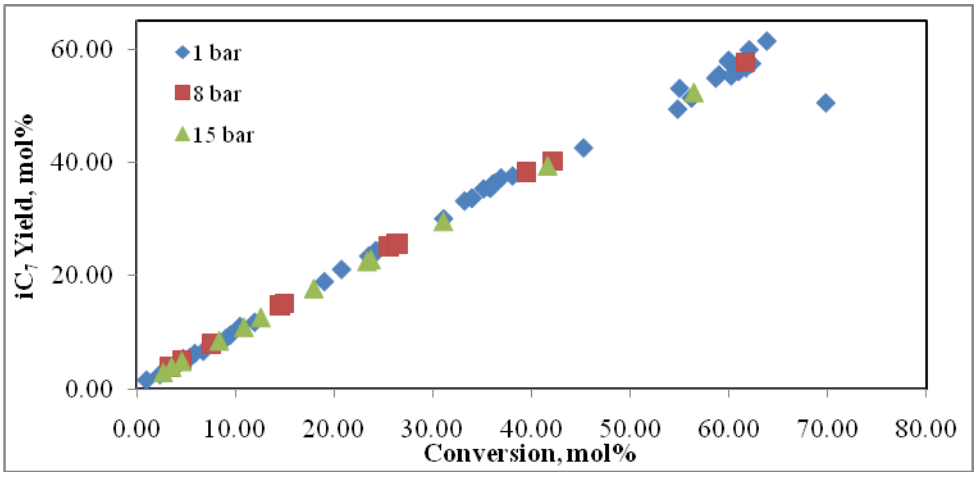

Figure 6-28. Heptane isomers yield as a function of overall conversion at different pressures for CBV-760.

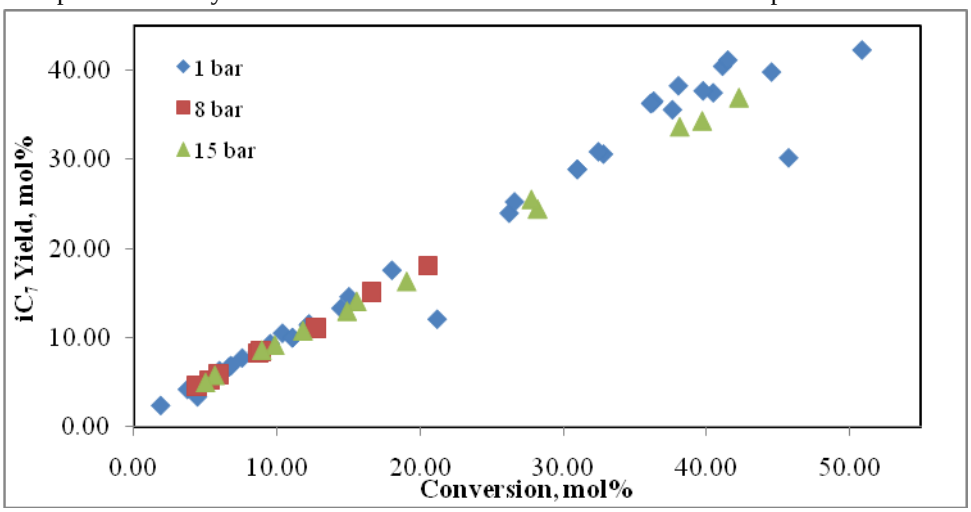

Figures 6-29, 6-30, and 6-31 show comparisons between the heptane isomer yields of all catalysts versus overall conversion at total pressures of 1, 8, and 15 bar, respectively. Despite USY-D performing poorly at 1 bar, with isomer yield comparable to that of USY-C, it is clear how its selectivity increased gradually at 8 bar, and substantially at 15 bar. This behaviour is normal for bifunctional zeolite catalysts as seen from the literature (sub-section 3.3.3), since pressure reduces overall conversion but improves hydroisomerization selectivity versus that of cracking. This, clearly, was not the case for catalyst USY-C, whose small average pore diameter has probably resulted in limited movement of larger molecules at high pressures, and promoted cracking.

Figure 6-29. Heptane isomers yield as a function of overall conversion at 1 bar for all catalysts.

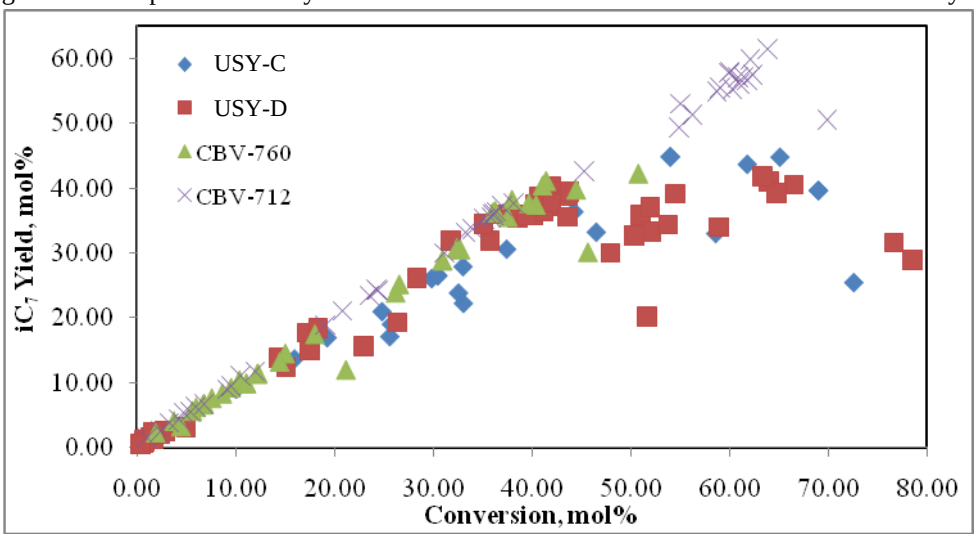

Figure 6-30. Heptane isomers yield as a function of overall conversion at 8 bar for all catalysts.

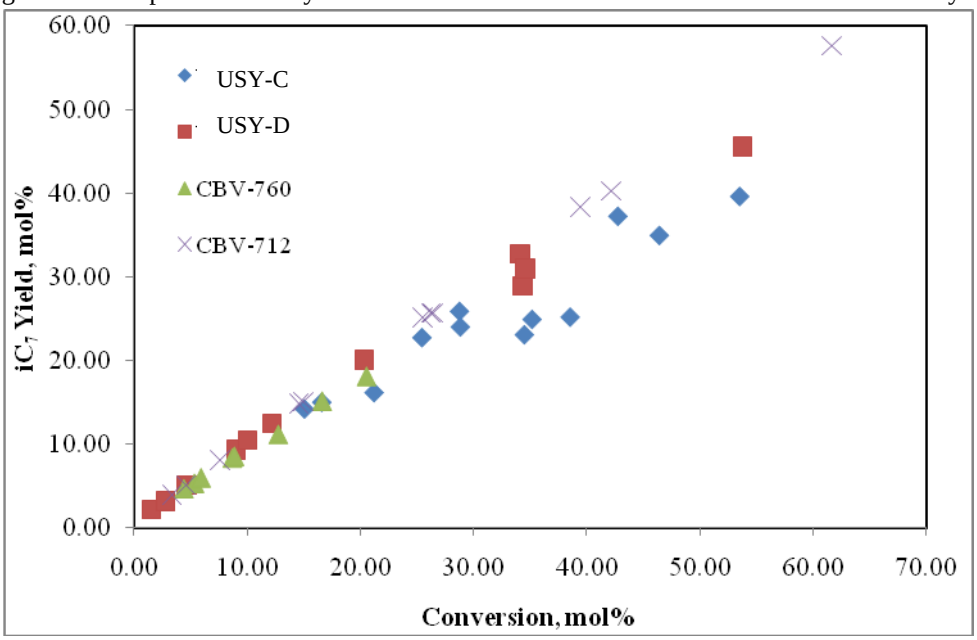

Figure 6-31. Heptane isomers yield as a function of overall conversion at 15 bar for all catalysts.

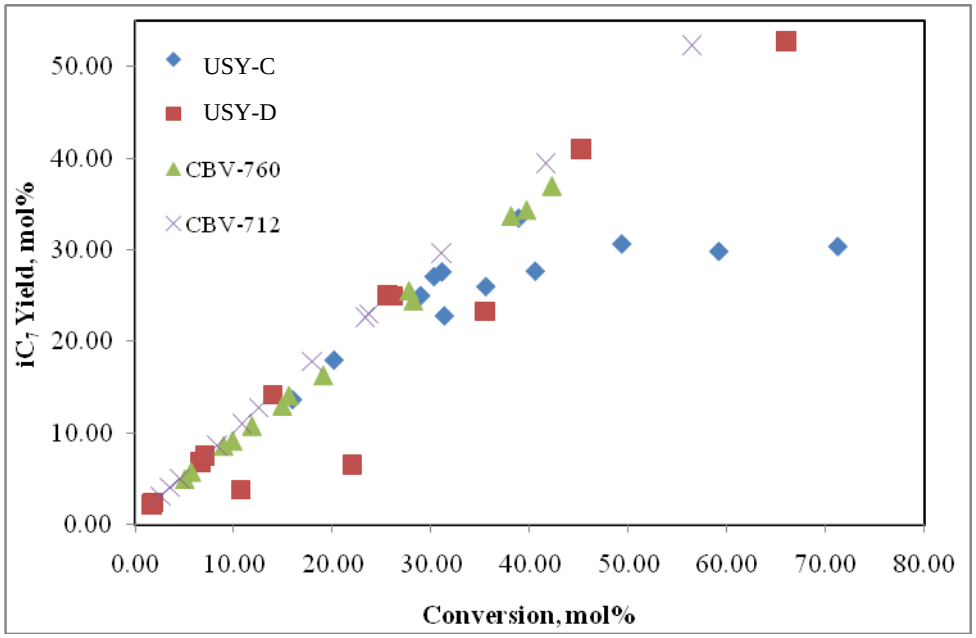

Figures 6-32 to 6-34 show the effect of pressure on the cracking yield for all catalysts at 1, 8, and 15 bar, respectively. The performance of catalysts is in agreement with what was witnessed with the isomer yield in Figures 6-29 to 6-31. Specifically, the cracking yield for USY-D was quite high at 1 bar and comparable to that of USY-C, but this yield has dropped moderately at 8 bar, and considerably at 15 bar, getting close to the yield of CBV-712. This, again, suggests diffusional limitations for USY-C at higher pressures, due to its lower average pore size. In order to further clarify the role of pressure on the performance of tested catalysts, I/C ratios have been plotted against overall conversion at

different pressures, and plots are shown in Figures 6-35 to 6-37. It is evident from the figures how the increase in pressure generally increases the ratio, but the improvement of the ratio for USY-D, especially at low conversions, is clear, since it exceeded that for CBV-712 at the lower conversion levels.

Figure 6-32. Cracking yield as a function of overall conversion at 1 bar for all catalysts.

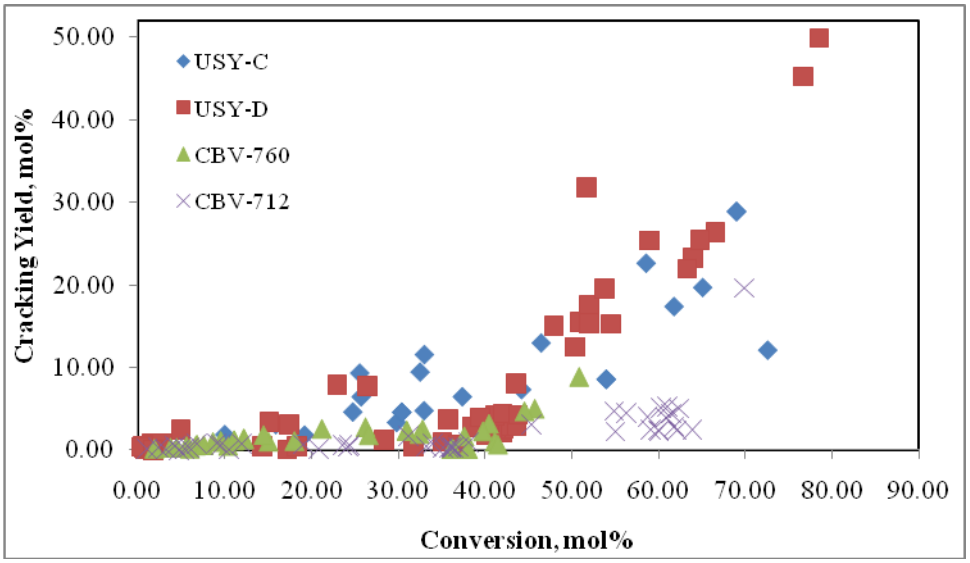

Figure 6-33. Cracking yield as a function of overall conversion at 8 bar for all catalysts.

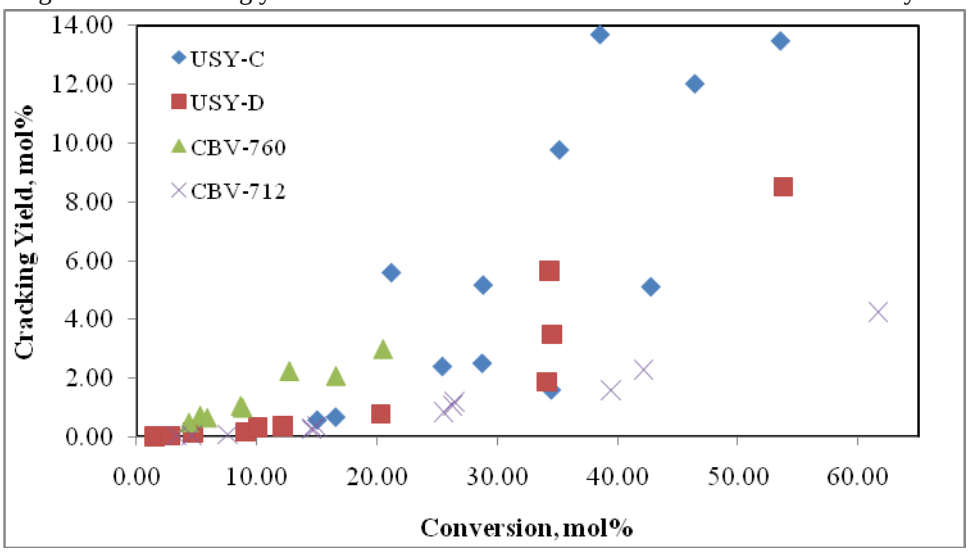

Figure 6-34. Cracking yield as a function of overall conversion at 15 bar for all catalysts.

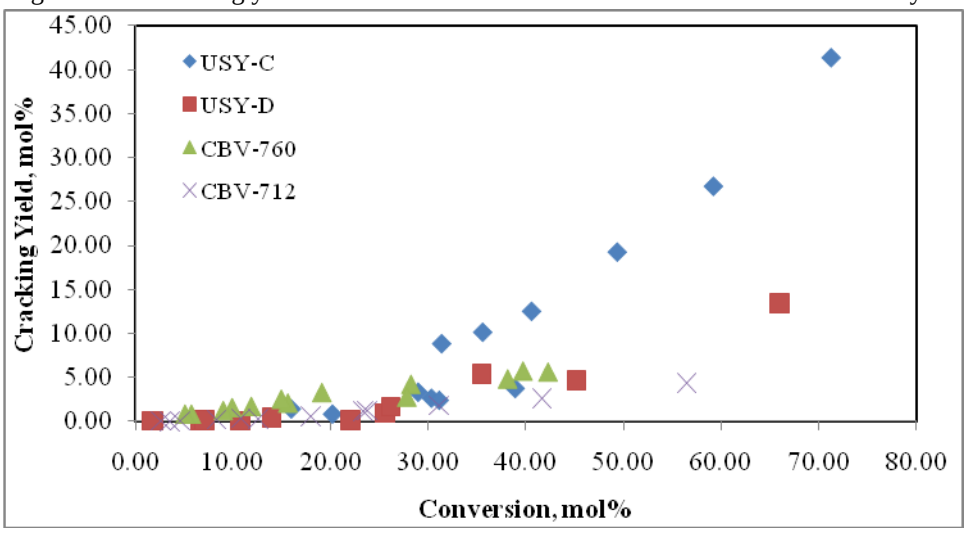

Figure 6-35. Isomer to cracking products ratio as a function of overall conversion at 1 bar for all catalysts.

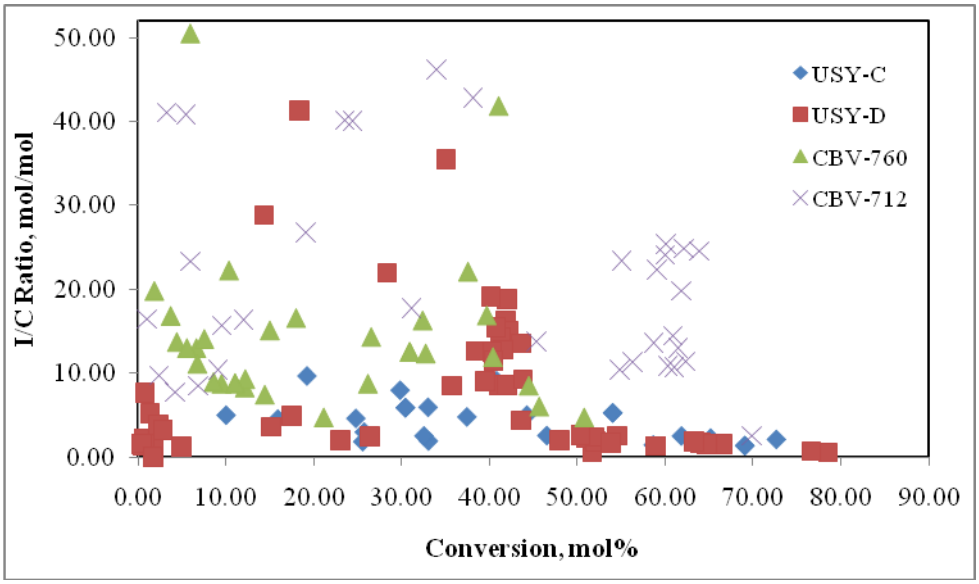

Figure 6-36. Isomer to cracking products ratio as a function of overall conversion at 8 bar for all catalysts.

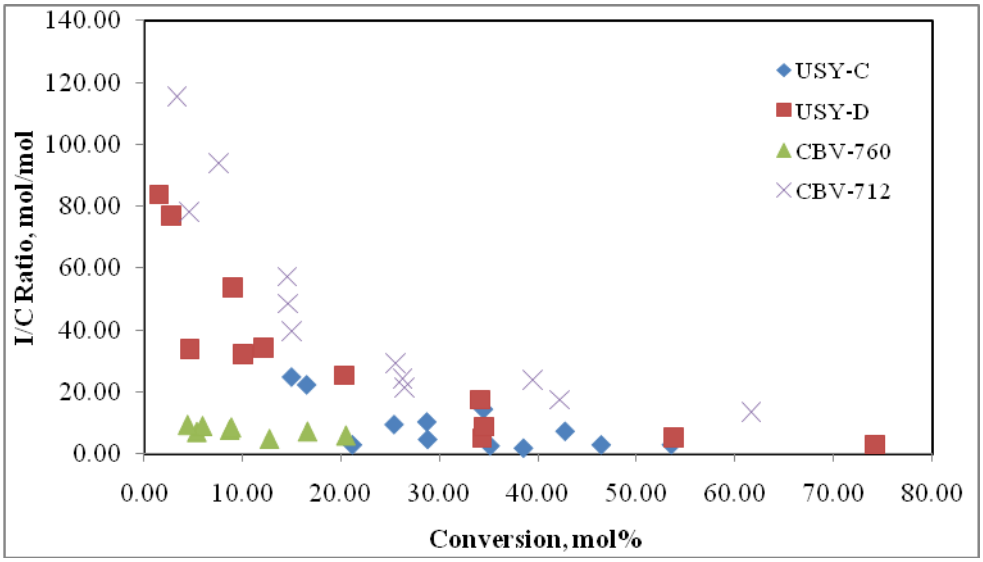

Figure 6-37. Isomer to cracking products ratio as a function of overall conversion at 15 bar for all catalysts.

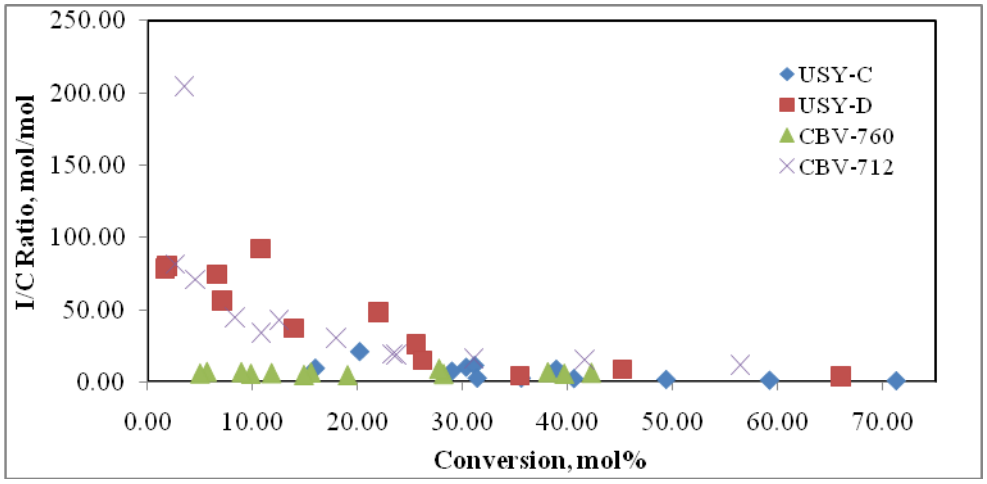

6.3.4 Effect of Contact Time

Figures 6-38 to 6-41 show the impact of changing space time on the yield of heptane isomers for temperatures 210 – 250°C as a function of overall conversion for catalysts USY-C, USY-D, CBV-712, and CBV-760, respectively. The unit for contact time is kg.s/mol. From the figures, conversion increased as the contact time increased for all catalysts, as expected and discussed previously in Chapter 3 (sub-section 3.3.4). However, increasing contact time between normal heptane and the catalyst seems to cause a reduction in isomer yield and, hence, an increase in cracking selectivity for catalysts USY-C and USY-D, which was not noticed for the acid-leached catalysts. It seems that the removal of the EFAL species from the structure of these catalysts has allowed for them to be operable at higher contact times without encountering excessive cracking, which suggests that the EFAL species are responsible for cracking through either the additional acidity they provide to the catalyst or by adding diffusion limitations on the catalysts.

Figure 6-38. Heptane isomers yield as a function of overall conversion at different contact times for USY-C.

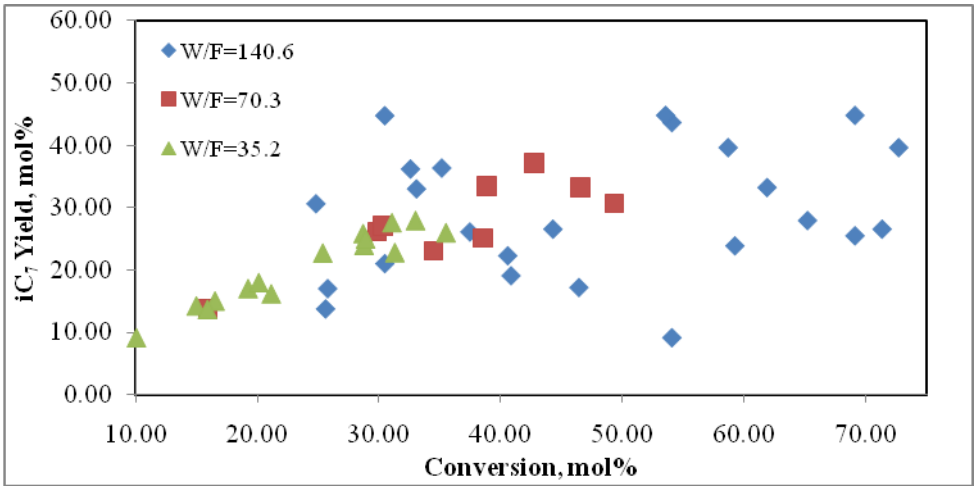

Figure 6-39. Heptane isomers yield as a function of overall conversion at different contact times for USY-D.

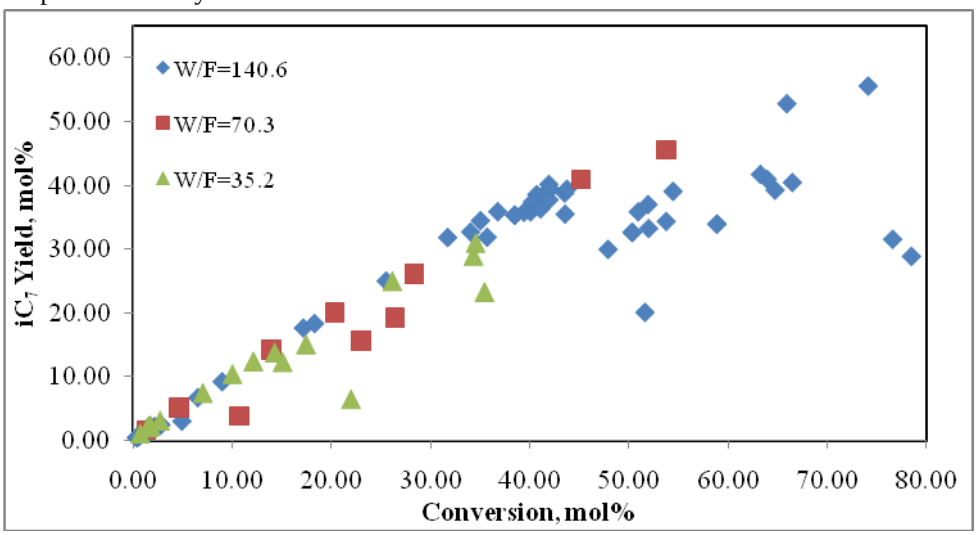

Figure 6-40. Heptane isomers yield as a function of overall conversion at different contact times for CBV-712.

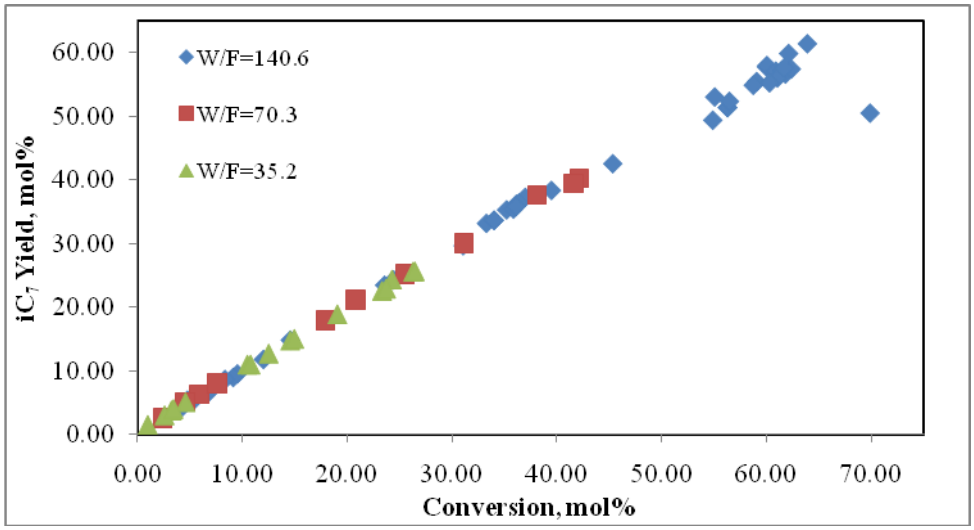

Figure 6-41. Heptane isomers yield as a function of overall conversion at different contact times for CBV-760.

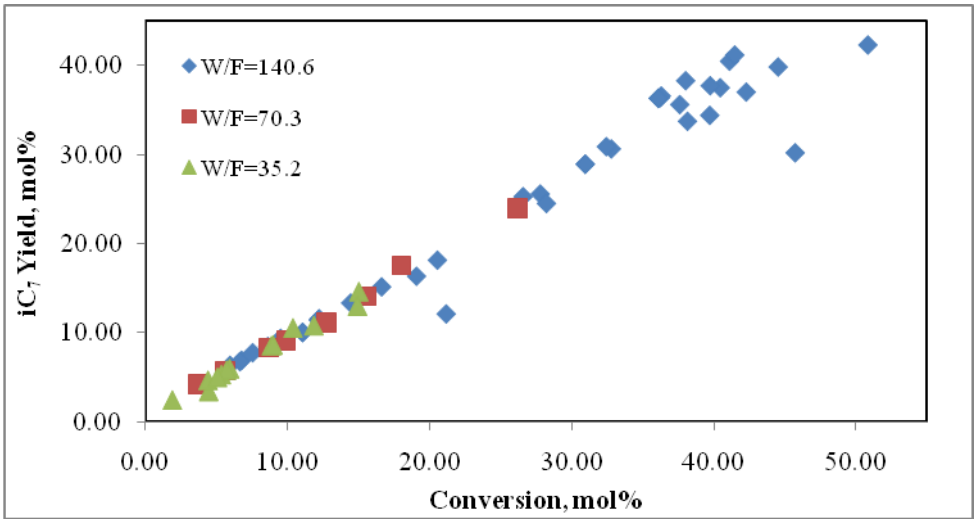

6.3.5 Effect of Acid-metal Balance

When the hydroisomerization reaction proceeds via an ideal bifunctional mechanism, a proper balance has to exist between the hydrogenation/dehydrogenation function, provided here by the platinum sites, and the acidic functions, provided by Brönsted and Lewis sites, as discussed previously. When this balance of platinum and acid sites exists, the transformation in the case of normal heptane during the reaction proceeds to first form mono-branched isomers, which, in turn, convert to multi-branched isomers upon further rearrangement. Here, multi-branched isomers would be the source of cracking products. However, when the balance between functions does not exist and the ratio of n_{Pt}/n_A is less than 0.17, as reported in sub-section 3.3.8, the reaction does not proceed in this successive manner, but different product categories are seen simultaneously. In order to check whether the tested catalysts in this work behave in an ideal bifunctional manner, yields of mono-branched isomers, multi-branched isomers and cracking products were plotted against overall conversion for all catalysts at 1, 8 and 15 bar.

Figures 6-42 to 6-44 show the results for catalyst USY-C. It can be noticed from the figures that cracking products yield exceeds that of multi-branched isomers at different levels of conversion, especially at high ones. This means that this catalyst did not behave in the ideal bifunctional fashion, since cracking products yield should be always lower than that of multi-branched isomers, indicating that the formation of multi-branched isomers precedes the formation of cracking products, as illustrated by the following equation:

$$nC_7 \rightleftarrows MB \rightleftarrows MuB \rightleftarrows CR \qquad (8)$$

This suggests that there is a deficiency in accessible platinum sites for this catalyst, which could be due to either a poor platinum dispersion or the need to load platinum in levels higher than 1 wt% in order to achieve a proper balance of its functions.

Figure 6-42. Yields of mono-branched isomers, multi-branched isomers, and cracking products as functions of overall conversion at 1 bar for USY-C.

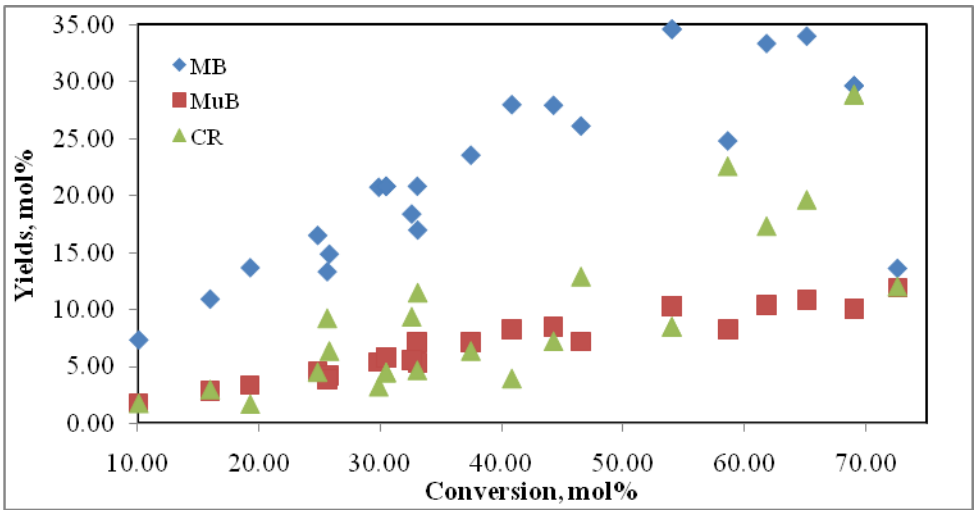

Figure 6-43. Yields of mono-branched isomers, multi-branched isomers, and cracking products as functions of overall conversion at 8 bar for USY-C.

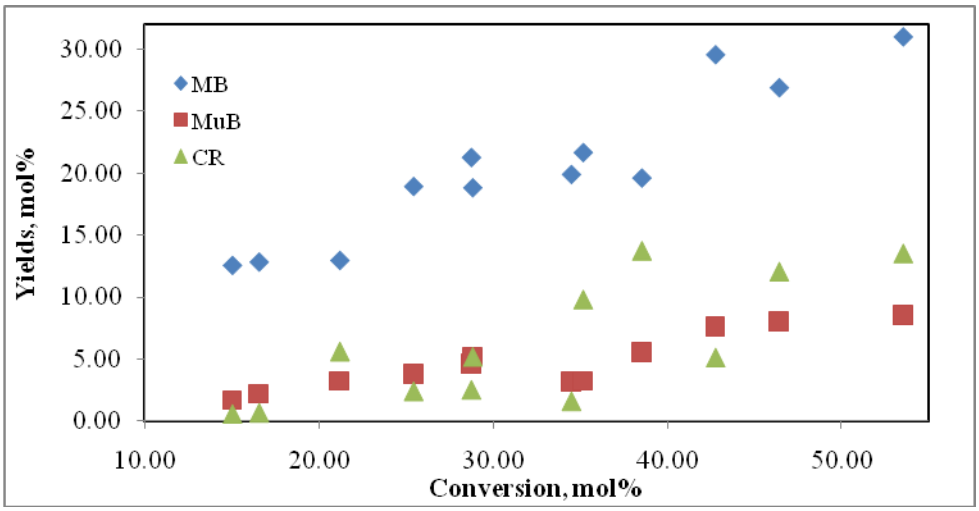

Figure 6-44. Yields of mono-branched isomers, multi-branched isomers, and cracking products as functions of overall conversion at 15 bar for USY-C.

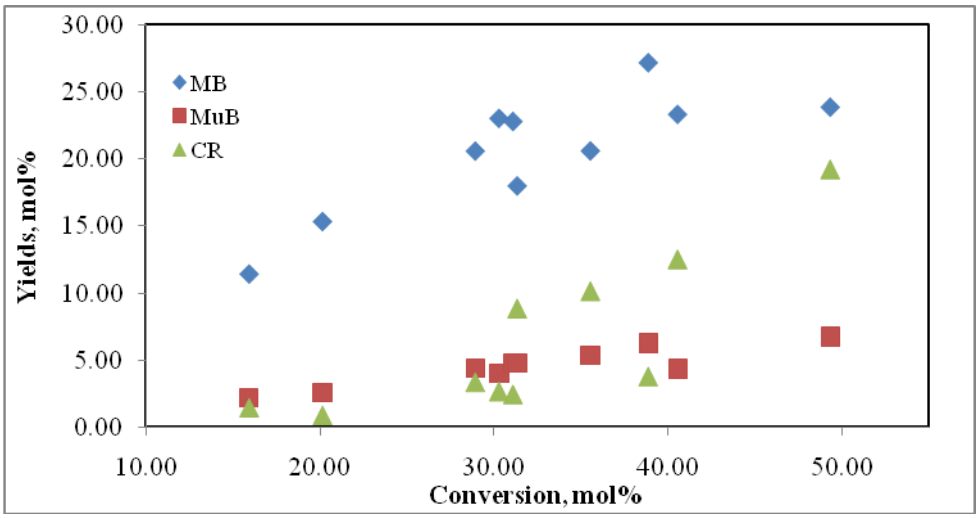

Figures 6-45 to 6-47 show the results for catalyst USY-D. This catalyst's performance shows a shift more towards the ideal bifunctional mechanism at higher pressures, indicated by the lower level of cracking products versus multi-branched ones at atmospheric pressure compared to 8 and 15 bar. This might be explained by a shorter residence time of mono-branched isomers inside the pores of this catalyst at higher pressure, resulting in a lower probability of cracking before converting into multi-branched isomers. Note worthy for this catalyst is the decline in the mono-branched isomers yield at 1 bar, which was taken up solely by cracking products. The high presence of EFAL species in this catalyst might have contributed to its high tendency for cracking at atmospheric pressure.

Figure 6-45. Yields of mono-branched isomers, multi-branched isomers, and cracking products as functions of overall conversion at 1 bar for USY-D.

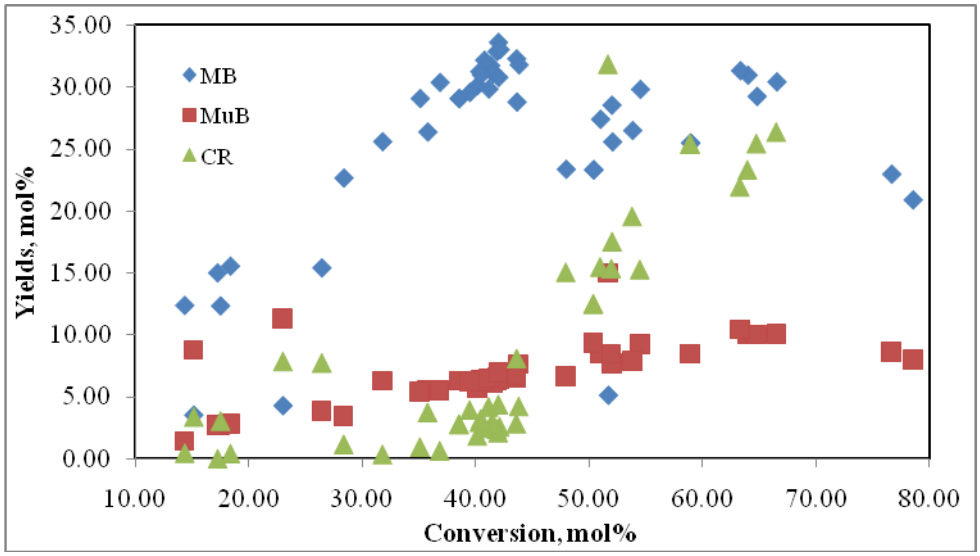

Figure 6-46. Yields of mono-branched isomers, multi-branched isomers, and cracking products as functions of overall conversion at 8 bar for USY-D.

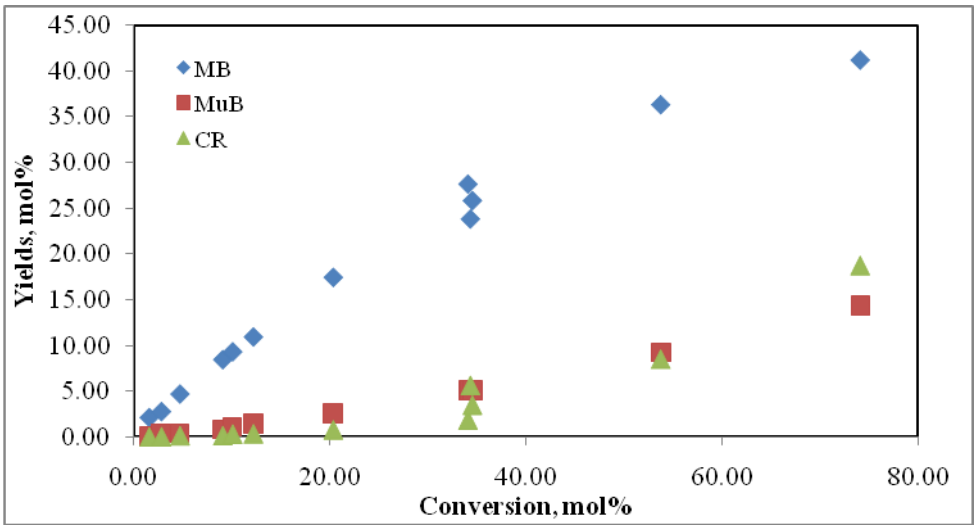

Figure 6-47. Yields of mono-branched isomers, multi-branched isomers, and cracking products as functions of overall conversion at 15 bar for USY-D.

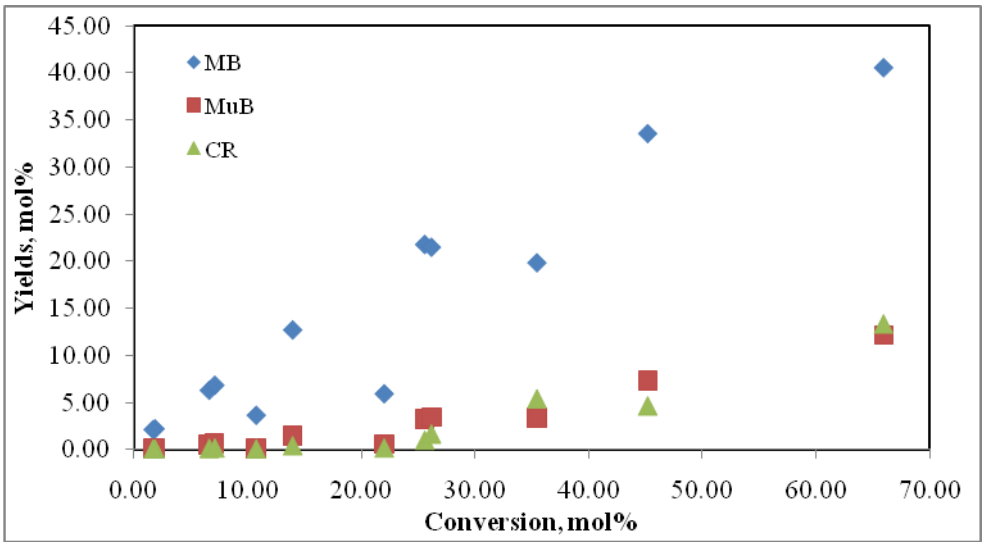

Figures 6-48 to 6-50 show the results for catalyst CBV-760. This catalyst appears to possess ideal bifunctional behaviour at 1 bar. However, the performance changes at higher pressures as more cracking products are observed. Potentially, this could mean that at higher pressures, mono-branched isomers are more prone to cracking, suggesting an imbalance of the functions of this catalyst. However, since this proposed imbalance exists at higher pressure, one explanation is that the imbalance is towards a stronger platinum function, which could be due to a very high platinum dispersion or the requirement of platinum loadings lower than 1 wt% for this catalyst, resulting in the contribution of hydrogenolysis to the overall reaction scheme.

Figure 6-48. Yields of mono-branched isomers, multi-branched isomers, and cracking products as functions of overall conversion at 1 bar for CBV-760.

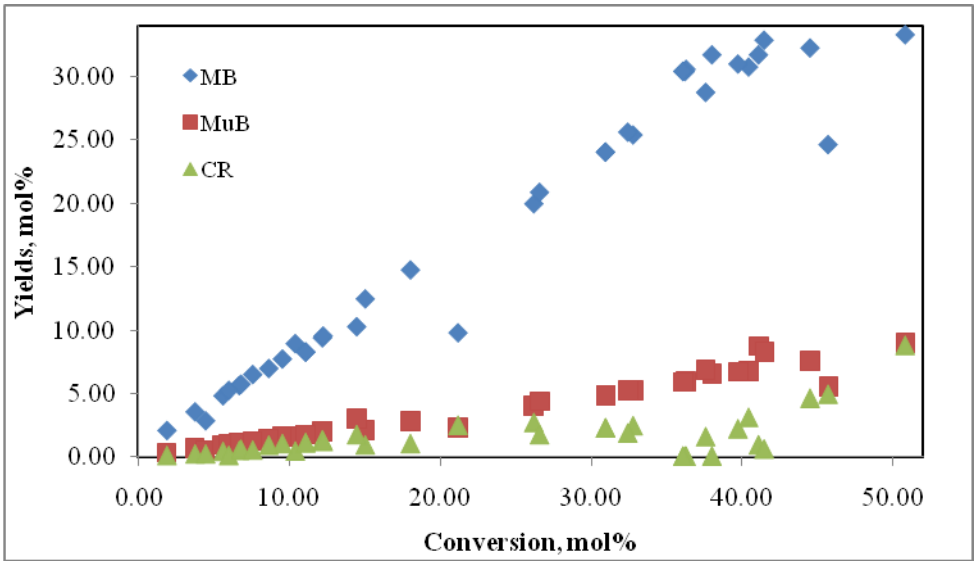

Figure 6-49. Yields of mono-branched isomers, multi-branched isomers, and cracking products as functions of overall conversion at 8 bar for CBV-760.

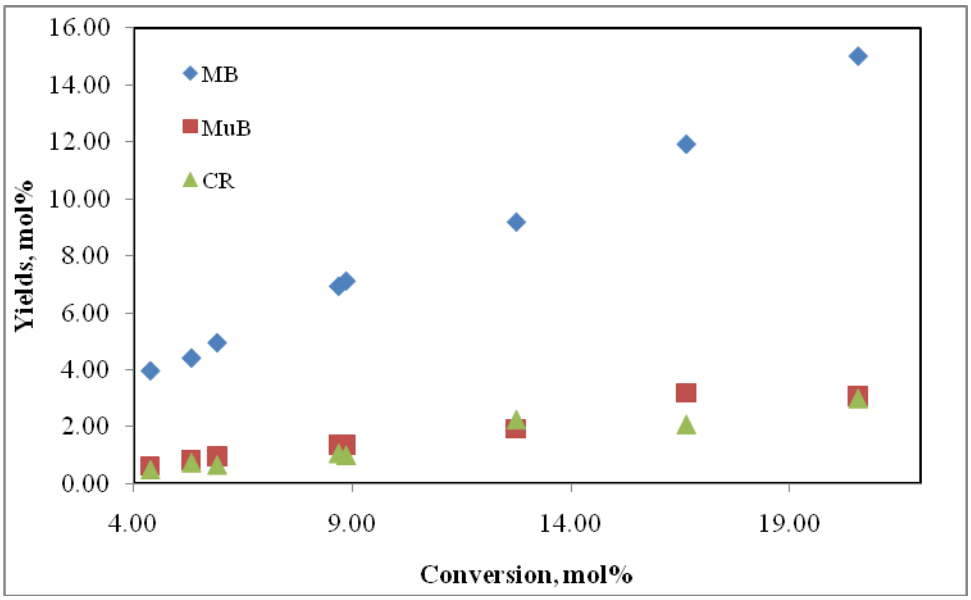

Figure 6-50. Yields of mono-branched isomers, multi-branched isomers, and cracking products as functions of overall conversion at 15 bar for CBV-760.

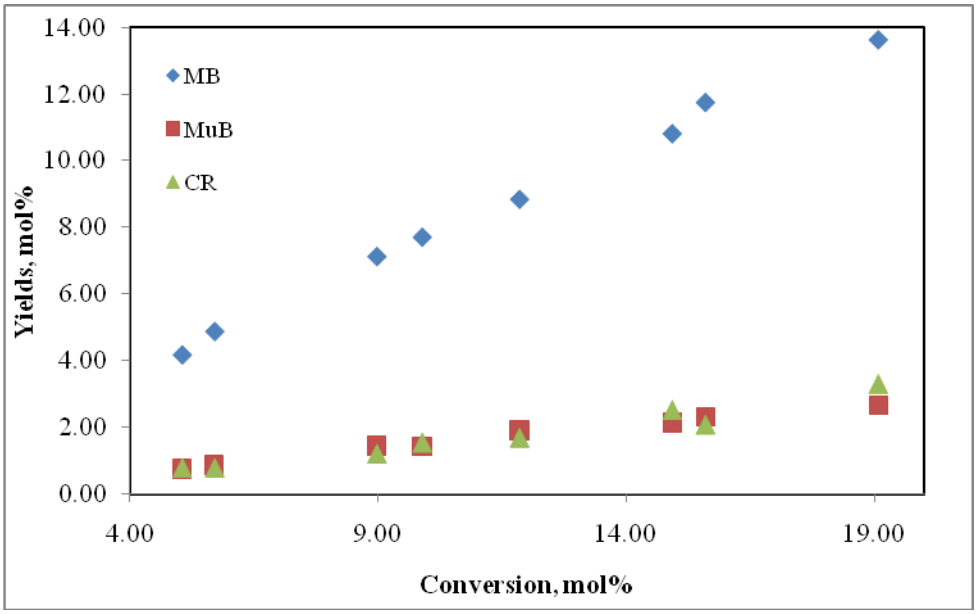

Figures 6-51 to 6-53 show the results for catalyst CBV-712. This catalyst clearly behaves in an ideal bifunctional manner, evident by the successive formation of mono-branched isomers to multi-branched isomers to cracking products at all studied pressures. This means that a platinum loading of 1 wt% is very suitable for the number and nature of acid sites of this catalyst. Also, a function of the stability seen by this catalyst maybe an optimum balance of its Brönsted/Lewis acid site ratio and the removal of EFAL species from its structure.

Figure 6-51. Yields of mono-branched isomers, multi-branched isomers, and cracking products as functions of overall conversion at 1 bar for CBV-712.

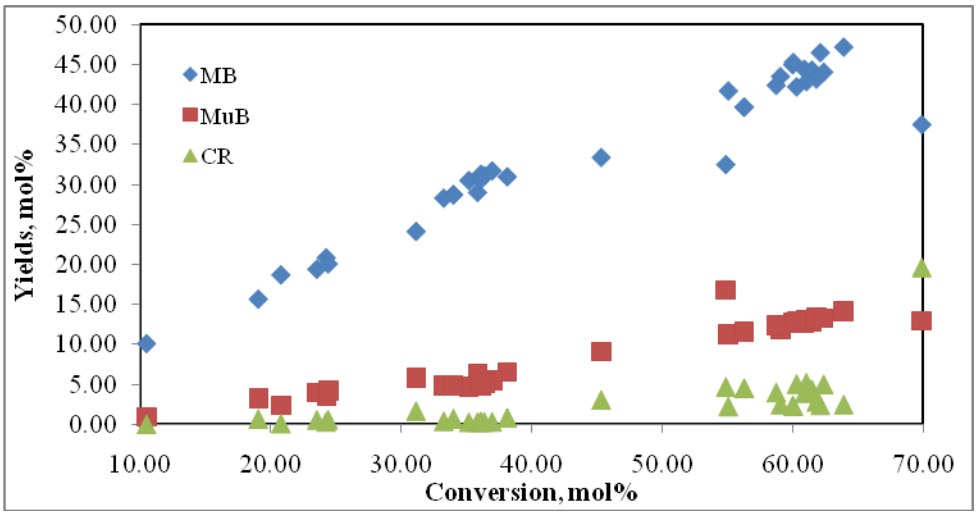

Figure 6-52. Yields of mono-branched isomers, multi-branched isomers, and cracking products as functions of overall conversion at 8 bar for CBV-712.

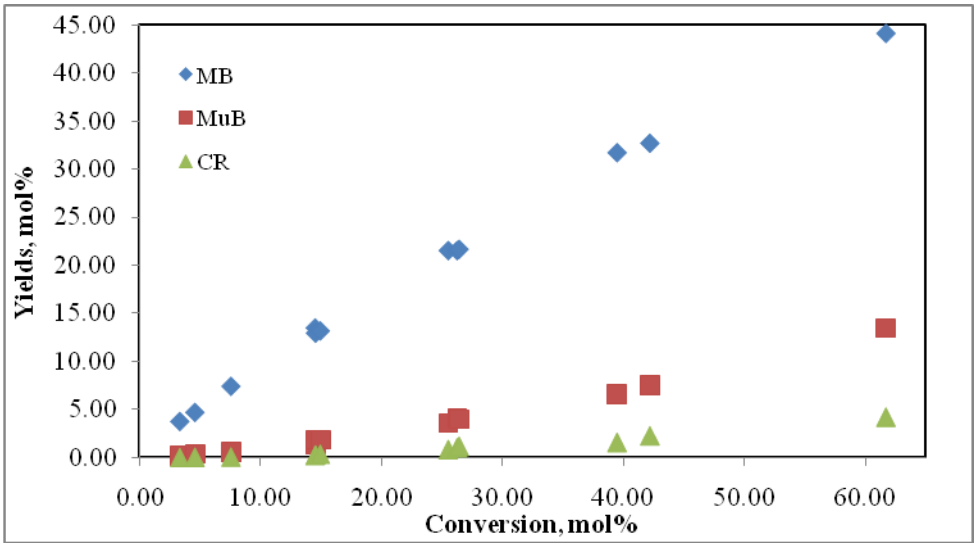

Figure 6-53. Yields of mono-branched isomers, multi-branched isomers, and cracking products as functions of overall conversion at 15 bar for CBV-712.

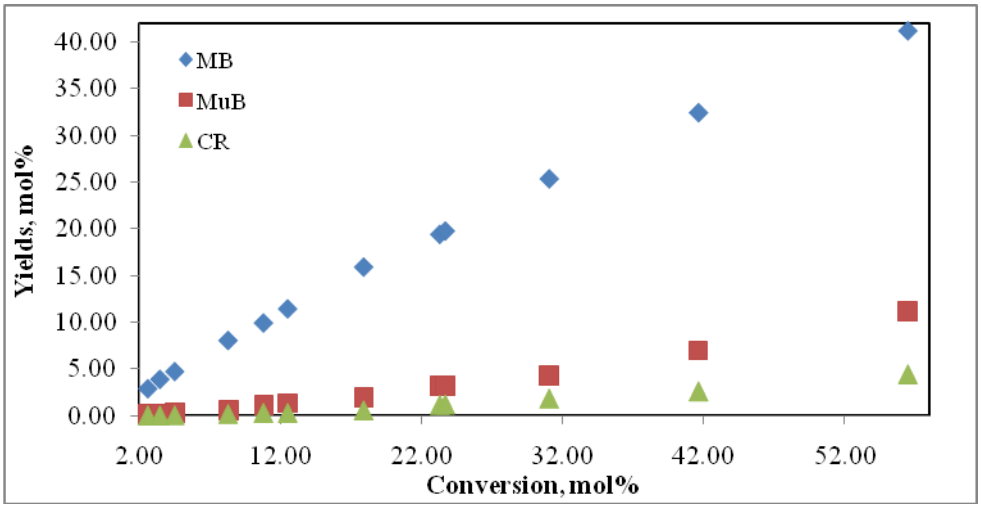

6.3.6 Effect of Zeolite Structure

The structure of a zeolite catalyst plays an important role in its catalytic properties during the hydroisomerization of normal heptane, as discussed in section 3.3.6. It has been shown by Patrigeon et al [3] that specific product ratios can be used to measure the level of constraint in different zeolites. These ratios are 2-MeC_6/3-MeC_6 and R, which is defined as:

$$R = \frac{2,3-DiMeC5 + 2,4-DiMeC5}{2,2-DiMeC5 + 3,3-DiMeC5 + 2,2,3-TriMeC4} \quad (9)$$

These ratios are important because in their denominators are isomers that are bulkier than ones in their numerators. Thus, a ratio close or equal to unity indicates the absence of diffusion limitations within the catalyst. Even though all tested catalysts in this work possess the 3D FAU structure, which has been shown not to have diffusion limitations, these ratios have been plotted versus overall conversion at different pressures for all catalysts in order to compare and examine the level of constraint, if any, of these catalysts at tested experimental conditions.

Figures 6-54 to 6-56 show results for the ratio of 2-MeC_6/3-MeC_6 at different pressures. Catalyst USY-C seems to be the one with the highest tendency to cause constraint, as it has many ratio values lower than 1 and its data points are slanted downwards when moving in the direction of higher conversions. All the other catalysts show close to straight horizontal lines, with USY-D with about the straightest line, indicating almost no constraint with this ratio.

Figure 6-54. Ratio of 2-MeC_6 to 3-MeC_6 as a function of overall conversion at 1 bar for all catalysts.

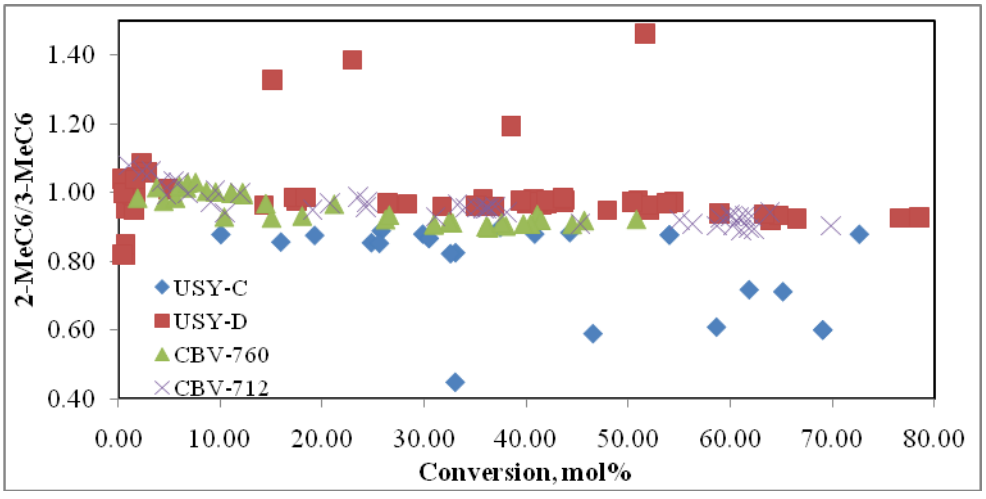

Figure 6-55. Ratio of 2-MeC_6 to 3-MeC_6 as a function of overall conversion at 8 bar for all catalysts.

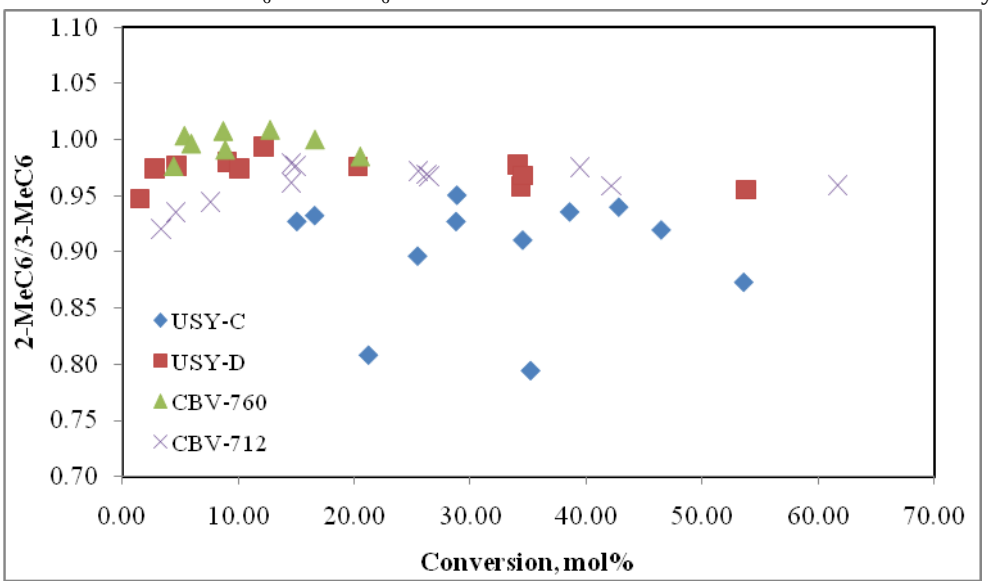

Figure 6-56. Ratio of 2-MeC_6 to 3-MeC_6 as a function of overall conversion at 15 bar for all catalysts.

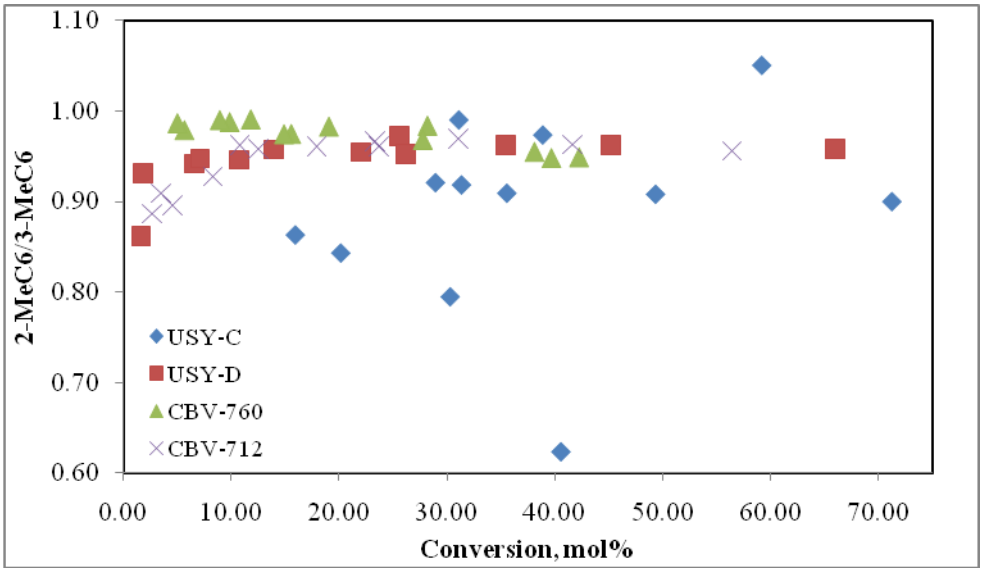

Figures 6-57 to 6-59 show results for the R ratio at different pressures. All the catalysts seem to have some constraint with this highly sensitive ratio, as the ratio is mostly tending to decrease for all of them. However, the downward trend for these catalysts is not as steep as reported by Patrigeon et al for one-dimensional zeolites (See section 3.3.6). As expected, all catalysts showed similar levels of constraint typical of the 3D network of zeolite Y.

Figure 6-57. R Ratio as a function of overall conversion at 1 bar for all catalysts.

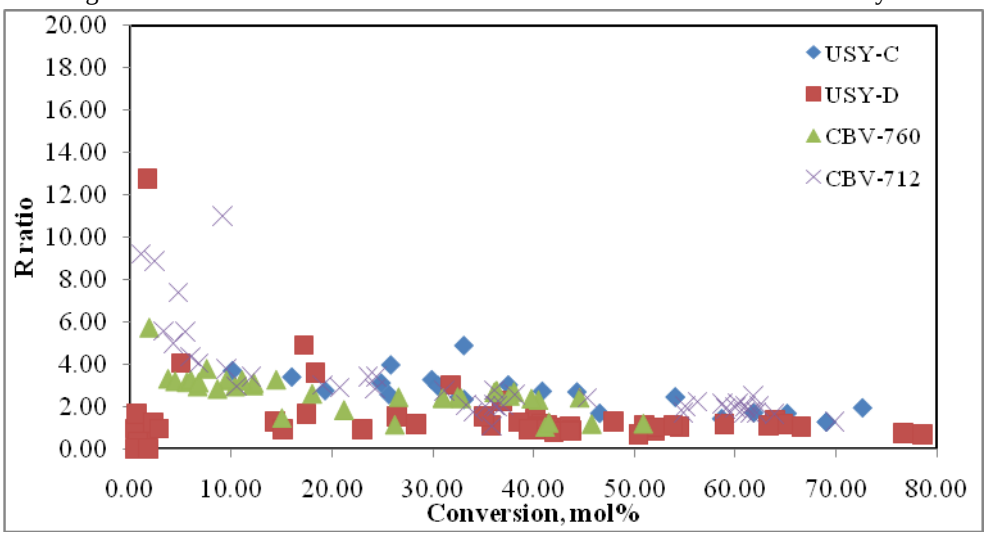

Figure 6-58. R Ratio as a function of overall conversion at 8 bar for all catalysts.

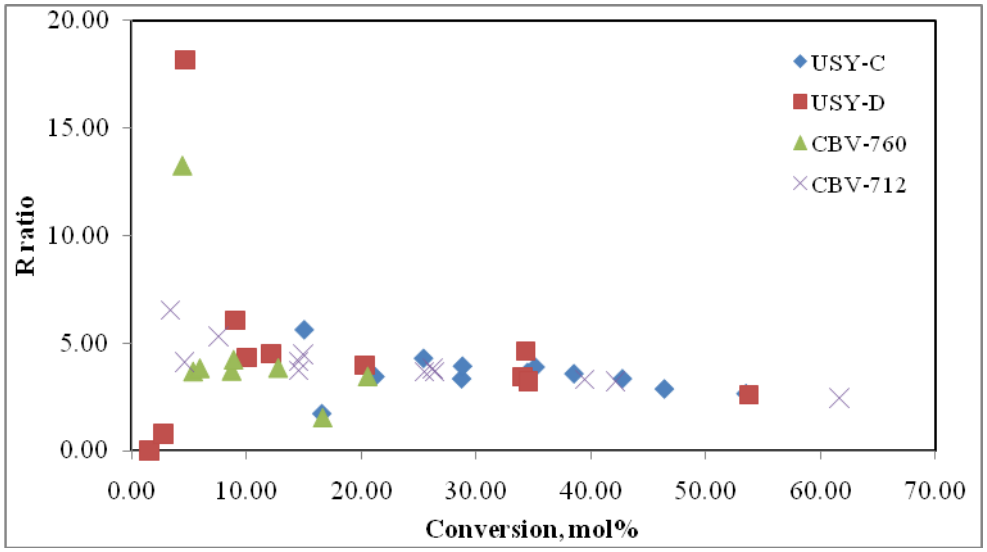

Figure 6-59. R Ratio as a function of overall conversion at 15 bar for all catalysts.

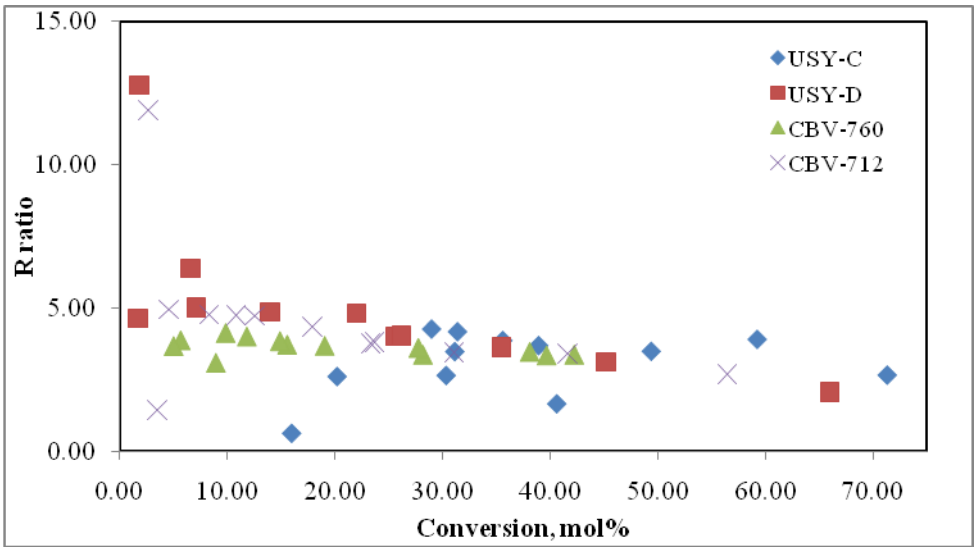

6.3.7 Selectivity & RON

Simulation for the research octane number (RON) for the reaction products was performed based on a new method developed by Nikolaou et al [4] to estimate RON for gasoline. In this method, influence of individual hydrocarbon products is taken into account when calculating the total blended RON, based on the following equation:

$$\mathrm{RON} = \sum_{i=1}^{n} \mathrm{K}i\mathrm{RON}iyi \tag{10}$$

In this equation, y_i is the volume fraction of the individual product hydrocarbon determined by GC, RON_i is the pure RON for each product, and K_i is a weighting factor, calculated as follows:

$$\mathrm{Ki} = \frac{\mathrm{RON}i}{\mathrm{BRON}i} \frac{\sum_{i=0}^{n} yi\mathrm{BRON}i}{\sum_{i=0}^{n} yi\mathrm{RON}i} \tag{11}$$

Here, $BRON_i$ is the blending RON for individual product hydrocarbons. When calculating total blended RON values for products of reaction in this work, the generated isomers were only taken into account, ignoring the contribution of cracked products to the RON, since some of the cracked products are gases in addition to cracking products being the undesired product in this reaction. RON_i and $BRON_i$ were obtained from the same reference [4] for all isomers except 2-MeC6, whose RON_i and $BRON_i$ values were obtained from [5], and the calculated total blended RON values were plotted against overall conversion for all catalysts at different pressure, and are shown in Figures 6-60 to 6-62. At 1 bar, catalyst CBV-712 is the one generating the highest RON isomers, reaching close to 35. Catalysts USY-C and USY-D have RON values reaching 25 then dropping as the conversion increases. CBV-712 generates the maximum RON at 8 bar as well. However, catalyst USY-D seems to be approaching the performance of CBV-712 at 15 bar, with a RON value exceeding 30 at 66% conversion. This means that the higher pressure resulted in a suppressed cracking activity for this catalyst, paving the way for enhanced isomer selectivity and, hence, higher RON values. The performance of catalyst USY-C at 15 bar is poor, and it has been argued before in previous sections that diffusion limitations might be the reason for the low isomer selectivity (RON) of this catalyst.

Figure 6-60. Blended research octane number as a function of overall conversion at 1 bar for all catalysts.

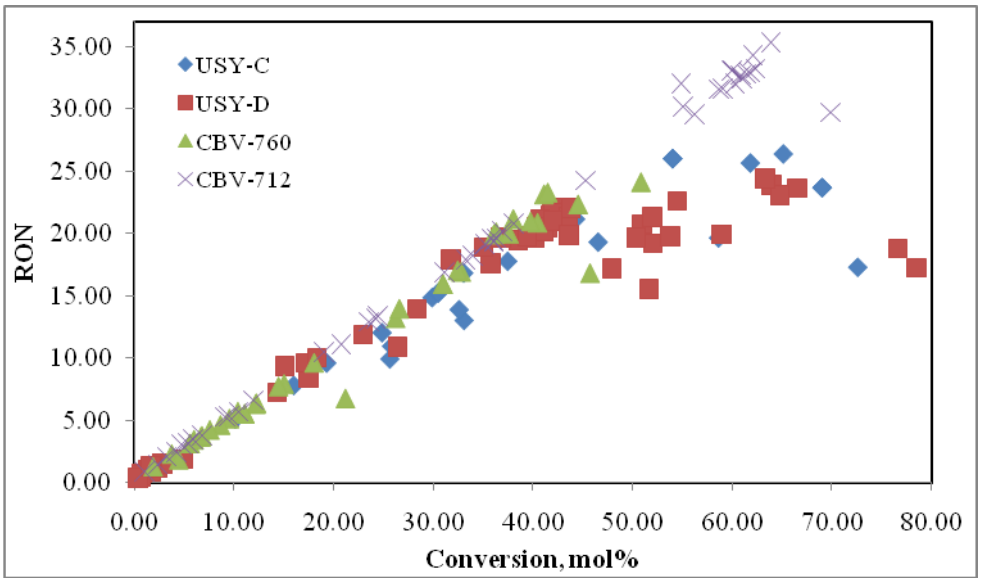

Figure 6-61. Blended research octane number as a function of overall conversion at 8 bar for all catalysts.

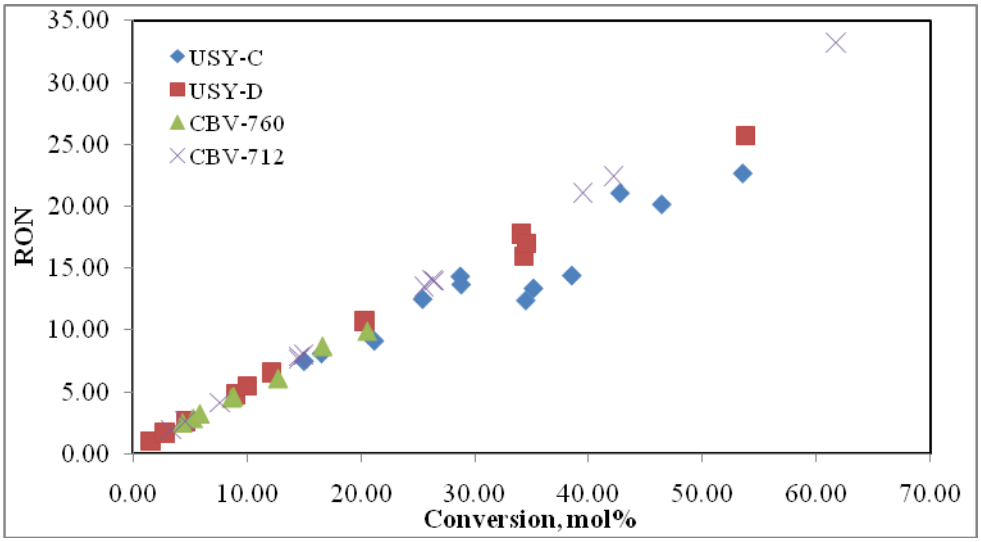

Figure 6-62. Blended research octane number as a function of overall conversion at 15 bar for all catalysts.

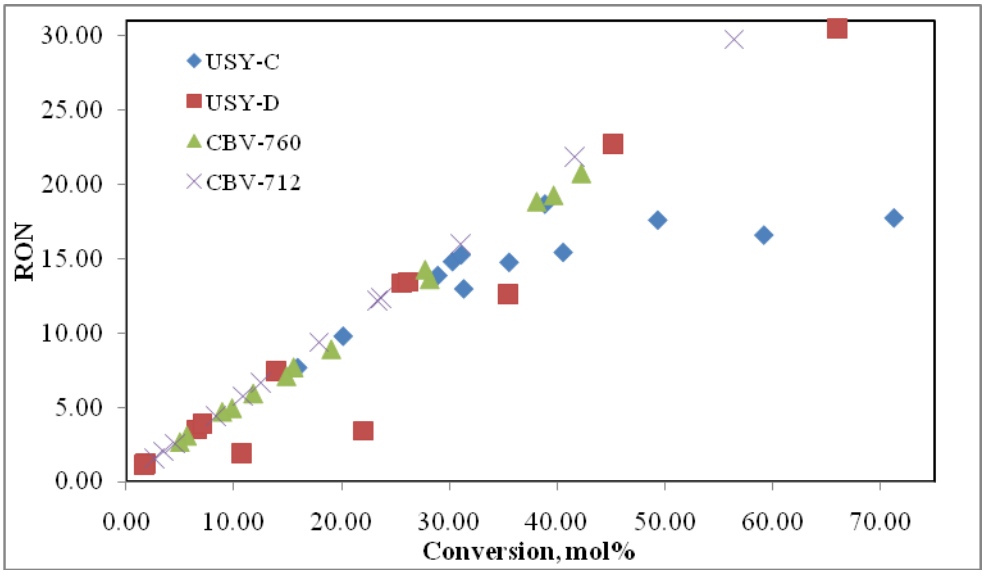

To best judge on how these catalysts differ in their selective properties, a good way is to evaluate their yield structure at comparable normal heptane conversions. Table 6-1 lists selective properties, product distributions, blended RON, in addition to key selectivity ratios for each catalyst at 1, 8, and 15 bar. Results in the table were carefully chosen so that they reflect a catalyst's performance at as close an overall conversion as possible to that achieved by other catalysts at the same pressure. At atmospheric pressure, it is noticed that the acid leached catalysts are more selective than the steamed-only ones, with CBV-712 being the one most selective to isomers. USY-C was less selective than others due to its high cracking yield, whereas USY-D was less selective because it generated other products, which were mainly cyclic compounds that result probably from heptane dehydrocyclization reactions. These cyclic products were mainly found with USY-C and USY-D, suggesting that the high presence of EFAL species (higher Lewis acidity) in these two catalysts might be the cause to their higher dehydrogenation activity. At 8 and 15 bar, USY-D was the most selective catalyst, with both cracking and dehydrocyclization activities greatly suppressed. Cracking selectivity generally decreased for all catalysts, except for CBV-760, whose cracking selectivity almost doubled. This is possibly due to it having the least porosity and average pore diameter among the four catalysts, which might be responsible for diffusion limitation imposition on this catalyst at high pressures.

The high yield of C_6 products with USY-C compared to the other catalysts, given the almost complete absence of methane in its products, suggests that some oligomerization-cracking (also called dimerization-cracking) takes place on this catalyst, since the only way for C_6 to be produced without producing C_1 is for heptane to oligomerize to C_{14}, which then cracks to C_6 and C_8, which further cracks to C_5 and C_2 or to two C_4s. Interestingly, the BET characterization of this catalyst shows that this assumption of oligomerization-cracking existence is entirely valid. This catalyst has the biggest porosity among the four catalysts, which provides enough room for heptane to oligomerize into the bulky C_{14} inside the zeolite cages. This high porosity, however, comes in conjunction with a low average pore diameter, which means that when the bulky C_{14} molecule forms, it cannot leave the zeolite structure through the narrow pores, resulting in its cracking.

Table 6-1. Selectivity, product distribution, blended RON, and key ratios for all catalysts at comparable conversions.

Catalyst	USY-C	USY-D	CBV-712	CBV-760	USY-C	USY-D	CBV-712	CBV-760	USY-C	USY-D	CBV-712	CBV-760
P, bar	1	1	1	1	8	8	8	8	15	15	15	15
Conversion, mol%	30.5	28.4	31.2	31.0	16.5	12.2	14.6	12.7	15.9	14.0	18.0	15.6
T, ^{o}C	252.0	214.0	252.0	311.8	213.0	233.8	211.4	292.2	215.0	233.0	231.0	296.0
Selectivity, mol%												
Hydroisomerization	84.5	85.9	93.5	89.4	87.2	95.0	93.6	79.6	86.4	93.8	93.0	83.5
Cracking	14.9	7.9	5.9	8.8	8.3	2.8	4.0	18.2	9.0	4.4	5.0	14.5
Other, including hydrodecyclization	0.6	6.2	0.6	1.8	4.5	2.2	2.4	2.2	4.6	1.8	2.0	2.0
Product Distribution, mol%												
Hydroisomerization												
2-MeC_6	35.0	41.5	37.2	38.0	39.6	42.1	43.2	39.8	37.5	42.3	42.2	39.6
3-MeC_6	40.3	42.8	40.1	42.0	42.5	42.4	44.9	39.5	43.4	44.2	43.9	40.7
3-EthC_5	3.0	2.5	3.2	3.2	3.1	3.6	3.2	3.3	3.0	3.3	3.2	3.2
2,2-DiMeC_5	3.4	4.4	3.1	2.9	4.6	1.6	1.4	2.4	5.4	1.2	1.3	2.1
2,3-DiMeC_5	10.1	4.2	9.0	8.0	5.4	5.5	4.0	8.2	5.3	4.9	5.0	8.0
2,4-DiMeC_5	6.2	2.9	5.3	3.9	4.0	4.3	2.9	5.5	1.0	3.6	3.7	5.0
3,3-DiMeC_5	1.4	1.3	1.7	1.7	0.6	0.6	0.4	1.1	0.4	0.5	0.5	1.1
2,2,3-TriMeC_4	0.7	0.3	0.5	0.3	0.2	0.0	0.1	0.1	3.9	0.0	0.2	0.3
Cracking												
C_1	0.0	0.0	0.0	0.0	0.0	0.0	0.0	0.0	1.4	0.0	0.0	0.6
C_2	0.1	1.6	0.1	0.0	0.0	1.2	0.0	0.9	2.1	2.3	1.7	0.9
C_3	42.9	45.0	44.5	48.5	40.5	47.9	43.0	48.8	39.3	51.4	46.8	50.4
C_4	50.4	50.7	53.1	49.8	47.5	46.4	52.5	49.6	48.6	45.4	51.6	47.4
C_5	2.8	1.8	1.6	1.3	0.0	4.4	4.5	0.7	5.7	0.9	0.0	0.6
C_6	3.9	0.9	0.7	0.4	11.9	0.0	0.0	0.0	3.0	0.0	0.0	0.0
RON	15.2	14.0	16.9	15.9	8.2	6.6	7.6	6.1	7.7	7.4	9.4	7.7
I/C ratio	5.9	22.0	17.8	12.6	22.3	34.2	57.3	5.0	9.6	37.3	30.6	6.7
Mono/Multi ratio	3.6	6.6	4.1	4.9	5.8	7.4	10.4	4.8	5.2	8.7	8.4	5.1
iC_4/C_4 ratio	23.6	16.0	31.0	7.6	128.4	17.6	13.6	11.9	17.4	18.6	24.2	11.1

Catalyst CBV-712 generated isomers with the highest blended RON among these catalysts at 1 and 15 bar, and USY-D was the one with the least. The reason for the low RON of USY-D isomers despite the high isomers yield is because it produces the most quantities of mono-branched isomers, which have lower RON values than multi-branched ones, resulting in a lower blended RON than achieved with the other catalysts. This behaviour could be due to the low crystallinity and surface area of this catalyst compared to the others, which might have resulted in a high diffusion of mono-branched isomers out of the catalyst before they transform into multi-branched ones. This also would explain the very low cracking selectivity of this catalyst, especially at higher pressures.

6.3.8 Effect of Sulfur Addition

Normal heptane is a typical component of heavy naphtha, which has sulfur contents ranging from 0.02 to 0.06 wt% for straight-run heavy naphtha [6], and can reach as high as 1 wt% for heavy naphtha derived from thermally cracked heavier petroleum fractions [7]. So, in order to test the effect of sulfur presence in the normal heptane feed to the studied catalysts, the deactivation behaviour for catalysts USY-D and CBV-712 was studied with feeds containing 1 wt% and 100 ppm dimethyldisulfide (DMDS), respectively. The former feed contained 0.64 wt% sulfur and the latter contained 64 ppm, versus a sulfur content of 4 ppm for the normal heptane feed used throughout experiments. Poisoning experiments were performed at 210^{o}C, atmospheric pressure and at a space time of 140.6 kg.s/mol. In each experiment, DMDS-free feed was fed over the catalyst bed until conversion stabilized. Then, DMDS + nC_7 was introduced and conversion measured until it stabilized. Finally, DMDS-free feed was re-introduced until catalyst activity stabilized with the new condition.

Figures 6-63 to 6-65 show the results for the poisoning experiment with catalyst USY-D. A severe drop in conversion was noticed right after the introduction of the 1 wt% DMDS feed, followed by a lesser decline before conversion stabilized around 0.5 mol%. Switching back to sulfur-free feed caused conversion to partially regain some of its losses to close to 3 mol%. This means that sulfur almost completely inhibited the catalyst activity, especially during its presence inside the catalyst structure. The ratio of mono- to multi-branched isomers generated during reaction generally rose during poison introduction, but dropped to levels lower than the initial ones after normal feed was re-introduced. This

could either mean that sulfur was competing with mono-branched isomers over metal sites responsible for their further rearrangement or it was, instead, competing with their olefinic intermediates over acidic sites, thus preventing their isomerization into multi-branched isomers and promoting their cracking. The behaviour of the I/C ratio during that time (being almost constant at low levels) suggests that the former interpretation is more valid, where the metal function of the catalyst was more affected with sulfur presence than the acidic one.

Figure 6-63. Overall Conversion as a function of time-on-stream before, during, and after the introduction of 1 mol% DMDS to the feed at 210°C and 1 bar for catalyst USY-D.

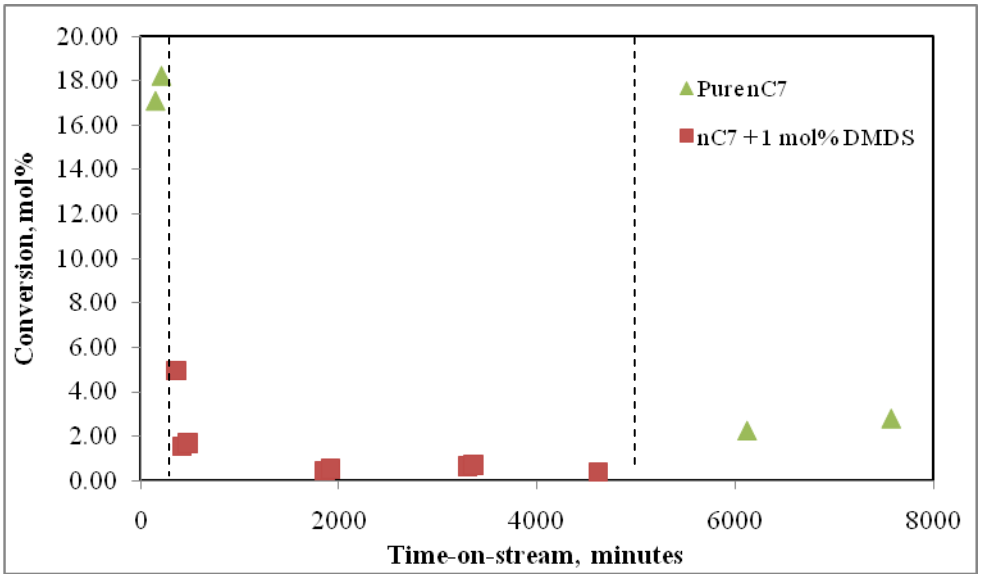

Figure 6-64. Mono to multi-branched isomers ratio as a function of time-on-stream before, during, and after the introduction of 1 mol% DMDS to the feed at 210°C and 1 bar for catalyst USY-D.

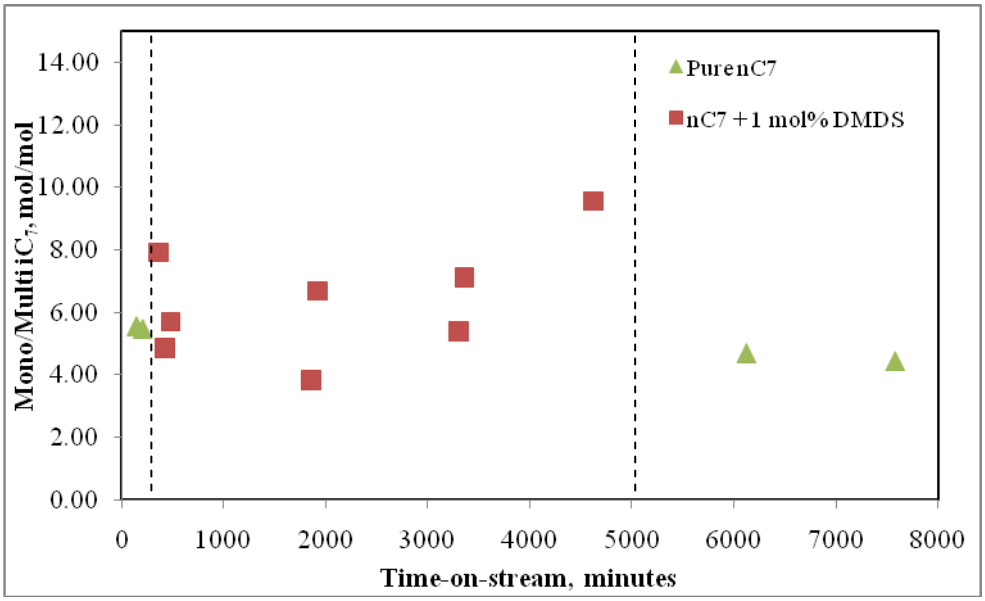

Figure 6-65. Isomer to cracking products ratio as a function of time-on-stream before, during, and after the introduction of 1 mol% DMDS to the feed at 210°C and 1 bar for catalyst USY-D.

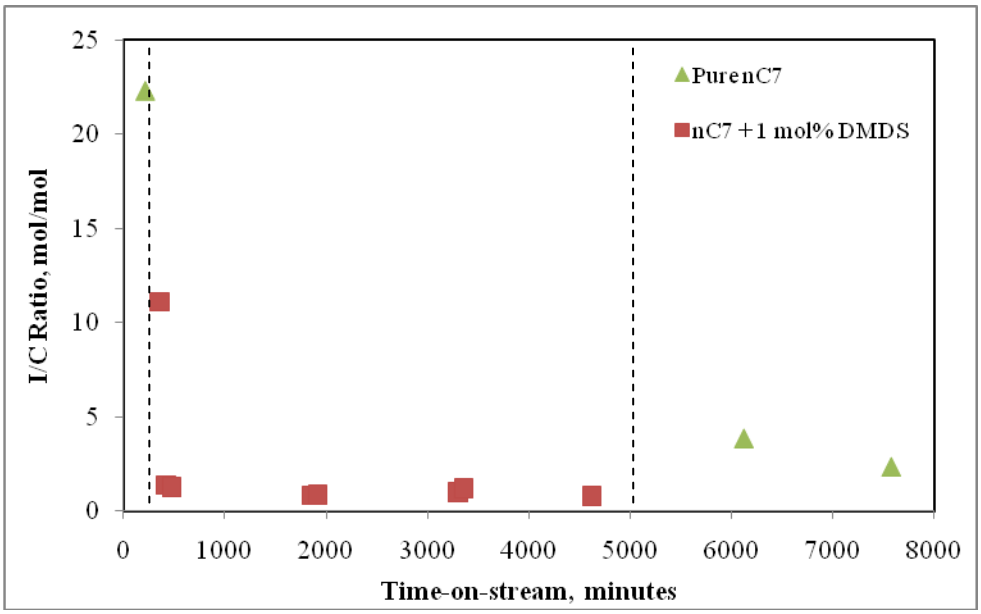

Figures 6-66 to 6-68 show the results for the poisoning experiment with catalyst CBV-712. The drop in this catalysts conversion upon sulfur introduction was less severe due to the lesser degree of sulfur content in the feed. The almost no difference noted in the mono/multi and I/C ratios after sulfur removal from the feed suggest that at the lower level of 100 ppm of DMDS in the feed, both metal and acidic functions were equally affected, and that higher sulfur levels can cause a further but somewhat reversible deactivation in the metal sites.

Figure 6-66. Overall Conversion as a function of time-on-stream before, during, and after the introduction of 100 ppm DMDS to the feed at 210°C and 1 bar for catalyst CBV-712.

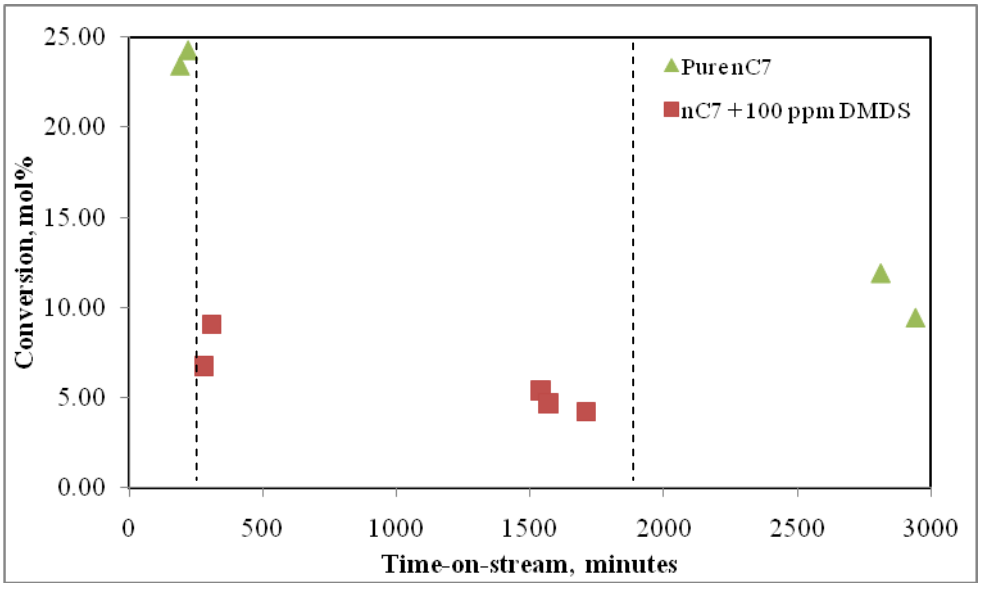

Figure 6-67. Mono to multi-branched isomers ratio as a function of time-on-stream before, during, and after the introduction of 100 ppm DMDS to the feed at 210°C and 1 bar for catalyst CBV-712.

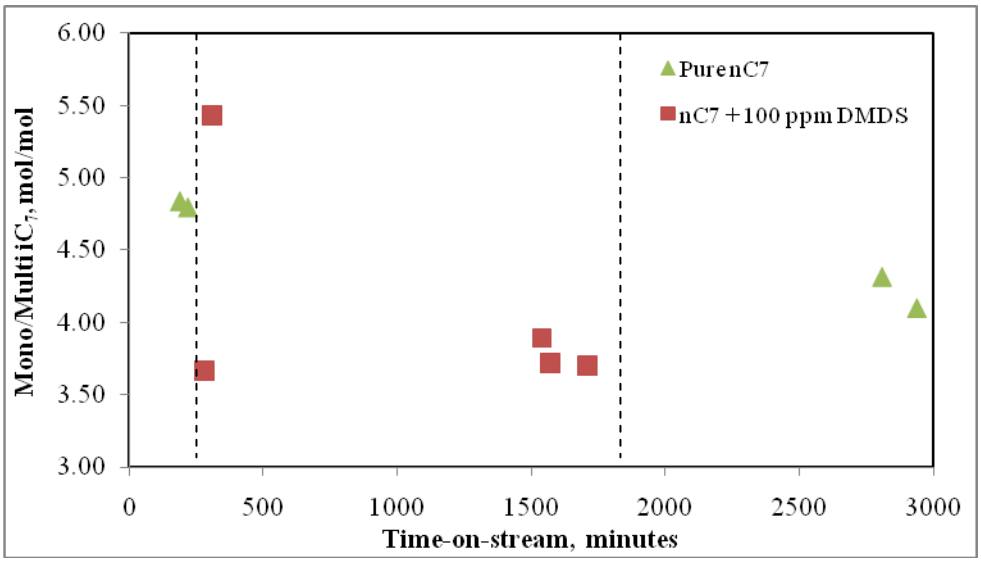

Figure 6-68. Isomer to cracking products ratio as a function of time-on-stream before, during, and after the introduction of 100 ppm DMDS to the feed at 210°C and 1 bar for catalyst CBV-712.

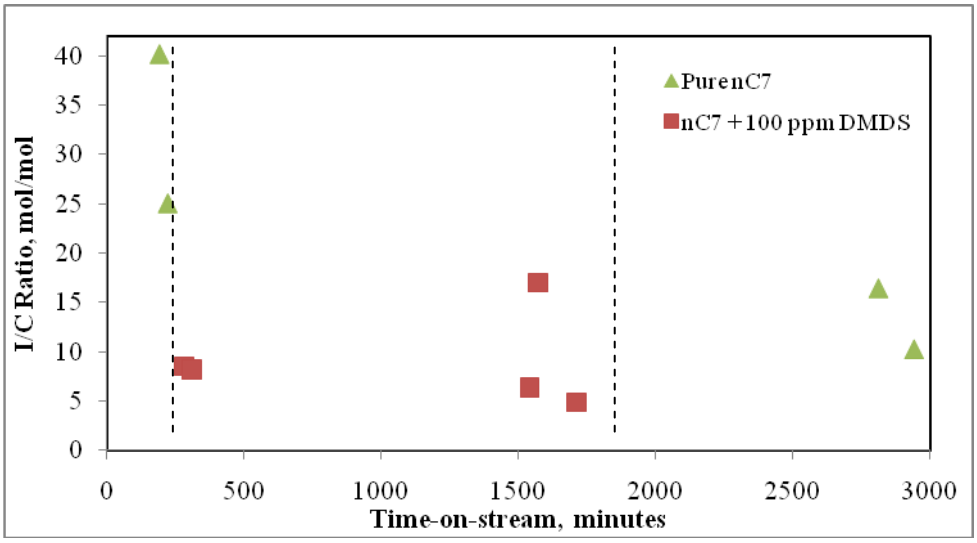

6.4 Kinetic Modelling

The global rate of reaction for the hydroisomerization of normal heptane, which includes rates of heptane diffusion into the catalyst, adsorption on the active sites, its reaction to form isomers or cracking products, their desorption from active sites, and the products' diffusion out of the catalyst, can be written in the following power law equation:

$$-r = k(P_{C7})^n(P_{H2})^m \qquad (12)$$

Here, r is the rate of reaction, P_{C7} is the partial pressure of normal heptane, P_{H2} is the partial pressure of hydrogen, n is the order of reaction in normal heptane, m is the order of reaction in hydrogen, and k is the rate constant. The reaction rate is defined by the rate of change of overall conversion with respect to space time, which is expressed as follows:

$$-r = \frac{dX}{d(\frac{W}{F_o})} \tag{13}$$

Here, X is the overall conversion of normal heptane, W is the weight of catalyst, F_o is the molar flow rate of normal heptane at the reactor entrance. The rate constant is given by the Arrhenius equation, where A is a pre-exponential factor, E is the apparent activation energy of the overall reaction, R is the gas constant, and T is the reaction temperature:

$$k = Ae^{(\frac{-E}{RT})} \tag{14}$$

Conversion data generated with the pressure reactor for catalysts USY-C, USY-D, CBV-712, and CBV-760 was kinetically modelled based on an (initial rates) approach that was used by Saberi and Le Van Mao [8]. Utilizing their used approach, the conversion versus space time data was fitted into a polynomial function of 3rd degree using non-linear regression with Sigmaplot software. The correlation factor for all regression made was above 0.95 for the cubic function used (1 being a perfect fit). An example is shown in Figure 6-69 for the fit for catalyst USY-C for data at 230°C and atmospheric pressure. Taking the derivative of the cubic function shown in the figure with respect to space time results in the following equation, with a, b, and c being constants determined by the regression software:

$$\frac{dX}{d(\frac{W}{Fo})} = 3a(\frac{W}{Fo})^2 + b(\frac{W}{Fo}) + c \tag{15}$$

Thus, at initial rates conditions when space time equals zero, the rate of reaction is equal to constant c. Repeating this procedure for conversion data to form mono-branched isomers, multi-branched isomers, total isomers, and cracking products, enables the calculation of relative rate constants for these types of products since concentrations of normal heptane and hydrogen are constant, per the example equation:

$$\frac{r_{o\,isom}}{r_{o\,cracking}} = \frac{k_{o\,isom}}{k_{o\,cracking}} \tag{16}$$

In this equation, $r_{o\ isom}$ is the initial rate of hydroisomerization and $k_{o\ isom}$ is the rate constant for hydroisomerization at initial conditions, and likewise for cracking.

Figure 6-69. Cubic fit by Sigmaplot for the conversion data as a function of space time for catalyst USY-C.

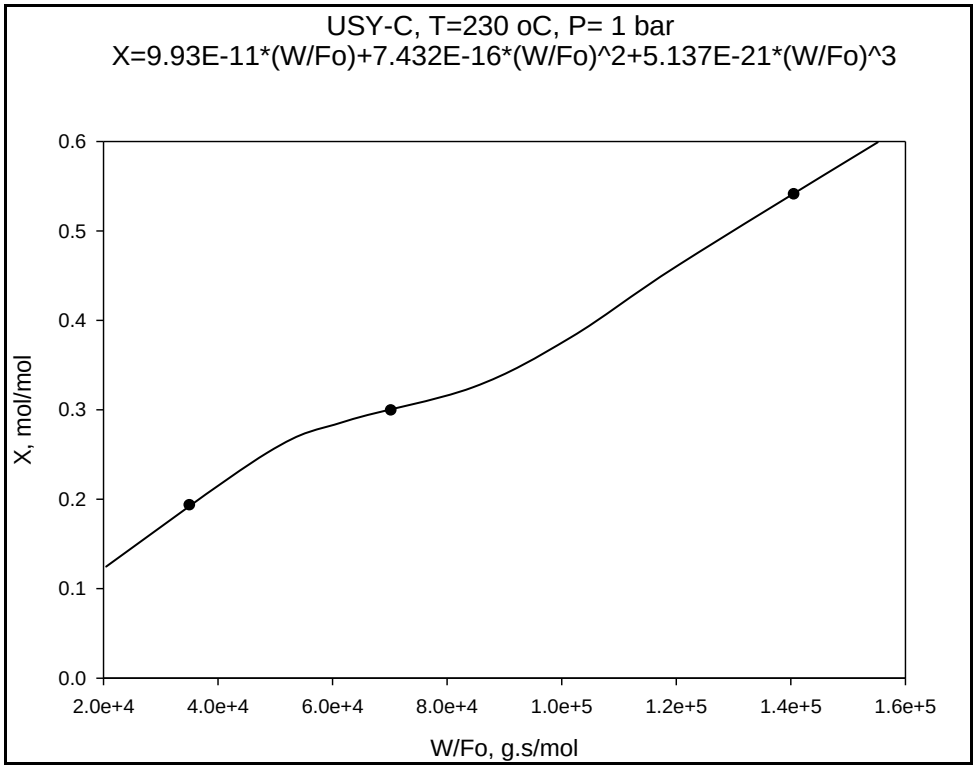

Table 6-2 shows ratios of rate constants at zero space time for all catalysts at different pressure and 210^{o}C, except for CBV-760, whose ratios were taken for 270^{o}C. The effect of sulfur poisoning on rate constant ratios for USY-D and CBV-712 has also been included in the table. The highest ratio for the isomerization to cracking rate constants is 77.99, obtained for USY-D at 15 bar, and the lowest was 1.74 for USY-C at 1 bar. This stark contrast is evidence of the big impact pressure as well as the modification of the catalyst structure and acidic properties have on the selectivity of the catalyst. However, the most influence was due to the catalyst structure difference, which suggests that the more severe steaming treatment that USY-D has undergone opened up enough pores to substantially reduce cracking. Both USY-D and CBV-712 had much higher isom/cracking ratios than USY-C and CBV-760. Increasing pressure resulted in a suppressed cracking rate compared to isomerisation for in-house catalysts, as evident in USY-C's value at 1 bar versus 8 and 15 bars and USY-D's rapidly rising ratios with pressure. CBV-712's ratio was relatively constant at different pressures, which again, points to this catalyst's high stability and consistency at different conditions. The sulfur poisoning experiments did indeed cause a larger drop of catalysts hydroisomerization activity versus the cracking one, as evident

from the drop in the rate constant ratio of isomerization to cracking for both poisoned catalysts compared to their pre-poisoned state. The impact of poison was even bigger during its introduction to CBV-712 than after sulfur-free feed was re-introduced over the catalyst. This is in agreement with what was found and discussed in sub-section 6.3.8. For the purpose of comparison with values reported in the literature, rate constant ratios reported by Saberi and Le Van Mao [8] were included in the table for a 1%Pt/HY sample they used that has a framework Si/Al ratio of 5.8 (very similar to CBV-712) and tested at 1 bar and 210^{o}C. Values for both catalysts seem to be quite comparable with a little less cracking activity for CBV-712 that seems to have moved towards generating more multibranched isomers than the catalyst they used.

Table 6-2. Rate constant ratios for all catalysts tested at different conditions at space time = 0. (t = total)

Catalyst	T, ^{o}C	P, bar	k^{o}_{isom}/k^{o}_{t}	k^{o}_{crack}/k^{o}_{t}	$k^{o}_{isom}/k^{o}_{crack}$	k^{o}_{mono}/k^{o}_{t}	k^{o}_{multi}/k^{o}_{t}	$k^{o}_{mono}/k^{o}_{multi}$	Remarks
USY-C	214.2	1	0.63	0.36	1.74	0.48	0.15	3.10	
USY-C	214	8	0.71	0.19	3.74	0.62	0.096	6.44	
USY-C	214.4	15	0.75	0.24	3.15	0.63	0.17	5.46	
USY-D	213.2	1	0.92	0.06	14.78	0.77	0.15	5.20	
USY-D	213.4	8	0.98	0.02	44.46	0.89	0.086	10.37	
USY-D	213	15	0.75	0.01	77.99	0.70	0.049	14.27	
USY-D	213	1	0.79	0.21	3.72	0.64	0.15	4.36	after 1 wt% DMDS
CBV-712	213.6	1	0.98	0.017	57.82	0.85	0.13	6.39	
CBV-712	211.4	8	0.99	0.015	65.67	0.91	0.08	11.31	
CBV-712	211.4	15	0.98	0.019	51.63	0.92	0.061	15.08	
CBV-712	210	1	0.89	0.11	8.43	0.71	0.18	3.89	during 100 ppm DMDS
CBV-712	210	1	0.95	0.053	17.87	0.77	0.17	4.47	after 100 ppm DMDS
CBV-760	271	1	0.91	0.093	9.75	0.75	0.16	4.78	
CBV-760	272	8	0.88	0.12	7.40	0.70	0.18	4.03	
CBV-760	273	15	0.84	0.16	5.21	0.70	0.14	5.22	
1%Pt-HY	210	1	0.92	0.03	30.67	0.84	0.08	10.50	Source [8]

In order to estimate the activation energy of reaction and the reaction orders with respect to heptane and hydrogen, the power law rate equation was utilized while substituting for the rate constant in it with its definition from Arrhenius equation. This gave the following equation:

$$-r = Ae^{\left(\frac{-E}{RT}\right)}(P_{C7})^n(P_{H2})^m \quad (17)$$

In this equation, rates of reaction at initial conditions were used along with experimental values for temperature heptane and hydrogen partial pressures. The remaining variables were determined by defining the equation in Sigmaplot software and using the dynamic fit option of the software to fit the data into 2000 fits, and choosing values of the variables that gave the best fit. The estimated kinetic parameters are listed in Table 6-3 for catalysts tested at the pressure hydroisomerization reactor, and in Table 6-4 for data generated using 200 fits. The apparent activation energy values are higher than those found in the literature and reported in table 3-2, probably because, here, the activation energy is for the global rate of reaction, which not only includes the intrinsic reaction rate, but also accounts for adsorption, desorption, and diffusion effects. Nonetheless, the reaction orders found for catalysts USY-D and CBV-712 were very close to the ones reported in the literature (Table 3-2) for Pt/USY catalysts, which indicated that the estimation method used here was quite beneficial. The high activation energy of CBV-760 and its high order in heptane agree with its low activity due to a high level of dealumination, which causes its acidic sites to possibly be far apart, raising the catalyst's dependence on the concentration of heptane inside its structure.

Table 6-3. Apparent activation energy and reaction orders in heptane and hydrogen for all catalysts using 2000 fits.

Catalyst	E_A, kJ/mol	Order in C_7	Order in H_2
USY-C	167.0	0.61	-0.42
USY-D	163.7	0.57	-0.61
CBV-712	163.7	0.57	-0.61
CBV-760	174.4	1.49	-1.04

Table 6-4. Apparent activation energy and reaction orders in heptane and hydrogen for all catalysts using 200 fits.

Catalyst	E_A, kJ/mol	Order in C_7	Order in H_2
USY-C	157.8	1.44	-1.21
USY-D	165.7	0.68	-1.0
CBV-712	165.7	0.68	-1.0
CBV-760	174.4	1.49	-1.04

6.5 Conclusion

In this chapter, results of experiments performed in the glass atmospheric reactor were discussed. It was shown how catalyst USY-D was the best among the catalysts tested in this reactor. Catalyst USY-B was very acidic and produced a lot of cracking products when compared to USY-C and USY-D, and therefore, the latter two catalysts were further investigated in pressure runs in the stainless-steel reactor. In pressure reactor runs, deactivation studies showed that catalyst USY-A deactivated very quickly, while others, including the commercial catalysts CBV-712 and CBV-760 were pretty stable. Activity studies showed that catalysts USY-C and CBV-760 were not as selective to heptane isomers as USY-D and CBV-712, and it was argued that this was mainly due to diffusion limitations in the former catalysts. Catalyst USY-D's performance was greatly improved with pressure, pushing it closer to that of CBV-712, which generated the highest blended RON values. The enhancement of USY-D's performance with pressure was argued to be due to its high dehydrogenation activity at lower pressures, possibly due to the high presence of Lewis sites in its structure. Catalyst CBV-712 appears to have a balanced ratio of Brönsted to Lewis acid sites and probably a better platinum dispersion through its structure due to its cleaner pores and less EFAL species, which have contributed to the catalyst's superior performance. Sulfur was found to impact the hydroisomerization activity of catalysts, though its impact becomes less severe once pure heptane is re-introduced to catalysts.

6.6 References

[1] Chica. A and Corma. A. (1999). Hydroisomerization of Pentane, Hexane and Heptane for Improving the Octane Number of Gasoline. *Journal of Catalysis*, 187, 167-176.

[2] Alotaibi, F. M. (2009). *Deactivation Behaviour of Metal-loaded Zeolite Catalysts during High n-Alkane Selective Hydroisomerisation. 1st Year PhD Transfer Report,* University of Manchester.

[3] Patrigeon, A; Benazzi, E; Travers, Ch. and Bernhard, J. Y. (2001). Influence of the Zeolite Structure and Acidity on the Hydroisomerization of *n*-heptane. *Catalysis Today*, 65, 149-155.

[4] Nikolaou, N; Papadopoulos, C. E; Gaglia, I. A. and Pitarakis, K. G. (2004). A New Non-linear Calculation Method of Isomerisation Gasoline Research Octane Number Based on Gas Chromatographic Data. *Fuel*, 83, 517-523.

[5] Internet FAQ Archives, Gasoline FAQ [Website]. Available from: <http://www.faqs.org/faqs/autos/gasoline-faq/part2/preamble.html> [Accessed: 1 June 2010].

[6] Jones, D. S. J. and Pujadó, P. R. (2006). *Handbook of Petroleum Processing*. Netherlands: Springer. p. 53.

[7] Cottingham, P. L; Antweiler, J. C; Mayfield, L. G; Keller, R. E. and Coker, W. P. (1956). Hydrofining Thermally Cracked Shale-Oil Naphtha. *Industrial & Engineering Chemistry*, 48:7, 1146-1151.

[8] Saberi, M. A. and Le Van Mao, R. (2003). Comparative Study of Kinetic Behaviour of the Bifunctional and Trifunctional Catalysts in the Hydroisomerization of *n*-Heptane. *Applied Catalysis A: General*, 242, 139-150.

CHAPTER SEVEN

CONCLUSIONS & FUTURE WORK

The utilization of zeolite USY catalysts seem to be promising in the application of octane boosting of normal heptane, given the 30+ points increase in RON achieved with the best catalysts among the ones tested. The dealumination treatment, be it steaming to change the acidic properties and create mesopores within the catalyst, or acid leaching to remove EFAL species from the catalyst structure, can result in a considerably enhanced selectivity and stability of zeolite Y in the hydroisomerization of normal heptane. The resulting catalysts, though, cannot accommodate the presence of sulfur species in the feed with their current formulations, as they seem to quickly lose their metal functions by sulfur poisoning.

Despite the success found with catalysts USY-D and CBV-712 in this research, improvements in the experimental setup and a variation in catalyst formulation and type could have improved observed results. In addition, there exists a big gap between the application of these catalysts with normal alkane and the ultimate objective of formulating a catalyst system that is capable of processing heavy naphtha into a higher octane stream. Many steps towards achieving that goal lie ahead. Following is a look at some of the ways that might help close that gap and ones that could improve the results of similar research in the future:

1. Varying the hydrogen to feed ratio: in this work, a molar ratio of 9 was used throughout. Varying this ratio would have enabled studying the effect of different hydrogen partial pressures on catalyst performance, in addition to the ability to empirically determine the reaction order with respect to the hydrocarbon feed or hydrogen for each catalyst by fixing the partial pressure of one component of the feed while varying the other, and vice versa.

2. Acid-leaching steamed samples: a mild acid treating for catalyst USY-D might result in a catalyst of lower cracking at atmospheric pressure due to altered Brönsted/Lewis acid site ratio and one that is better than CBV-712.

3. Improved characterization using TEM, metal surface area and dispersion: the former technique might help in investigating metal position and lumping, if any, in the catalyst in addition to analyzing if there is pore-blockage by coke. The latter technique enables the calculation of accessible metal sites on the catalyst, which leads to determining the key n_{Pt}/n_A ratio of tested catalysts.

4. Running at differential conditions: carrying out experiments at low overall conversions (< 10 mol%) allows a straight forward estimation of apparent activation energies.

5. Including cracking products in RON estimation: even though this would be more difficult to carry out than to do it for heptane isomers only, a better estimation, with possibly higher values, of RON can be performed.

6. Building a more comprehensive kinetic model: time did not allow a detailed modelling study, but modelling with an adsorption-desorption approach might enable building a high-precision reaction model similar to that used by Denayer et al (Table 3-3). This would allow predicting catalyst activity and selectivity at various reaction conditions, which would provide a roadmap for experimental setup.

7. Varying metal type and loading: as seen from the literature, different metals in addition to different combinations and loadings can considerably alter catalyst performance. CBV-712 would be an excellent starting point for a new study as CBV-712 proved extremely stable in performance with good conversion and constant selectivity with changing pressure, contact time, and temperature. Its clean pore structure would allow the incorporation of a second metal or more. For instance, studying the effect of adding an alkaline earth metal such as Ba, which proved to be very good in enhancing the catalyst selectivity in Liu et al's study (see sub-section 3.3.9), to platinum and/or loading Pd, Ni, or Al might greatly enhance product RON and reduce cracking substantially.

8. Testing a mixture of normal heptane to decane: this way, there will be a more realistic representation of the heavy naphtha range, though this would only simulate the paraffinic portion of heavy naphtha. The best catalysts with this feed would be later tested with a desulfurized real heavy naphtha feed.

9. Comparison with zeolite Beta: this type of zeolite proved highly active and selective in this reaction, as per the literature. Therefore, comparing the performance of USY samples with Beta ones or even testing a hybrid catalyst of both types can achieve better results.

10. Pilot-plant testing: using a binding material with these catalysts and testing a bigger mass of catalyst at a pilot plant would better simulate real-plant conditions.

A publication based on this work has been drafted and will be submitted to appropriate journals for review. It can be found in Appendix E. A later publication is planned to cover advanced modelling of data generated in this work, with the aim of developing a more realistic model that allows predicting catalyst behaviour at untested reaction conditions.

APPENDIX A

Bill OF MATERIALS & COST OF HYDROISOMERIZATION PRESSURE UNIT

Table A-1. Bill and cost of materials required to build the pressure hydroisomerization unit.

Part	Specification	Manufacturer	Supplier	Model	Quantity	Price (£)
1/4" Stainless Steel Tube	OD = 1/4” Wall thickness = 0.028” Max pressure = 4000 psig	Swagelok	M .F .S.	Swagelok (SS-T4-S-035-6ME)	6 Meters	25.8
Needle Valve	Body Material: 316-SS Kel-F Stem 1/4" Swagelok	Swagelok	M .F .S.	Swagelok (SS-1KS4)	15	634.5
Pressure Regulator	Body material: 316-SS Max inlet pressure: 50 bar	Wika		Tescom	3	available
H_2 Pressure Regulator	0-28 bar outlet pressure		Freshfords	GA400	1	208.89
Pressure Gauge	Body material: 316-SS Pressure range: 0 – 60 bar 1/4" NPT connector Filled with Glycerin	Wika	BKW	Wika (232.30.63)	6	354
Compact Inline Filter	316 Stainless Steel 1/4" Swagelok 7 micron wire mesh 3000 psig			Swagelok (SS-4F-7)	1	38.2
Check Valve	316 Stainless Steel 1/4" Swagelok Working pressure = 206 bar Back pressure = 70 bar Cracking pressure = 0.7 bar			Swagelok (SS-4C-10)	4	115.2

Mass Flow Controller	Fluid: H_2/N_2/air Flow = 10 – 20,000 ml/min Max pressure = 100 bar Operating temp. = ambient I/O signal = 0 – 5 Vdc	Brooks	Flotech	Brooks (5850 TR)	3	available
Readout & Control Unit	I/O signal: 0 – 5 Vdc Supply output: 15 V 4 channels	Brooks	Flotech	Brooks Instruments (0154/CC1A10)	1	1245
Pressure Controller	1 – 40 Bar 0 – 20 mA	Brooks	Flotech	Brooks Instruments (5866/A1C1B2EE1A)	1	1674
Mass Flow Controller Cables	6 M long interconnecting cable D-D	Brooks	Flotech	Brooks Instruments (124-Z-237-AAA)	4	352
Temperature Controller	7.5 VA 24V AC	Omron	Farnell	Omron (E5CN-R2MT 500)	3	474.93
Temperature Cut-out Policeman					1	available
Weighing Scale	Max range = 5 Kg Readability = 0.01 g				1	available
HPLC Pump	Flow rate range = 2.5 – 50 ml/hr	Gilson		305	1	available
Pressure Relief Valve	Body material: 316-SS Seal: Viton Inlet: 1/4" male NPT Outlet: 1/4" female NPT Spring range: 50 – 499 psig Spring setting: 435 psig (30 bar)		Tamo Ltd.	Circle Seal Control (PEDMR6032-2MP-CC)	2	303.16
Double Tube Heat	Body material: 316-SS				1	available

Exchanger	Outer tube diameter: 1/2" Inner tube diameter: 1/4"					
Separator	Body material: 304L Volume = 150 ml			Swagelok (304L-HDF4-150-PD)	1	89.75
Cooling Bath	5.75 L -40^{o}C	Fryka	Camlab	Fryka (FR/KT06-43)	1	2252.5
Bath Circulating Pump	External circulating pump	Fryka	Camlab	Fryka (FR/EP 20)	1	418
Knock-out Vessel	Body material: 304L Volume = 50 ml			Swagelok (304L-HDF4-50-PD)	1	67.75
Reactor	Body material: 316-SS Total length = 64.5 cm Bed length = 53.5 cm External diameter = 1.27 cm Internal diameter = 1.02 cm Wall thickness = 0.1245 cm Thermo well diameter = 0.3175 cm Total volume = 43.7 ml Bed volume = 39.92 ml				1	available
Furnace	Three-zone			Vectstar	1	available
Multi-trend Temperature Indicator	6 independent readings 85 – 250 Vac 50 – 60 Hz 50 VA			Penny & Giles Instruments Ltd. (D53087/C848TPAO)	1	available

Bed Thermocouples	Type = K-Type Diameter = 1.0 mm Grounded	A J Thermosensor		A J Thermosensor (PR11-K-10-500-3-PV-MZ)	2	59
Ceramic Thermowells	THE tubes Closed one end (COE) Length 65 mm External diameter: 3 mm Internal diameter: 1.5 mm	Anderman Ceramics			50	875
Union Cross	Body Material: 316-SS 1/4" OD	Swagelok	M .F .S.	Swagelok (SS-400-4)	2	50.6
Male Elbow	Body Material: 316-SS 1/4" OD x 1/4" NPT	Swagelok	M .F .S.	Swagelok (SS-400-2-4)	6	51
Union Tee	Body Material: 316-SS 1/4" OD	Swagelok	M .F .S.	Swagelok (SS-400-3)	6	83.4
Female Branch Tee	Body Material: 316-SS 1/4" OD x 1/4" NPT	Swagelok	M .F .S.	Swagelok (SS-400-3-4TTF)	6	120.3
Reducer	Body Material: 316-SS 1/16" OD x 1/4" tube ST	Swagelok	M .F .S.	Swagelok (SS-100-R-4)	1	10.1
Ferrule set (front & back)	Body Material: 316-SS 1/4" OD	Swagelok	M .F .S.	Swagelok (SS-400-SET)	20	24
Reducing Union	Body Material: 316-SS 1/4" OD x 1/8" OD	Swagelok	M .F .S.	Swagelok (SS-400-6-2)	1	7
Female Connector	Body Material: 316-SS 1/4" OD x 1/4" NPT	Swagelok	M .F .S.	Swagelok (SS-400-7-4)	3	21
Pressure Gauge Shipping						27.5
Pressure Controller Shipping						30
Ceramic Thermowells						14

Shipping						
Cooling Bath Shipping						20.63
Circulator Pump Shipping						20.63
Swagelok Shipping						25
Thermocouples Shipping						25
Relief Valves Shipping						13.5
Unit Steel Frames						194.95
TOTAL						**£9926.29**

APPENDIX B

ZEOLITE Y GEL & Pt-LOADING CALCULATIONS

Zeolite Y Gel Calculations

Seed Gel: **(10.67 Na_2O: Al_2O_3: 10 SiO_2: 180 H_2O)**

- To get 1 mole of Al_2O_3, we need N grams of Sodium Aluminate (SA).
  1 gram of SA contains 0.509 g of Al_2O_3 = 0.004992 moles.

  So, N = 1 mole/ 0.004992 = 200.32 g of SA

- Now we have (0.312)(200.32) = 62.5 g of Na_2O = 1.0084 moles.
  So, we need 10.67 – 1.0084 = 9.6616 moles of Na_2O = 2(9.6616) moles of NaOH = (19.3232)(39.99717 g/mole) = 772.8733 g of NaOH

- We need 10 moles of SiO_2 = 600.848 g. To get it, we need N grams of Ludox.
  N = 600.848g/0.4 = 1502.12 g of Ludox

- For Hydrogen, we have (0.179)(200.32 g SA)(2/18.01534) = 3.98075 moles from SA
  + 19.3232 moles from NaOH

  + (0.6)(1502.12 g Ludox)(2/18.01534) = 100.056 moles from Ludox AS-40.

  Total is 123.36 moles. We need 360 – 123.36 = 236.64 moles of Hydrogen.

  So, we need 236.64/2 = 118.32 moles of H_2O = 2131.575 g of H_2O

- To check for Oxygen, we have 3 moles from Al_2O_3 + 1.0084 moles from Na_2O
  + 19.3232 moles from NaOH + 3.98075/2 moles from SA + 20 moles from SiO_2

  + 100.056/2 moles from Ludox water + 118.32 moles of H_2O = 213.67 moles (correct!)

Seed Gel weight ratio: 1 SA: 3.8582 NaOH: 7.4986 Ludox: 10.6408 H_2O

Feed Stock Gel: **(4.3 Na_2O: Al_2O_3: 10 SiO_2: 180 H_2O)**

- As in the seed gel, we need 200.32 g of SA
- We have 1.0084 moles of Na_2O and need 4.3 – 1.0084 = 3.2916 moles of Na_2O = 6.5832 mole of NaOH = 263.3094 g of NaOH
- As in the seed gel, we need 1502.12 g of Ludox
- For Hydrogen, we have 3.98075 moles (SA) + 6.5832 moles (NaOH) + 100.056 moles (Ludox) = 110.61995 moles. We need 360 – 110.61995 = 249.38005 moles of Hydrogen = 124.690025 moles of H_2O = 2246.3332 g of H_2O
- To check for Oxygen, we have 3 + 1.0084 + 6.5832 + 3.98075/2 + 20 + 100.056/2 + 124.690025 = 207.3 (correct!)

Feed Stock gel weight ratio: 1 SA: 1.3144 NaOH: 7.4986 Ludox: 11.2137 H_2O

Pt-loading Calculations

- Tetra-ammine platinum (II) chloride ($Pt(NH_3)_4Cl_2$) has a molecular weight of 334.11, which means that Pt constitute 195.08 × 0.98 ÷ 334.11 × 100 = 57.22 wt% of the salt
- To have a 1 wt% loading of Pt on a 1 gram catalyst sample, we need 0.99 grams of catalyst and 0.01 gram of Pt. To get 0.01 grams of Pt, we need 100 ÷ 57.22 × 0.01 = 0.0175 g of salt
- To prepare a 5×10^{-3} M solution of salt, we need 0.005 moles for each 1 liter (1000 ml) of water, so for 0.0175 ÷ 334.11 = 5.24×10^{-5} moles of salt we need 5.24×10^{-5} ÷ 0.005 × 1000 = 10.48 ml of water

APPENDIX C

W/F_o, YIELD & MASS BALANCE CALCULATIONS

W/F_o Calculations

- The weight of catalyst used was always W = 2 grams

- The HPLC pump fed nC_7 at 7.5, 15, and 30 ml/hr. For 7.5, that is equal to 0.00833 ml/s. The density of nC_7 at room temperature is 0.684 g/ml, which means that for the lowest pump setting the flow = $0.00833 \times 0.684 = 0.0057$ g/s

- The molecular weight of nC_7 is 100.2 g/mol, which means that the flow rate is $0.0057 \div 100.2 = 5.69 \times 10^{-5}$ mol/s

- Therefore, $W/F_o = 2 \div 5.69 \times 10^{-5} = 35{,}140$ g.s/mol = 35.14 Kg.s/mol

Yield Calculations

- GCs separate each component in the injected sample into peaks, and for liquid samples each peak represents the weight % of its corresponding product

- So, for one sample of liquid product, nC_7's wt% is multiplied by the total liquid sample weight to give the yield in grams

- The yield in grams is converted to mols to enable the calculation of nC_7 conversion and key molar ratios such as mono/multi, I/C, etc

- For gas samples, the GC produces peaks for individual components of the injected sample

- Each peak area is multiplied by the corresponding RF of its representative component to give its mol% of the gas product

- Then, the mol% of the individual component is divided by the total mol% of components to get the mol% of the individual component with respect to the total hydrocarbon conent of the gas product

- The mol% of each component in the hydrocarbon mixture is multiplied by its molecular weight, and the resulting values for all components are summed to get the average molecular weight of hydrocarbons in the gas product

- Then, the average flow rate of gas during run time is calculated in liters per hour and then multiplied by run time to get total product volume, which is multiplied by the total mol% of the gas sample to calculate the volume of hydrocarbons during run time, which, in turn, is multiplied by the sample average molecular weight and divided by 24.2 (liters per mol using the idea gas law) to give the total mass of hydrocarbons in the gas product.

- Finally, to calculate the yield in grams for an individual component of gas product, its mole ratio in the hydrocarbon content of the gas product is multiplied by its molecular weight and the result is multiplied by the total mass of hydrocarbons in the gas product then divided by their average molecular weight

- The yield in grams for individual gas components is later converted to moles to enable the calculation of nC_7 conversion and key molar ratios such as mono/multi, I/C, etc

Mass Balance Calculations

- To conduct a hydrocarbon mass balance for a given experimental run, the inlet mass of nC_7 is measured by recording the weight change of the feed vessel

- Then the total mass of liquid plus gas products calculated above is calculated

- Finally, the mass balance is calculated as:

$$\text{Mass Balance} = (\text{Liquid out} + \text{Gas out}) \div \text{Liquid in} \times 100$$

APPENDIX D

IDENTIFICATION OF NORMAL HEPTANE ISOMERS BY GC

Using Varian's Galaxie Chromatography Data System in conjunction with GC instruments allowed for an easy quantitative and qualitative analysis of reaction products. Figure C-1 shows an example of a liquid sample separation using this software. Each peak was assigned to an isomer after using GC-MS analysis in addition to the used GC PONA column's data sheet to anticipate isomer elution order.

Figure D-1. Identification of normal heptane isomers using Varian's Galaxie Chromatography Data System.

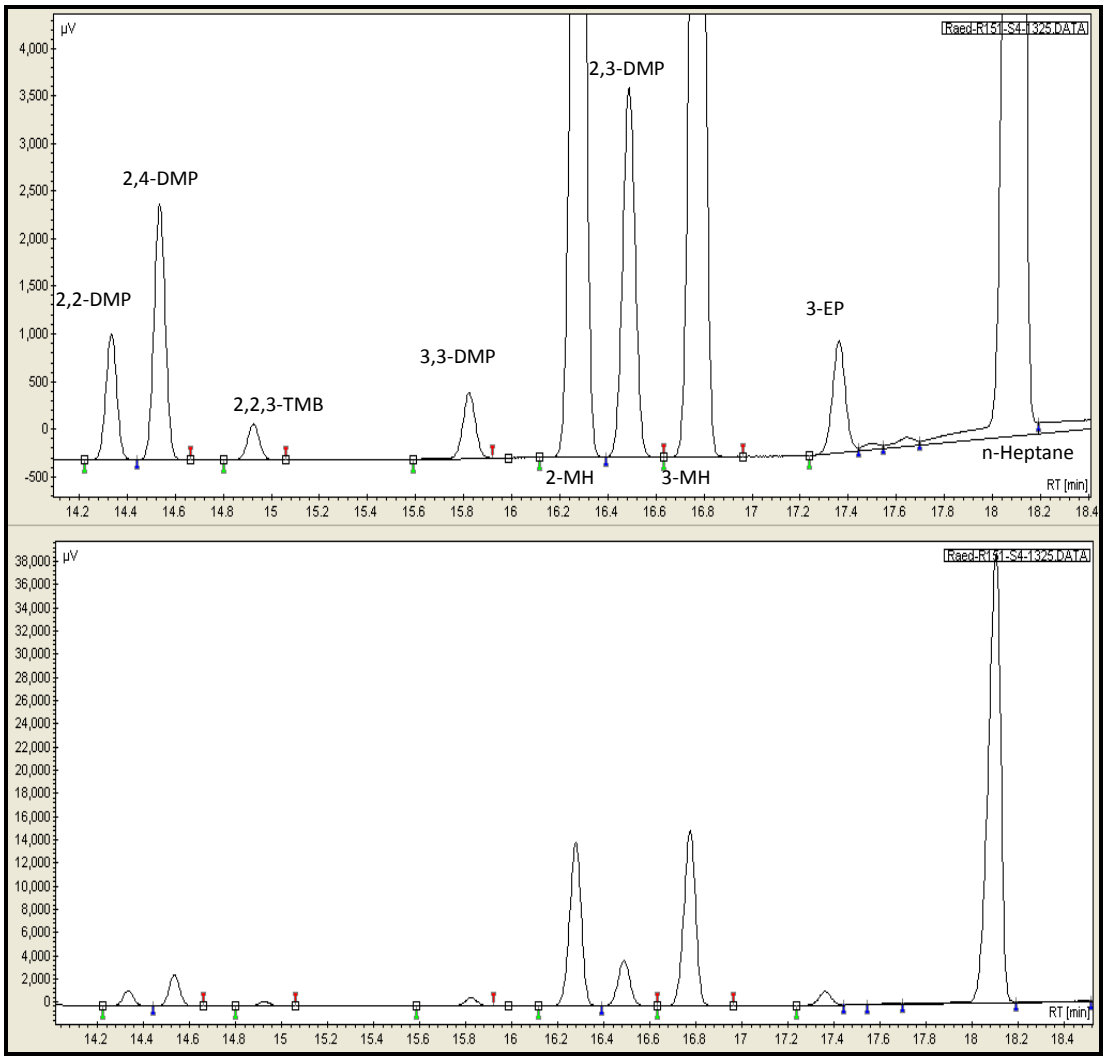

APPENDIX E

DRAFT PUBLICATION

Hydroisomerization of Normal Heptane over Pt-Loaded USY Zeolites. Effect of Steaming, De-Alumination and the Resulting Catalyst Structure on Catalytic Properties.

Raed H. Abudawood, Faisal M. Alotaibi, and Arthur A. Garforth*

Abstract

The hydroconversion of normal heptane was studied on five USY zeolite samples loaded with 1 wt% Pt. Experiments were performed on a continuous fixed-bed stainless steel reactor at 210 – 310^{o}C and pressures up to 15 bar. Three in-house samples were subjected to steaming treatment and the remaining were acid-leached commercial ones. Results have shown that steamed samples generate more cracked products at higher conversions when compared to acid-leached ones, possibly due to a high presence of EFAL species. The degree of steaming played a role in decreasing cracking tendency at higher pressures, which is attributed to pore structure change and decreasing acidity. It also resulted in a catalyst sample capable of generating isomers with blended Research Octane Numbers close to those achieved with a robust commercial catalyst. However, poisoning experiments have shown that these two catalysts are highly sensitive to sulfur and require sulfur-free feeds in order to demonstrate their full capacities.

*To whom correspondence should be addressed.

Introduction

Stricter environmental regulations imposed worldwide on gasoline automotive fuel quality have left refiners facing a challenge; the content of environmentally-unfriendly aromatics in gasoline fuel has to be reduced [1-3] with the fuel still meeting the minimum combustion efficiency requirement, expressed by its Research Octane Number (RON) [4-6]. Finding a high-octane substituent for aromatics is not a straight forward task. For instance, main octane enhancers blended in gasoline have either been completely phased out due to their toxicity, such as in the case of lead-containing additives, or seen their use decline due to their environmental concerns, like oxygenates such as MTBE [7-9]. Moreover, adding high-octane reformates to gasoline fails to do the trick, since aromatics are a major constituent of reformates [10-12]. A potential solution to this problem has been proposed in the hydroisomerization of lower-value refinery heavy naphtha streams to improve their RON, thus enabling the blending of higher amounts of heavy naphtha into gasoline, allowing

for a weaker need to blend the aforementioned additives with gasoline. The application of specifically-made bifunctional zeolite catalysts in upgrading the RON of refinery light naphtha streams through hydroisomerization has already been commercialized [13-15]. This application, however, has not yet been expanded commercially to include the processing of heavy naphtha, which typically contains normal alkanes from the range of heptane to decane [16-18]. In the present work, normal heptane, having a RON of 0, is chosen as a proxy to heavy naphtha in studying the hydroisomerization reaction over bifunctional USY zeolite catalysts.

Zeolites are crystalline aluminosilicates [19,20] that have unique pore structures and catalytic properties, promoting their use in many industries, most importantly the refining industry [21,22]. Of these zeolites utilized in the oil industry is Y Zeolite, which has a 3D structure with large pore openings [23]. It can be hydrothermally treated with steam to form its ultrastable form USY. Steaming treatments introduce extraframework alumina (EFAL) species within USY. These EFAL species are responsible for the presence of Lewis acid sites within USY zeolites [24,25].

Hydroisomerization of normal alkanes proceeds ideally by the bifunctional mechanism in which a noble metal, usually platinum, provides the hydrogenation/dehydrogenation functions of the catalyst, and a zeolitic support provides the acidic function responsible for carbenium ion rearrangments [26]. The presence of EFAL species in USY catalysts has an impact on their acidic properties, leading to a modified selectivity. Wang, Giannetto, and Guisnet [27] reported that a higher presense of EFAL species in the zeolite unit cell contributes to a higher cracking activity and coking rate. They noticed also that they positively affect the isomerisation activity of calaysts, possibly due to the inductive effect their introduced Lewis acid sites have on existing Brønsted ones. This inductive effect has been highlighted by Remy et al [28] who found that deep dealumination of USY samples by acid leaching and the removal of most EFAL species from the catalyst results in smaller turnover frequencies (TOF) over framework aluminium atoms ($Al(IV)_F$), suggesting the inductive effect.

In this work, we examine the effect of different dealumination treatments and impacted USY catalyst properties on the activity, selectivity, and

stability of Pt-loaded samples, in addition to studying the effect of reaction conditions on isomers RON and product distribution. Catalyst sensitivity to feed sulfur is also tested.

Experimental

The three in-house USY samples were generated as follows: A parent Y zeolite material with a soda content of 2.5 wt% was steamed at 425^{o}C then underwent a mild ion-exchange treatment with ammonium sulfate at 70^{o}C for half an hour, which caused a drop in its soda content to 0.57 wt%. The resulting sample was used to generate the three USY samples by first steaming at 560^{o}C for half an hour, followed by further ion-exchange with ammonium sulfate at 80 ^{o}C for one hour to generate the sample USY-A, and by severely ion-exchanging it at 95^{o}C for 3 hours down to 0.1 wt% soda followed by steaming at 600^{o}C for half an hour then ion-exchange at 80^{o}C for one hour to generate sample USY-B, and steaming at 710^{o}C for half an hour then ion-exchange at 80^{o}C for half an hour to generate sample USY-C. In addition to the 3 in-house samples, samples CBV-712, which is steamed and mildly acid-leached, and CBV-760, which is steamed and deeply acid-leached, were obtained from Zeolyst for this research.

Each sample was platinum-loaded while in its ammonium forms by ion-exchanging it at room temperature overnight in a 5 x 10^{-3} molar aqueous solution of tetra-ammine platinum (II) chloride ($Pt(NH_3)_4Cl_2$), whose amount was calculated such that it results in 1 wt% platinum loading, assuming complete uptake of platinum by the sample. The mixture was later centrifuged and washed with 10 times its volume of de-ionized water to ensure the sample is free of chloride ions.

Characterization techniques used were XRD, elemental analysis, ^{27}Al and ^{29}Si solid-state NMR, BET surface area, pyridine FTIR, and hydrogen chemisorption. Results of sample characterization are shown in Table 1. The number of Al atoms per zeolite unit cell appears to increase with increasing steaming severity for in-house samples, indicating increasing quantities of EFAL species and the retention of Al in the catalyst structure upon steaming, and it is lower for acid-leached samples, reaching as low as 6.2 atoms for the deeply dealuminated CBV-760 sample. Platinum dispersion in analyzed in-house catalysts suggests the presence of large metal crystallites responsible for the somewhat poor dispersion within the samples.

Table 1: Properties of Pt/USY samples.

Sample	Crystallinity (%)*	NaO_2 (wt%)**	Bulk Si/Al^+	Al per UC^{++}	BET surface area $(m^2/g)^x$	Pore volume $(cm3/g)^x$	Average pore diameter $(Å)^x$	Brønsted/Lewis acid sites$^+$	Metal dispersion $(\%)^{xx}$
USY-A	80.6	<0.09	2.95	54.9	646.2	0.477	29.53	4.48	-
USY-B	79.1	0.09	2.90	59.6	576.7	0.506	35.09	2.70	54.9
USY-C	71.8	0.09	2.85	61.2	456.8	0.457	40.04	1.60	51.8
CBV-712	81.0	0.05	6.00	28.0	816.3	0.452	42.75	0.63	-
CBV-760	72.0	0.03	30.00	6.2	814.0	0.449	24.38	0.60	75.8

*Assuming 100% crystallinity for Y zeolite parent material for in-house samples and reported by [29] for commercial ones.
**Reported by Zeolyst for commercial samples.
$^+$Performed at 150^{o}C for in-house samples and reported by [29] for commercial ones.
$^{++}$Based on a unit cell of 192 Al + Si and assuming 100% crystallinity. Values for commercial samples were reported by [28].
^{x}Degassing was performed at 300^{o}C for in-house samples and 350^{o}C for commercial ones.
^{xx}Performed at 35^{o}C.

To prepare for experiments, samples were each pelletized and sieved into a 40 – 60 mesh size prior to loading into the reactor. 2 grams of sample was sandwiched in the reactor between two layers of inert glass beads with glass wool in between to form the catalytic bed. Then, calcination was performed in-situ using air flow at 500^{o}C for two hours followed by reduction by hydrogen at 450^{o}C for six hours before going to the desired experimental temperature. An illustration of the used reaction rig is given in Figure 1.

Figure 1: Reaction rig.

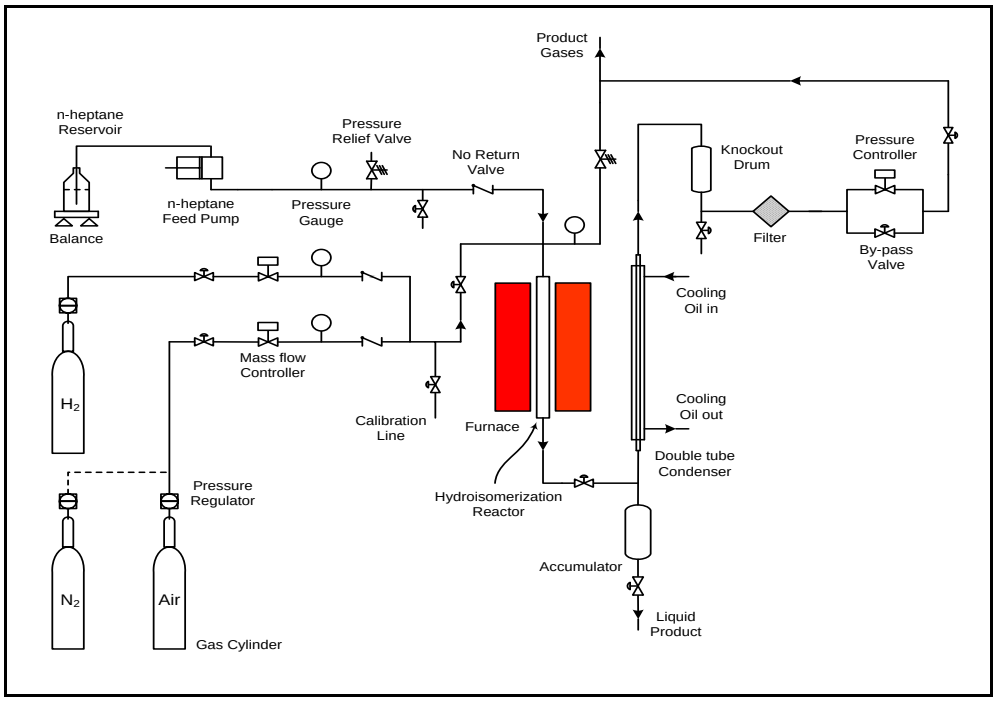

Normal heptane with >99% purity (Sigmaaldrich) was fed to the catalyst bed using an HPLC pump and hydrogen of high purity was introduced to give an H_2/HC molar ratio of 9. Catalytic runs were done at temperatures from 210 to 310^{o}C in order to achieve comparable conversions among all samples. Overall pressure ranged from 1 and 15 bar and space time ranged from 35.14 to 140.6 kg.s/mol. Products were analyzed using a Varian 3400 GC equipped with a 50m x 0.32mm i.d. PLOT Al_2O_3/KCl capillary column fitted to an FID detector for gas products and a CP-Sil PONA CB optimized gasoline column fitted to an FID detector for liquid products. In poisoning experiments, 1 wt% and 100 ppm solutions of dimethyldisulfide (DMDS) (0.64 wt% and 64 ppm sulfur) in normal heptane were prepared for tests with sample USY-C and CBV-712, respectively at 210^{o}C, atmospheric pressure and a space time of 140.6 kg.s/mol.

Results

I) Deactivation behaviour

The deactivation behaviour of all samples was studied at 230^{o}C, atmospheric pressure and a space time of 70.6 kg.s/mol. Overall conversion of normal heptanes, calculated either in mole or weight % as $X = [(n_{C7})_0 - (n_{C7})_f]/(n_{C7})_0 \times 100$, where $(n_{C7})_0$ and $(n_{C7})_f$ are the initial and final concentrations of normal heptane, respectively. Figure 2 shows the overall conversion of normal heptane as a function of time-on-stream. CBV-760 was not active at this temperature and its results are shown at 290^{o}C and a space time of 140.6 kg.s/mol. Sample USY-A

Figure 2: Overall conversion of nC_7 (T = 230^{o}C, P = 1 bar, W/F_o = 70.6 kg.s/mol).

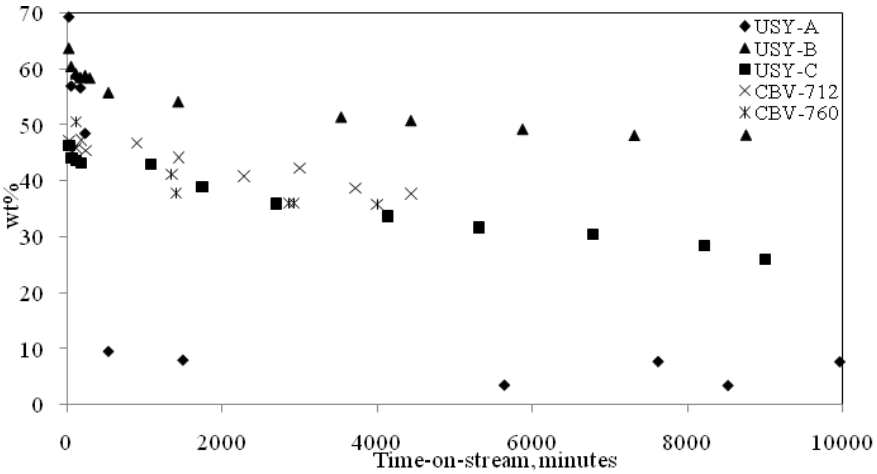

has shown a very rapid deactivation, possibly due to its high acidity and low average pore diameter, which might have caused excessive cracking and/or diffusion limitation inside its tight pores. Therefore, further testing of this sample was halted. Despite sample USY-B's initial sharp drop in activity from around 70 to 55 wt% conversion, its activity has dropped gently thereafter, reaching steady state sooner than the remaining samples, whose activities seemed to be trending lower throughout the course of experiments. It is worth mentioning that sample USY-B has the largest pore volume among all samples, which might suggest the absence of diffusion limitations.

II) Product yield & RON

All possible isomers were generated and identified in activity tests. After reaching steady conversion levels, product selectivities for mono-branched isomers (MB), multi-branched isomers (MuB), and cracking products (CR) were calculated and plotted against normal heptane conversion, as shown in Figure 3. Among the 4 samples, USY-B seems to generate the most cracking products, with the yield of cracking products exceeding that of multi-branched isomers at most conversion levels. This is indicative of poor acid-metal balance in this sample, evidenced by a low metal dispersion, since a proper balance would normally generate products in a successive manner as shown in the equation:

$$nC_7 \rightleftharpoons MB \rightleftharpoons MuB \rightleftharpoons CR$$

This successive generation of product categories is characteristic of ideal bifunctional catalysts, an observation made by Guisnet et al [30]. They found that for a proper balance between acidic and metal functions to exist, the ratio of accessible platinum sites to acidic sites, expressed by n_{Pt}/n_A, for the hydroisomerization of normal heptane over platinum-loaded Y zeolite has to exceed 0.17, a value also confirmed later for normal decane hydroisomerization by Alvarez et al [31]. Guisnet et al reported that at lower values than 0.17, catalysts generated mono-branched, multi-branched, and cracking products simultaneously from normal heptane. Despite sample USY-C showing non-ideal behaviour at 1 bar, its performance seems to approach ideal bifunctional behaviour as pressure increases, almost matching that of CBV-712. Cracking on USY-C seems to be suppressed at higher pressures. Quite the contrary to USY-C, CBV-760 appears to generate more cracking products as system pressure increases, most probably due its

considerably lower average pore diameter than its peers, which could have promoted cracking within its pores as its structure became increasingly more restricted to the passage of bulky molecules at elevated pressures.

Figure 3: Product selectivity at steady conversions.

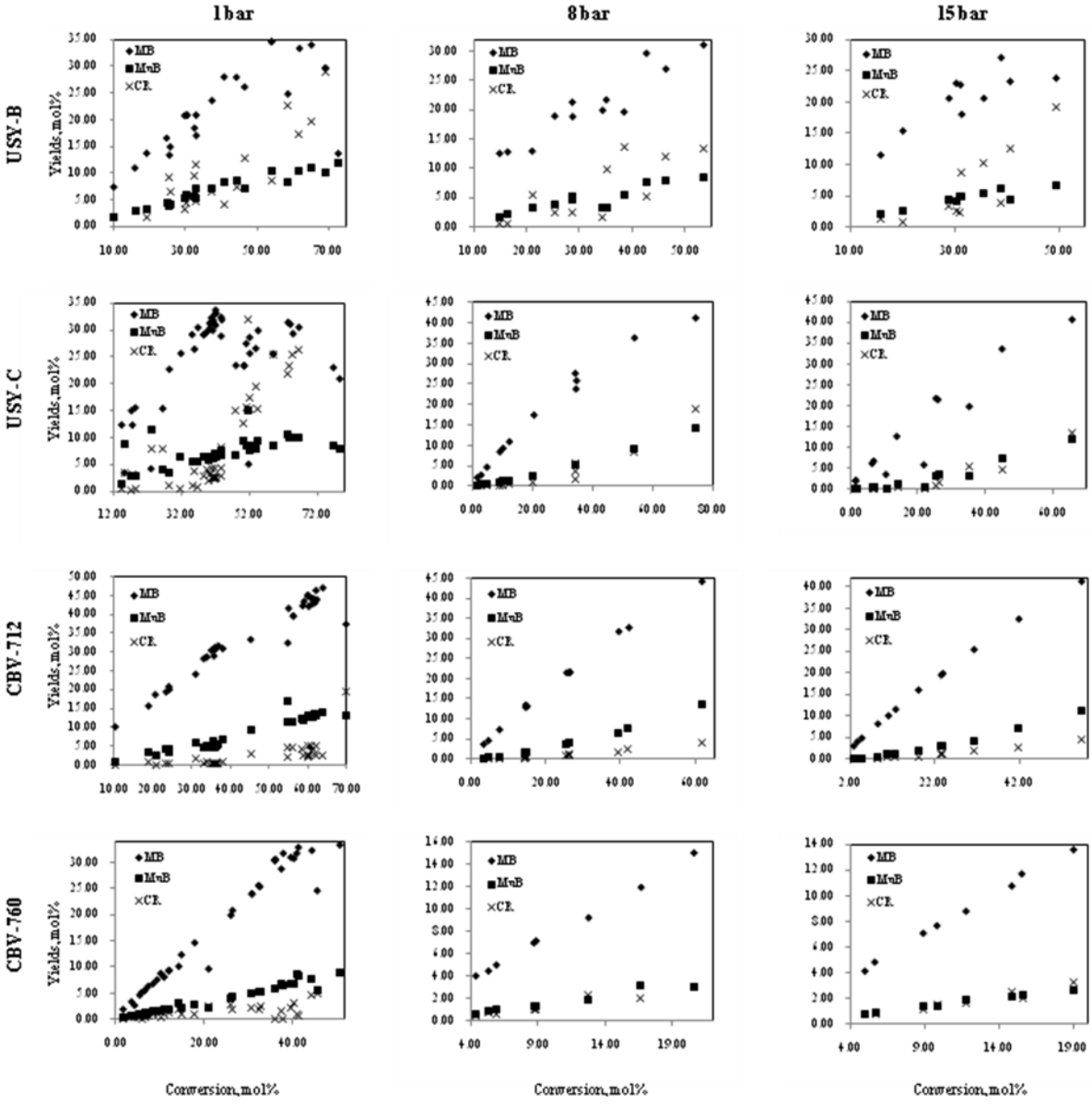

In order to have a more realistic view of the selectivites of these USY samples, the RON of blended product isomers has been estimated by a method developed by Nikolaou et al [32], where the influence of individual hydrocarbon products is taken into account when calculating the total blended RON for the product stream. Estimated blended RON values were plotted against normal

heptane conversion and are shown in Figure 4. It appears that sample USY-B fails to show improvement in product RON upon raising pressure, with the value reaching a plateau around 17 at 15 bar, whereas USY-C's maximum RON increases from around 23 to above 30 as the pressure increases from 1 to 15 bar. USY-C seems to behave differently to other samples, since they generate less RON values with increasing pressures, which is the expected outcome since the selectivity to multi-branched isomers, which have high RON contributions, is negatively impacted the higher the pressure [33]. Nevertheless, sample CBV-712 superbly maintained RON values close to or above 30 at all tested pressures.

Figure 4: Blended RON at steady conversions.

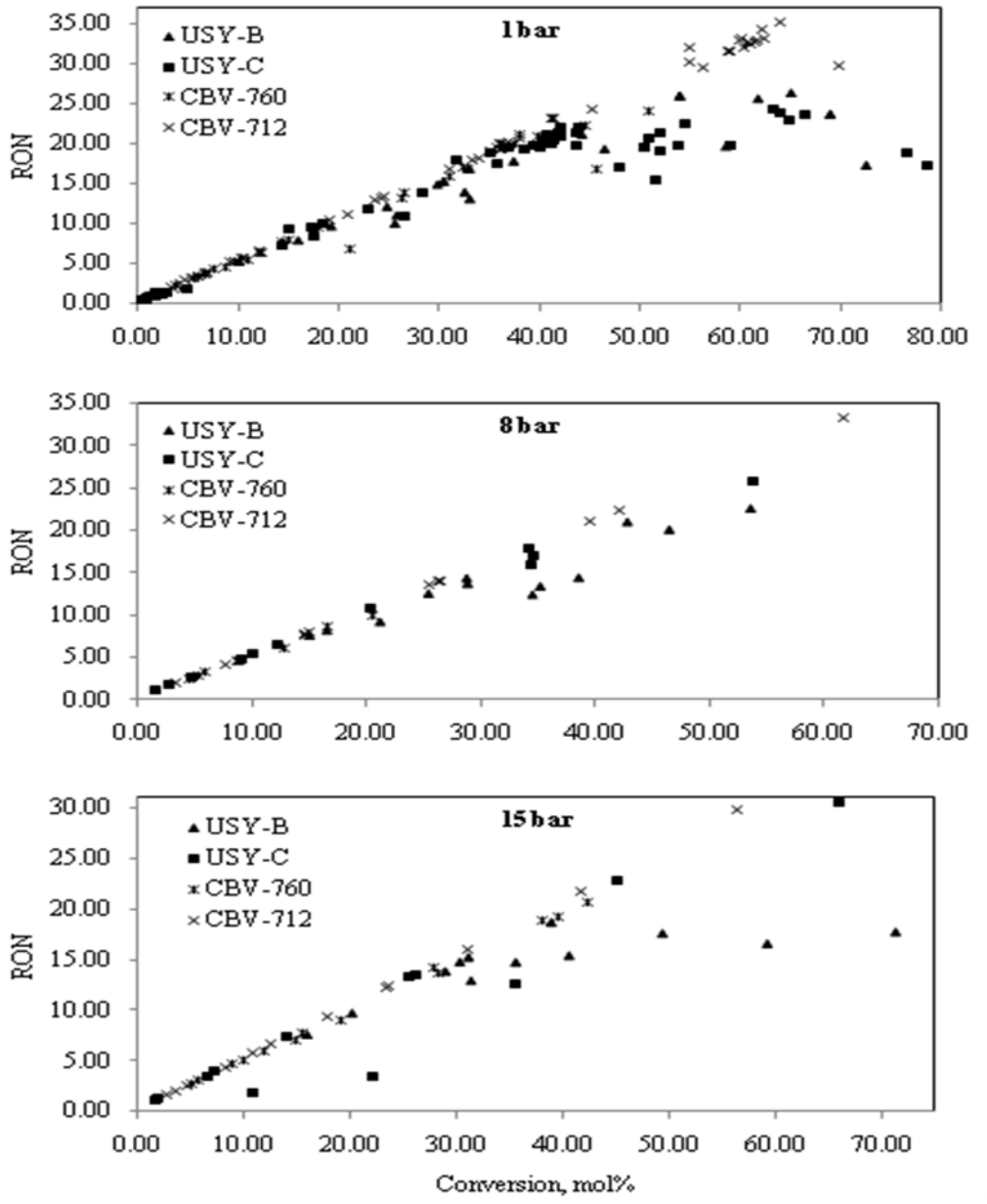

III) Effect of sulfur

Figure 5 shows the results of the two poisoning experiments. It seems both tested samples are very sensitive to sulfur in the feed, since they undergo sharp drops in conversion once the feed was switched from pure nC_7, which has a total sulfur content of 4.6 ppm, to nC_7 plus DMDS, with the fall in USY-C being greater due to the higher sulfur content it suffered. However, activity was partially recovered upon resumption of nC_7 feeding on both cases, though to a lesser degree for USY-C. This is a similar behaviour to what was reported by Romero et al [72] for the hydroisomerization of normal decane over Pt-loaded mordenite, with the exception of a greater loss of isomerisation activity versus that of cracking, evidenced by a drop to less than one fifth the original value of the I/C ratio in the case of USY-C (it dropped to one third the original value as reported by Romero et al). The drop in the I/C ratio was shallower for CBV-712, since it was treated with only 100 ppm of DMDS. The mono/multi ratio was less affected, indicating that both categories of isomers have a larger dependence on metal sites for their formation.

Figure 5: Effect of sulfur addition.

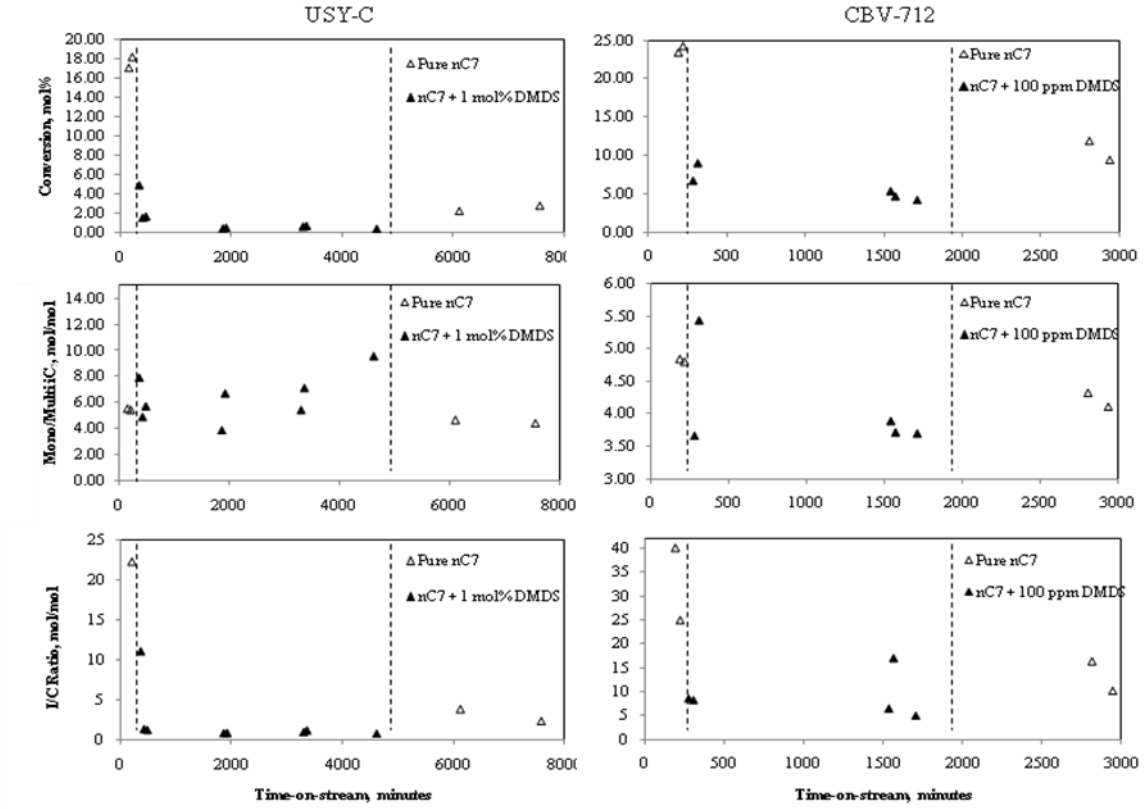

VI) Analysis of spent samples

After all tests were completed, analysis of spent catalyst samples was performed to determine their crystallinity and coke content. Crystallinities were determined by XRD and were calculated as a percentage of the crystallinities of fresh samples. Table 2 lists the crystallinities of all samples tested. Sample USY-A lost a bit of its crystallinity due to its short testing duration. The rest of the samples were tested for almost equal total durations, allowing for a better comparison. Both in-house samples lost more of their original crystallinity when compared to acid-leached samples, with sample USY-C losing the most. It is worth noting, however, that the XRD analysis was performed on samples without regeneration (coke oxidation), and thus coke might have caused the observed loss of crystallinity to be aggravated, since coke is amorphous.

Table 2: Crystallinity of spent samples.

Sample	Crystallinity, %
USY-A	80
USY-B	52
USY-C	50
CBV-712	67
CBV-760	73

Coke content was measured by thermogravimetric analysis (TGA) for the top, middle, and bottom portions of the catalytic bed in order to see the distribution of coke in samples. Table 3 shows the results for the TGA analysis for all samples.

Table 3: Coke content of spent samples.

Sample	Coke Content, wt%		
	Top	Middle	Bottom
USY-A	1.903	1.204	0.804
USY-B	2.078	0.723	0.219
USY-C	0.991	1.088	1.096
CBV-712	0.083	0.022	0.061
CBV-760	0.252	0.136	0.137

Despite its short testing duration, sample USY-A accumulated a high content of coke on all zones of the catalyst bed. A similar observation is noticed for USY-B, though its coke content is mostly located in the top zone of the bed, suggesting pore blockage by excessive cracking, which most probably occurred at elevated temperatures, since its deactivation behaviour suggested the least diffusion limitation compared to other samples. For sample USY-C, the very uniform distribution of coke in all

zones of its bed despite the high coke content indicates that no diffusion limitations are imposed on this sample. The very low coke content in CBV-712 and, to a lesser degree, CBV-760 suggests that the EFAL species, richly present in in-house samples, might have acted as coke precursors, promoting cracking in those samples.

Discussion

To best judge on how tested samples differ in their selective properties, a good way is to evaluate their yield structure at comparable overall conversions. Table 4 lists selective properties, product distributions, RON, in addition to key selectivity ratios for each catalyst at 1, 8, and 15 bar. Results in the table were carefully chosen so that they reflect a catalyst's performance at as close an overall conversion as possible to that achieved by other samples at the same pressure. At atmospheric pressure, it is noticed that the acid leached samples are more selective than the steamed-only ones, with CBV-712 being the most selective to isomers. USY-B was less selective than others due to its high cracking yield, whereas USY-C was less selective because it generated other products, which were mainly cyclic compounds that result from heptane dehydrocyclization reactions. These dehydrocyclization products were mainly found with USY-B and USY-C, suggesting that the high presence of EFAL species (higher Lewis acidity) in these two samples might be the cause to their higher dehydrogenation activity. At 8 and 15 bar, USY-C was the most selective catalyst, with both cracking and dehydrocyclization activities greatly suppressed. Cracking selectivity generally decreased for all catalysts, except for CBV-760, whose cracking selectivity almost doubled. This is possibly due to it having the least porosity and average pore diameter among the four samples, which might be responsible for diffusion limitation imposition on this catalyst at high pressures.

The high yield of C_6 products with USY-B compared to the other catalysts, given the almost complete absence of methane in its products, suggests that some oligomerization-cracking (also called dimerization-cracking) takes place on this catalyst, since the only way for C_6 to be produced without producing C_1 is for heptane to oligomerize to C_{14}, which then cracks to C_6 and C_8, with the latter further cracking to C_5 and C_2 or to two C_4s. Interestingly, the BET characterization of this catalyst shows that this assumption of oligomerization-

cracking existence is entirely valid. This catalyst has the biggest porosity among

Table 4: Selectivity, product distribution, RON, and key ratios at comparable conversions.

Catalyst	USY-C	USY-D	CBV-712	CBV-760	USY-C	USY-D	CBV-712	CBV-760	USY-C	USY-D	CBV-712	CBV-760
P, bar	1	1	1	1	8	8	8	8	15	15	15	15
Conversion, mol%	30.5	28.4	31.2	31.0	16.5	12.2	14.6	12.7	15.9	14.0	18.0	15.6
T, ^{o}C	252.0	214.0	252.0	311.8	213.0	233.8	211.4	292.2	215.0	233.0	231.0	296.0
Selectivity, mol%												
Hydroisomerization	84.5	85.9	93.5	89.4	87.2	95.0	93.6	79.6	86.4	93.8	93.0	83.5
Cracking	14.9	7.9	5.9	8.8	8.3	2.8	4.0	18.2	9.0	4.4	5.0	14.5
Other, including dehydrocyclization	0.6	6.2	0.6	1.8	4.5	2.2	2.4	2.2	4.6	1.8	2.0	2.0
Product Distribution, mol%												
Hydroisomerization												
2-MeC_6	35.0	41.5	37.2	38.0	39.6	42.1	43.2	39.8	37.5	42.3	42.2	39.6
3-MeC_6	40.3	42.8	40.1	42.0	42.5	42.4	44.9	39.5	43.4	44.2	43.9	40.7
3-EthC_5	3.0	2.5	3.2	3.2	3.1	3.6	3.2	3.3	3.0	3.3	3.2	3.2
2,2-DiMeC_5	3.4	4.4	3.1	2.9	4.6	1.6	1.4	2.4	5.4	1.2	1.3	2.1
2,3-DiMeC_5	10.1	4.2	9.0	8.0	5.4	5.5	4.0	8.2	5.3	4.9	5.0	8.0
2,4-DiMeC_5	6.2	2.9	5.3	3.9	4.0	4.3	2.9	5.5	1.0	3.6	3.7	5.0
3,3-DiMeC_5	1.4	1.3	1.7	1.7	0.6	0.6	0.4	1.1	0.4	0.5	0.5	1.1
2,2,3-TriMeC_4	0.7	0.3	0.5	0.3	0.2	0.0	0.1	0.1	3.9	0.0	0.2	0.3
Cracking												
C_1	0.0	0.0	0.0	0.0	0.0	0.0	0.0	0.0	1.4	0.0	0.0	0.6
C_2	0.1	1.6	0.1	0.0	0.0	1.2	0.0	0.9	2.1	2.3	1.7	0.9
C_3	42.9	45.0	44.5	48.5	40.5	47.9	43.0	48.8	39.3	51.4	46.8	50.4
C_4	50.4	50.7	53.1	49.8	47.5	46.4	52.5	49.6	48.6	45.4	51.6	47.4
C_5	2.8	1.8	1.6	1.3	0.0	4.4	4.5	0.7	5.7	0.9	0.0	0.6
C_6	3.9	0.9	0.7	0.4	11.9	0.0	0.0	0.0	3.0	0.0	0.0	0.0
RON	15.2	14.0	16.9	15.9	8.2	6.6	7.6	6.1	7.7	7.4	9.4	7.7
I/C	5.9	22.0	17.8	12.6	22.3	34.2	57.3	5.0	9.6	37.3	30.6	6.7
Mono/Multi	3.6	6.6	4.1	4.9	5.8	7.4	10.4	4.8	5.2	8.7	8.4	5.1
iC_4/C_4	23.6	16.0	31.0	7.6	128.4	17.6	13.6	11.9	17.4	18.6	24.2	11.1

the four catalysts, which provides enough room for heptane to oligomerize into the bulky C_{14} inside the zeolite cages. This high porosity, however, comes in

conjunction with a low average pore diameter, which means that once the bulky C_{14} molecule forms, it cannot leave the zeolite structure through the narrow pores, resulting in its cracking. Sample CBV-712 generated isomers with the highest blended RON among these samples at 1 and 15 bar, and USY-C was the one with the least. The reason for the low RON of USY-C isomers despite this sample's high isomers yield is because it produces the most quantities of mono-branched isomers, which have lower RON values than multi-branched ones, resulting in a lower blended RON than achieved with the other catalysts. This behaviour could be due to the low crystallinity and surface area of this catalyst compared to the others, which might have resulted in a high diffusion of mono-branched isomers out of the catalyst before they transform into multi-branched ones. This also would explain the very low cracking selectivity of this catalyst, especially at higher pressures.

Conclusion

Studying Pt-USY zeolite catalysis in the hydroisomerization of normal alkanes is of great interest. Many factors can play a significant role in shaping the catalyst's activity, selectivity and stability. In-house samples that were generated by steaming Y zeolite at different severities behaved very differently to each other and to acid-leached commercial samples. Mild steaming produced a sample that deactivates rapidly due to high Brønsted acidity and small pores. Medium strength steaming produced a stable sample, but one that generates a lot of cracking and cyclic products. Severe steaming did generate a sample that produces a lot of coke and loses crystallinity, but it operates in a near-ideal bifunctional fashion at high pressures, producing isomers with a RON reaching 30, which is a substantial achievement, given that the feed (nC_7) has a RON = 0. EFAL species appear to contribute to coke generation, especially when present at high concentrations. A mild acid-leaching treatment can therefore greatly enhance catalyst performance, since deep dealumination causes activity to drop sharply, resulting in a requirement of very high temperatures to achieve high RONs, as in the case of CBV-760. CBV-760 requires very high temperatures to achieve high RON. A well-balanced acid-metal function results in the highest RON for product isomers, as demonstrated by sample CBV-712, which probably has an optimum ratio of Brønsted to Lewis acid

sites and a high Pt dispersion due its clean pore structure. One drawback of Pt-USY zeolites is their extremely high sensitivity to sulfur presence in the feed, especially their metallic function, and thus require a hydrotreated feed to express their full potential.

Acknowledgement

The authors would like to thank Dr. Aaron Akah from the University of Manchester for his kind help in carrying out the TGA analysis for spent samples.

References

1. Eswaramoorthi, I. and Lingappan, N. (2003). *Catalysis Letters*, 87, 3-4, 133-142.

2. Sakagami, H; Ohno, T; Takahashi, N. and Matsuda, T. (2006). *Journal of Catalysis*, 241, 296-303.

3. Liu, Y; Guo, W; Zhao, X. S; Lian, J; Dou, J. and Kooli, F. (2006). *Journal of Porous Materials*, 13, 359-364.

4. Arribas, M. A; Márquez, F. and Martínez, A. (2000). *Journal of Catalysis*, 190, 309-319.

5. Khurshid, M, Al-Khattaf, S. S. (2009). *Applied Catalysis A: General*, 368, 56-64.

6. Akhmedov, V. M. and Al-Khowaiter, S. H. (2007). *Catalysis Reviews*, 49, 33-139.

7. Barsi, F. V. and Cardoso, D. (2009). *Brazilian Journal of Chemical Engineering*, 26-2, 353-360.

8. Ali, L. I; Ali, A. A; Aboul-Fotouh, S. M. and Aboul-Gheit, A. K. (2001). *Applied Catalysis A: General*, 205, 129-146.

9. Karthikeyan, D; Lingappan, N. and Sivasankar, B. (2008). *Industrial & Engineering Chemistry Research*, 47, 6538-6546.

10. Pope, T. D; Kriz, J. F; Stanciulescu, M. and Monnier, J. (2002). *Applied Catalysis A: General*, 233, 45-62.

11. Ramos, M. J; Gómez, J. P; Dorado, F; Sánchez, P. and Valverde, J. L. (2007). *Chemical Engineering Journal*, 126, 13-21.

12. Raybaud, P; Patrigeon, A. and Toulhoat, H. (2001). *Journal of Catalysis*, 197, 98-112.

13. Maloncy, M. L; Maschmeyer, Th. and Jansen, J. C. (2005). *Chemical Engineering Journal*, 106, 187-195.

14. Matsuda, T; Watanabe, K; Sakagami, H. and Takahashi, N. (2003). *Applied Catalysis A: General*, 242, 267-274.

15. Wei, R; Wang, J. and Xiao, G. (2009). *Catalysis Letters*, 127, 360-367.

16. Pham-Huu, C; Del Gallo, P; Peschiera, E. and Ledoux, M. J. (1995). *Applied Catalysis A: General*, 132, 77-96.

17. Li, X; Yang, J; Liu, Z; Asami, K. and Fujimoto, K. (2006). *Journal of the Japan Petroleum Institute*, 49, 2, 86-90.

18. Liu, P; Zhang, X; Yao, Y. and Wang, J. (2010). *Reaction Kinetics, Mechanisms and Catalysis*, 100, 217-226.

19. Barrer, R. M. (1978). *Zeolites and Clay Minerals as Sorbents and Molecular Sieves.* London; New York: Academic Press, Inc. p. 1, 4-5.

20. Barrer, R. M. (1982). *Hydrothermal Chemistry of Zeolites*. London; New York: Academic Press, Inc.

21. Bekkum, H. V; Flanigen, E. M; Jacobs, P. A. and Jansen, J. C. (2001). *Introduction to Zeolite Science and Practice*. 2nd Edition. Amsterdam: Elsevier. p. 1-7.

22. Frillette, V. J; Haag, W. O. And Lago, R. M. (1981). *Journal of Catalysis*, 67, 218-222.

23. Price, G. L; TU Chemical Engineering Zeolite Page [Website]. Available from: www.personal.utulsa.edu/~geoffrey-price/zeolite/fau.htm

24. Simon-Masseron, A; Marques, J. P; Lopes, J. M; Ribeiro, F. R; Gener, I. and Guisnet, M. (2007). *Applied Catalysis*, 316, 75-82.

25. Marques, J. P; Gener, I; Ayrault, P; Bordado, J. C; Lopes, J. M; Ribeiro, F. R. and Guisnet, M. (2003). *Microporous and Mesoporous Materials*, 60, 251-262.

26. Wang, Z. B; Kamo, A; Yoneda, T; Komatsu, T. and Yashima, T. (1997). *Applied Catalysis*, 159, 119-132.

27. Wang, Q. L; Giannetto, G. and Guisnet, M. (1991). *Journal of Catalysis*, 130, 471-482.

28. Remy, M. J; Stanica, D; Poncelet, G; Feijen, E. J. P; Grobet, P. J; Martens, J. A. and Jacobs, P. A. (1996). *Journal of Physical Chemistry*, 100, 12440-12447.

29. Burckle, E. C. (2000). *Comparison of One-, Two-, and Three-Dimensional Zeolites for the Alkylation of Isobutane with 2-Butene.* Masters' Thesis, University of Cincinnati, Cincinnati, Ohio.

30. Guisnet, M; Alvarez, F. Giannetto, G. and Perot, G. (1987). *Catalysis Today*, l, 415-433.

31. Alvarez, F; Rebeiro, F. R; Perot, G. Thomazeau, C. and Guisnet, M. (1996). *Journal of Catalysis*, 162, 179-189.

32. Nikolaou, N; Papadopoulos, C. E; Gaglia, I. A. and Pitarakis, K. G. (2004). *Fuel*, 83, 517-523.

33. Chao, K; Lin, C; Lin, C; Wu, H; Tseng C. and Chen, S. (2000). *Applied Catalysis A: General*, 203, 211-220.